THE UNIVERSITY OF CALGARY

A New Non-Metallic Anchorage System For Post-Tensioning Applications Using CFRP Tendons

by

Mahmoud Reda Taha

A DISSERTATION
SUBMITTED TO THE FACULTY OF GRADUATE STUDIES
IN PARTIAL FULFILLMENT OF THE REQUIREMENTS FOR THE
DEGREE OF DOCTOR OF PHILOSOPHY

DEPARTMENT OF CIVIL ENGINEERING

CALGARY- ALBERTA
November, 1999

ABSTRACT

The objective of the work described in this thesis is to design, develop and test a new non-metallic anchorage system for post-tensioning applications using CFRP tendons. The use of a non-metallic anchorage system should eliminate corrosion and deterioration concerns in the anchorage zone. The development of a reliable non-metallic anchorage would provide an important contribution to this field of knowledge.

The idea of the new anchorage is to hold the tendon through mechanical gripping. The anchorage consists of a barrel with a conical housing and four wedges. The anchorage components are made of ultra high performance concrete (UHPC) specially developed for the anchorage. Sixteen concrete mixtures with different casting and curing regimes were examined to develop four UHPC mixtures with compressive strengths in excess of 200 MPa. The UHPC mixtures showed very dense microstructures with some unique characteristics. To enhance the fracture toughness of the newly developed UHPC, analytical and experimental analyses were performed. Using 3 mm chopped carbon fibres, a significant increase in the fracture toughness of UHPC was achieved.

The non-metallic anchorage was developed with the UHPC with enhanced fracture toughness. The barrel required careful wrapping with CFRP sheets to provide the confinement required to utilize the strength and toughness of the UHPC. Thirty-three anchorages were tested under both static and dynamic loading conditions. The non-metallic anchorage showed excellent mechanical performance and fulfilled the different requirements of a post-tensioning anchorage system. The development of the new non-metallic anchorage will widen the inclusion of CFRP tendons in post-tensioned concrete/masonry structures. The new system will offer the opportunity to exploit CFRP tendons effectively creating an innovative generation of corrosion-free, smart structures.

PREFACE

This dissertation is the result of three years of research work since September 1996 for the Degree of Doctor of Philosophy under the supervision of Dr. N. G. Shrive at the Department of Civil Engineering, the University of Calgary, Calgary, Alberta, Canada. During the preparation of this dissertation, the following papers have been published or submitted for publication

1. Reda, M.M., Sayed-Ahmed, E.Y., and Shrive, N.G., 1997, "Towards a New Non-Metallic Anchorage System for Post-Tensioned Applications With Carbon Fibre Reinforced Plastic Tendons", Proceedings of the 42nd International SAMPE Symposium, Anaheim, USA, pp. 288-297.

2. Reda, M.M., Sayed-Ahmed, E.Y., and Shrive, N.G., 1997, "Advanced Composite Materials for Post-Tensioning Applications: Merits, Shortcomings and Possibilities", Proceedings of the Int. Conference on Engineering Materials, Ottawa, Canada, CSCE and JSCE, Vol. 1, pp. 271-279.

3. Reda, M.M. and Shrive, N.G., 1998, "A New Ultra High Performance Concrete Using Micro Carbon Fibres", Proceedings of the 12th CSCE annual Conference, Halifax, pp. 329-338.

4. Reda, M.M., Shrive, N.G. and Gillott, J.E., 1999, "Microstructural Investigations of Ultra High Performance Concrete", Cement and Concrete Research, Vol. 29, pp. 323-329.

5. Campbell, T.I., Shrive, N. G., Soudki, K.A., AL-Mayah, A., Keatley, J. P., and Reda, M. M., 2000, "Design and Evaluation of a Wedge-Type Anchor for FRP Tendons", Submitted for Publication in Canadian Journal of Civil Engineering, July 1999.

ACKNOWLEDGMENTS

Praise and thanks to Allah, the Most Gracious, the Most Merciful, and peace be upon his prophet.

I would like to extend my thanks and gratitude to my supervisor Dr. Nigel Shrive for his continuous support, constructive criticism, guidance and endless encouragement throughout the entire program. I deeply appreciate the interest in the project expressed by Dr. Jack Gillott and Dr. Robert Loov, and I thank them for their time and their fruitful discussions. The early support and guidance from Dr. Ezz Sayed-Ahmed and Dr. Amr El-Dieb should not go without a special thank. I would like also to thank my colleagues Ahmed El-Metwally, A. Noureldin, David Blakeney, and Shelley Lissel for their help in different aspects throughout the project.

Great thanks to the technical staff of the Department of Civil Engineering for their invaluable help and donation of time. Special thanks go to Mr. Don McCullough whose technical expertise and sincere help in testing and instrumentation were invaluable; Mr. Dan Tilleman for his help in developing the microstructure work and Mr. Terry Quinn for his time. Special thanks also to the University of Calgary machine shop; Mr. Rob Scorey and Mr. Gunther Hehr for their patience and help in developing the casting moulds.

The financial support of ISIS Canada (The Network of Centres of Excellence on Intelligent Sensing for Innovative Structures), NSERC (The Natural Sciences and Engineering Research Council) and the Department of Civil Engineering, the University of Calgary is gratefully acknowledged. The donation of different materials in the project by Zoltek Inc., Mitsubishi Chemicals America Inc., Lafarge Canada, NAPCO Inc., and Sika Canada is greatly appreciated.

Finally, I would like to express my gratitude to my parents for their continuous love and support throughout all my study period and my recognition for the patience, support, continuous encouragement and love of my wife Abeer Ibrahim to whom I dedicate this work.

To Abeer

TABLE OF CONTENTS

LIST OF TABLES

LIST OF FIGURES

LIST OF SYMBOLS

α	notch-depth ratio
α_c	critical notch-depth ratio
β_1	mathematical parameter [Equation 4.3]
Γ	contour line for line integral
γ_m	matrix surface energy
δ	beam deflection
Δ	distance between the top of the wedges and the top of the barrel [Figure 5.3]
Δ	displacement
δ_1	elastic deflection
δ_{11}	elastic deflection at centre span due to concentrated load
δ_{12}	elastic deflection at centre span due to uniform loads
Δa	crack depth change
δ_{crack}	vertical beam deflection due to cracking
δ_i	beam deflection corresponding to elastic load Pi
$\delta_{maximum}$	maximum beam vertical deflection
ΔU_f	increase in fibre elastic energy due to matrix cracking
ΔU_m	reduction of matrix elastic energy due to cracking
ΔW	work done by applied stress
η	anchorage efficiency factor
θ	anchorage wedge slope angle
μ_{WB}	coefficient of friction between the wedges and the barrel
ν	Poisson's ratio
$\sigma(w)$	cohesive pressure function
$\sigma(x)$	tensile stress of fibre at distance x from fibre end
σ_c	critical stress based on peak load Pc
σ_{fu}	ultimate tensile strength of fibre
σ_T	tangential stress developed in the barrel due to wedge pressure

σ_{WB}	radial stress exerted on the outer barrel by the wedges
$\tau(x)$	interface shear stress at distance x from fibre end
τ_{av}	interface shear strength of the matrix
ϕ_c	material saftey factor of concrete strength
ϕ_{sheets}	material factor of tensile strength of CFRP sheets
ε_m	matrix cracking strain
a	crack depth
a_0	initial crack depth
a_c	critical crack depth
A_1	area under load-deflection curve of notched beams up to the peak load
A_2	area under load-deflection curve of unnotched beams up to the peak load of a similar notched beam
A_3	total area under the load-deflection curve of notched beams
A_{total}	area under the whole load-deflection curve of notched beams including own weight
b	beam width
c	deflection due to cracking
C	compliance
d	beam depth
d	fibre diameter
d_B	barrel outer diameter
d_{Bb}	barrel bottom inner diameter
d_{Bt}	barrel top inner diameter
d_i	aggregate particle size
ds	length increment along contour line
d_{WB}	bottom diameter of the wedges
d_{WT}	top diameter of the wedges

dA	dummy load acting on the beam
D	aggregate nominal maximum size
E	modulus of elasticity of the beam
$E_{cracked}$	modulus of elasticity of cracked beam
E_f	fibre modulus of elasticity
E_m	matrix modulus of elasticity
f'_c	concrete characteristic compressive strength
$f_{bearing}$	bearing strength of concrete
f_r	modulus of rupture of concrete
f_{sheets}	tensile strength of sheets
F	force developed in the fibre
F_{TW}	friction force between the tendon and the wedges
F_{WB}	friction force between the wedges and the barrel
$g(\alpha)$	geometry function for stress intensity factor
$g_2(\alpha)$	geometry function for critical mouth opening displacement
G	modulus of rigidity
G_F	fracture energy
G_{IC}	critical energy release rate
G_m	matrix shear modulus
H	uncracked ligament
H_0	initial uncracked ligament
H_c	critical uncracked ligament
I	moment of inertia
J	The J-Integral
J_{IC}	critical J-integral
K	shear geometry constant equals 3/2 for rectangular sections
K_{IC}	critical stress intensity factor

l	fibre length
l_B	barrel length
l_{Bc}	wedge barrel contact length
lc	critical fibre length
l_f	fibre rupture length without any debonding
l_p	minimum fibre bond length
l_W	wedge length
L	beam length
M_c	critical moment based on peak load Pc and beam own weight
P	applied load
P	aggregate passing percent
P_c	peak load
P_i	elastic load
$P_{seating}$	anchorage seating load
Q	shear force
r	fibre radius
R	matrix radius around the fibre
R	bearing force of the outer barrel
R_{TW}	radial force exerted on the tendon by the wedges
R_{WB}	radial force exerted on the barrel by the wedges
S	loaded span
T	Traction vector
t_{Bb}	barrel bottom wall thickness
t_{Bt}	barrel top wall thickness
U	Strain energy
U_{db}	work required to debond fibres from the matrix
U_s	work of friction during fibre pull-out

U_t	total work of fracture
u	displacement vector
v	shear deflection
V_m	matrix volume
V_f	fibre volume
w	self weight of the beam per unit length
w	crack opening displacement
w	strain energy density
W	beam own weight
W_T	total fibre pull-out work
W_p	average fibre pull-out work per unit fibre length
x	distance from fibre end to a specific point on the fibre
x	distance from support to a specific point on the beam

LIST OF ABBREVIATIONS

ACI	American Concrete Institute
ACK	Aveston, Cooper and Kelly model.
ACM	Advanced Composite Materials
AFRP	Aramid Fibre Reinforced Polymers
CSH	Calcium Silicate Hydrates
CCOA	Critical Crack Opening Angle
CFRP	Carbon Fibre Reinforced Polymers
CH	Calcium Hydroxide
CMOD	Crack Mouth Opening Displacement
COA	Crack Opening Angle
COD	Crack Opening Displacement
CTOD	Crack Tip Opening Displacement
EPFM	Elasto-Plastic Fracture Mechanics
FPZ	Fracture Process Zone
FRC	Fibre Reinforced Concrete
FRP	Fibre Reinforced Polymers
GFRP	Glass Fibre Reinforced Polymers
HPC	High Performance Concrete
LEFM	Linear Elastic Fracture Mechanics
MTS	Material Testing System
PTI	Post-Tensioning Institute
Pult	Ultimate Load
SEM	Scanning Electron Microscope
Test #	Test Number
UHPC	Ultra High Performance Concrete
XRD	X-ray diffraction

CHAPTER 1

INTRODUCTION

1.1. General

The durability of much of the world's infrastructure has become of concern. Corrosion of steel is a major contributor to durability concerns. In recent years, the use of advanced composite materials (ACMs) in structures has grown widely as ACMs offer an alternative strong options in material selection. More recently, fibre reinforced polymers (FRP) have been introduced into reinforced and prestressed concrete applications. A considerable development in technology is expected if the applications of these fibres in concrete/masonry structures can be spread widely. The new fibres do not corrode and they offer the possibility of integrating monitoring capability through the use of fibre optic structural sensing technology. Sensors can be integrated in FRPs to provide the opportunity to monitor the structures in various ways throughout their working life. The fibre optic sensor systems are immune to electromagnetic interference, which will make them more durable than other conventional systems. However, the use of FRP tendons in post-tensioned structures is limited because of the absence of a simple and reliable anchorage system which fulfills all the technological requirements of an anchor. The production of this anchorage system will be very useful to extend the applications of FRP tendons.

1.2. Scope of the research programme

The objective of this research is to design, develop and test a new non-metallic anchorage system for CFRP prestressing tendons. The new anchorage should be easy to assemble, economic to produce and as durable as the FRP tendons. The use of non-metallic components in the new anchorage system should eliminate corrosion and deterioration concerns

of the anchorage zone, and should create a highly reliable system from both the mechanical and environmental points of view. Previous systems have shown several shortcomings which should be eliminated in the proposed anchorage system. The development of a reliable non-metallic anchorage would provide an important contribution to this field of knowledge.

The idea of the new anchorage is to hold the tendon through mechanical gripping. The anchorage consists of a barrel with a conical housing and four wedges. Structural analysis of recently developed metallic anchorages, in conjunction with preliminary experimental investigations of a concrete anchorage system, have shown the need for a material of very high toughness to work as the wedges and a material of ultra high tensile strength to work as the outer barrel. Examining the different non-metallic alternatives, concrete was chosen to be used in developing the non-metallic anchorage system.

Therefore, an ultra high performance concrete (UHPC) using chopped carbon fibres has been developed to produce the precast concrete wedges and barrel for the non-metallic anchorage. The UHPC showed enhanced mechanical performance with compressive strength in excess of 200 MPa. Microstructural investigations including SEM and XRD analysis of the newly developed concrete have also been performed to understand the microstructural behaviour of the material in order to enhance its production process. The UHPC mixtures examined have shown very dense microstructures with some unique characteristics. The microstructural investigation revealed the role of the carbon fibres in controlling cracking and toughness of the UHPC.

The fracture mechanics of fibre reinforced concrete were reviewed, followed by the application of an analytical model to predict the optimum fibre length which can provide the maximum fracture toughness. Experimental investigation of the fracture of the UHPC showed the sensitivity of the J-integral as a fracture parameter for fibre reinforced concrete. The J-integral was used to determine the optimum fibre length to enhance the fracture toughness of UHPC.

The new non-metallic anchorage was made with the UHPC with enhanced fracture toughness. A linear elastic model was used to propose the dimensions of the new anchorage

system. The barrel was reinforced with a special wrapping using carbon fibre reinforced polymer (CFRP) sheets. This provided the necessary increase in the load carrying capacity of the anchorage system. Thirty-three anchorages were tested with sequential modifications of the anchorage geometry, the number of layers of CFRP sheets and the wedge seating load. The testing programme examined both the static and dynamic performance of the anchorage system.

The new non-metallic anchorage fulfills the different requirements of the anchorage system. The development of the non-metallic anchorage system will widen the inclusion of FRP in post-tensioned concrete/masonry structures. The new system offers the opportunity of avoiding the corrosion problems associated with metallic parts in concrete structures. Use of a non-metallic anchorage and FRP's would create an innovative generation of smart structures with enhanced durability.

1.3. Thesis organization

Knowledge of the new FRP materials and previous research on FRP prestressing anchorage systems is first reviewed. The different anchoring concepts are discussed and the optimum anchorage system for post-tensioning applications is described. The anchorage required the development of a new UHPC to provide the necessary material properties for the different non-metallic anchorage components. Different production parameters were examined experimentally and the new concrete was developed. The role of fibres in controlling the fracture behaviour of fibre reinforced concrete was reviewed. This was followed by an experimental investigation of the fracture of HPC and UHPC to determine the optimum fibre length for enhanced fracture toughness. The anchorage was then developed and tested. The test results showed the effect of the different parameters on the performance of the non-metallic anchorage system. Finally, the conclusions and recommendations of this work are summarized.

Three appendixes are included. In Appendix A the test data are presented together with the statistical analysis of the experimental work in the development of the UHPC. Appendix B

includes derivation of the formula used, the MathCad™ worksheet developed for the fracture mechanics analysis, the test data and statistical analysis of the experimental results of work performed towards enhancing the fracture toughness of the UHPC. In Appendix C the test data and statistical analysis of the experimental related to the development of the non-metallic anchorage system are listed.

CHAPTER 2

LITERATURE REVIEW

2.1. Historical review

The ancient Egyptians initiated the idea of using fibres as a reinforcing material through using straw to reinforce their mud. The idea of using fibres to reinforce materials to improve toughness and structural performance is therefore not new, but has been not exploited extensively until recently. Iron rods were used to reinforce masonry in the eighteenth century, leading to the development of steel-reinforced concrete. By the beginning of the twentieth century asbestos fibres were used to reinforce phenolic resin. However, the beginnings of engineering applications of new ACMs can be traced back to the early 1940s when a fibreglass boat was invented.

Technology development produced the filament winding process by 1946 which was used for the missile industry in the 1950s. In 1954 fibre reinforced polymer products were used to reinforce concrete structures for the first time [Rubinsky and Rubinsky 1954]. The application of high strength carbon fibres began in the 1960s when such fibres were used in the aircraft industry. Aramid fibres (Kevlar™) were developed by the 1970s when the application of fibre reinforced polymers was expanded to the automotive industry. A significant jump in the applications of fibre reinforced polymer composites was achieved by the 1980s when they were introduced as a new structural material, especially for rehabilitation purposes [Daniel and Ishai 1994].

2.2. ACM: Basic concepts and characteristics

Conventional monolithic materials can be divided into three basic categories: metals, ceramics, and polymers. Experimental analysis of these categories with all their varied sub-types has shown that no single category has all the advantages for a specific application and a

combination of these categories can result in enhanced performance while making use of each individual constituent. A composite material can be defined as a material system which consists of two or more phases. The mechanical performance and properties of the composites are designed to be of superior performance to either of the constituent materials. Typically, the composite material is a multi-phase material in which the weaker phase is used as the matrix and the stiffer phase is discontinuous and used as the reinforcement. The volume fraction of the reinforcement phase and its distribution and the matrix properties determine the stiffness and homogeneity of the composite. The large variety of possible combinations of fibres and matrices is a source of difficulty when trying to characterize Advanced Composite Materials (ACM). The orientation and the geometry "dimension" of the reinforcement affect the anisotropy of the system which is expressed by reinforcement efficiency factors. The less uniform the reinforcement distribution, the more heterogenous is the composite material [Bentur and Mindess 1990].

Based on the geometry and orientation of the fibre reinforcement, two-phase composite materials can be classified into three types: particulate composites, discontinuous short fibre composites and continuous fibre composites. In particulate composites, the first phase is the matrix while the second phase consists of randomly distributed particles dispersed within the matrix. Concrete is a simple example of a particulate composite. When short fibres are included in the composite with random distribution they provide a limited enhancement of the composite material compared to the basic matrix properties. The third type of composite is continuous fibre composites: these materials are very efficient and the fibre orientation can be either unidirectional or multidirectional according to the application requirements. Laminated composites constitute another type of composite materials in which thin layers of different materials are bonded together. A laminate is made of two or more unidirectional laminae. The laminae may be of different materials and thicknesses. Composite laminates are designated in a manner indicating the number, type, orientation and stacking sequence of the different number of laminae used [Matthews and Rawlings 1994].

ACMs may have many advantages over the monolithic materials, such as high strength,

high stiffness, long fatigue life, low density, excellent corrosion resistance, wear resistance, and appearance. The superior structural performance of composite materials can be expressed in the high specific strength and specific stiffness parameters. The former represents the strength/density ratio while the latter represents the elastic modulus/density ratio. Figure [2.1] shows a comparative representation of the structural performance of different ACM from the specific strength and modulus point of view. Among the different types of composites, carbon/epoxy combinations seem to have the highest specific modulus and strength.

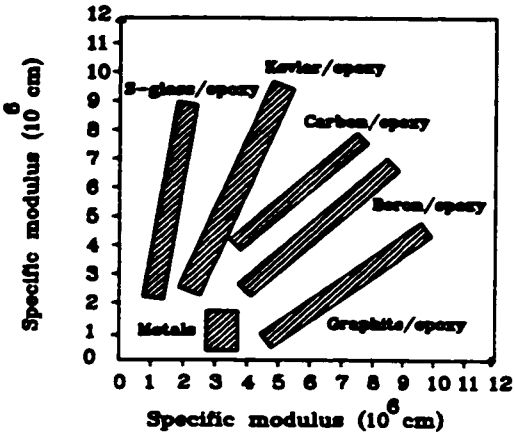

Figure [2.1]: Performance map of structural composites [Daniel and Ishai 1994].

The mechanical performance, especially the stiffness, of unidirectional composites in the fibre direction can be attributed to the properties of the fibre reinforcement. While the behaviour of the composite in the transverse direction with respect to the fibres is dominated by the matrix properties. This can explain the limited transverse capacity of most ACM. It was observed that increasing the composite stiffness detracts from the ability of the material to withstand high strain values [Daniel and Ishai 1994 and Matthews and Rawlings 1994]. The heterogenous nature of ACM especially the fibre/polymer composites (e.g. FRP) provides mechanisms for high energy absorption on a micro-scale comparable to the yielding process of metals [ACI committee 440. 1996].

2.3. Fibre Reinforced Polymers (FRP): A new structural material

Fibre reinforced polymers (FRP) have been introduced to prestressing technology as a potential replacement for steel tendons basically due to the corrosion problem. Technical reports during the last decade from different regions of the world, especially North America, repeat the same theme: an epidemic of corrosion, particularly in bridge decks. More than 35,000 bridges are added annually in the USA alone to the list of those suffering from corrosion [Mehta 1986]. The corrosion problem becomes of more and dangerous concern when prestressing is involved. The corrosion issue has become a multi-billion dollar problem and one of the most innovative applications of FRP is its use instead of steel tendons in prestressed concrete/masonry structures.

Different types of FRP reinforcement are currently produced. They are typically made of high modulus fibres and a resin matrix and are produced by a pultrusion method in which fibres are bundled together and drawn through a resin matrix then pulled through a shaping die. Figure [2.2] shows a schematic representation of the pultrusion process which is crucially important in the production of FRP reinforcement. Other fabrication processes include autoclave moulding, filament winding and resin transfer moulding. There is limited automation of these processes which are therefore dependent on highly skilled hand labour requiring extensive quality control resulting in high cost. Special techniques including wrapping additional epoxied fibre to the surface, pulling a tight fibre around the rod, and fibre twisting to enhance FRP bond strength have been recently reported [Naaman 1998 and Dolan 1993].

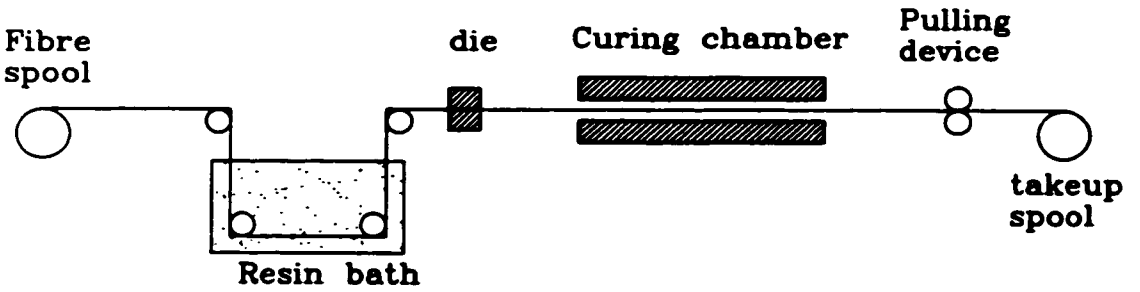

Figure [2.2]: Schematic representation of the pultrusion process [Dolan 1993].

2.3.1. Constituent materials

2.3.1.1. Matrices

Four types of matrices are used in ACM: polymeric, metallic, ceramic, and carbon. In FRP the ones commonly used are the polymeric matrices. Most of the published literature focuses on the reinforcing fibres as the principal load carrying element of FRP. However, it is essential to consider the important role of the polymer matrix. The polymer matrix constitutes about 25-50 percent of the FRP composite by weight. The polymer matrix is the stress transfer medium from the FRP structure to the constituent reinforcing fibres and the matrix also protects the fibres from the outer environment.

Two major types of polymer matrices are considered for FRP production; thermosetting polymers (e.g. polyester and vinyl ester, epoxy, etc.) and thermoplastic polymers (e.g. nylon, polyethylene and terephthalate, etc.). To date most FRP composites have consisted of thermosetting polymer matrices. This can be attributed to the ability of thermosetting polymers to provide good thermal stability, good chemical resistance, and limited creep and relaxation when compared to thermoplastic polymers. While a detailed discussion about polymer matrices, their structures and differences is beyond the scope of this study, the basic engineering properties of both epoxy and vinyl ester resins widely used in FRP are presented in Table [2.1] for reference.

Table [2.1]: Engineering Properties of epoxy and vinyl ester resins [Benmokrane et al. 1997].

Property	Epoxy	Vinyl ester
Density (g/cm^3)	1.2-1.3	1.12-1.32
Tensile Strength (MPa)	55-130	73-81
Tensile Modulus (GPa)	2.75-4.1	3.0-3.5
Ultimate Strain %	1-9	3.5-5.5
Coefficient of thermal expansion (10^{-6}/°C)	50-80	N/A
Poisson's ratio	0.2-0.33	0.37

Under loading the matrix resin deforms and distributes the stress to the higher modulus fibre constituents. The matrix should have an ultimate strain at failure higher than that of the reinforcing fibres and it should not shrink excessively during curing to avoid placing internal strains on the reinforcing fibres. The polymer matrix is characterized by its highly viscoelastic behaviour which means that the material exhibits an instantaneous elastic deformation followed by a viscous deformation when it is subjected to any external loading. Temperature has a great effect on the mechanical performance of the polymer matrix. The matrix tends to behave as a solid brittle material when subjected to high loading rates but in a more ductile fashion if subjected to slow loading rates [ACI committee 440, 1996].

2.3.1.2. Fibre reinforcement

The desirable characteristics of most reinforcing fibres are high strength, high stiffness, low creep and relaxation and relatively low density. Three high-modulus fibres are generally considered for FRP reinforcement; carbon, aramid and glass. Recently, ultra high molecular weight polyethylene fibres have successfully been used to produce FRP reinforcement in The Netherlands; however, the resulting material has shown poor creep performance. The small production and the high cost of PBO (Poly(p-phenylene-2, 6 benzobisoxazole)) has limited its application in the construction industry [Burgoyne 1998].

Fibres usually are manufactured by drawing fibre stock to very small diameters (in the range of 5 to 10 μm). This allows the fibres to exhibit very high tensile strengths due to the lack of individual flaws and impurities in the fibres [Griffith 1921]. Most of the fibres show linear mechanical performance with limited ultimate strain. The lack of a yield plateau constitutes the major common feature of all these fibres. Fibres also show relatively low shear strength, typically in the range of five percent of the tensile strength. This is very low when compared to steel fibres which have a shear strength about one third of the tensile strength. On the other hand, DuPont [1987] proved experimentally that high modulus fibres are not able to sustain their ultimate strength over a long period of time: creep-rupture limits the load capacity of the fibres to less than eighty percent of the theoretical strength. However, carbon fibres showed excellent creep performance under short and long term loading [Anigol 1991].

2.3.1.2.1. Glass fibres

Glass was one of the early fibres which attracted engineering researchers. Griffith [1921] established the basic principles of fracture mechanics based on his experiments on glass fibres. However, the new form of glass fibres was developed in 1931 by Owens Illinois Glass Company with a continuous production line in 1936 [Hercules Aerospace1995]. Glass fibre is an amorphous material consisting mainly of a silica network. Glass is made by fusing silicates with soda or with potash, lime or various metallic oxides. To prevent crystallization, the molten mass is cooled rapidly and then extruded through a very thin orifice [Holte et al. 1993[a]]. Five basic types of glass fibre are available commercially: the following is a brief note about each type [ACI committee 440, 1996 and Hercules Aerospace 1995]:

A-Glass: A-glass is a high alkali glass with adequate tensile strength (3000 MPa) with a high coefficient of thermal expansion.

E-Glass: E-glass stands for electrical grade glass. The glass is composed of calcium-alumina-silicate glass and is used for virtually all electrical applications. This glass constitutes more than 80 percent of glass fibre production.

S-Glass: S-glass is basically a magnesium alumino-silicate which is characterized by its very high strength, as well as high temperature performance. S-Glass fibres are the most expensive type of glass fibres and they are usually produced under very high quality control regulations for military purposes.

ECR-Glass: A modified E-glass with good chemical resistance.

C-Glass: C-glass is highly chemical resistance glass which is used for applications when corrosion-resistant materials are required.

R-Glass : High strength and high modulus fibres rarely used for structural applications.

Glass fibres are hydrophilic and very surface-active. They can be easily damaged in handling. Glass fibres can easily corrode when serving in alkaline environments such as concrete with pH value > 12. This corrosion can be of major concerns for structural applications [ACI committee 440, 1996 and Holte et al. 1993[a]]

2.3.1.2.2. Aramid fibres

The fibre-forming substance in aramid fibres is a long chain synthetic polyamide in which at least 85 percent of the aramid links are attached directly to two aromatic rings. This definition is very important to distinguish aramid from conventional polyamides such as Nylon [Hercules Aerospace 1995]. Aramid fibres have an organic base of poly-para-phenyleneterephthalamide known as "PPD-T" providing very high thermal stability, high strength and high elastic modulus. Aramid fibres were introduced to the market for the first time under the name "Kevlar™" by DuPont in 1973 and were then produced under other names such as "Twaron™" by Akzo Nobel in 1987. The aromatic ring provides high thermal stability, while the para configuration provides the high stiffness and strength. Aramid fibres have very good mechanical properties which permits possible use in structural applications. The low thermal conductivity enables good initial fire resistance. Aramid fibres can be degraded by very strong bases and acids, show strength loss in wet environment and severe degradation under ultra violet light [Mukae et al. 1993].

ACI committee 440 [1996] recommended against the use Aramid fibres in structural elements subjected to compressive stresses because the fibres exhibit nonlinear, ductile behaviour under compression with yielding being observed. This was attributed to the formation of structural defects known as "kink" bands which are related to buckling of p-aramid molecules under compressive stresses. If the fibres are hybridized with glass and/or carbon fibres they can be used in shell structures exposed to compressive and bending stresses.

2.3.1.2.3. Carbon fibres

Commercial quantities of carbon fibres are derived from three major precursors: PAN which is polyacrylonitrile; Pitch which is a by-product of petroleum distillation; and Rayon which is produced from cellulosic materials. Waste in the range of 75 percent results in high cost for the Rayon process. The first two types are therefore used for engineering applications. The production process always includes stabilization, carbonisation, graphitization, surface treatment, finishing and spooling.

Table [2.2]: Typical properties of commercial composite reinforcing fibres.

Fibre	Specific gravity	Tensile strength (MPa)	Tensile Modulus (GPa)	Strain to failure percent	Coefficient of thermal expansion x 10^{-6}/ °C	Poisson's ratio
Glass						
A-Glass	2.58	3000	70.0	N/A	8.6	N/A
E-Glass	2.54	3450	72.4	4.8	5.07	0.2
S-Glass	2.49	4300	86.9	5.0	2.9	0.22
ECR-glass	2.62	3670	87.5	N/A	5.0	N/A
Aramid						
Kevlar™	1.45	3620	131	2.8	-2.0	0.35
Twaron™	1.45	3600	127	2.5	-2.0	0.35
Pan-Carbon						
T-300	1.76	3650	231	1.4	-0.1 to -0.5	-0.2
AS	1.77	3100	220	1.2	-0.5 to -1.2	N/A
HSB	1.85	2340	344.5	0.58	N/A	N/A
Fortafil3™	1.8	3800	227	1.7	-0.1	N/A
Fortafil5™	1.8	2760	345	0.8	N/A	N/A
Pitch-Carbon						
P-555	2.0	1900	380	0.5	-0.9	N/A
P-100	2.16	2410	758	0.32	-1.6	N/A

The formation of carbon fibres requires processing temperatures above 1000 °C at which most synthetic fibres melt [Hercules Aerospace 1995, and Diefendorf 1989]. More than twenty different types of carbon fibres are available commercially. Table [2.2] is a collection of data showing the mechanical properties of seven types of fibres widely used in the construction industry [Hercules Aerospace 1995 and ACI committee 440, 1996]. The superior mechanical performance of carbon fibres can be attributed to their unique microstructure. The

excellent mechanical performance of pan based fibres is related to the two-dimensional parallel arrangement of the hexagonal graphene layers. Carbon fibres are not affected by moisture and have excellent durability performance in hostile environments. Oxidation of carbon fibres becomes a problem at elevated temperatures higher than 1000 °C [Holte et al. 1993[a] and ACI committee 440, 1996].

2.3.2.Types of FRP reinforcement

Different types of FRP reinforcement are currently being produced. Cables, tendons, rods, grids, strips and finally sheets are the most widely known FRP reinforcement. Cables are typically three- or seven- multi-wire strand. Solid rods, with or without deformed surfaces, are known as bars when they are used as conventional reinforcement and as tendons for prestressing applications. The focus in the following discussion will be on FRP bars and tendons as they constitute the major concern of this work in addition to FRP sheets which were used in the experimental programme.

2.3.2.1. FRP bars and tendons

2.3.2.1.1. Arapree™

Arapree™ is the commercial name of FRP rods and tendons of the Netherlands from the co-operation of the Akzo Nobel and HGB companies, and stands for (Aramid Prestressing Element). Arapree™ utilizes Twaron™ aramid fibres embedded in epoxy resin. Arapree™ tendons have good serviceability and durability performance [Taerwe 1993 and Gerritse and Werner 1991]. Arapree™ tendons were used in the Netherlands in different structural applications and in the Bridie post-tensioned pedestrian bridge in Japan[Erki and Rizkalla 1993[a] and Gerritse and Werner 1991].

2.3.2.1.2. BRI-TEN™

Generic FRP tendons consist of E-glass, aramid or carbon fibres embedded in a thermosetting resin matrix. BRI-TEN™ bars are produced by British Ropes Ltd. in the UK. BRI-TEN™ has been used in limited applications up till now [Erki and Rizkalla 1993[a]].

2.3.2.1.3. CFCC™

CFCC stands for carbon fibre composite cable which is produced by Tokyo Rope as

prestressing tendons. The tendons are made from unidirectional PAN fibres wrapped with a synthetic yarn. CFCC cables were successfully used in Canada, Japan and Europe. This includes the Beddington trail prestressed highway bridge in Calgary, Canada, the Shinmiya roadway bridge in Ishikawa, Japan and BASF post-tensioned railroad bridge in Ludwigshafen, Germany [Hercules Aerospace 1995 and Yamashita and Inukai 1990].

2.3.2.1.4. Carbon Stress™

Carbon Stress™ is the trade name of prestressing tendons manufactured in the Netherlands. It was basically developed by the producers of Arapree™. The tendons are manufactured through the pultrusion of epoxy-impregnated carbon fibres [Nanni et al. 1996].

2.3.2.1.5. FiBRA™

Mitsui Construction in Japan developed FiBRA™ reinforcement. FiBRA rods and/or tendons are produced by impregnation of Kevlar™ aramid fibres in epoxy resin. FiBRA™ was used as prestressing strands in Tabras Golf Club bridge and Tahahiko floating bridge in Japan [Tanigaki and Mikami 1990, Sumida et al. 1995].

2.3.2.1.6. JONC J.T.™

A French production of a mixed carbon or glass fibres in a polyester or/epoxy resin matrix. The cable consists of resin-impregnated parallel fibres encased in a braided sheath. The cable was not basically manufactured for construction purposes and no reports are available about its performance in prestressed or reinforced concrete structures [ACI committee 440, 1996].

2.3.2.1.7. Lightline™

An American FRP cable produced by Neptco, Inc. Lightline™ is a seven individual wire strand like a conventional steel strand. The composite cable is made of E-glass and epoxy resin. Lightline™ has shown good on site performance in spite of the limited number of reported applications [Nanni et al. 1996].

2.3.2.1.8. Leadline™

Carbon fibre prestressing tendons and bars produced by Mitsubishi Chemical using pitch based carbon fibres known commercially as Dialead™. Leadline™ is available in diameters

ranging from 1 to 17 mm and is produced in both smooth and deformed bars. Engineering properties of Leadline™ have been examined and the material has been proved to be an excellent alternative for steel reinforcement [Sayed-Ahmed and Shrive 1998 and Benmokrane et al. 1997]. In 1993, CFCC™ and Leadline™ were used to prestress a highway bridge in Calgary [Grant et al. 1995]. More recently, the first masonry diaphragm wall post-tensioned with FRP tendons was built in Calgary using Leadline™ tendons [Sayed -Ahmed et al. 1999]. Leadline™ is the tendon for which a non-metallic anchorage system is to be developed in the work described here [Reda et al. 1997 [a and b]].

2.3.2.1.9. Parafil™

Parafil™ ropes developed by ICI Company consists of a closely packed parallel filament core of continuous Kevlar™ aramid fibres encapsulated within a thermoplastic sheath without a polymer resin [Erki and Rizkalla 1993[b]]. Parafil™ tendons are recommended to be used in unbonded external prestressed structures. Parafil™ bars were used in the Aberfeldy Golf Club pedestrian bridge in Scotland [Burgoyne 1990 and Taewre 1993].

2.3.2.1.10. Polystal™

By the end of 1970s, Strabag Bau-AG and Bayer AG companies in Germany were using E-glass fibres and unsaturated polyester resin to produce Poylstal™ bars and tendons. The fibres have the ability to resist alkaline attack because of the polyamide sheath. Recently Polystal™ has been produced using S-glass fibres impregnated in epoxy resin by Mobay Chemical Company. Polystal™ reinforcement was used extensively in the 1980s in Europe including the Ulenberg-Strasse bridge in Germany, the Notsch bridge in Austria, and in subway stations in France. Recently Poylstal™ tendons were used in a prestressed bridge in New Brunswick in Canada [Taewre 1993 and Erki and Rizkalla 1993[a]].

2.3.2.1.11. SPIFLEX™

SPIFLEX™ is mixed carbon, E-glass and aramid fibres pultruded and embedded in a thermosetting matrix. SPIFLEX™ bars are manufactured by Bay Mills in France. There is no detailed description of this type of FRP bar [ACI committee 440, 1996].

2.3.2.1.12. Technora™

A product of Sumitomo Construction and Teijin Corp. in Japan, Technora ™ aramid fibres especially manufactured for Technora™ bars and tendons are pultruded and then impregnated in vinyl ester resin. Three prestressed concrete bridges in Japan were erected using Technora ™ tendons [ACI committee 440, 1996, Nanni et al. 1996 and Hercules Aerospace 1995].

Many other types of FRP tendons and bars are also available in the market (e.g. Jitec™, Isorod™, Kodiak™ and Plalloy™ etc.). Very recently Naaman [1998] proposed a new fibre tendon technology by allowing the fibre cross section to change in conjunction with the fibre twisting. The new technology has been shown to enhance the performance of FRP structures.

2.3.2.2. FRP sheets

Rehabilitation and retrofitting are two major areas of FRP reinforcement applications. Different commercial products of FRP sheets are available. However, Forca Tow™ and Replark™ are the major products widely used as wrapping material to enhance shear and/or flexural strength of concrete beams and to provide better seismic resistance and ductility to concrete columns and piers. Both sheets are produced by impregnating carbon fibres in high performance epoxy matrix and then rolled down the product. Forca Tow ™ is produced by Tonen, while Replark™ is the product of Mitsubishi chemicals, both from Japan [Nanni 1997].

2.3.3. Mechanical properties of FRP tendons

FRP tendons are anisotropic being strong parallel to the longitudinal axis and weak parallel to the transverse axis. There can be significant variation of mechanical properties from one bar to another. When fibres are pultruded in a rod, the properties of the rods become a combination of the properties of both the fibres and the resin. FRP properties are influenced by many factors including resin matrix properties, fibre sizing, fibre volume fraction, fibre alignment, environmental effects and manufacturing variation [Hercules Aerospace 1995].

The simple rule of mixtures can predict the mechanical performance of the composite material based on the properties of the constituents and the volume fraction of each constituent.

$$E_{cr} = E_f V_f + E_r(1 - V_f) \approx E_f V_f \qquad [2.1]$$

where E_{cr}, E_f, and E_r are the modulus of elasticity of the composite material, the fibre reinforcement and the resin matrix respectively. V_f is the volume fraction of the fibres which is always in the range of sixty to seventy percent. The approximation used is due to the high volume of fibres with respect to resin in most FRP reinforcement. Umoto and Hodhod [1993] reported the inaccuracy of the previous equation in predicting the tensile strength of FRP reinforcement. They attributed that to the difference in Poisson's ratio between the fibres and the resin for most FRP which is not considered in the equation.

Holte et al. [1993] deemed the mechanical performance of FRP tendons to be due to their unique microstructure which offers high strength/weight ratio, low strain values, brittle failure and low transverse stiffness. The latter initiates most failure modes of FRP tendons. Table [2.3] shows the mechanical properties of most commercially available FRP tendons [Sayed-Ahmed and Shrive 1998, Benmokrane et al. 1997, ACI Committee 440 1996, Nanni et al. 1996, Hercules Aerospace 1995, Daniel and Ishai 1994, Holte et al. 1993[a], Dolan 1993 and Erki and Rizkalla 1993[a]]. An important feature of FRP reinforcement is its ability to incorporate optical fibre sensors which allows permanent monitoring of the structures. A Canadian fibre optic integrated monitoring system for structures with FRP materials has been developed [Measures et al. 1995].

2.3.3.1. Tensile strength

While GFRP and AFRP tendons show tensile strength in the same range of steel tendons, CFRP tendons have 15-20 percent higher tensile strength than that of steel tendons. However, tensile strength can not be considered as an intrinsic value of FRP tendon as it is significantly affected by the tendon diameter. The smaller the FRP tendon diameter, the higher its tensile strength. This can be attributed to the shear lag phenomenon, as the surface bond stresses are transferred to the core of the tendon through shear stresses. Excessive shear stresses in the matrix can initiate a progressive failure of the tendon due to relatively low shear strength of that constituent matrix. This possibility increases as the fibre diameter increases

[ACI Committee 440, 1996, Nikolic-Brzev and Pantazopoulou 1995, and GangaRao and Faza, 1992].

Table [2.3] Basic Engineering Properties of FRP Reinforcement

FRP tendon	Fibre volume ratio	Density (g/cm3)	Tensile strength (MPa)	Tensile Modulus (GPa)	Strain to failure percent	Coefficient of thermal expansion x 10^{-6} m/m/°C
Arapree™	0.45	1.25	1200	62	2.9	5.00
BRI-TEN™	0.63	N/A	1480	136	1.1	0.00
CFCC™	0.65	1.5	1800	N/A	1.57	0.50
Carbon Stress™	N/A	N/A	2140	160	1.6	N/A
FiBRA™	0.65	1.28	1250	65	2.4	-2.00
Lightline™	N/A	N/A	1340	51.8	2.5	N/A
Leadline™	0.65	1.53	2250	142	1.3	-0.90
Parafil™	N/A	1.44	1210	120	1.5	N/A
Phillystran™	N/A	N/A	1900	124	N/A	N/A
Polystal™	0.68	2.4	1670	48	3.3	7.00
Technora™	0.65	1.3	1700	54	3.7	-3.00
Steel strands	—	7.85	1860	190	4.0	11.70

2.3.3.2. Stress-Strain relationship

It is evident that all FRP tendons exhibit a linear elastic response up to failure, and failure is generally observed to occur through fibre rupture. GFRP tendons usually show an elastic modulus in the range of 25 -30 percent of that of steel tendons, whereas, CFRP tendons have elastic moduli 75-85 percent of that of steel. The low failure strain values observed for most types of FRP tendons, and the obvious lack of yield plateaux constitute the main structural disadvantages for FRP materials. There will be an inherent lack of ductility in the overall structural response. However, this may be negated with CFRP tendons because of their high strength and relatively high stiffness [Sayed-Ahmed and Shrive 1998, Benmokrane at al. 1997, Reda et al. 1997[a], Nanni et al. 1996, Dolan 1993, Erki and Rizkalla 1993[a], Taerwe 1993 and

Holte et al. 1993[a] .

Alternatively, when mixed fibres are used, the stress-strain curves can change significantly and non-linear behaviour similar to that of a steel tendon may be obtained [Nikolic-Brzev and Pantazopoulu 1995]. Figure [2.3] shows a schematic representation of the stress-strain relationship of the different types of FRP tendons. A different design approach with respect to that well known for steel tendons must be used [ACI Committee 440, 1996]. Taerwe [1993] reported that under increased temperatures, glass fibres have shown very slight changes in stress-strain relationship. This means FRP tendons have an acceptable fire resistance for most structural applications.

Umoto and Hodhod [1993] reported that AFRP tendons have an initial non-linear stress-strain relation which is converted to a linear one when higher stresses are applied to aramid tendons and /or rods. The initial softening mechanism observed can be interpreted by recalling the chain polymeric structure of aramid fibres which will need loading to be straightened. The ultimate strain of both CFRP and AFRP is much lower than that of the steel tendons. However, GFRP shew high ultimate strains.

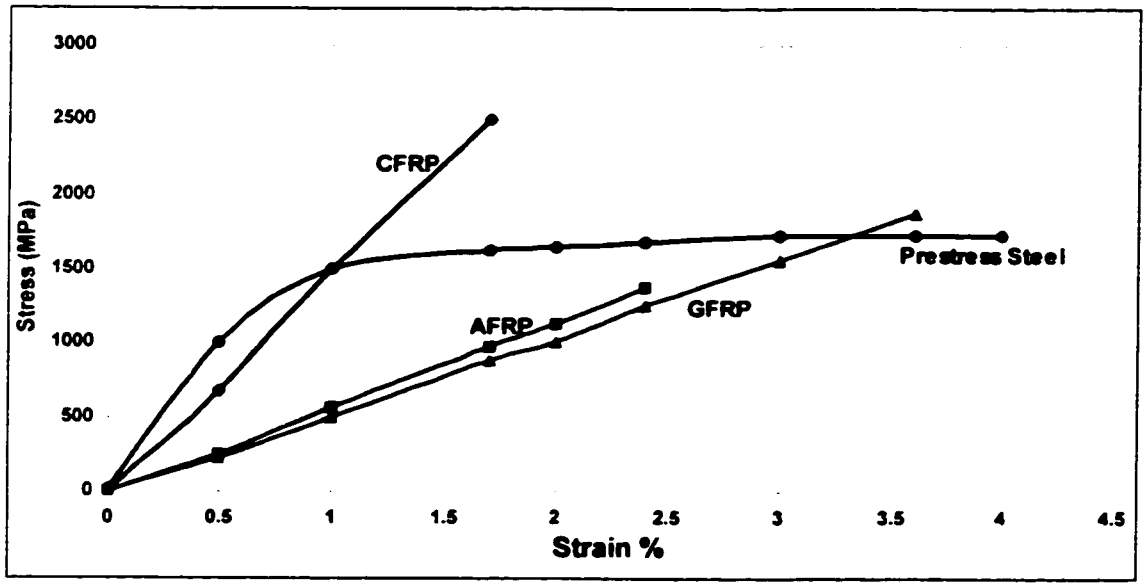

Figure [2.3]: Stress-Strain relationship of different types of FRP tendons [Taerwe 1993].

2.3.3.3. Shear strength

The shear strength of FRP tendons is very low compared to steel ones. Designers try to overcome this shortcoming by orienting tendons to resist applied loads using axial strength only.

2.3.3.4. Compressive strength

FRP tendons show very weak compressive strength when compared to their tensile strength. However, it should be noted that appropriate testing conditions for FRP in compression still of controversy with many difficulties in the gripping, aligning procedures, and stability [ACI committee 440, 1996]. Also, the compressive strength of FRP tendons is not of concern for most structural applications.

2.3.3.5. Creep and creep-rupture

Creep is defined as the observed increase in the material strain while the stress is kept constant [Dowling 1993]. While aramid and carbon fibres have adequate creep resistance, glass has very poor creep performance. Most resins have low creep resistance which means most FRP tendons are susceptible to creep regardless of the fibre type. However, the orientation and volume fraction of the constituent fibres in an FRP tendon have a great effect on its creep performance. Creep rupture is known as the disability of a material to sustain a load lower than its ultimate capacity over a long period of time. The observed creep rupture of most FRP tendons prevents them from being used for long periods at much more than a defined ratio of their ultimate strength [Dolan 1993].

Buldemann and Rostasy [1993], recommended that the service stress level of FRP should not exceed 60 percent of the ultimate strength of FRP tendons. They also proposed the use of a characteristic creep rupture strength based on a 95 percent survival probability during creep rupture tests. Recent experiments by Yamaguchi et al. [1997] showed CFRP tendons to have superior creep-rupture performance with creep-rupture strength in excess of 90 percent of their ultimate strength. This is about three times the creep-rupture strength of GFRP tendons.

2.3.3.6. Fatigue performance

FRP tendons usually show good fatigue performance. CFRP and AFRP prestressing

tendons have shown fatigue performance superior to that of steel ones [Schwarz 1992]. On the other hand, GFRP tendons have shown poor fatigue performance especially when tested at elevated stress levels. The poor performance was attributed to the loss of stiffness due to creep of the resin [Ellyin and Kujawski 1992 and Walton and Yeung 1986]. This stiffness deterioration is in contrast to that of CFRP and AFRP tendons which have shown stiffness gain under cyclic loading [Dolan 1993]. This was explained by the tendency of carbon and aramid fibres to straighten when subjected to cyclic loading. Adimi and Benmokrane [1997] showed GFRP bars to be able to withstand the desired fatigue life of 4 million cycles only when loaded to 22 percent of ultimate capacity. This was shown to be independent of the pH of the surrounding concrete. Fatigue tests carried out on a CFRP-anchorage assembly revealed that neither the mean stress nor the cyclic loading rate have a significant effect on CFRP fatigue performance. The stress range seems to have the most pronounced effect [Saadatmanesh and Tannous 1999 and Sayed-Ahmed and Shrive 1998].

2.3.3.7. Relaxation

Stress relaxation represents the stress loss observed in materials held at a constant length. Stress relaxation is a time dependent phenomenon which is also a function of the stress level [Dowling 1993]. Stress relaxation depends on both the strain loss of the material and its stiffness. This means a low stiffness material like glass can show the same stress relaxation as a high stiffness one like steel. Hercules Aerospace [1995] has proposed that GFRP may have the highest stress relaxation based on its performance in both fatigue and creep tests. Santoh et al. [1993] have reported CFCC™ cable to have a stress relaxation about half of that of the steel tendons, while Sayed-Ahmed and Shrive [1998] reported Leadline™ to have the same value as prestressed steel tendons (4 percent of ultimate strength). AFRP tendons have been reported to have stress relaxation in the range of 10-15 percent which is high compared to either steel or CFRP tendon [Dolan 1993].

2.3.4. Environmental effects and durability performance of FRP

FRP tendons have the attractive feature of good chemical stability in hostile environments such as concrete in contrast to steel tendons which can be easily corroded.

While the problems of steel durability begin when a reduction in pH happens due to carbonation or chloride ion diffusion, durability problems with FRP (with the emphasis on glass) occur in alkaline environments. GFRP tendons were reported to lose more than 50 percent of their strength when used in contact with concrete [Dolan 1993]. The degradation mechanism of GFRP in alkaline solutions is due to ion exchange between hydrogen ions in the surrounding medium and alkali ions, especially sodium, in the glass fibres. The process begins by affecting a very thin layer of the fibre surface which would tend to shrink . The shrinkage would crack the GFRP surface, allowing a continuous degradation process, stress concentrations and finally premature failure [Jones and Rock 1983]. Other deterioration mechanisms supported with analytical studies of the different diffusion mechanisms have been reported recently by Tannous and Saadatmanesh [1998].

Although, aramid fibres have been reported to show strength loss when exposed to continuous moisture conditions, they are able to survive in alkaline environments [Gerritse 1992, and Kakihara et al. 1991]. This moisture effect on aramid fibres was attributed to the loss of the horizontal shear capacity of the FRP composite due to deterioration of the bond strength between the fibres and the polymer matrix [Doxsee et al. 1991].

Carbon fibres tendons have shown superior durability performance in moist, alkaline, and acidic environments. There is a significant amount of literature which examines the durability properties of different carbon fibres especially in the aerospace industry and the data show that mechanical properties of CFRP are not affected by the surrounding environmental conditions. However, CFRP tendons and bars have been reported to react with aluminium and titanium through a galvanic reaction. This would recommend the need to prevent the existence of these metals in the anchorage zone when CFRP tendons are used [Hercules Aerospace 1995].

2.4. Anchorage systems for FRP

2.4.1. Introduction

In 1936 Eugene Freyssinet announced the creation of an entirely new material/structural system, "Prestressed Concrete". Prestressed concrete is an extension of reinforced concrete in which the steel is tensioned against the concrete. This tensioning can be operated either pre- or post- construction resulting in different prestressing technology for pre- and post-tensioned structures. Prestressing technology was developed to overcome problems associated with the tensile strength of concrete which is not only very low, (about 10 percent of the compressive strength), but also, non-predictable and associated with very small deformation prior to failure. Prestressing was shown to enhance the structural behaviour of concrete members, particularly under flexural loading. Prestressing technology has grown widely during the last half of this century. Recently, the same concept has been applied to masonry structures which have the same weak tensile strength problem. Post-tensioning with unbonded tendons is the most common technology used with masonry structures. The effect of prestressing on masonry walls is very pronounced. Curtin et al. [1982] have shown experimentally that applying prestressing to a masonry cavity wall can enhance its flexural capacity up to 150 times that of the original wall. Recent research by Shaw [1996] has shown that the enhancement can be even higher, in the range of 500.

The first FRP prestressed concrete structure was a highway bridge in Germany in 1986. Many prestressed structures have been constructed after that making use of FRP tendons for example; a masonry foot bridge in UK [Ballinger 1991], the Bridie post-tensioned pedestrian bridge in Japan [Erki and Rizkalla 1993[a]], and Aberfeldy Golf Club Pedestrian bridge in Scotland [Burgoyne 1990].

2.4.2. The need to a new anchorage system

The introduction of FRP in prestressing technology needs knowledge about the behaviour of both FRP tendons themselves and the tendon-anchorage assemblage so as to provide a system of an acceptable performance. The key problem of the FRP prestressing and

specifically post-tensioned system is anchoring the tendons. Steel tendons are usually anchored using serrated wedges which can grip the tendon, or by using end button heads and bearing nuts. Because of the relative weakness of FRP tendons in the transverse direction when compared to steel ones, these conventional anchorage systems are not suitable as they dig into the sensitive surface of the FRP tendons causing a premature failure. Most current anchorages have been developed mainly for pre-tensioning techniques and as a result they are frequently not suitable for post-tensioning.

An anchorage system should be able to develop the ultimate strength of the tendon without allowing premature failure in the anchorage zone. Therefore, the current absence of a simple and reliable anchorage system for post-tensioning FRP tendons constitutes a technical obstacle to widespread use of FRP in post-tensioning: a new anchorage which can satisfy all the technical requirements for the new system becomes necessary.

2.4.3. Requirements of a prestressing anchorage system

For a prestressing anchorage system some main requirements should be fulfilled to ensure durable performance of the tendon/anchorage system. The following may summarize these requirements [Sayed-Ahmed and Shrive 1998, Reda et al. 1997[b], Nanni et al. 1996, Hercules Aerospace 1995, Holte et al. 1993[a], and Rostasy and Budelmann 1993].

1- The anchorage efficiency must exceed 0.95. This means that the anchorage must develop a minimum of 95% of the nominal ultimate strength of the tendon. The anchorage efficiency η was defined by Rostasy and Budelmann [1993] and [1991] as the ratio between the measured tendon strength using this anchorage system and the theoretical tendon strength as provided by the manufacturer. Equation [2.2] defines η

$$\eta = \frac{F_{tu(measured)}}{F_{tu(theoretical)}} \qquad [2.2]$$

Where $F_{tu(measured)}$ is the failure force of the tendon-anchorage assembly obtained in a direct test and $F_{tu(theoretical)}$ is the ultimate tendon force based on the nominal tendon strength.

2- The anchorage system should allow the elongation of the tendon to be correlated with

the prestressing force exerted. However, the anchorage itself should only deform with a relatively small, predictable displacement during "seating" when the jacking force is released. This would allow very small prestressing losses which is very important for post-tensioning applications where short masonry walls and concrete beams are prestressed.

3- The anchorage system should be of reliable mechanical performance. This means that the stressing operation should only have to be completed once. This can be achieved through minimal creep deformation.

4- The tendon-anchorage assembly should have excellent creep-rupture resistance. This will provide the prestressing system with the ability to keep the same tensile strength of the tendon even with the application of the long-term static prestressing force for the life time of the structure.

5- Fatigue failure of the anchorage should not occur. The provisions for adequate fatigue performance have been specified for steel tendons by the Post-Tensioning Institute [PTI 1985] which recommends that 500 000 load cycles between 60 percent and 66 percent of the specified tendon strength should be withstood. The same sample should then resist at least 50 load cycles between 50 and 80 percent of the tendon strength without failure. Finally, the anchorage then should provide at least 95 percent efficiency in a direct monotonic loading test. Although, this has been developed for steel tendons, it is reasonable that it can be applied to FRP ones.

6- The anchorage should have excellent durability performance under different environmental conditions which should not detract from the strength of the anchorage-tendon assembly.

7- The anchorage should be simple to assemble and use, so that it can provide easy and effective constructability.

Although, many anchorage systems have been developed to allow the utilization of FRP tendons in post-tensioning applications, none of the developed systems have fulfilled all the basic requirements of a fully reliable and durable tendon-anchorage assembly. A review of the

different anchorage systems follows.

2.4.4. Modes of failure for FRP anchorage systems

For a better understanding of the difficulties encountered in the development of the new anchorage system, the common failure modes of the different anchorage-tendon assemblies should be considered as summarized below [Sayed-Ahmed and Shrive 1998 and Holte et al. 1993[a and b]].

1- Rupture of the tendon within its free length. This is the optimum performance of an anchorage system because this means that the anchor is not affecting the tensile capacity of the tendon.

2- Shear failure in the anchorage zone. Different anchorage systems may result in excessive shear stresses due to certain anchorage geometry. FRP tendons are known to have very low shear strength and to have a very sensitive surface. Thus, shear stresses can result in premature failure of the tendon. This kind of failure was observed when anchorages developed for steel were used to anchor FRP tendons.

3- Bond failure between the resin and the tendon. This can occur in resin bonded anchorages when the bond strength of the tendon/resin assembly is insufficient to withstand the full strength of the tendons. The solution for weak bond strength has been to increase the anchorage length, often resulting in impractical anchorage dimensions.

4- Slip failure between the tendon and the anchorage in wedge type anchorages. This type of failure results in a complete loss of the prestressing force which can result in a catastrophic failure of the structure.

5- Long term creep of the anchorage-tendon assembly. Most resins have low elastic modulus and are very sensitive to high temperatures which results in excessive creep deformation. These deformations can result in significant prestress losses with associated serviceability problems.

2.4.5. Anchorage systems for FRP prestressed tendons

As previously mentioned, conventional anchorage systems developed for steel tendons consist basically of wedges with teeth and an outer barrel. The wedges can hold the tendons by

the tooth action and by exerting high lateral pressure on the tendons. This concept is not suitable to hold FRP tendons as they have very poor lateral and shear strength which will result in premature failure of the tendons. New anchorage concepts are required for the utilization of the new FRP tendons in prestressing applications.

2.4.5.1. Split wedge anchorage

This anchorage consists of two main parts. An outer conical barrel and inner wedges with or without teeth. This system was basically developed for anchoring steel tendons. Figure [2.4] shows a schematic representation of this anchorage system. The anchorage action depends mainly on the gripping action of the wedge and/or its teeth around the tendon perimeter accompanied with the compression exerted by the wedges. The common failure mode of this system is local damage in FRP tendons due to the gripping effect of the wedges. Erka [1986] used plastic wedges for the same anchorage system which were reported to work satisfactorily but limited only to pre-tensioning applications. Kakihara et al. [1991] used a two piece wedge anchorage system for prestressed concrete using AFRP. This system was reported to develop 97 percent efficiency when the CFRP tendons were used with a bonded steel sleeve.

2.4.5.2. Plug-in-cone anchorage

The plug-in cone anchorage is somewhat similar to the split wedge system. However, multiple tendons can be stressed by using a conical solid cone (spike) instead of the wedges as shown in Figure [2.4]. The anchorage action depends on the gripping effect from the teeth in the outer conical socket. The system is based on the Freyssinet system developed in 1936 for prestressed steel tendons. The plug- in- cone anchorage system was basically developed for Parafil™ tendons. The steel spike in the system presses the dry fibre against the wall of the conical socket. The end parts are usually sealed with a resin to prevent moisture penetration.

The system has performed very well when used for Parafil™ tendons made of aramid fibres without a resin [Erki and Rizkalla 1993[b]]. This can be explained by the high transverse stiffness of aramid fibres when compared to either glass and/or carbon fibres. However, stress concentration in the tendons usually initiates premature failure of the tendons. This anchorage failure usually happens due to stress concentrations of FRP tendons at the anchorage entrance.

2.4.5.3. Resin sleeve anchorage

This system is mainly composed of a cylindrical metallic shell or sleeve with threaded or deformed inside surface as shown in Figure [2.4]. The anchorage action is developed by injecting resin (typically epoxy) in the sleeve, then the cylindrical sleeve is anchored using a bearing nut. The common failure modes observed are either bond failure or excessive creep strain of the epoxy resin. A number of parameters affect the anchorage capacity. However, the shear strength of the bonding resin can be considered the most important. Zhang and Benmokrane [1997] introduced a theoretical analysis of resin sleeve anchorage showing the bond strength of the anchorage to be independent of the anchoring length. Many disadvantages have been reported regarding this system: poor impact resistance which can resulted in premature failure of the anchorage, excessive creep deformation, and durability problems regarding moisture and thermal effects [Holte et al. 1993[b] and Naaman et al. 1993.]

Wolff and Miesser [1989] proposed a successful resin sleeve system for anchoring Polystal™ tendons using a steel sleeve with epoxy-sand grout. Tokyo Rope [1990] also reported a 100 percent efficiency with the resin sleeve system developed for CFCC™. Rostasy [1993] reported a successful application of a resin sleeve anchorage using a steel sleeve with threaded attachment. Hercules Aerospace [1995] has reported successful combination of resin sleeve and split wedge anchorages. Tokyo Rope provided different types of anchorages with CFCC™. A metallic and a non-metallic resin sleeve anchorage which is filled by a polymer resin to bond the tendon. The sleeve is usually threaded to allow anchoring using a bearing nut.

Harada et al. [1995] and Khin et al. [1996] have proposed a non-metallic resin sleeve anchorage system for prestressed CFRP tendons. The system consists of a non-metallic outer sleeve made of mortar epoxy reinforced with two layers of CFRP spiral and longitudinal reinforcement. An expansive epoxy resin mortar is used as the bonding material. Experimental evaluation of this system showed its ability to anchor the tendons up to their maximum tensile strength. Good fatigue performance was also observed. However, prestress losses in the range of 4 percent were developed due to tendon slippage and expansive mortar creep. It is suggested that the effect of the slippage would be negligible when long prestressed members will be used.

This means the anchorage would not be suitable for post tensioning applications involving short concrete/masonry panels.

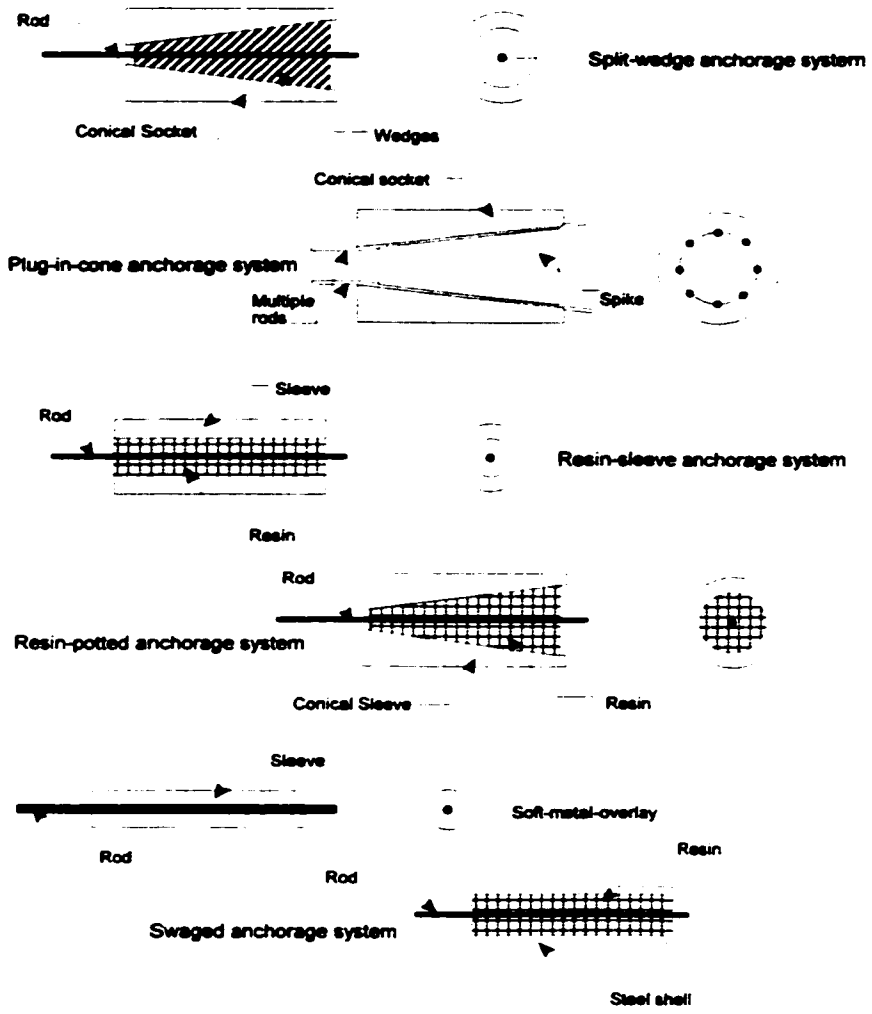

Figure [2.4]: Different FRP anchorage systems [Sayed-Ahmed and Shrive 1998].

2.4.5.4. Resin-Potted anchorage

This is an anchorage system which combines the benefits of both the wedge -type anchorage and the resin sleeve anchorage. Figure[2.4] shows a schematic diagram of a resin potted anchorage. The resin is used to bond the tendon to a conical sleeve rather than a

cylindrical one. The anchorage action depends on the compressive stress exerted by the wedges while the resin eliminates the biting action of the wedges. The most common mode of failure is related to excessive creep deformation of the resin. In addition, there is high susceptibility to thermal and durability deterioration. Conventional resin potted anchorages have generally shown unreliable performance [Hercules Aerospace 1995]. Holte et al. [1993 [a and b]] examined the effect of different parameters on the performance of a resin potted anchorage using both a finite element model and experiments. Both methods proved that an anchor with a bond release between the resin plug and the metallic socket would produce a substantial reduction in the shear stress at the tendon surface. They also found that if the inside surface of the sleeve had a segmentally-varying taper, especially a parabolic one, the anchorage was able to develop the tendon strength.

Meier [1995] and Patrick and Meier [1991] in the Swiss Federal Laboratories for Materials Testing and Research (EMPA) developed a resin potted anchorage system which developed 92 percent of the tendon tensile strength. The anchorage was reported to use a resin with a stiffness gradient. The resin consists of an epoxy matrix with high modulus ceramic and polymer fillers. The change of the resin stiffness was deemed to allow better shear stress distribution than occurs with a constant modulus resin, thereby preventing the common slippage failure of such anchorage.

However, excessive creep is a big concern for this anchorage. The anchorage may also face durability problems as it utilizes aluminum based ceramics which may have a galvanic reaction with the carbon fibre tendons [Hercules Aerospace 1995]. Further discussion of the soft zone concept will be considered in the next section. Resin potted anchorage is usually used with Technora™ prestressed tendons. Nanni et al. [1996] examined this anchorage system and reported the anchorage to be inefficient due to anchor/tendon slippage.

2.4.5.5. Swaged anchorage

A system which has a limited use is the swaged anchorage which consists of a steel shell into which a resin is injected. The gripping action is accomplished by using nuts or bolts. Two steel plate grips with a semi-circular groove and epoxy sand coating were successfully used to

anchor FRP prestressed tendons [GangaRao and Faza 1992]. Slight slippage was reported when the system was tested [ACI committee 440, 1996]. Slippage can result in considerable prestress losses especially for short post-tensioned concrete/masonry members. Figure [2.4] shows a schematic representation of this system.

Sippel [1992] developed a multi-tendon swaged anchorage system in which each single rod is embedded in clamping sleeves of copper filled with a resin mortar. The sleeve is then anchored between two steel blocks using bolts and nuts. The sleeve geometry provides a compact arrangement for the tendons which allows relatively uniform distribution of transverse stresses. The system had an efficiency factor of 98 percent, however, no data were reported regarding fatigue performance.

2.4.5.6. Soft metal overlay

A soft metal overlay system mainly consists of a soft metal tube made of aluminum alloy to grip the tendon. The cable is then anchored using conventional steel grips. Figure [2.5] shows a schematic diagram of this system. Tokyo Rope developed a permanently bonded soft metal overlay for its CFRP cables. While this anchorage works well it does not have the required flexibility for field modifications (cables have to be ordered with the location of the metal overlay specified). In addition, aluminum is highly sensitive to both concrete and carbon, raising concerns about long-term durability [Sayed-Ahmed and Shrive 1998, and Hercules Aerospace 1995]. A soft metal overlay anchorage has been used with CFCC™. Anchoring is achieved using steel wedge anchorage system. Neither system works with 100 percent efficiency and failure is usually expected within the anchorage zone.

2.4.5.7. Link Cable Connection

The link cable is fabricated by the continuous winding method in order to produce an eye bat that has a solid central section and circular eyes. The end eye is reinforced with fibre to reduce stress concentrations [Hercules Aerospace 1995]. This type of anchorage has been successfully used with GFRP tendons. Due to the nonuniform contact surface between the end anchorage and the supporting pin, an aluminum spool is inserted at the end eyes to improve both the strength and fatigue performance of this anchorage [Erki and Rizkalla 1993[b]].

2.4.5.8. New anchorage system

A new metallic anchorage system for post-tensioning applications using single Leadline™ tendon has been developed in the University of Calgary [Sayed-Ahmed and Shrive 1998]. The new anchorage merges the split-wedge, the plug-in and the soft-metal overlay systems and consists of an outer steel barrel with a conical hole, four piece metallic wedges and a copper soft-metal sleeve [Figure 2.5]. A small differential angle between the outer sleeve and the inner wedges is used which results in relatively uniform contact pressure. The system has performed well when tested under both static and fatigue loading [Sayed-Ahmed and Shrive 1998]. However, the stainless steel used as the inner wedges and the outer barrel is still susceptible to corrosion, especially in chloride environments. A similar anchorage has also been developed by Kerstens et al. [1998] for CFRP tendons and has been reported to achieve a 90 percent efficiency factor.

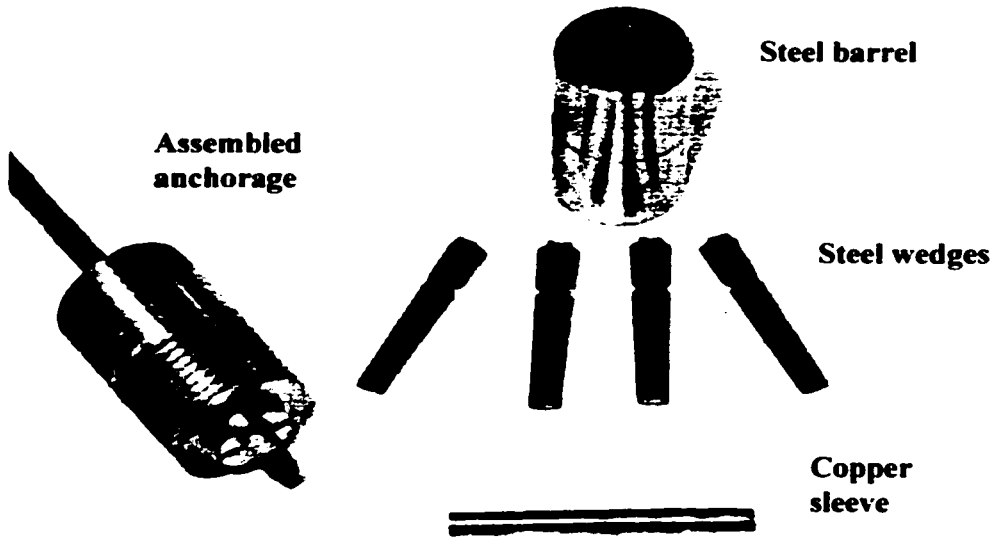

Figure [2.5]: The metallic anchorage barrel, wedges, sleeve and assembled anchorage.

2. 5. Analysis and design of FRP anchorage systems

In order to develop an improved anchorage system, it was decided to examine the different mechanical models already developed for FRP anchorages, in conjunction with conducting preliminary experimental investigation. The basic principle of pulling conical wedges into an outer housing in the longitudinal direction is to apply uniform transverse radial pressure on the tendon to grip it. Rostasy and Budelmann [1991] showed that the change of uniaxial state of stress to a multiaxial one at the anchorage zone markedly affects the axial tensile strength of FRP tendons. This was attributed to the sensitivity of the FRP tendons to transverse stresses which results in a premature failure. Therefore, a successful anchorage system would be able to exert uniform radial pressure without any stress singularity points.

2.5.1. Soft Zone Concept

Meier [1995] developed the soft zone concept for bonded type anchorage. This concept was invoked to counteract the fact that using a constant stiffness bonding material initiates peaks of shear stress at the end of the anchorage resulting in premature rupture of the CFRP tendon. On the other hand, if a material with varying stiffness is used, the shear peak will be avoided and the anchorage will be able to withstand the ultimate capacity of the tendon provided that the bond length is enough.

The anchor matrix at the anchorage termination has a very low stiffness and the stiffness continuously increases towards the other end. Meier [1995] applied this concept and developed a resin potted anchorage system with a gradient stiffness using epoxy resin and ceramic filling powders. The static load carrying capacity of this anchorage reached 92 percent of the tendon ultimate load. Figure [2.6] shows the soft zone concept and the effect of varying stiffness resin matrix on the shear stress distribution of the anchorage.

However, a bonded type anchorage may not be the most suitable type for post-tensioning applications. Such an anchorage requires the total anchorage to be in place on the tendon prior to stressing which will not be as flexible in construction as the wedge type which can be used only during stressing. Applying the soft zone concept to a wedge type anchorage

can be accomplished by giving the conical wedges varying local stiffness in order to reduce the compressive radial stresses at the anchorage entrance. However, this can result practically in tendon slip. On the other hand, similar reduction of the shear peak stresses can be accomplished by using a differential angle between the inner wedges and the outer barrel in a wedge-type anchorage.

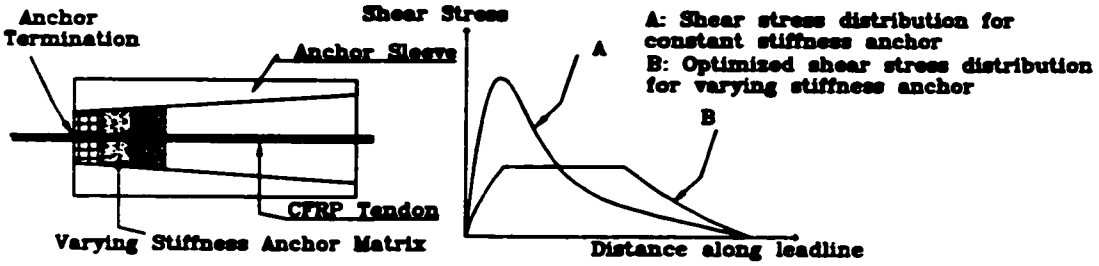

Figure [2.6]: Soft zone concept and the effect of using gradient stiffness anchoring material [Meier 1995].

2.5.2. Differential angle concept

Sayed-Ahmed and Shrive [1998], proposed the concept of the differential angle and proved using the finite element method that reasonably uniform shear and radial stresses around the tendon can be exerted by the wedges if a suitable differential angle is utilized. The differential angle allows the anchor to grip the tendon on the rear end first and to increase the gripping pressure gradually towards the front end. Experimental verification of the concept was established by the new metallic wedge type anchorage systems developed in the University of Calgary [Sayed-Ahmed and Shrive 1998] and in the Netherlands [Kerstens et al. 1998].

2.5.3. Finite Element models

Noisternig and Jungwirth [1996] proved using finite element analysis that optimizing the radial stress distribution can reduce the shear stress peaks at the end of the anchorage. Sayed-Ahmed and Shrive [1998] developed an axisymmetric finite element model to determine the stress distribution along the CFRP tendon inside the anchorage zone. Both linear and non-linear analysis were considered.

Analysis was performed on three steps including seating the anchorage, releasing the load and finally applying the force. Non-linear analysis proved that a nearly uniform radial stress distribution is developed along the Leadline™ length. Although, high radial stresses can be developed at the anchorage front during anchorage seating, these stresses are relieved after load application to the tendon. Relatively uniform shear stresses along the tendon in the anchorage zone are developed with the same observation regarding stress increase and reduction during loading. The model in conjunction with the static and fatigue testing performed on this type of anchorage has proved the reliability of the differential angle concept [Sayed-Ahmed and Shrive 1998].

Campbell et al. [1998 and 1997] proposed a finite element model to analyse the same wedge type anchorage with differential angle using linear elastic analysis. Similar results were reported. This model examined the effect of friction between the outer barrel and the inner wedges and proved that the smaller the coefficient of friction between the outer barrel and the inner wedges the higher the pressure exerted on the outer barrel and the hoop force developed inside the barrel as a result.

Although this may not be of concern for the steel anchor, as using grease can reduce this friction to negligible values, this will be of concern for the non-metallic anchorage as it can affect the internal stresses on both the inner wedges and the outer barrel. The study also proved that linear elastic models can be used to give a reasonable estimation of the stresses and strains developed in the anchorage parts. This will be further considered when an estimation of the non-metallic anchorage dimensions will be considered.

2.5.4. Elasticity simulation analysis

Kerstens et al. [1998] developed an elasticity simulation model to analyse CFRP wedge-type anchorage based on the differential angle concept. The anchorage consists of an outer conical housing and two-piece inner wedges. The model distributed the forces over a number of thin disc elements each having a finite thickness. The disc consists of the steel housing, the conical wedges and the carbon rod composite.

Three springs were used to model the discs. Figure [2.7] shows the basic components of the model. Plane stress conditions were assumed in spite of the fact that these conditions may not be actual due to the expected contraction of the FRP tendon when tensioned. Applying sensitivity analysis to the model, the effect of lateral contraction of the tendon appeared to have a negligible effect.

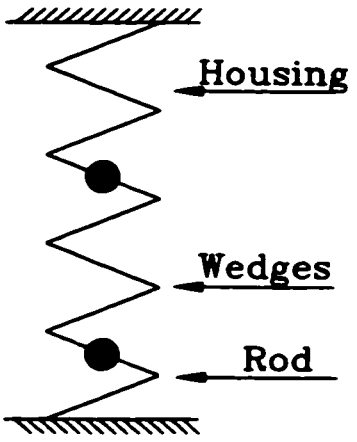

Figure [2.7]: Elasticity Simulation Model [Kerstens et al. 1998].

The model addressed both the material and geometric non-linearity of the anchorage. Based on the theory of elasticity, both the tangential and radial stresses can be computed. Material non-linearity was used both for the steel of the outer housing and the Nylon of the wedges, while geometric non-linearity was included for the differential angle between the housing and the wedges. The analysis of a non-differential wedge type system showed the

development of very high radial stresses at the anchorage entrance which would cause pinch action on the FRP tendons. However, a wedge-anchorage with a differential angle has shown more uniform radial stresses allowing the anchorage to withstand 90 percent of the ultimate load of the tendon.

2.6. Closure

The previous review sheds light on the different aspects of the FRP prestressing tendons as a relatively new structural material and the anchorage problem. To anchor prestressed FRP tendons, enough, relatively uniform, radial pressure is required on the tendon. Such stress should be developed without exceeding the shear strength of the tendon material in order to prevent premature failure. The two techniques available to achieve these requirements are either to use a varying gradient bonded-type matrix or a differential angle wedge-type anchorage. The latter is preferred for post-tensioning applications due to the ease of use. In the following chapters an experimental programme is described in which a non-metallic wedge-type anchorage system was developed for post-tensioning applications using CFRP (Leadline™) tendons.

CHAPTER 3

DEVELOPMENT AND INVESTIGATION OF UHPC

3.1. Introduction

When a mechanical gripping wedge-type anchorage is considered, the wedges should be tough enough so that sufficient pressure can be developed around the tendon without the wedges or tendon being deformed, cracked or crushed. To support this concept, preliminary experimental investigation included testing of anchorages with 0.1° differential angle was considered. The anchorage consisted of an outer barrel and four inner wedges and all were made of epoxy cement grout. The grout used was characterised by 70 MPa compressive strength. Slippage of the tendon from the wedges was observed and the anchorage carried no load. In all tests slippage occurred as a result of either early transverse tensile cracking of the wedges (i.e. perpendicular to the longitudinal axis) and/or radial tensile cracking of the barrel. This preliminary series of tests revealed the need for the wedges to be made of a material characterized by high fracture toughness to be able to grip the tendon without fracturing itself. High strength would also be required in both the barrel and the wedges.

Three main alternative materials were considered; plastics, ceramics and ultra high performance concrete (UHPC). Creep problems with plastic anchorages have been widely reported which reduced the probability of utilizing plastic parts in the new anchorage. The very high cost associated with ceramics production excluded this option. The choice was to develop the required UHPC with very high compressive strengths, enhanced durability and high fracture toughness.

3.2. Background

Ultra high performance concrete (UHPC) forms a family of micro-defect-free-cement composites. These relatively new materials are characterized by an extremely dense

microstructure, compressive strengths in the range of 150-250 MPa and superior durability performance. Ultra high strength concrete (UHSC) is defined as concrete with compressive strength greater than 200 MPa [Shah 1996]. Although high performance concrete (HPC) is different from high strength concrete when durability criteria are taken into account, the compressive strength is still used as a parameter to distinguish and identify both HPC and UHPC. The main differences between HPC and UHPC are summarized in Table [3.1].

Table [3.1]: Characteristics of HPC and UHPC [Shah 1996].

Characteristic	HPC	UHPC
Compressive Strength (MPa)	~ 100	> 150
Water/Cementitious ratio	< 0.3	< 0.2
Chemical admixtures	Superplasticizers	Superplasticizers
Mineral admixtures	fly ash, silica fume and /or slag	silica fume
Fibres	beneficial	essential
Processing	conventional	heat treatment and pressure

The most well known UHPCs are the Silica Infiltrated Fibre Concrete (SIFCON), Compacted Reinforced Concrete (CRC), High Performance MultiModal Fibre Reinforced Cement Composites (HPMFRCC), Reactive Powder Concrete (RPC), and Densified Systems containing homogeneously arranged ultra fine Particles (DSP) (known commercially as DENSIT®), in addition to some recent mixtures which exhibit very high compressive strength [De Larrard et al. 1995].

Different theoretical bases are behind the production of different types of UHPC. The principal characteristics of DSP [Baché 1981] and the recent UHPC mixtures developed by De Larrard et al. [1995] are based on the arrangement of different particles in a very dense arrangement. The mix proportions were developed from a theoretical packing model which takes into account all the concrete components (coarse aggregate, fine aggregate, cement, pozzolans..etc.). According to Sedran and De Larrard [1996] the production of UHPC seems to depend mainly on the improvement of the packing density of the aggregate skeleton. It is

widely believed that part of the mixing water is consumed in filling the porosity of the aggregate skeleton. Thus, improving the packing density of the aggregate skeleton leads to less water requirement for the same concrete workability. Rossi and Renwez [1996] argued that because of the confining effect of the aggregate on the cement paste, the more dense the aggregate skeleton, the higher the strength that will be achieved. Clearly, there are different opinions on how to create UHPC's.

The production of UHPC requires careful selection of suitable concrete ingredients, as low a water/binder ratio as possible and the removal of entrapped air. The choice of the materials and techniques used to produce UHPC are centred on the capability of these materials to reach maximum strengths with minimum water demand [Gutierrez and Canovas 1996]. High strengths can be achieved through use of aluminous cement and/or very strong, reactive aggregate (like Calcined Bauxite) of small nominal size [Aitcin 1992]. Two different curing techniques are known to help develop UHPC: applying high compacting pressure to fresh concrete by either direct pressure or vibration, or applying a high curing temperature to increase interface bond. Any of these techniques and materials may be used alone or in combination with the others for the production of UHPC.

Some recent experimental approaches such as Reactive Powder Concrete (RPC) have achieved remarkable results illustrating that the above are not the only approaches to producing UHPC [Richard and Cheyrezy 1995]. Monosize aggregate in the range of 150-60 μm is used with a high cement and silica fume content to provide high compressive strength. The idea of RPC is that when coarse aggregate is eliminated and pressure is applied to fresh concrete for 6-12 hours, the compacted density of concrete can be increased significantly. Steel fibres were also used to increase the ductility of the concrete [Richard 1996]. A brief summary of some published UHPC mixtures is given in Table [3.2].

The mixing and compacting techniques are recognized as important processes in the production of UHPC. Bresson [1996] recommended preliminary mixing of the dry ingredients for sufficient time to achieve a good mix before water is incorporated. Special mixing techniques were reported to achieve the high workability of HPC especially when very low

water/binder ratios were used [Gjϕrv, 1996]. To achieve moderate workability when fibres are included in the mixture, the mixing and compaction processes are expected to require a longer time than usual [Banthia 1994]. Schmiedmayer and Schachinger [1998] reported the importance of using high performance shear mixers to develop ultra high performance concrete.

Table [3.2]: Mixture proportions of some published UHPC mixtures [Richard 1996, De Larrard and Sedran 1995 and Aitcin 1992].

Mixture	1	2	3	4	5	6
Type 50 Cement (kg/m³)	400	955	1080	1148	1013	713
Silica Fume (kg/m³)	130	240	334	357	313	232
Aggregate (kg/m³)	1850	1051	813	725	763	1233
Water (L/m³)	100	153	167	200	207	143
Steel Fibre (Vol. %)	—	1.5-2	—	—	5-7	196
Superplasticizers (L/m³)	13	13	52	N/A	N/A	43
Water/cementitious ratio	0.19	0.18	0.18	0.17	0.16	0.15
28 days comp. strength (MPa)	268	230	236	233	193	216

3.3. Development of UHPC

3.3.1. Materials

3.3.1.1. Cementing materials

Type 10 and Type 50 Portland cement were used, with only silica fume as a supplementary cementing material (SCM) due to the necessity for high early strength. The choice of cementing material depends mainly on both the potential strength gain and workability. Type 50 was considered due to its relatively small C3A content which can enhance workability especially when very low water/binder ratios are considered. Silica fume has been proven to have a substantial role in achieving a uniform and easy dispersion of carbon fibres in the cement matrix [Ohama et al. 1985].

3.3.1.2. Aggregate

Different combinations of limestone, calcined bauxite and silica aggregate were used.

The limestone and calcined bauxite aggregate were of nominal maximum size of 4 mm. The inclusion of fibres in these mixtures limited the maximum size of the fine aggregate in the mixtures to a maximum of 200 μm to provide the required density in the vicinity of a fibre [Banthia 1994]. On the other hand, the need for very high strengths limited the nominal maximum size of coarse aggregate to 4 mm [Aitcin 1992].

Two types of siliceous aggregate were incorporated, Ottawa sand of uniform size > 150 μm and Silica flour (pulverized quartz) of a uniform size < 75 μm. Silica flour has been reported to work as a pozzolanic material when the concrete is cured at temperatures above 150 °C [Grabowski and Gillott 1989]. The aggregates were combined considering an exponential grading curve with a (0.415) exponential value as suggested by Loov [1996]. Equation [3.1] includes the newly suggested exponential value. The basic equation was initially developed by Fuller and Thompson [1907] with exponential value of (0.5). Other exponents between 0.4 and 0.5 have also been suggested [Goode and Lufsey 1962].

$$P\% = 100\left(\frac{d_i}{D}\right)^{0.415} \qquad [3.1]$$

Where P% is the percent passing, d_i is any particle size and D is the nominal maximum size of the aggregate. This means that to achieve a dense packing system, the percent passing of any sieve depends on the nominal aggregate maximum size. Figure [3.1] shows the theoretical aggregate grading curve for different nominal maximum sizes used in the development of UHPC. The concept of achieving optimum mixture design through the development of a densified system of packed particles has received more attention lately [Nehdi and Mindess 1998, Kronlöf 1997, Young 1997, Goltermann et al. 1997, De Larrard 1995 and Baché 1981].

In preliminary stages of this work, experiments have been carried out to verify the ability to develop high strength concrete mixtures based on determining the mix proportions of all the concrete ingredients to match the exponential grading curve. These trials resulted in concrete mixtures which show 28 days compressive strengths less than 70 MPa. These trials also showed

the difficulty encountered for practical production of HPC which depends on dense packing system including all the concrete particles. Similar conclusions were reported by Domone and Soutsos [1994] who disagreed with the idea of filling the voids of aggregate skeleton when developing HPC as it results in a small cement paste volume, which makes it difficult to attain very high strength. They indicated that cement paste overfill is required to increase concrete workability and strength. On the other hand, when the aggregate skeleton only was considered, higher strengths were attained and better concrete was easily produced.

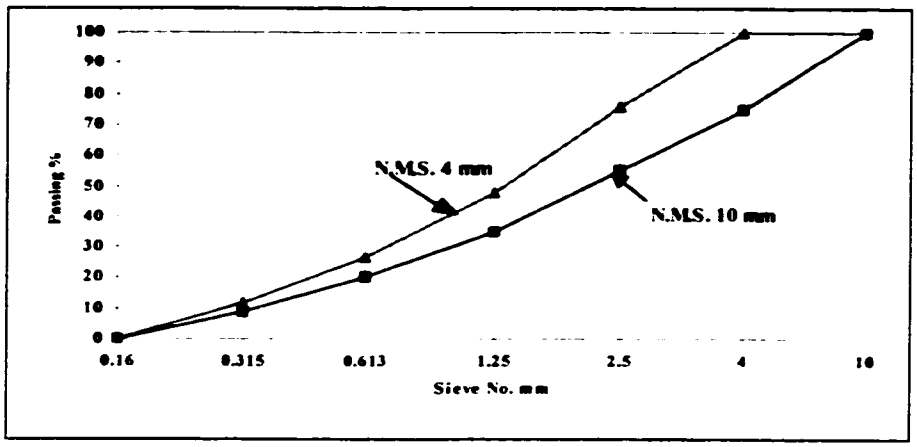

Figure [3.1]: Theoretical grading curve for aggregate used in the development of UHPC.

3.3.1.3. Superplasticizer

Liquid and powder polynaphthalene formaldehyde sulfonates were examined as superplasticizers for the production of UHPC. The Marsh cone test was used to determine the superplasticizer dosage, which was about 2% of the cementing material by weight. This dosage is known as the saturation dosage because it is the dosage beyond which only small effects of further dispersion can be observed.

3.3.1.4. Fibres

The inclusion of carbon fibres in cement matrix materials has been considered in the last decade. The pan-based and the pitch-based carbon fibres are the most well known carbon fibres that have been used to enhance the performance of cement based materials. However, the

difficulties encountered in mixing concretes including these fibres, the inability of long fibres to enhance the mechanical performance of concrete and the relatively high cost of these fibres has limited their use in structural applications.

Chopped carbon fibres 3-6 mm long were incorporated in the mixes. The fibres were included to enhance fracture toughness and to allow thermal curing of the specimens at temperatures above 200 °C. Carbon fibres were selected instead of steel fibres to develop corrosion free concrete elements. Although carbon chopped fibres may be the most expensive fibres, they have the highest tensile strength, the highest strength/weight ratio, the highest modulus of elasticity, the highest thermal resistance, excellent finishability, and long term chemical stability compared to conventional steel, glass and polypropylene fibres used in the cement composites. The low failure strain values observed for most types of carbon fibres, and the obvious lack of yield plateaux constitute their main disadvantages. The different physical and mechanical properties of these fibres have been discussed in chapter 2. A comparison between conventional steel fibres and these carbon fibres is shown in Table [3.3]. Fibre content in the mixtures was limited to a maximum value of 2% by volume to obtain acceptable workability, especially since no dispersing agents were used when the carbon fibres where included. Banthia [1994] recommended a 1% volume of carbon fibres when normal mortar mixers are used.

Table [3.3]: Engineering properties of steel and carbon chopped fibres

Characteristic	Steel fibres	Carbon fibres
Diameter (μm)	25	10
Length (mm)	12-25	3-25
Unit Weight (kg/m³)	7850	2000-2100
Ultimate Strength (MPa)	1900	2400-3300
Strength/wt. Ratio	0.24	1.2-1.6
Modulus of Elasticity (GPa)	200	210-300

3.3.2. Mixture Proportions

Sixteen trial mixtures were developed and examined in this experimental programme. Table [3.4] shows the mixture proportions of these trial mixtures. The mixtures can be divided into five basic groups.:

Group 1: mixtures A, B, C, and D. This group includes a combination of crushed lime stone, silica sand and silica flour. Mixtures B, C, and D have high cement contents with respect to mixture A, while, mixture D is the only one of the group incorporating carbon fibres.

Group 2: mixtures E, F and G. This group includes a combination of only silica sand and silica flour. The rationale behind this group was to investigate the effect of eliminating the coarse aggregate and developing mixtures with nominal maximum size of 160 μm. Mixture G is the only mixture of this group to incorporate carbon fibres.

Group 3: mixtures H, I and J. This group uses high volumes of silica flour as the only aggregate. The rationale behind this group was to investigate the pozzolanic and filler effect of silica flour and making use of its small nominal maximum size. Mixture J is the only mixture of this group to incorporate carbon fibres.

Group 4: mixtures K and L. This group utilizes well graded calcined bauxite aggregate without any combinations of any types of sand. The nominal maximum size of this aggregate was 4.0 mm. Mixture L is the only mixture of this group to incorporate carbon fibres.

Group 5: mixtures M, N, O and P. This group includes a well graded combination of calcined bauxite aggregate, silica sand and silica flour. The rationale behind this group was based on the testing results of the previous mixture groups which proved the superior performance of calcined bauxite, and silica flour. The mixtures have normal cement content (35% cement paste by volume). Mixtures O and P were further trials to reduce the cement content so that no shrinkage cracks develop and to examine the effect of using Type 50 Portland cement. Mixtures N and P incorporate carbon fibres.

3.3.3. Production of UHPC

From the sixteen trial mixtures, twenty seven concrete groups were developed. The large number of groups examined is related to the different production parameters (pressure on fresh concrete and curing regimes) utilized. The following describes the techniques used in developing these groups.

3.3.3.1. Mixing and pressuring of fresh concrete

A conventional 3 speed mortar mixer was used to blend these mixtures. A special mixing technique was required due to the limited superplasticizer content (so that no retardation took place), the very low water content and the high specific surface area of carbon fibres. Mixing parameters including mixer speed, mixing time, and time of adding the ingredients especially the water and superplasticizers, were taken into consideration.

The best workability was achieved when the aggregate was mixed for 2 minutes in the dry state, the cement, the silica fume and the fibres were then added and mixed for another 2 minutes, half of the water was added to the dry mixture and mixed at high speed for 2 minutes and finally the superplasticizer was added to the rest of mixing water and then the fresh concrete was mixed for 3 minutes. Similar results have been reported by Gjφrv [1996].

The concrete was cast in special moulds designed to resist high pressure. The moulds included little grooves parallel to the base of the mould at the mould component interfaces to allow excess fluid to egress. Each mould included three 5 cm cubes. Specimens were then well compacted during casting and vibrated for 15 minutes. Pressure was applied using head plates designed to fit on the top of the fresh concrete within these moulds. The load was applied downward to create a stress in the range of 10 - 80 MPa using Material Testing System (MTS) machine with a load capacity of 1000 kN. The pressure was and increased gradually to its maximum value (in 5 minutes) at a slow rate of loading (2 kN/s) and kept constant for 4 hours. The maximum value of applied pressure to fresh concrete was governed by the compaction attained and varied with the workability of the concrete. Specimens were demoulded after 24 hours and one of three curing regimes was used for each group.

Table [3.4]: Mixture proportions of UHPC trial mixtures

Mixture No.	A	B	C	D	E	F	G	H
Cement (kg/m³)	600	850	1040	1040	850	1000	1000	1000
Silica fume (kg/m³)	70	150	310	310	150	200	200	300
Lime stone (kg/m³)	1200	900	600	600	—	—	—	—
Calcined Bauxite (kg/m³)	—	—	—	—	—	—	—	—
Ottawa sand (kg/m³)	300	200	100	100	950	500	500	—
Silica flour (kg/m³)	200	100	100	100	350	200	200	800
Fibres (Vol. %)	—	—	—	2	—	—	2	—
Superplasticizer/Cement %	2	2	2	2	2	2	2	2
Water (kg/m³)	135	210	240	240	230	330	330	230
Cement Type	10	10	10	10	10	10	10	10
Nominal maximum size (mm)	10	10	4	4	0.16	0.16	0.16	0.16
Water/binder ratio	0.20	0.18	0.18	0.18	0.23	0.28	0.28	0.18
Mixture No.	**I**	**J**	**K**	**L**	**M**	**N**	**O**	**P**
Cement (kg/m³)	1000	1000	1040	1040	510	510	450	450
Silica fume (kg/m³)	150	150	310	310	65	65	50	50
Lime stone (kg/m³)	—	—	—	—	—	—	—	—
Calcined Bauxite (kg/m³)	—	—	800	800	1140	1140	1000	1000
Ottawa sand (kg/m³)	—	—	—	—	280	280	360	360
Silica flour (kg/m³)	1000	1000	—	—	280	280	360	360
Fibres (Vol. %)	—	0.8	—	2	—	0.5	—	0.5
Superplasticizer/Cement %	2	2	2	2	2	2	2	2
Water (kg/m³)	250	250	240	240	140	140	180	140
Cement Type	10	10	10	10	10	10	50	50
Nominal maximum size (mm)	0.16	0.16	4	4	4	4	4	4
Water/binder ratio	0.22	0.22	0.18	0.18	0.24	0.24	0.28	0.28

Table [3.5]: Production parameters of the UHPC groups.

Group No.	1	2	3	4	5	6	7	8	9
Mixture No.	A	B	C	C	D	D	D	D	D
Pressure on fresh concrete (MPa)	0	0	0	40	0	0	0	40	40
Curing regime	SC	SC	HW	OV	HW	SC	OV	HW	SC
Group No.	**10**	**11**	**12**	**13**	**14**	**15**	**16**	**17**	**18**
Mixture No.	D	E	F	G	H	I	J	K	L
Pressure on fresh concrete (MPa)	40	10	20	20	20	20	20	0	0
Curing regime	OV	SC	HW	SC	HW	HW	OV	HW	HW
Group No.	**19**	**20**	**21**	**22**	**23**	**24**	**25**	**26**	**27**
Mixture No.	L	L	M	N	N	N	O	P	P
Pressure on fresh concrete (MPa)	0	0	80	0	80	80	0	0	12
Curing regime	SC	OV	HW	OV	HW	OV	HW	OV	OV

3.3.3.2. Curing of hardened concrete

Specimens immersed until testing in the hot water bath at 50 °C, to minimize the shrinkage and thermal cracking expected from the hydration of these high cement-content mixtures, were denoted hot water cured (HW). Specimens cured in the hot water bath at 50 °C until 2 days prior to testing when they were steam cured at 95 °C, were denoted as having been steam cured (SC). Finally, specimens cured in the hot water bath at 50 °C until 2 days prior to testing when they were oven dried at 200 °C, were denoted as having been oven cured (OV). Table [3.5] shows the different production parameters of the prepared UHPC groups including the mixture number, the pressure applied to fresh concrete and the curing regime used.

3.4. Testing of UHPC

3.4.1. Compressive strength test

Compressive strengths were determined at ages of 7 and 28 days on 5 cm cubes tested in triplicate: average results and standard deviations are shown in Tables [3.6] and [3.7]

respectively. Detailed results for both 7 and 28 days are provided in appendix [A.1].

Table [3.6]: 7 and 28 days compressive strength of UHPC mixtures

Group No.	1	2	3	4	5	6	7	8	9
7 days Compressive strength (MPa)	120	130	120	160	130	140	190	180	190
28 days Compressive strength (MPa)	132	143	140	165	140	142	195	193	195
Group No.	**10**	**11**	**12**	**13**	**14**	**15**	**16**	**17**	**18**
7 days Compressive strength (MPa)	220	130	138	170	182	164	210	130	150
28 days Compressive strength (MPa)	230	143	163	175	191	185	217	140	182
Group No.	**19**	**20**	**21**	**22**	**23**	**24**	**25**	**26**	**27**
7 days Compressive strength (MPa)	160	200	160	190	180	240	117	130	170
28 days Compressive strength (MPa)	170	210	175	195	198	240	143	145	175

Table [3.7]: Standard deviation (MPa) of 7 and 28 days compressive strength of UHPC mixtures

Group No.	1	2	3	4	5	6	7	8	9
7 days standard deviation (MPa)	1.6	1.6	1.6	2.9	0.8	3.3	1.7	2.6	4.1
28 days standard deviation (MPa)	1.2	1.9	1.6	1.9	0.5	5.1	2.4	5.4	5.7
Group No.	**10**	**11**	**12**	**13**	**14**	**15**	**16**	**17**	**18**
7 days standard deviation (MPa)	4.5	0.5	0.5	2.6	0.5	4.5	0.5	2.6	1.3
28 days standard deviation (MPa)	2.6	0.9	0.9	2.4	0.9	3.3	0.9	1.6	1.9
Group No.	**19**	**20**	**21**	**22**	**23**	**24**	**25**	**26**	**27**
7 days standard deviation (MPa)	2.2	5.0	3.4	3.6	5.2	4..9	2.2	6.5	1.3
28 days standard deviation (MPa)	1.7	4.2	4.1	2.9	3.4	4.8	1.9	4.1	1.4

3.4.2.Discussion of test results

From the twenty seven examined concrete groups, four UHPC groups (10, 20, 22, and 24) were developed with 7 and 28 day compressive strengths over 200 MPa and up to 240 MPa. All these groups incorporated carbon fibres. Various well-graded aggregates were involved, and three of the four mixtures were pressurized after casting (groups 10, 22 and 24).

The pressure squeezes water out, dropping the water/cement ratio and increasing the packing density of the cement matrix. Therefore, the improvement achieved appears to be mainly a result of the reduced porosity of concrete.

The superior performance of the UHPC trial mixtures containing crushed limestone, calcined bauxite and/or silica sand may be due in part to the epitactic growth of cement hydration products on these aggregates [Gutierrez and Canovas 1996 and Aitcin and Mehta 1990]. Establishment of this hypothesis was beyond the scope of this work and was difficult to prove due to the involvement of many variables in this investigation. Further work should be able to shed light on the influence of epitaxy on bond strength. The high compressive strength of the mixed limestone/silica sand mixtures (A, B, C and D) is consistent with HPC results reported by Luciano et al. [1991] explained by a balance between water demand and bond strength when a combination of these types of aggregate is used. In this work, strengths up to 200 MPa were achieved in a mixture containing only about 35% cement paste by volume (group 24). This is thought to be due to the combined effect of the bauxite aggregate at elevated temperatures (see below) and the application of pressure during fabrication. On the other hand, concrete made with limestone aggregate (group 8 and 10) required 60-70 % cement paste by volume to attain the same strength level.

Due to the mineralogical nature of the calcined bauxite aggregate [Mehta and Aitcin 1990] a reaction between the aggregate surface and the cement paste may be expected to occur when elevated temperatures are applied. In comparison to group (3) (limestone aggregate) group (17) (bauxite aggregate) (hot water curing) shows a slight increase in compressive strength at 7 days but no effect at 28. When elevated temperature curing is applied, compressive strengths in excess of 200 MPa were attained when the fresh limestone concrete (group 10) was also pressurized up to 40 MPa. The same level of strength was obtained under the same curing conditions but with no pressure applied to the fresh concrete, by group (20) incorporating bauxite aggregate. Improved bonding of the cement paste to the aggregate, at elevated temperatures, may well be partly responsible for these high compressive strengths.

3.5. Microstructural investigation of UHPC

Two main techniques were used to examine the microstructure of the mixes. The first was direct observation with Scanning Electron Microscope (SEM) and the second was qualitative mineralogical analysis by X-ray Diffraction (XRD). Combined use of the two techniques facilitates an understanding of the link between engineering behaviour and composition and microstructure.

3.5.1. Scanning Electron Microscope (SEM)

Specimens of eight groups (8,10,18,20, 22,24,26 and 27), that had been tested for strength at 7 days, were subsequently examined on the SEM at an age of 14 days. SEM specimens were taken from the inner part of the strength test specimens to avoid possible artifacts caused by thermal effects at the surface. Specimens were fractured and coated with gold prior to examination.

3.5.2. X-Ray Diffraction (XRD)

Similar samples as above (section 3.5.1) were examined by XRD. X- ray diffractograms were recorded from samples of powdered concrete compacted in Al holders, over a 2θ angular range from 2° to 140°, using Fe filtered Co Kα radiation. Phases were identified by the use of the Joint Committee on Powder Diffraction Standards (JCPDS) powder data file.

3.5.3. SEM micrograph interpretations

3.5.3.1. Dense and homogeneous microstructure

All the UHPC mixtures examined showed a very dense microstructure compared to the known microstructure of conventional concrete and even High Performance Concrete (HPC). The calcined bauxite groups (20,22,24,26 and 27) showed a more homogeneous and dense microstructure than the limestone ones (groups 8 and 10).

The dense microstructure of the cement phase in these groups extended to the aggregate boundary and as a result, the well-known microstructural gradient of the cement paste towards the transition zone was absent. This was observed even when no pressure was applied to fresh concrete of such mixtures (group 18 and 20). It is worth mentioning that mixtures containing

both silica fume and silica flour generally showed a very dense and homogeneous microstructure. The carbon fibres are randomly distributed within the hydration products. Figure [3.2] shows the distribution of some carbon fibres within the homogeneous microstructure of the UHPC mixtures.

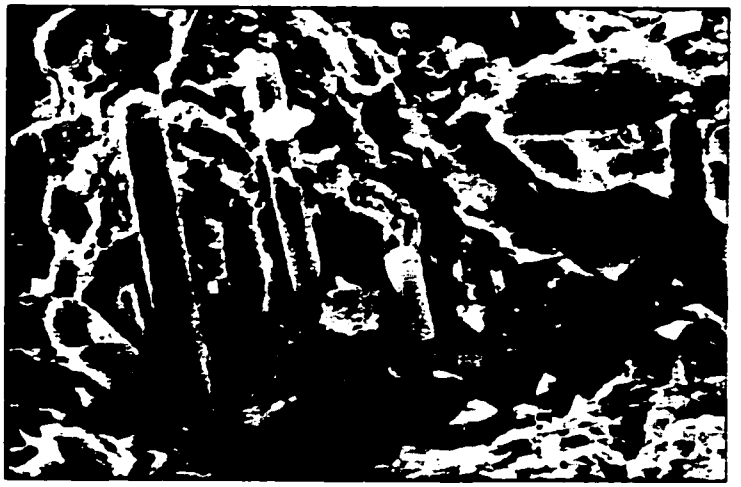

Figure [3.2] : SEM micrograph showing the carbon fibres distributed within the microstructure (group 10 - X 616 - Reda et al. 1999)

3.5.3.2. Absence of CH crystals

The UHPC mixtures differed from conventional concrete in that large crystals of CH were generally absent. However, CH crystals were only found in mixtures made with limestone aggregate and cured in the hot water bath, Figure [3.3], and in the calcined bauxite mixture made with a relatively high water/binder ratio (group 26). It is believed that the very low water/binder ratio and the pressure applied to the fresh concrete results in a very low porosity, which restricts the space available for the growth of CH crystals. The relatively high content of silica fume, especially in groups 3 to 20, together with the inclusion of silica flour and the elevated temperature curing regime, created an effective pozzolanic environment which consumed most of the weak CH crystals produced during hydration. These crystals were converted to strong C-S-H. The combined effect provided excellent mechanical properties.

However, the effect of dry curing seems very pronounced especially at 28 days age.

Comparing groups (8, 18 and 22) where hot water curing is used to groups (10,20, and 24) where oven curing is used, a significant enhancement in strength can be observed for the oven cured groups. The effect of oven curing was confirmed when CH crystals were observed in group (8) where only the hot water curing regime was applied.

Figure [3.3]: SEM micrograph showing dense packed CH crystals in the limestone mixtures (group 8 - X 2480 - Reda et al. 1999)

3.5.3.3. Characteristics of UHPC transition zone

The transition zone observed in the UHPC mixtures examined was of very small thickness with respect to that of HPC and conventional concrete. Microcracks in the vicinity of the aggregate particles were very small and no CH crystals were deposited in this vicinity. These fracture cracks are well known in SEM specimens and have been attributed to the preparation process. The reduction in the width of the transition zone may indicate a well-developed bond between the cement paste and the aggregate surface. Figure [3.4] shows the vicinity of an aggregate particle with a very small microcrack in a UHPC mixture.

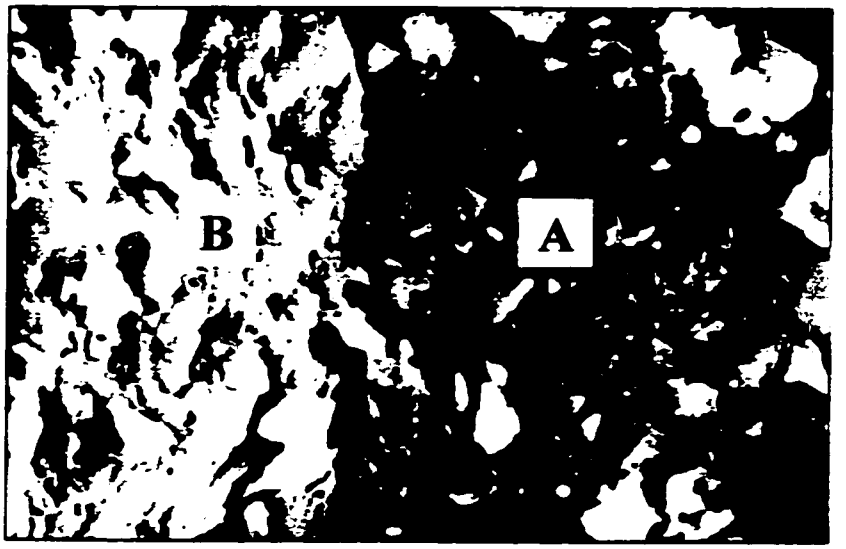

Figure [3.4]: SEM micrograph showing the transition zone characteristics in UHPC mixture (group 20 - A aggregate , B cement paste - X 1210 - Reda et al. 1999)

3.5.3.4. Unidentified microstructure region

An unidentified microstructure region of fibre/cement paste was found (groups 8,10,18 and 20). The materials in these regions were gel-like and of amorphous appearance. Figure [3.5] shows a typical unidentified region. It was initially suspected that an epoxy coating material on the fibres may have had a secondary material attached which melted at the high curing temperature, but similar features were found in specimens cured in hot water at only 50 °C. Additionally, when the carbon fibres were examined separately before and after exposure to 200 °C for 2 days, no significant difference was noticed on the surface of the fibres indicating that the unidentified material was not caused by the mechanism suspected.

The gel-like amorphous nature of this unidentified material suggests that it may result from a reaction between silica fume and sodium hydroxide (NaOH) released early during the hydration process. This probability is supported by the very high silica fume content of groups 8,10,18 and 20 and the absence of this unidentified material in the other groups which had a relatively small silica fume content. The unidentified region is not expected to involve any kind of alkali-aggregate reaction due to the large amount of silica provided to the mixture by silica fume and silica flour and the pozzolanic effect of both. High availability of silica will inhibit any

possible potential for alkali-aggregate reaction [Neville 1996]. The potential implications of the new material on the engineering behaviour of UHPC are unknown. but will depend on its composition, the amount present, and the long-term stability. Further work is clearly needed to identify this material.

Figure [3.5]: SEM micrograph showing the interactive fibre/cement paste unidentified region (group 10 - X 329 - Reda et al. 1999)

3.5.3.5 The role of carbon fibres in UHPC

The enhancement of the mechanical properties of UHPC mixtures can be attributed to the role of carbon fibres in addition to the microstructural improvements of the concrete matrix. This can be verified from Table [3.6] by comparing the compressive strengths of UHPC groups including carbon fibres (groups 8,10,18,20,20,24,26 and 27) with those which do not include carbon fibres (groups 1,2, 3,4,17, and 21). A statistical analysis using the student t-distribution has been performed on these experimental data to examine the significance of micro carbon fibre incorporation on the compressive strength of UHPC groups [Appendix A-2]. The numerical increase in compressive strength due to incorporation of carbon fibres is not as large as that associated with oven curing, but is nevertheless statistically significant.

In contrast with the known microstructure of conventional fibre-reinforced concrete

[Sarkar 1994] no additional transition zones were found in the region of the reinforcing fibres, no special air entrapment was observed in the fibre vicinity, nor was inefficient packing of particles. Figure [3.6] shows a schematic diagram of the fibre transition zone model developed by Bentur and Mindess [1990]. The existence of such transition zones should result in a weak matrix/fibre link [Wei et al. 1996].

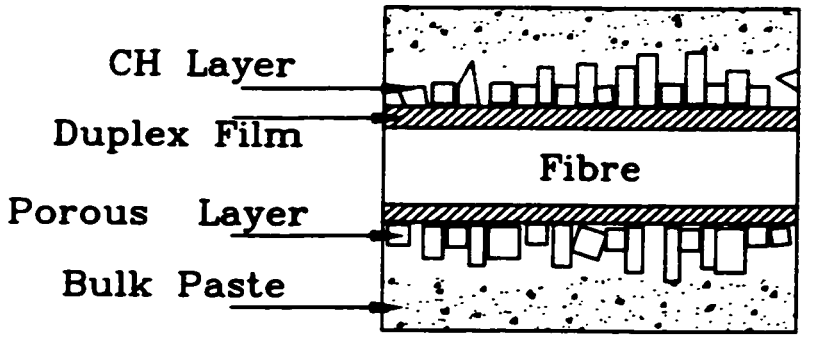

Figure [3.6]: Schematic representation of the fibre transition zone in conventional fibre reinforced concrete [Bentur and Mindess 1990].

Figure [3.7]: SEM micrograph showing a ruptured carbon fibre bridging a micro crack (Group 9 - X 138 - Reda et al. 1999).

SEM micrographs have shown both fibre pull-out and fibre rupture. Banthia [1994] also observed both fracture mechanisms as did Beaudoin [1990]. He performed experiments on

autoclaved wood-fibre-reinforced cement mortars and attributed both fibre pull-out and fracture to the very strong bond strength between the fibres and the cement matrix. Figure [3.7] shows a ruptured carbon fibre bridging a micro crack in one of the UHPC mixes.

3.5.4. XRD analysis

The main observation from the XRD analysis was that the strongest Portlandite (CH) peaks at 2.6° A and 4.9° A were absent on diffractograms of the UHPC mixture examined with the exception of groups 3 and 7. This confirms the conclusion from the SEM micrographs that CH was largely consumed by the pozzolanic reaction and converted to strong C-S-H gel. The principal calcium silicate hydrate identified was Xonotlite (C_6S_6H) with smaller amounts of Tobermorite ($C_5S_6H_5$) and Scawtite ($C_7S_6CH_2$). Xonotlite has been associated with strong and moderately permeable cement.

Ettringite peaks were not identified on diffractograms of any samples, confirming the SEM observation that ettringite needles were absent. The absence of ettringite may simply reflect the stage of maturity of the samples studied in these mixtures and under the curing conditions used. Under some conditions accelerated curing at elevated temperatures appears to favour ettringite formation at later ages, which is known as delayed ettringite formation (DEF). However, very recent studies on DEF [Collepardi 1999] proposed that micro cracking rather than the elevated temperature curing is a basic requirement for DEF. The UHPC mixes studied in this work may be susceptible to DEF at later ages. However the limitation of microcracking from the inclusion of fibres should reduce this possibility. The absence of a simple and reliable short term DEF test did not allow investigation of this possibility. Long term durability of UHPC is beyond the scope of this work.

3.6. Closure

Through the previous experimental investigation four UHPC groups with 7 day compressive strengths in excess of 200 MPa have been developed and investigated. These groups are group 10,16, 20 and 24. Group 24 was chosen to be used to produce both the

barrel and the wedges of the new non-metallic anchorage system, because of its relatively low cementing material content (Portland cement + silica fume) compared to the other three UHPC groups. The low content of cementing materials should reduce shrinkage and creep strains of UHPC compared to the mixes with higher cementing material contents. Shrinkage and creep could be a major source of prestress loss for the non-metallic anchorage system. Further investigation of the fracture toughness of this UHPC mixture is needed to optimize that property before the UHPC is used to make the anchorage.

CHAPTER 4

FRACTURE OF ULTRA HIGH PERFORMANCE CONCRETE; CONCEPTS, ANALYSIS AND RESULTS

4.1. Introduction

The preliminary investigation of the non-metallic anchorage system established the need for ultra high performance concrete (UHPC) to serve as both the outer barrel and inner wedges. The wedges need high fracture toughness to hold the tendon without being crushed. It was thought that cracking of these wedges would relieve the pressure exerted on the tendon resulting in tendon slip. The fracture toughness of the UHPC mixtures was therefore examined, with a view to maximizing this property.

Simple stress based models, to large extent, oversimplify the problem of fracture of fibre reinforced concrete (FRC). Factors which affect the fracture mechanism of FRC include fibre geometry (length and diameter), fibre-concrete matrix bond, and concrete matrix properties. In the following, the mechanism by which fibres increase the toughness of concrete will be discussed, then the fracture mechanics of FRC will be reviewed. An analysis of how to enhance the fracture toughness of UHPC as a fibre reinforced concrete was developed and assessed experimentally.

4.2. Mechanics of fibres in concrete

4.2.1. Stress transfer mechanism

The presence of fibres in concrete results in a minimal increase of stiffness prior to cracking and holds the matrix together after cracking. During the early stages of loading, the interaction between the fibre and the concrete matrix is elastic, with stress transfer occurring through shear at the fibre-concrete interface [Cox 1952]. As load increases, the matrix can fracture due to shear or the fibres debond. Fibre debonding activates a combination of elastic

and frictional stress transfer mechanisms [Bentur and Mindess 1990].

The first analytical model of stress transfer to and from fibres embedded in an elastic matrix was developed by Cox [1952]. The analysis assumes that the matrix and the fibres were linear elastic materials perfectly bonded together. The fibres are assumed to be arranged in a regular, repeated array with no stresses transmitted through their ends. The requirement of compatibility results in a tensile strain in the matrix at distance R (matrix radius) from the fibre equal to the tensile strain of the composite. Equations [4.1] and [4.2] evaluate the fibre tensile stress $\sigma(x)$ and the interface shear stress $\tau(x)$ respectively at distance x from the fibre end. Figure [4.1] shows both shear and tensile stress distributions based on Cox' [1952] analysis. Experimental values indicate higher shear stresses at the end of the fibres than those predicted by this model [Piggot 1970].

$$\sigma(x) = E_f \varepsilon_m \left[1 - \frac{\cosh \beta_1 (\frac{l}{2} - x)}{\cosh \frac{\beta_1 l}{2}} \right] \qquad [4.1]$$

$$\tau(x) = \frac{l}{2} E_f \varepsilon_m \beta_1 \cdot \left[\frac{\sinh \beta_1 (\frac{l}{2} - x)}{\cosh \frac{\beta_1 l}{2}} \right] \qquad [4.2]$$

where ε_m is the matrix strain, R is the radius of the matrix around the fibre, r is the fibre radius, l is the fibre length, E_f is the fibre modulus of elasticity, G_m is the matrix shear modulus, and β_1 is a mathematical parameter defined by equation [4.3];

$$\beta_1 = \sqrt{\frac{2G_m}{E_f r^2 \ln(R/r)}} \qquad [4.3]$$

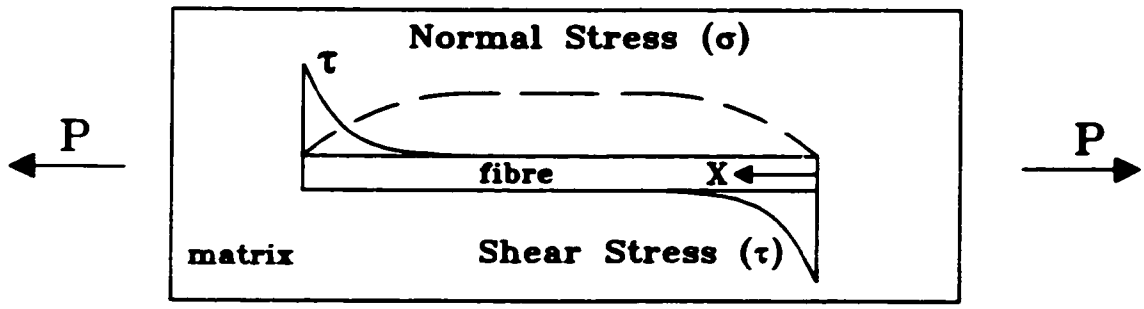

Figure [4.1]: Shear and tensile stress distribution along fibre length [Cox 1952].

Stress transfer in FRC taken as a quasi-brittle material with considerable non-linear deformation is different to that shown in Figure [4.1]. In the initial (elastic) period of loading, there will be no difference compared to the Cox [1952] model: the maximum interfacial shear stress will occur at the fibre end. In cracked concrete however, the maximum shear will occur at the point at which full bond between the fibre and the matrix still exists. Figure [4.2] shows two possibilities of stress transfer in a cracked matrix.

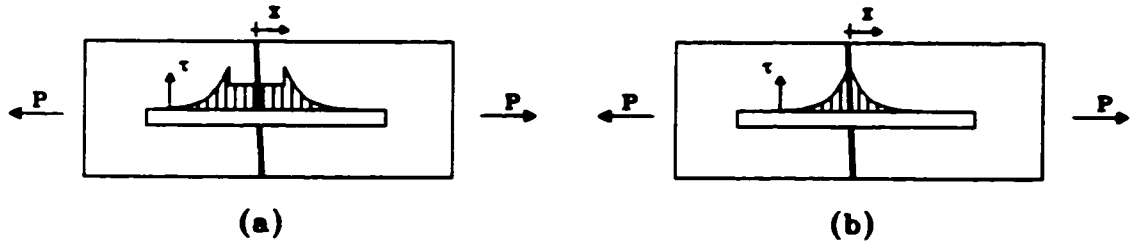

Figure [4.2]: Interfacial shear stress along a fibre crossing a crack just after cracking [a] debonding prior to cracking [b] no debonding prior to cracking [Bentur and Mindess 1990].

First, in figure [4.2-a] when debonding takes place at the cracked zone, the shear stress will be of a combined mode, with frictional shear adjacent to the crack and decreasing elastic shear stresses away from it. On the other hand, in Figure [4.2-b] where no debonding occurs prior to cracking, the shear stress distribution at the fibre-crack intersection will initially be elastic following Cox' model. Bartos [1980]examined the effect of fibre length on the fracture mode of FRC. Three different cases of stress transfer were considered: elastic shear stress transfer where no debonding can occur, frictional stress transfer without any elastic stress transfer and combined elastic and frictional stress transfer. Shear force per unit length of the fibre (shear flow) was used in the analysis instead of the average shear stress. The analysis defined three basic fibre lengths, l_c the critical fibre length beyond which fibres will be ruptured rather than being pulled-out, l_p the minimum bond length needed to prevent catastrophic bond failure, and l_f the fibre rupture length at which the fibre will be ruptured without any debonding occuring. Table [4.1] represents the fracture possibilities based on these fibre lengths. Assuming stress equilibrium of a single brittle fibre in an infinite matrix, the critical fibre length can be determined as shown in equation [4.4] where σ_{fu} is the ultimate tensile strength of the fibre, τ_{av} is the average interface shear strength of the matrix and d is the fibre diameter.

$$l_c = \frac{\sigma_{fu} d}{2\tau_{av}} \qquad [4.4]$$

Table [4.1]: Effect of fibre length on the fracture mode and fibre tensile stress.

Length condition	Fracture mode	Fibre tensile stress
$l < l_p$	Fibre pull-out followed by sudden debonding	$\sigma<\sigma_{fu}$
$l_p < l < l_c$	Fibre pull-out followed by gradual debonding.	$\sigma< \sigma_{fu}$
$l_c < l < l_f$	Fibre rupture with possible gradual debonding	$\sigma> \sigma_{fu}$
$l_f < l$	Fibre rupture without any debonding	$\sigma > \sigma_{fu}$

4.2.2. Fibre-matrix bond

Experimental investigations using fibre pull-out tests revealed a linear load-slip relation of FRC up to a peak value, followed by a non-linear descending part. This was reported for both steel fibres [Naaman and Shah 1976] and polyethylene and carbon fibres [Katz and Li 1995]. These experiments showed the governing factors for pull-out strength to be the interface shear strength and fibre dowel action. However, dowel action seems to damage the matrix at the crack surface making multiple fibres less effective [Balguru and Shah 1992]. Many micro-mechanical models were developed which successfully predicted the pull-out strength of fibres in cement matrix [eg: Laws 1982 and Lawrence 1972]. Gray [1984[a] and 1984[b]] verified a number of these models with different pull-out test results and concluded that the major difference between all these models is their definition of the elastic shear stress transfer parameters.

4.2.3. Fibre work of fracture

Fibres are used in concrete to provide high fracture toughness by providing further toughening mechanisms in the fracture process zone (FPZ) of concrete. The role of toughening mechanisms is to consume energy increasing the total energy required for fracture. Fibre pull-out and fibre debonding are two possible toughening mechanisms provided by fibres in concrete. Pull-out work is defined as the work done against sliding friction extracting fibres from a broken matrix, while fibre debonding is defined as the work done in destroying the bond strength between the fibre and matrix [Bentur and Mindess 1990]. Fibre pull-out is preferred to fibre debonding as the former consumes much more energy and does not result in a catastrophic failure. Beaumont [1974] showed how both fibre pull-out and fibre debonding can contribute to final fracture in the process zone [Figure 4.3]. Mindess [1983[a]] reported that fibre pull-out and/or debonding energy could consume more than 95% of the fracture energy. Li et al. [1995] suggested that fibres suppress crack growth through fibre bridging, interfacial debonding and frictional sliding. The last two mechanisms absorb a considerable amount of fracture energy.

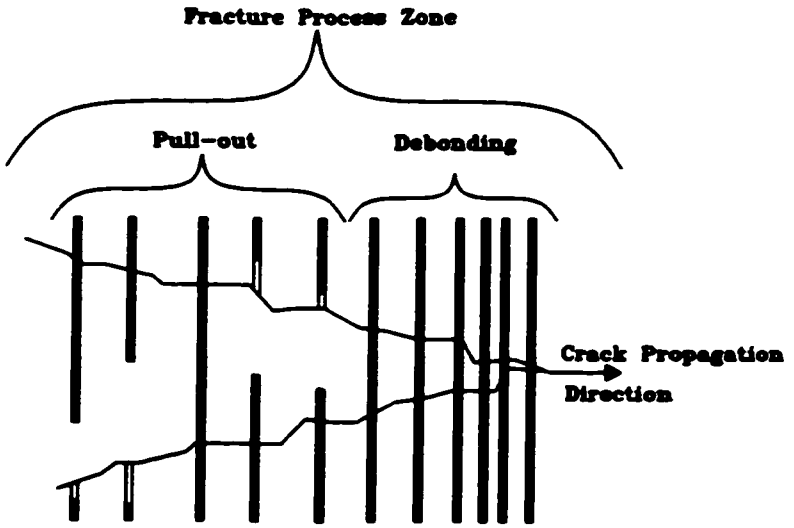

Figure [4.3]: Contribution of fibre pull-out/debonding in the FPZ [Beaumont 1974].

Piggott [1970] proposed a method for estimating the fracture surface energy of fibre-reinforced material. The surface energy increases with increasing fibre content, strength and diameter, and decreases with increasing fibre modulus and matrix shear strength. Mathematical expressions of the work done to allow fibre pull-out can be easily derived by assuming an infinitesimal fibre displacement and by integrating with pre-defined boundary conditions related to the fibre length [Appendix B.1]. Equations [4.5] and [4.6] represent these mathematical expressions.

$$W_p = \frac{l}{24}\pi d \tau_{av} l^2 \qquad \text{for } l < l_c \qquad [4.5]$$

$$W_p = \frac{l}{24}\left(\frac{l_c}{l}\right)\pi d \tau_{av} l_c^2 \qquad \text{for } l > l_c \qquad [4.6]$$

Where W_p is the pull-out work of fracture, l_c is the critical length of the fibre given by equation [4.4]. Kelly [1973] proved that the maximum work of fracture is achieved when the fibre length is equal to the critical length (l_c). Similarly, Bartos [1980] proved that the maximum

energy demand for fracture can be achieved by limiting the fibre length to a maximum value of (l_c) to allow fibre pull-out rather than fibre rupture.

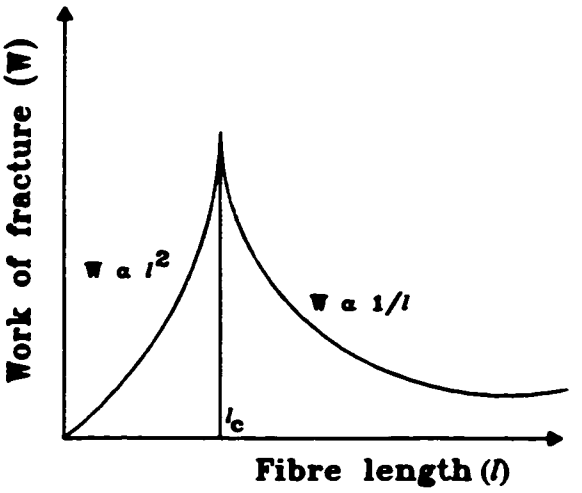

Figure [4.4] Variation of work of fracture with changing fibre length [Kelly 1973].

Figure [4.4] shows the variation of the work of fracture per fibre when fibre length is changed for discontinuous fibres. However, this was proved for polymer matrices and different types of ductile fibres. No reports were found in the literature for applying this concept to FRC with brittle fibres.

4.3. Fracture mechanics of FRC

4.3.1. Fracture mechanics of concrete

It is well established that two basic criteria govern fracture of materials in either tension or compression [Wang and Shrive 1995, Shrive 1983, Broek 1982, Cotterell 1972 and Griffith 1924]. These are the stress and the energy criteria. The stress criterion is based on the fact that the local tensile stress developed around a flaw must be large enough to overcome the cohesive strength of the material. The energy criterion is that extension of a crack requires a certain amount of energy. Although these two conditions can explain the fracture behaviour of any

material, the complexity is how to determine accurately the amount of energy consumed in the fracture process under specific boundary conditions.

Three different types of structural material can be identified. Brittle elastic materials (e.g. glass and FRP materials), quasi-brittle materials (e.g. concrete) and ductile elastic-plastic materials (e.g. steel). The difference between these materials is the shape and dimension of the fracture process zone (FPZ) which is formed ahead of the crack tip prior to fracture. In brittle materials, elastic energies are consumed in the form of surface energy with no FPZ [Griffith 1921]. In ductile materials the FPZ is known as the plastic zone which can consume a considerable amount of energy, much more than the surface energy [Barenblatt 1962 and Dugdale 1960]. For quasi-brittle materials, a large FPZ is usually formed which consumes large amounts of energy prior to failure. This provides concrete with its non-linear (softening) response. The FPZ is also the source of size effect phenomena observed in concrete testing [Bazant and Kazemi 1990]. Figure [4.5] shows a schematic representation of the FPZ in concrete.

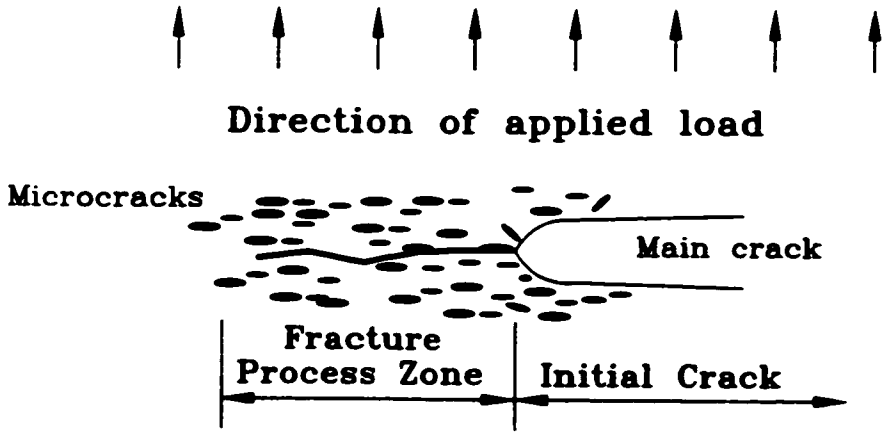

Figure [4.5]: Fracture process zone (FPZ) in concrete [Shah et al. 1995].

Studies of concrete crack growth have proved the existence of FPZ [Shah et al. 1995]. The reason for the difficulties encountered in the application of fracture mechanics to concrete comes from the different toughening mechanisms taking place in the FPZ of concrete compared

to the plastic zone of ductile materials. These toughening mechanisms are shown in Figure [4.6] and include microcracking, crack branching, crack deflection [Shah et al. 1995], crack bridging [Cox and Marshall 1994], crack-face friction, and crack tip blunting [Mindess and Diamond 1982].

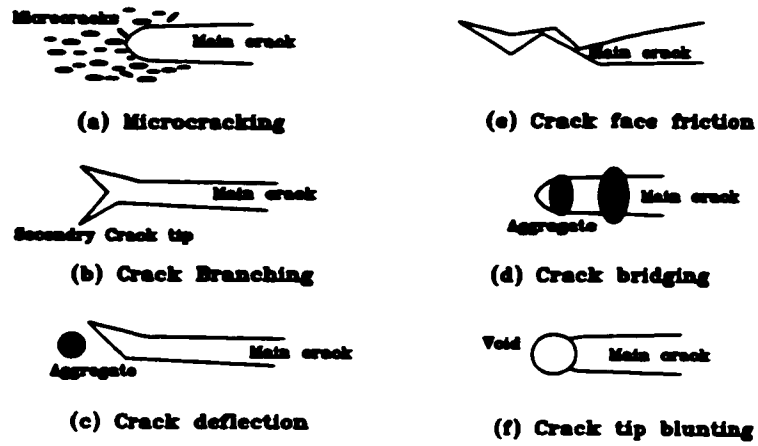

Figure [4.6]: Toughening mechanisms of FPZ in concrete [Shah et al. 1995].

Developing other energy consuming (i.e. toughening) mechanisms in concrete will increase its fracture toughness further. This is because fibres can consume a large amount of energy through fibre crack bridging, fibre pull-out and/or fibre debonding. Other toughening mechanisms of fibres have been reported by Beaudoin [1990] including fibre bending and the internal work of fibre fracture.

4.3.2. Models of fracture mechanics applied to FRC

4.3.2.1. Linear elastic fracture mechanics (LEFM)

Linear elastic fracture mechanics (LEFM) models were the first to be applied to both concrete [Kaplan 1961] and fibre concrete [Romoualdi and Batson 1963]. A summary of the main different LEFM models applied to FRC follows:

4.3.2.1.1. Crack suspension models

Romoualdi and Batson [1963] developed a LEFM model including the effect of the

fibres on crack growth as "pinching forces". These forces suspend crack growth and further energy has to be supplied to the system to overcome these forces. A spacing factor was introduced as a parameter representing the fibre efficiency in the cement matrix. Romoualdi and Mandel [1964] modified the crack suspension model by showing the ability of the fibres to reduce the stress intensity factor K_I at the crack tip so that the composite can continue to carry loads. The crack suspension model has shown little agreement with experimental results.

4.3.2.1.2. The compliance approach

Stang and Shah [1986] applied the compliance approach to FRC to calculate the fibre pull-out force. The approach relates the displacement to the load through a linear relation using the cracked body stiffness or "compliance" as shown in equation [4.7].

$$P = C\,\Delta \qquad [4.7]$$

Where Δ is the displacement P is the applied load and C is the compliance which is a function of many parameters including crack depth. The strain energy release rate G_I has been derived as a function of the compliance. The approach has shown good agreement with experimental data and was successfully used to predict the tensile strength of FRC [Balaguru and Shah 1992].

4.3.2.1.3. Energy models

Aveston, Cooper and Kelly [1971] developed the ACK model in which the energy absorbed during fracture of FRC includes the work done by the applied stress (ΔW), the work required to debond the fibres from the matrix (U_{db}), the work of friction during fibre pull-out (U_s), an increase in the elastic strain energy of the fibres after matrix cracking (ΔU_f), a reduction of the elastic strain energy in the matrix due to cracking (ΔU_m), and the work of matrix fracture ($2\gamma_m V_m$)based on Griffith [1921] assumptions. Equations [4.8] and [4.9] represent this energy condition for cracking and the matrix cracking strain respectively as proposed by the ACK model.

$$\Delta W + \Delta U_m \geq 2\gamma_m V_m + U_{db} + U_s + \Delta U_f \qquad [4.8]$$

$$\varepsilon_m = \left[\frac{12\tau\gamma_m E_f V_f}{E_c E_m^2 r V_m} \right]^{1/3} \qquad [4.9]$$

The model was able to predict the matrix cracking strain (ε_m) accurately. This strain depends on the bond strength between the fibre and the matrix. The ACK model was also able to predict the total work of fracture (U_t) of FRC by mathematically estimating the area under the stress-strain curve [Equation 4.10].

$$U_t = \frac{E_c \varepsilon_{mu}^2}{8} + \frac{E_f \varepsilon_{fu}^2 V_f}{2} \qquad [4.10]$$

Hannant et al. [1983] proposed the strain relief model known as the Nottingham model using similar assumptions. The model predicted the total fracture energy of FRC through an iterative approach determining the final shape and dimensions of the crack. The total reduction in the strain energy is then obtained by numerical integration. Beaudoin [1990] has shown the Nottingham model to be more realistic in predicting the matrix strain than the ACK model. Weiss [1973] showed how fibre reinforcement increases the energy demand for crack growth highly. Kasperkiewiecz [1983] proposed a surface energy model for FRC including material in- homogeneity. The model was able to model strain softening of FRC. Korczynskyj et al. [1981] proposed the fibres to provide a jump in the energy demand similar to that provided by the aggregate in plain concrete as suggested by Glucklich [1963]. The model predicted the fibre volume limits required to suppress crack growth.

4.3.2.2. Elasto-Plastic fracture mechanics (EPFM)

Moavenzadeh and Kuguel [1969] applied Griffith theory to concrete and reported a large difference between theoretical and experimental results. Shah and McGarry [1971] reported that the application of LEFM to FRC was not successful due to the existence of a large FPZ. Patterson and Chan [1975] tested specimens made of high alumina cement and E-glass fibres, and reported a relatively large zone of microcracks around the crack tip. The zone extended as extra loading was applied, which violated the definition of the crack tip for LEFM.

Gjϕrv et al. [1977] concluded that LEFM is not applicable to small concrete specimens. Mindess et al. [1977] found K_{IC} and G_{IC} of the FRC insensitive to fibre volume showing only a small marginal change with increasing fibre volume. Many experimental results of both concrete and FRC revealed the inconsistency of LEFM models. Swamy [1979] pointed out that all LEFM data applied to concrete show considerable scatter and definite size dependence which makes LEFM useful only for qualitative comparisons rather than for absolute values.

4.3.2.2.1. Application of COD to FRC

Crack opening displacement (COD) has been used to characterize fracture behaviour of FRC. Nishioka et al. [1978] applied COD analysis to FRC specimens with different fibre volumes and concluded that COD is applicable to FRC. However, other researchers showed that COD does not provide an appropriate criterion for fracture of FRC because COD is geometry and size dependent [Mindess 1983[a] and Velazco et al. 1980]. Crack tip opening displacement (CTOD) was suggested to be the most suitable fracture parameter due to the significant non-linear behaviour within the FPZ of FRC. Wecharatana and Shah [1983] developed the CTOD-closing pressure model using an iterative process to determine the size of the FPZ. This showed good agreement with experimental results.

Visalvanich and Naaman [1983] proposed the crack opening angle (COA). Fracture of FRC is expected to take place when the COA reaches its critical value. The critical crack opening angle (CCOA) was found to be 0.13° for plain concrete and 0.29° for fibre concrete. However, CCOA shows little sensitivity to changes in fibre volume. Chern et al. [1985] related CTOD of FRC to the applied stress using a numerical approach. Recently Soroushian et al. [1995] proposed a theoretical optimization model for FRC by modelling the bridging mechanism of fibres at the crack tip using stress equilibrium, strain compatibility and COD conditions. Even more recently Taylor et al. [1996] used the crack mouth opening displacement (CMOD) to represent the fracture toughness of FRC. Zhang and Stang [1998] introduced a semi-analytical model for predicting the flexural behaviour of FRC using the stress-crack width constitutive relations and verified it with finite element modelling based on CMOD. The model showed good agreement with both the finite element model and experimental results.

4.3.2.2.2. Application of the J-integral to FRC

For a non-linear elastic body, the J-integral is defined as the energy available for crack extension. The J-integral is evaluated using the line integral defined in equation [4.11] [Rice 1968]. w is the strain energy density, T is the traction vector, u is the displacement vector and ds is the length increment along the contour Γ.

$$J = \int_{\Gamma} w\, dy - T\left[\frac{du}{dx}\right] ds \qquad [4.11]$$

Mindess et al. [1977]applied the J-integral for both plain and fibre concrete and reported J_{IC} to be able to represent the difference in the behaviour of concrete when fibres were incorporated. Figure [4.7] shows the effect of fibre content on both J_{IC} and G_{IC}. Although, the J-integral was able to reflect the difference in fibre length and aspect ratio, it was reported to be size and geometry dependent.

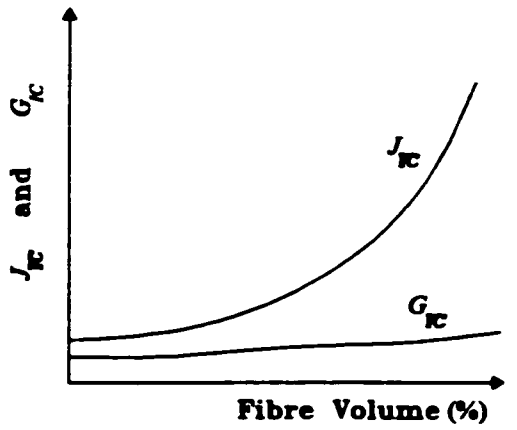

Figure [4.7]: Effect of fibre volume on both G_{IC} and J_{IC} [Mindess et al. 1977].

Halvorsen [1980] proved the J-integral can show the variation of fracture toughness of FRC due to changes in fibre type and content. The researchers in the experimental program developed at University of Illinois, U.S.A in the late 1970s came to similar conclusions on the suitability of the J-integral to represent the fracture toughness of FRC [Mindess 1983[b]]. Velazco et al. [1980] reported the J-integral to be crack dependent and not to be sensitive to

fibre changes. However, Ward et el. [1989] recommended the application of the J-integral rather than any other fracture parameter to describe the fracture toughness of FRC.

4.3.2.2.3. Application of the R-curve to FRC

R-curves are crack growth resistance graphs plotted as the energy release rate G or "R" versus the crack extension [Broek 1982]. Lenain and Bunsell [1979] applied the R-curve to asbestos cement sheets and identified three basic stages of crack growth. The first represents the creation of the FPZ, the second represents FPZ stable growth and the third shows main crack extension and stopping of FPZ growth. Andonian et al. [1979] developed an EPFM model based on fibre pull-out energy, predicting the R-curve with good agreement with experimental results. Velzaco et al. [1980] reported good sensitivity of the R-curve to changes in the fibre volume. Wecharatana and Shah [1983] predicted the R-curve of FRC using quasi-brittle fracture mechanics models. Balaguru ad Shah [1992] proposed a step-by-step procedure for the establishment of the different mathematical parameters of the R-curve for FRC. Mobasher et al. [1995] established the R-curve for different types of FRC including carbon and polypropylene fibres, providing significant information on the fracture of FRC.

4.3.2.3. Non-linear quasi brittle fracture mechanics

The existence of a large FPZ in concrete and FRC results in a different fracture behaviour than that usually observed in fully plastic materials (e.g. steel). Figure [4.8] shows the effect of the FPZ on the tensile stress distribution.

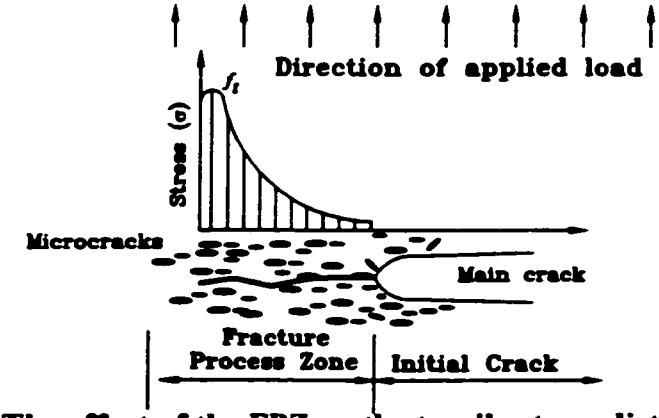

Figure [4.8]: The effect of the FPZ on the tensile stress distribution [Shah et al. 1995].

The tensile stress increases from the crack tip reaching a maximum and then dropping to the microcracking stress at the end of the FPZ. This is different from fully plastic materials which show full plasticity in the plastic zone. To predict accurately, the inelastic response of the FPZ should be taken into account. A cohesive pressure acting on the crack surfaces is used to model the different toughening mechanisms in the FPZ. The result is a modified version of the plastic zone model based on the Dugdale [1960] and Barenblatt [1962] assumptions. The cohesive pressure $\sigma(w)$ tends to close the crack and is a decreasing function of the crack opening displacement (COD) which is denoted here as (w). Figure [4.9] shows a cohesive crack with crack surfaces in contact.

Using the cohesive crack model the energy release rate G can be divided into two parts: the energy consumed in fracturing the material surfaces G_{IC} and the energy consumed to overcome the cohesive pressure as shown in equation [4.12]

$$G = G_{IC} + \int_0^{CTOD} \sigma(w)\, dw \qquad [4.12]$$

The first term of the equation represents the Griffith LEFM energy balance while the integration represents the Dugdale-Barenblatt correction for plastic materials. The difference is the shape of the $\sigma(w)$ function used to represent the cohesive pressure. Two groups of models for concrete and FRC were developed based on equation [4.12]. The first is the fictitious crack models and the second is the effective elastic crack models. A brief note about these models with respect to FRC follows.

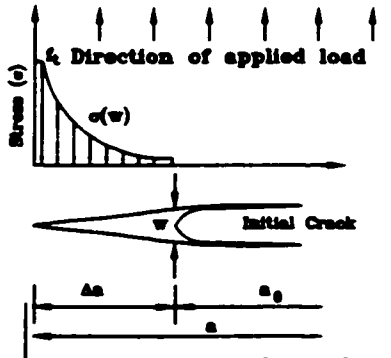

Figure [4.9]: Cohesive crack with crack surfaces in contact [Shah et al. 1995].

4.3.2.3.1. The fictitious crack models

In fictitious crack models the elastic energy release rate G_{IC} is assumed to be zero as the surface energy in quasi-brittle materials is negligible compared to the energy consumed in the FPZ. Equation [4.13] represents the main trend of all these models

$$G = \int_0^{CTOD} \sigma(w)\, dw \qquad [4.13]$$

Hillerborg et al. [1976] introduced the first fictitious crack model for concrete. The choice of $\sigma(w)$ function is the most significant part of the model. Linear, bi-linear, tri-linear, exponential, and power curve functions were examined and the bi-linear function seems to give the most reasonable results [Shah et al. 1995]. Other models based on the same concept were introduced to model concrete and FRC [Foote et al. 1987, Visalvanich and Namman 1983, Wecharatana and Shah 1983, and Bazant and Oh 1983].

4.3.2.3.2. The effective elastic crack models

In these models the second term in equation [4.12] is assumed to be zero by using an equivalent elastic traction-free crack. This means LEFM can be applied and equation [4.12]can be re-written as [4.14].

$$G = G_{IC} \qquad [4.14]$$

Jenq and Shah [1985] proposed the two-parameter fracture model for concrete [1985]. The new model used two fracture parameters (K_{IC} and $CTOD_C$) to describe the quasi-brittle material. Other equivalent elastic crack models for concrete were developed using different approaches in the determination of the equivalent crack dimensions but all used equation [4.14] [Bazant and Kazemi 1990, Karihaloo and Nallthambi1989 and Jenq and Shah 1986].

Through the previous review the main fracture mechanics approaches developed for FRC have been investigated. However, many other models have been developed for FRC. More detailed discussion of these models and their differences are provided by Balaguru and Shah [1992]. Bentur and Mindess [1990]. Beaudion [1990] Gopalaratnam and Shah [1987]. and Mindess [1983[a and b]].

4.4. Fracture toughness of UHPC

The reason for using strong fibres (carbon fibres) in a brittle matrix (concrete) is to enhance both strength and ductility. The insignificant increase in the composite strength of most conventional fibre cementitious composites is attributed to the small fibre fraction used, comprising less than 2% of the cement matrix by volume, and the weak bond between the fibre and the cement matrix. The effect of the weak bond seems to be more significant [Bentur and Mindess 1990]. Microstructural investigation of these UHPC mixtures [section 3.5] has shown the carbon fibres to have a non-smooth surface and the matrix to be very dense in the vicinity of the fibres. This would support the concept that fibre debonding is unlikely to take place prior to fibre rupture or fibre pull-out. However, this strong bond would also favour fibre rupture rather than fibre pull-out to be the dominant energy absorption mechanism. This interpretation has been supported by the micrographs presented in figure [3.7].

The dense microstructure of UHPC leaves no room for more enhancement of the cement matrix. Any further enhancement of the composite has to be achieved through changes in the fibres. Recalling the shear transfer model [section 4.2.1], higher fracture toughness can be attained if fibres shorter than the critical length (l_c) are used. The model assumes full bond between the fibre and the matrix, and stress transfer is based only on shear stresses as in Figure [4.10] and equation [4.4].

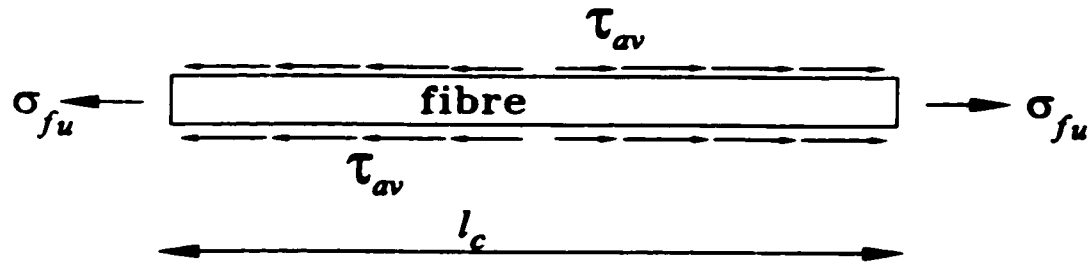

Figure [4.10]: Shear transfer model.

$$l_c = \frac{\sigma_{fu} d}{2\tau_{av}} \qquad [4.4]$$

Applying this model to the newly developed UHPC, the critical length (l_c) will depend on the ultimate strength of the fibres (σ_{fu}), the fibre diameter (d) and the average interface shear strength (τ_{av}) as shown in equation [4.4]. The carbon fibres are modeled using the properties shown in Table [3.3]. Bentur and Mindess [1990] showed that densification of the cement matrix resulted in enhancement of the fibre/matrix bond strength. τ_{av} is assumed to be a function of the matrix strength. Neville [1996] recommended relating the bond strength of concrete to its tensile strength and suggested using the power of 0.7 developed by Oluokun [1991] instead of the conventional square root. Equation [4.15] is used to predict the average interface shear strength of UPHC based on its compressive strength (f'_c) [Oluokun 1991].

$$\tau_{av} = 0.2(f'_c)^{0.7} \qquad [4.15]$$

The predicted critical fibre length (l_c) ranges from 1.9 to 1.6 mm for UHPC mixtures showing compressive strengths 190 up to 240 MPa respectively. The maximum critical fibre length is shorter than the fibres used of 3-6 mm. This means that fibres will be ruptured rather than being pulled-out which will result in limited fracture toughness. An experimental programme examining the effect of fibre length change on HPC and UHPC mixtures was therefore carried out to support the analysis above.

4.5. Experimental programme

The purpose of this experimental programme was to examine the effect of changing fibre length on the fracture toughness of UHPC. Two series of fracture toughness experiments were carried out. In the first series, high performance concrete (HPC) incorporating carbon fibres with four different fibre lengths were tested. In the second series UHPC mixtures incorporating carbon fibres with three different fibre lengths were tested. The rationale behind developing two series of test was to examine the effect of fibre length on a wide range of

concrete strengths. The shortest fibre length available was 3 mm..

4.5.1. Material properties and mix proportions

Table [4.2] gives the engineering properties of the carbon fibres incorporated in both testing series. These are the same carbon fibres used in developing the UHPC mixtures.

Table [4.2]: Engineering properties of carbon fibres used in HPC and UHPC.

Fibre length (mm)	3	6	10
Fibre diameter (μm)	10	10	17
Tensile strength (MPa)	2400	3300	1800
Unit weight (kg/m³)	2000	2100	1900
Modulus of elasticity (GPa)	210	300	180
Carbon content	99	99	99

Table [4.3]: Mixture proportions of HPC and UHPC mixtures.

	HPC	UHPC
Cement (Type 10) (kg/m3)	540	510
Silica fume (kgm³)	—	65
Calcined bauxite aggregate (kg/m³)	—	1140
Lime stone aggregate (kg/m³)	1050	—
Fine aggregate (kg/m³)	630	560
Water (Litre/m³)	180-200	140
Superplasticizer (litre/m³)	5 - 15	15
Fibre volume %	2	2
Water/Cement	0.33-0.37	0.24

In the first series four HPC mixtures including chopped carbon fibres were examined. The four mixtures are denoted as HPC0, HPC3 , HPC6 and HPC10 indicating carbon fibres with 0, 3 , 6, and 10 mm length respectively. These HPC mixtures included crushed lime stone aggregate with 10 mm nominal maximum size. Table [4.3] gives the HPC mixture proportions

used. In the second series the UHPC mixture [Table 4.3] including chopped carbon fibres with three different lengths were used. The three mixtures are denoted as UHPC0, UHPC3 and UHPC6 indicating carbon fibres with 0, 3 , and 6 mm length respectively. HPC specimens were cured in the fog room with 100 % RH at 23 °C till the testing time of 28 days. UHPC0 were cured for 7 days in 50 °C hot water bath while those of UHPC3 and UHPC6 were removed from the bath after 5 days and were oven dried at 200°C for 2 days. Different curing regimes were used to achieve the maximum strength of each mix due to the difference of the ingredients of HPC and UHPC .

4.5.2. Fracture toughness testing

Two sets of beams were tested to determine the different fracture parameters. The first set was unnotched specimens, while the second set was notched specimens. Each set was tested in triplicate. Selection of specimen dimensions for fracture toughness testing of HPC and UHPC was guided by the technical recommendations developed in the literature [Shah et al. 1995, Karihaloo and Nallathambi 1989, Broek 1982, Mindess et al. 1977 and Rice et al. 1973]. The beam dimensions were determined considering that no dimension is less than five times the maximum aggregate size which is 10 mm of HPC and 4 mm for UHPC. HPC series were tested using 100 x 75 x 350 mm beams with a loaded span of 300 mm while the UHPC series were tested using 25 x 25 x 100 mm beams with a loaded span of 75 mm. Small dimension specimens of UHPC were cast because of the difficulty encountered in the production of regular size specimens due to the need to pressure the fresh concrete. Very high loads and special moulds would have been required. The UHPC specimens were therefore cut from the UHPC wedges produced for the anchorage. The production of these wedges is described in section 5.4.

The span/depth ratio was 4.0 for the HPC series and 3.0 for the UHPC series. The HPC specimens were notched using a 3 mm wide carbide saw, while the UHPC ones were notched using 0.8 mm wide carbide saw. The initial notch/depth ratio was kept at one-third for both series. The dimension of both series are shown in Figure [4.11]. The load was applied downward to the specimens at the third points using two concentrated loads. The choice of the four-point bending set-up was based on the need to determine J_{IC}, which requires the

application of pure bending [Rice et al. 1973]. The application of four-point bending to determine the fracture toughness parameters of FRC was also supported by other researchers [Ward et al. 1989, Mindess 1983[b], Halvorsen 1980, Mindess et al. 1977 and Brown 1973].

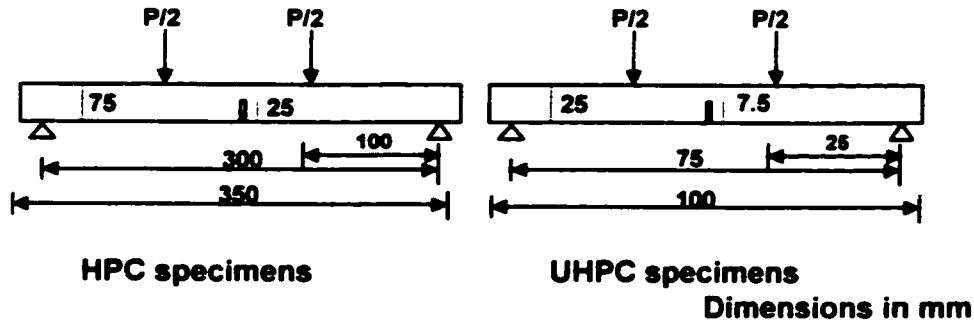

Figure [4.11]: HPC and UHPC testing specimens.

For the HPC series a closed-loop testing set-up was developed using a feed back signal from a Crack Mouth Opening Displacement (CMOD) clip gauge attached to the specimen. This feed back mechanism provided a stable controlled failure of the concrete. The CMOD and the applied load were recorded continuously during the test. The mid-span deflection was measured simultaneously with the load using Linear Variable Differential Transducers (LVDT). Two LVDTs were used over the supports to eliminate the error due to the deflections at the supports [Johnston 1982]. The machine was programmed to change the rate of loading from 0.01 mm/sec to 0.00033 mm/sec according to the CMOD feed back signals. The rate of loading was controlled by a constant rate of increment of CMOD. These rates provided a total loading period in the range of 120 to 180 seconds and a peak load after 30 seconds. Figure [4.12] shows both loading and displacement measurement devices for the HPC series.

The small dimensions of the UHPC specimens and test set-up did not allow the use of the CMOD clip gauge. The mid-span deflection was measured simultaneously with the load using a locally constructed and calibrated displacement transducer which provided the required

feed back mechanism. The loading rate provided a total loading period in the range of 300 seconds and a peak load after 60 seconds. In both series the loading machine and the different displacement transducers were connected to a data acquisition system which was linked to a computer. The readings were collected continuously using a sampling rate of 5 readings per second.

4.5.3. Test results

Different parameters from the load-deflection curves of the notched specimens were computed using spread sheets. These parameters include the peak load (P_c), its corresponding deflection (δ_c), an elastic load (P_i), its corresponding deflection (δ_i), the area under the load-deflection curve of the notched specimens up to the peak load (A_1), and the area under the whole load-deflection curve of the notched specimens up to failure (A_3). The graphs of the unnotched specimens were used to calculate the area under the curve up to the peak load of the corresponding notched specimens (A_2). The different calculated parameters for all tested specimens for both series are given in appendix [B.2]. In appendix [B.3] a sample spread sheet used to determine these parameters in both series is also provided.

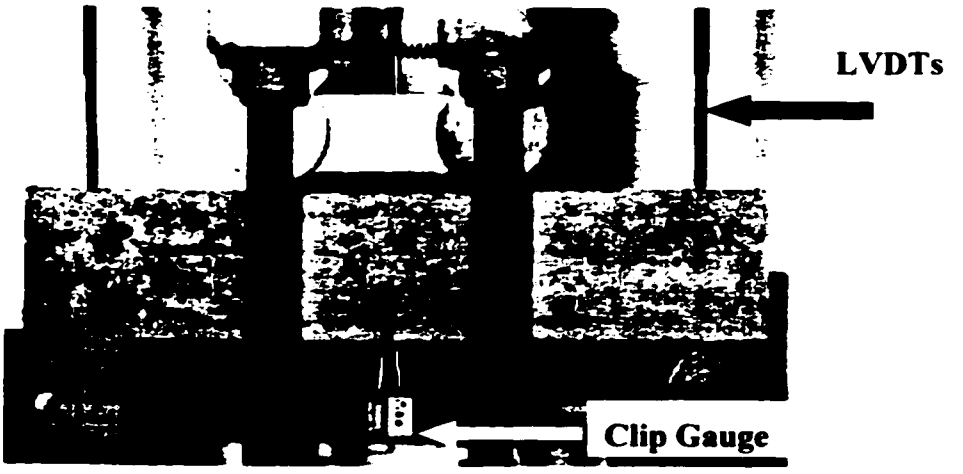

Figure [4.12]: Fracture toughness test set-up for HPC series.

4.5.3.1. HPC series

Two typical graphs of load-deflection and load-CMOD behaviour of the HPC series are shown in Figures [4.13] and [4.14] respectively. From the load-deflection graphs two distinct regions of the curves can be identified. The curve is linear up to 50-60% of the fracture load for HPC0, 60-70% for HPC3, 60-70% for HPC6 and 50-60% for HPC10, followed by non-linear region.

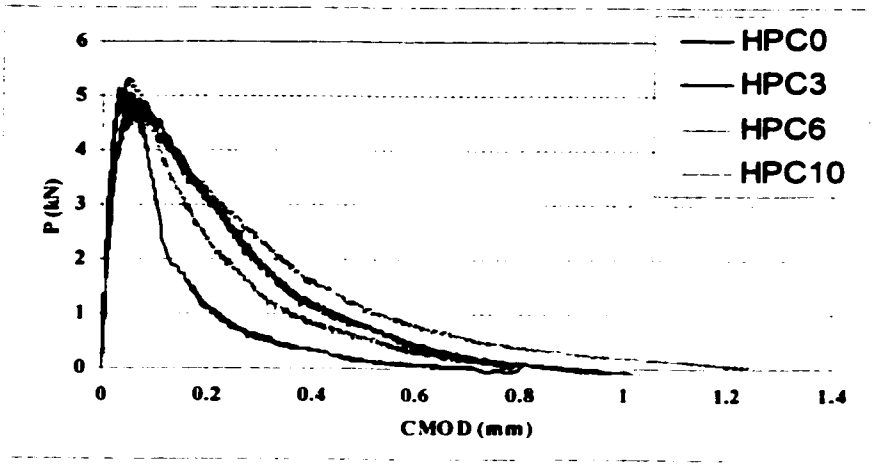

Figure [4.13]: Typical load-CMOD curves for HPC series.

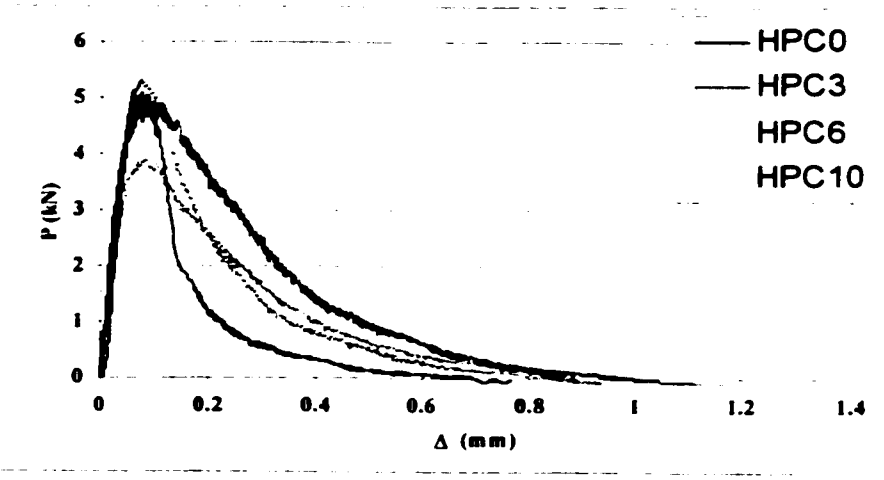

Figure [4.14]: Typical load-deflection curves for HPC series.

The strain hardening is more obvious in the fibre concrete curves with higher deflections achieved prior to the peak load. After the peak load larger deformations were exhibited with decreasing load, showing the tension softening mechanism. The rate of load loss to deformation in the post peak region is much higher in HPC than in fibre concrete.

4.5.3.2. UHPC series

Typical graphs of load-deflection of the UHPC series are shown in Figure [4.15]. As with the HPC graphs two distinct regions of the curves can be identified: linear region up to 70-80% of the fracture load of UHPC0, 85-90% of UHPC3 and 85-90% for UHPC6, followed by non-linear region.

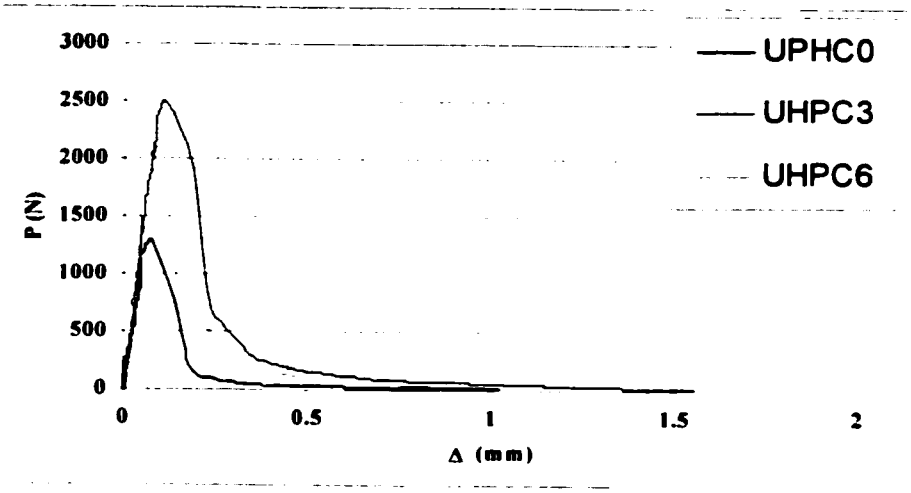

Figure [4.15]: Typical load-deflection curves for UHPC series.

4.5.4. Data analysis

4.5.4.1. Determination of the critical notch depth a_c

The critical notch depth was determined using the effective elastic crack model proposed by Karihaloo and Nallathambi [1989]. The model does not require any P-δ information beyond the peak load. The model uses a secant compliance at the maximum load which can be obtained from the load-deflection curve. The critical effective crack length (a_c) is assumed to correspond to the peak load (P_c). The model determines the modulus of

elasticity of the notched specimen (E) using an elastic load (P_i) within the proportional limit and the corresponding deflection (δ_i) as shown by equation [4.16]. In this analysis P_i was determined from the P-δ curves so that P_i is in the linear range of loading and before the elastic limit. This elastic limit is usually defined as a ratio of the peak load. All the elastic loads selected for analysis were about 65-75% within the linear region based on the load-deflection graphs.

$$E = \frac{P_i S^3}{\delta_i b d^3}\left[\left[\frac{23}{108} + \frac{5wS}{32P_i}\right] + \left[\frac{(1+\upsilon)d^2}{S^2}\left(\frac{1}{2} + \frac{23wS}{48P_i}\right)\right] + \left[F(\alpha_0)\left(3 + \frac{9wS}{4P_i}\right)\right]\right] \quad [4.16]$$

Karihaloo and Nallathambi [1989] developed this model for three-point loading. Therefore, equation [4.16] has been redeveloped for four point loading. The total deformation is evaluated taking into account the elastic deformation, the shear deformation and the plastic deformation due to cracking. This derivation is provided in appendix [B.4]. In equation [4.16] P_i is the elastic load within the proportional limit, δ_i is the corresponding deflection, b is the beam width, d is the beam depth, S is the loaded span, w is the self weight of the beam per unit length, ν is Poisson's ratio (taken as 0.17 for all specimens), α_i is the notch/depth ratio and $F(\alpha_i)$ is

$$F(\alpha_i) = \int_0^{\alpha_i} \alpha\, g^2(\alpha)\, d\alpha \quad [4.17]$$

$g(\alpha)$ in equation [4.17] is the geometric function for the stress intensity factor as given by Tada et al. [1985] for the case of pure bending.

$$g(\alpha) = 1.122 - 1.40\,\alpha + 7.33\,\alpha^2 - 13.08\,\alpha^3 + 14.0\,\alpha^4 \quad [4.18]$$

It is now assumed that the critical crack depth (a_c)can be determined by an imaginary "equivalent" beam including a notch a_c whose stiffness would be equal to the reduced stiffness of the real beam containing a notch of depth a_0. The equation of the stiffness (E) of the beam is expressed as

$$E_c = \frac{P_c S^3}{\delta_c b d^3}\left[\left[\frac{23}{108}+\frac{5wS}{32P_c}\right]+\left[\frac{(1+\upsilon)d^2}{S^2}\left(\frac{1}{2}+\frac{23wS}{48P_c}\right)\right]+\left[F(a_c)\left(3+\frac{9wS}{4P_c}\right)\right]\right] \quad [4.19]$$

Using a trial and error procedure, the initial crack length (a_0) is applied to equations [4.16], [4.17], and [4.18] to calculate E. The same crack length is then used to evaluate Ec from equation [4.19]. The new value E_c will be less than E. An increment is added to the crack length with ($\Delta a=0.001\ d$) and the calculation of E_c is repeated. The process is repeated until E_c is approximately equal to E. The crack length corresponding to this condition is the critical crack length. A computer program using MathCad™ was developed to evaluate the critical notch depth (a_c)and all the fracture toughness parameters based on the P-δ data. This program is provided in appendix [B.5].

4.5.4.2. Determination of K_{IC}

The critical stress intensity factor K_{IC} was used to express the fracture toughness of FRC. K_{IC} represents a measure of how much and how far the local stress field is altered [Shrive and El-Rahman 1985]. Equation [4.20] shows the mathematical expression of K_{IC} [Broek 1982].

$$K_{IC} = g(\alpha)\,\sigma_c\sqrt{\pi a_c} \quad [4.20]$$

The geometrical function $g(\alpha)$ for the case of pure bending is given by equation [4.17], a_c is the critical notch depth determined in the previous step and σ_c is the critical stress estimated using equation [4.21].

$$\sigma_c = \frac{6M_c}{bd^2} \quad [4.21]$$

M_c is the critical moment based on the peak load (P_c)and the self weight of the beam per unit length (w), b is the beam width and d is the beam depth.

4.5.4.3. Determination of G_{IC}

G_{IC} is the critical energy release rate usually used as a LEFM parameter to express the

fracture toughness. G_{IC} can be estimated using the plane strain relation shown in equation [4.22] [Broek 1982]. Both K_{IC} and E are determined experimentally and ν is Poisson's ratio, assumed to be 0.17 for all specimens.

$$G_{IC} = K_{IC}^2\left(\frac{1-\upsilon^2}{E}\right) \qquad [4.22]$$

4.5.4.4. Estimation of the $CTOD_c$

Although measurement of CMOD versus load was used to control the loading rate through a closed loop testing scheme, the determination of $CMOD_c$ and $CTOD_c$ through testing required a different loading sequence including loading and unloading cycles [Jenq and Shah 1985]. This requires a stiff machine to allow unloading after the peak load: this was difficult to attain especially with the HPC series. Therefore, the load-CMOD graphs were used only to show the change in toughness with different fibre lengths while both $CMOD_c$ and $CTOD_c$ were calculated based on the linear crack profile assumptions represented by equations [4.23] to [4.27] provided by Shah et al. [1995] and Tada et al. [1985].

$$CMOD_c = \frac{4\sigma_c a_c g_2(\alpha_c)}{E} \qquad [4.23]$$

$$\text{Where } g_2(\alpha) = 0.8 - 1.7\alpha + 2.4\alpha^2 + \frac{0.66}{1-\alpha^2} \qquad [4.24]$$

$$CTOD_c = CMOD_c\, g_2(\alpha, \chi) \qquad [4.25]$$

$$\text{Where } g_3(\alpha_c, x) = \left[1 - x^2 + (1.081 - 1.149\alpha_c)(x - \alpha_c{}^2)\right]^{0.5} \qquad [4.26]$$

$$x = \frac{a_0}{a_c} \text{ and } \alpha_c = \frac{a_c}{d} \qquad [4.27]$$

4.5.4.5. Determination of J_{IC}

Begley and Landes [1972] defined the J-integral as an average measure of the near tip

stress-strain environment of a cracked elastic plastic body. This was followed by a technique proposed by Rice et al. [1973] to measure J_{IC} for metals using two notched and unnotched specimens under pure bending. Equation [4.28] defines the J integral for a cracked specimen with uncracked ligament H_c [Appendix B.4] under pure bending [Equation 4.28].

$$J = \frac{2}{H_c} \int_0^{\theta_{crack}} M d\theta_{crack} \qquad [4.28]$$

For four point bending equation [4.28] can be written as:

$$J = \frac{2}{b H_c} \int_0^{\delta_{crack}} P \, d\delta_{crack} \qquad [4.29]$$

where P is the applied load, b is the specimen width and δ_{crack} is the vertical displacement of the load point due to the cracking of the specimen. Rice et al. [1973] pointed out that in a pure bending test the elastic displacement of uncracked specimen ($\delta_{uncracked}$) will be of considerable value with respect to elastic and plastic displacement due to the crack, therefore, it should be eliminated in evaluating J. Therefore, definition of J in equation [4.29] has been interpreted as the total absorbed energy of the cracked specimen minus its elastic energy.

Mindess et al. [1977] have reported the application of this technique in determining the J_{IC} of fibre cement composites using a four point bending test set-up. They proved the sensitivity of J_{IC} to change in fibre volume fraction. To avoid the expected complexity of sub-critical crack growth, post-peak behaviour was excluded. Mindess et al. [1977] recommended the estimation of J_{IC} using the area under the load-displacement curve up to the point of maximum load only. Equation [4.30] is used to evaluate the J_{IC} based on the load-displacement data.

$$J_{IC} = \frac{2}{H_c b}\left[A_2 - A_1\right] = \frac{2}{H_c b} A_c \qquad [4.30]$$

where A_2, A_1 and A_c are the areas under the load-displacement curves as shown in Figure [4.16]. The areas under the curves were calculated using spread sheets. The trapezoidal integration method [Ellis and Gulick 1990] was applied to the P-δ curves. The accuracy of this method for integration will be very good due to the fact that the data acquisition system was operating at 5 HZ.

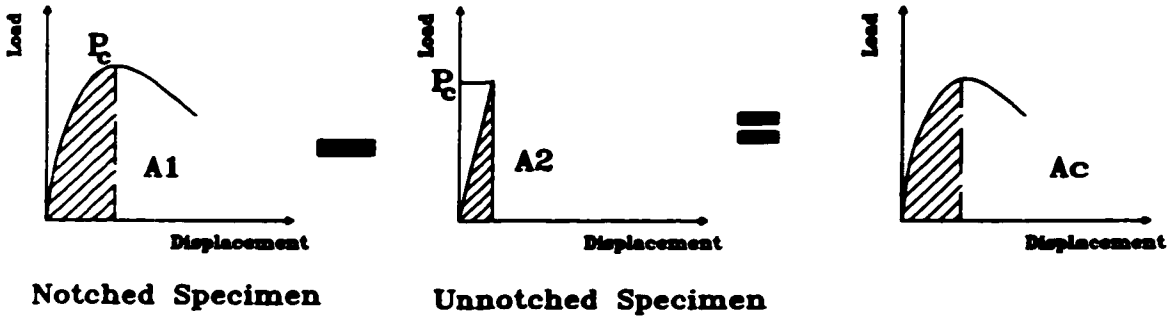

Figure [4.16]: Parameters in evaluating the J-integral [Mindess et al. 1977].

4.5.4.6. Determination of the fracture energy G_F

Although the use of four point bending does not comply with RILEM committee 50-FMC [1985] recommendation to evaluate the fracture energy G_F, the method used to determine G_F complies with the theoretical basis provided by Hillerborg [1985]. The fracture energy was evaluated based on its definition as the total energy absorbed till fracture. By assuming that the energy absorption takes place only in the fracture zone and all deformations outside this zone are purely elastic, G_F the fracture energy of the beam was calculated using equation [4.31].

$$G_F = \frac{A_{total} + W\delta_{max}}{H_0 b} \qquad [4.31]$$

A_{total} is the total area under the load-deflection curve after including the self-weight corrections, W is the self-weight of the beam, δ_{max} is the maximum deflection of the corrected curve at final failure of the beam, H_0 is the uncracked ligament thickness and b is the beam width.

4.5.5. Discussions of results

4.5.5.1. HPC series

Table [4.4] shows the average fracture toughness results for the HPC series. A distinct increase in the different fracture toughness parameters can be observed with the reduction of the fibre length. If the average interface shear strength is in the range of tensile strength, as assumed, the critical fibre length is in the range of 3-6 mm. This is in good agreement with the experimental results showing higher fracture toughness of HPC3 including 3mm long carbon fibres. Figure [4.17 to 4.21] show the effect of changing fibre length on the fracture parameters of the HPC series. Individual test results for HPC are given in appendix [B.7.1]

Table [4.4]: Mechanical properties and fracture parameters of the HPC series.

Mixture	HPC0	HPC3	HPC6	HPC10
l (mm)	0	3	6	10
f'c (MPa)*	52.1	51	53	55
fr (MPa)*	6	8	8.2	7.8
a_c (mm)	28.2	33.8	30.2	32.6
K_{IC} (MPa. $m^{1/2}$)	0.93	1.3	1.17	1.23
G_{IC} (N / m)	44.3	70	61	56.2
$CTOD_C$ (μm)	15.52	19.89	18.07	16.75
J_{IC} (N / m)	56.8	109.7	87.9	84.9
G_F (N / m)	145.3	338	271.6	325.1

* 28 days compressive strength and modulus of rupture in appendix [B.6].

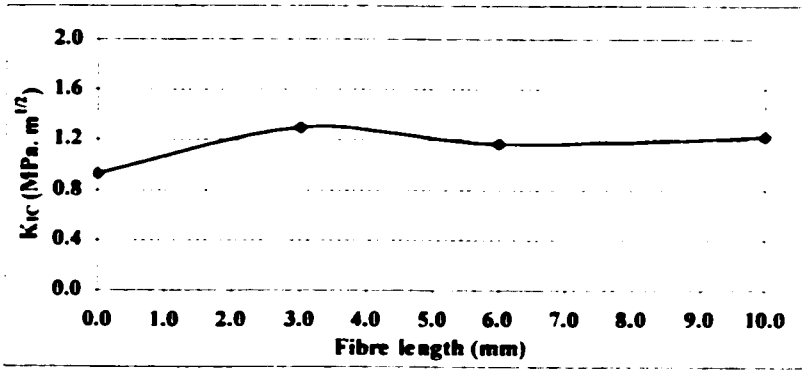

Figure [4.17]: Effect of changing fibre length on K_{IC} [HPC series].

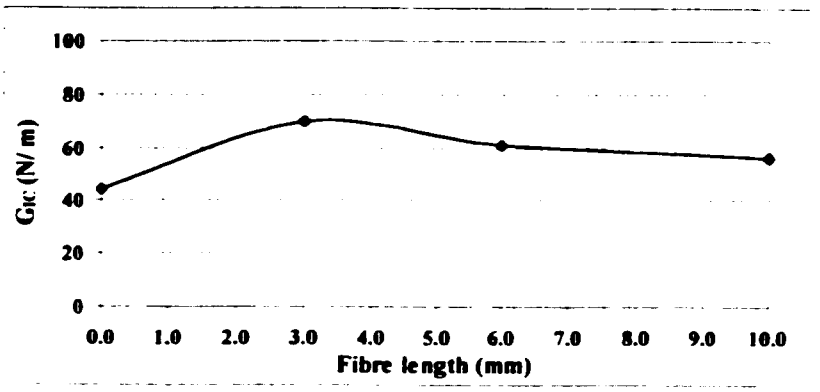

Figure [4.18]: Effect of changing fibre length on G_{IC} [HPC series].

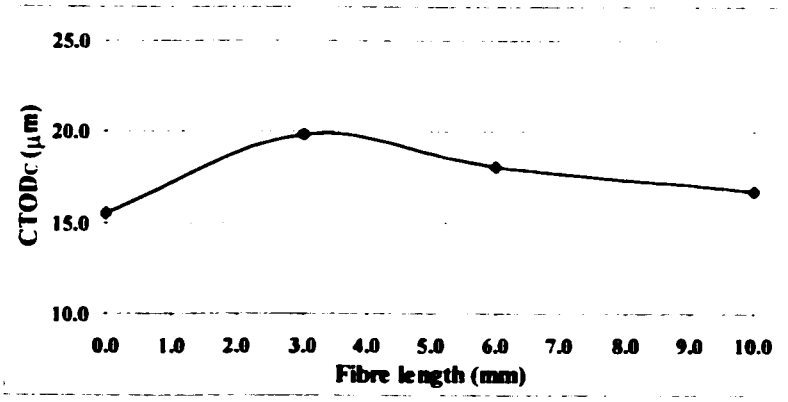

Figure [4.19]: Effect of changing fibre length on $CTOD_C$ [HPC series].

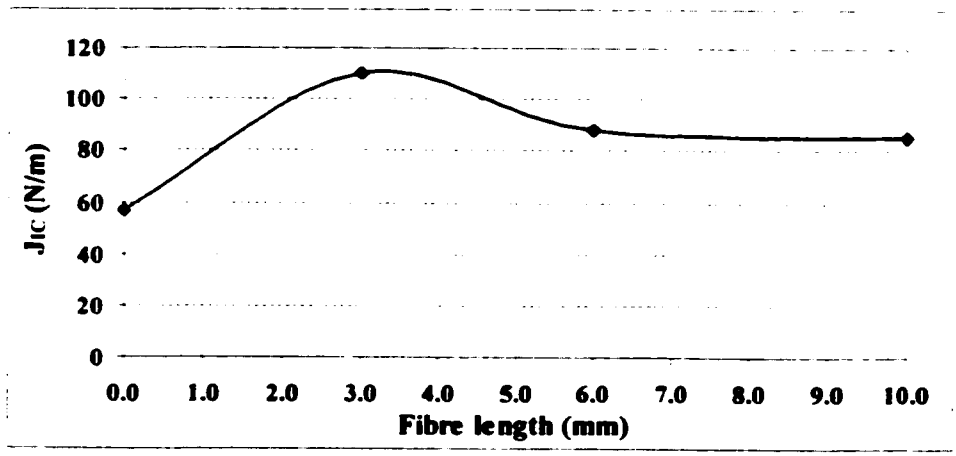

Figure [4.20]: Effect of changing fibre length on J_{IC} [HPC series].

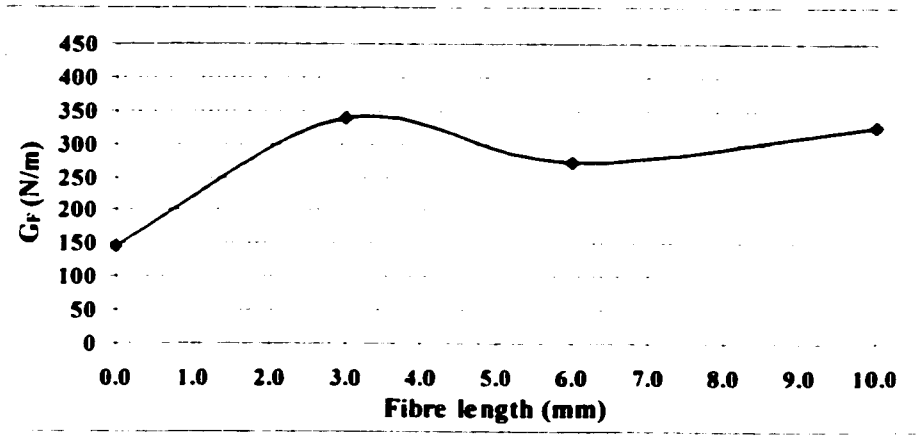

Figure [4.21]: Effect of changing fibre length on G_F [HPC series].

4.5.5.2. UHPC Series

All UHPC series show a fracture toughness three to four times higher than that of the HPC series using the same fibre lengths. This is attributed to the dense microstructure associated with the UHPC mixtures which has been shown through the SEM investigation [3.3.5]. The dense microstructure will result in a much smaller FPZ for UHPC than for HPC

[Shah et al. 1995], which would indicate a considerable reduction in the size effect associated with using small specimens of UHPC compared to HPC. However, this size effect should be taken into account when comparing the fracture toughness parameters of the two series. UHPC3 including 3mm carbon fibres showed the highest fracture toughness. Table [4.5] shows the average fracture toughness results for the UHPC series. Figure [4.22 to 4.24] show the effect of fibre length changing on the fracture parameters of the UHPC series. Individual test results for UHPC are given in appendix [B.7.2].

Table [4.5]: Fracture parameters of the UHPC* series.

Mixture	UHPC0	HPC3	HPC6
l (mm)	0	3	6
a_c (mm)	10.21	8.9	11.02
K_{IC} (MPa. $m^{1/2}$)	1.63	2.4	2.37
G_{IC} (N / m)	162	409	259
$CTOD_C$ (μm)	20.8	33.7	23.7
J_{IC} (N / m)	211	525	347
G_F (N / m)	457	1220	775

* Mechanical properties of this UHPC is provided in Table [3.4 to 3.7].

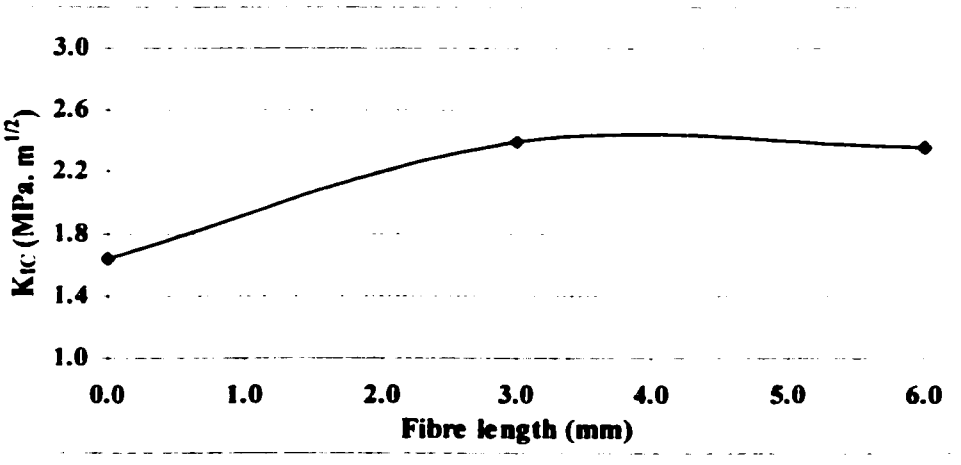

Figure [4.22]: Effect of changing fibre length on K_{IC} [UHPC series].

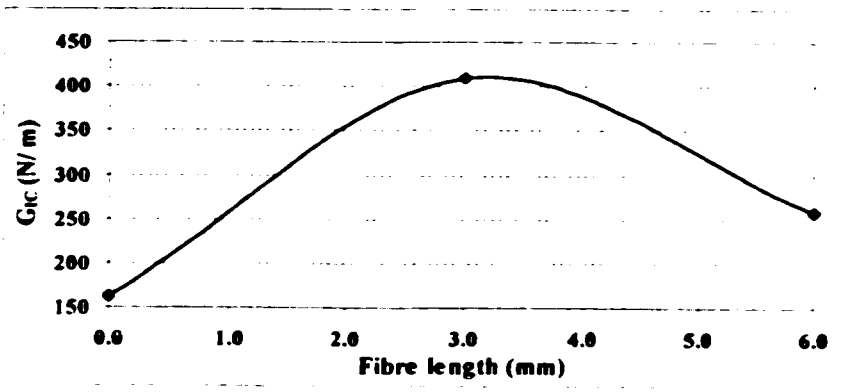

Figure [4.23]: Effect of fibre length on G_{IC} [UHPC series].

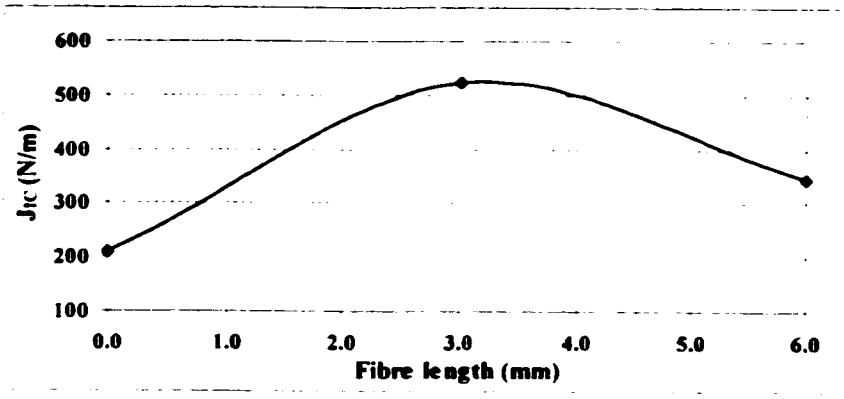

Figure [4.24]: Effect of changing fibre length on J_{IC} [UHPC series].

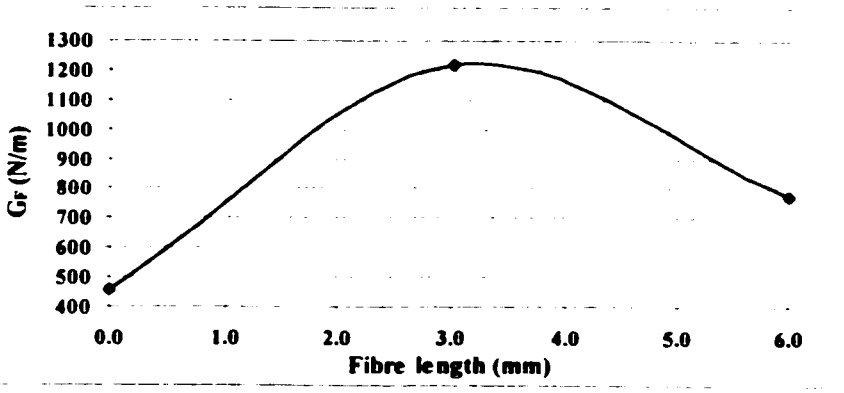

Figure [4.25]: Effect of changing fibre length on G_F [UHPC series].

The experimental work achieved the main goal of this investigation by finding the fibre length which provides most enhancement to the fracture toughness of the newly developed UHPC. However, the experiments can not verify the validity of the shear transfer model. The model would predict the critical fibre length to be 1.6 to 1.9 mm for UHPC of compressive strengths up to 240 MPa [Equation 4.4]. This means that only a small difference between the fracture toughness of UHPC3 and UHPC6 was expected as both are longer than the predicted critical length. However, the results of the UHPC series showed the difference between the fracture toughness of UHPC3 and UHPC6 to exceed 50% while it was 25% for the HPC series. The proposed increase in the interface shear strength due to the more dense packing of the mixtures should allow fibre rupture to be more dominant in both UHPC3 and UHPC6. However, fibre pull-out was very clear in the UHPC3 specimens. The prediction of the interface shear strength based on the tensile strength [Equation 4.15] seems not to be accurate when used for UHPC. Further research work may be required to predict the interface shear strength of FRC more accurately. This is beyond the scope of this work.

4.5.5.3. Statistical analysis

The test results of both the HPC and UHPC series show large discrepancies with some very large standard deviations. Hence there is a potential for misleading interpretations when absolute values only are used. The student t-distribution was applied to the results of both series comparing each fracture toughness parameter. Statistical analysis of both HPC and UHPC series are given in appendix [B.8.1 and B.8.2] respectively. Assuming a 5 % level of significance, the analysis proved J_{IC} to be the most sensitive fracture parameter to fibre reinforcement.

Both K_{IC} and G_{IC} showed sensitivity to fibre inclusions in the matrix but showed less sensitivity when the fibre length was changed. The *CTODc* seemed useless to judge either the inclusion of fibres or changes in fibre length. This insensitivity of the *CTODc* may be due to the method of determination of *CTOD* which did not make use of the CMOD measurements. Finally, G_F seems to be sensitive to fibre inclusion and fibre length change. G_F was the only measurement to show a different trend with changing fibre length compared to all other

parameters. While all parameters showed fracture toughness peaks at 3 mm fibre length and approximately similar values up to 10 mm fibre, G_F showed a further increase when the fibre length changed from 6 mm to 10 mm in the HPC series. This observation was not noticed in the UHPC series.

The sensitivity of the J-integral can be explained with the fact that J_{IC} is based on evaluating the plastic energy required for cracking up to the peak only. The contribution of fibres in this zone is governed by their ability to bridge the crack and being pulled-out. If fibre pull-out is achieved through cracking up to the peak this will significantly increase the plastic energy required for the pre-critical crack growth. Although short fibres proved to be able to provide higher fracture toughness up to the peak, long fibres seem to contribute more in the post-peak behaviour because of their longer anchorage compared to the short ones. Fibre pull-out of short fibres would not allow any kind of energy contribution after being pulled out of the matrix. Fibre rupture would allow the ruptured portions to contribute again to the energy consumption after the peak. The contribution of the ruptured portion will be through toughening the sub-critical cracks in the process zone, thus consuming a considerable amount of energy. This can explain why G_F seems to increase while J_{IC} seems to be constant after decreasing with increasing fibre length. The same effect has not been verified in the UHPC series due to the examination of three fibre lengths only due to difficulties encountered with mixing fibres longer than 6 mm with the UHPC mixes.

4.6. Closure

It is important to emphasize here that the purpose of this experimental work was not to provide general conclusions about the effect of changing fibre length on the fracture toughness of FRC. This would require a much more extensive experimental investigation beyond the scope of this work. The purpose here was to examine the effect of changing fibre length on the fracture toughness of UHPC so as to enhance its fracture toughness. The fracture mechanics analysis proved the possibility of increasing the fracture toughness of both HPC and

UHPC by reducing the fibre length to 3 mm. This was confirmed by the experiments. Hence, the newly developed UHPC [Table 4.3] will be used in the subsequent steps with 3 mm carbon fibres to produce the barrel and the wedges of the non-metallic anchorage.

CHAPTER 5

DEVELOPMENT AND TESTING OF THE NEW NON-METALLIC ANCHORAGE SYSTEM

5.1. Introduction

The objective of this work is to develop a new non-metallic anchorage system for FRP prestressing tendons that is easy to assemble, economic to produce and as durable as the FRP tendons themselves. The use of non-metallic components in the new anchorage system should eliminate corrosion and deterioration concerns at the anchorage zone and should create a highly reliable system from both the mechanical and environmental points of view. Previous systems have shown several shortcomings. These should be eliminated in the proposed system which will be used in steel-free structures enabling the utilization of the CFRP tendons.

The new anchorage is designed to anchor an 8 mm diameter indented spiral Leadline™ (CFRP) tendon. The mechanical properties of the Leadline™ are given in Table [2.3]. Experimental testing of the Leadline™ using a newly developed steel anchorage showed an ultimate strength of the tendon varying from 105 -124 kN [Sayed-Ahmed and Shrive 1998]. To remain conservative, the nominal failure strength of 104 kN cited by manufacturer was used to design and evaluate the new non-metallic anchorage system.

5.2. The new non-metallic anchorage system

The new non-metallic anchorage is both resin- and steel-free, combining the concepts of the split-wedge and the plug-in cone anchorage systems. The anchorage consists of an outer barrel with a conical hole and a four-piece wedge. Figure [5.1] is a schematic of the non-metallic anchorage components. The conical hole of the barrel is inclined at an angle $\theta_1 = 2°$ while the wedges are inclined by an angle of $\theta_2 = 2.1°$. The choice of these angles was based on the experiments done on the metallic anchorage [Sayed-Ahmed and Shrive 1998]. The inside surface of the barrel and the outer surface of the wedges are smooth enough to facilitate seating

of the wedges.

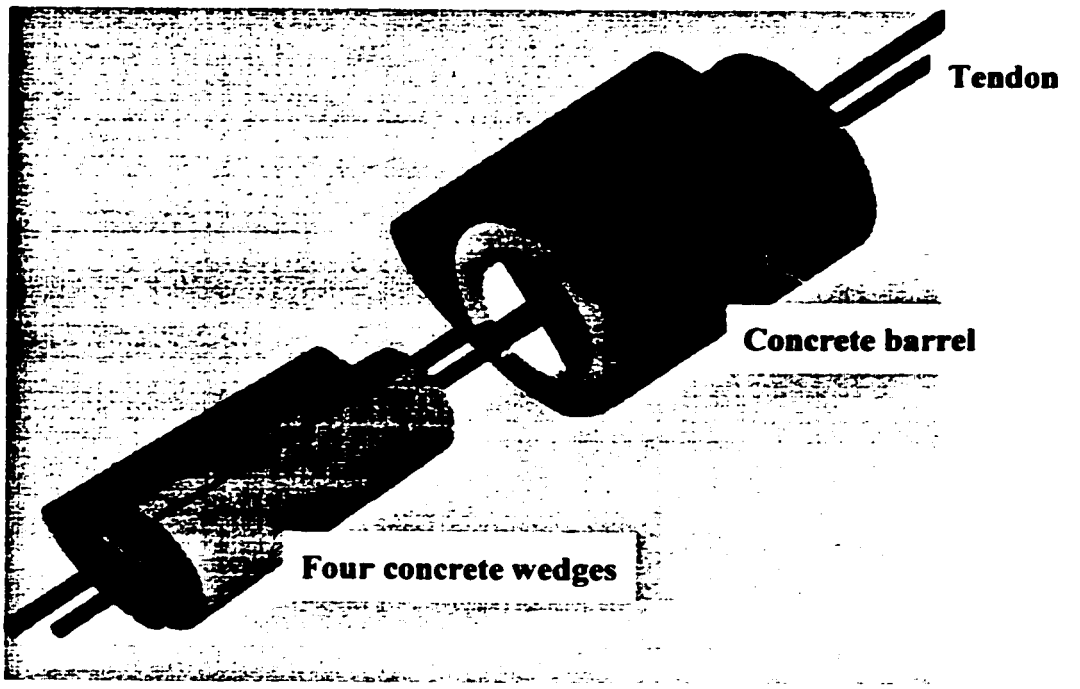

Figure [5.1]: Schematic of the non-metallic anchorage components.

A target anchorage efficiency factor (η) of 95 percent was established. The anchorage is set with a hydraulic jack before tendon load is applied. The wedges and barrel system grip the tendon directly - there being no equivalent to the copper sleeve (in the metallic anchorage) on the tendon. Different non-metallic materials were considered in the early stages of this work. Cast ceramics were considered given their strength and the high-stresses expected to develop in the wedges and the barrel. Cost ruled out these materials, so the ultra high performance concrete (UHPC) with 3 mm length carbon fibres was developed. The UHPC mix used in developing the anchorage components is given in Table [5.1] (very similar to the mix in Table 4.3.)

Table [5.1]: UHPC mixture used to develop the non-metallic anchorage components.

Item	Value
Type 50 Cement (kg/m³)	510
Silica fume (kg/m³)	65
Calcined bauxite aggregate (kg/m³)	1140
Silica flour (kg/m³)	280
Ottawa sand (kg/m³)	280
Superplasticizer/Cement %	2
3 mm long carbon fibres (Vol%)	2
Water (litre/m³)	140
Water/Cementitious ratio	0.24
Nominal maximum size aggregate (mm)	4
Applied pressure (MPa)	80
50 °C hot water curing (days)	5
200 °C dry curing (days)	2

5.3. Design of the non-metallic anchorage system

Preliminary design of the non-metallic anchorage system is provided here using a simple static model shown in Figure [5.2], developed by Campbell et al. [1997]. The purpose of this preliminary design is to propose anchorage dimensions for experimental investigation. Considering θ_2 to be the wedge angle, P is the tendon load, F_{TW} is the friction force between the tendon and the wedges, F_{WB} is the friction force between the wedges and the barrel, R_{TW} is the normal force exerting pressure on the tendon by the wedges, R_{WB} is the normal force exerting pressure on the barrel by the wedges and R is the bearing force of the barrel. Applying equilibrium conditions;

$$F_{TW} = P \qquad [5.1]$$

$$F_{TW} = R_{WB}Sin\theta_2 + F_{WB}Cos\theta_2 \qquad [5.2]$$

$$F_{WB} = \mu_{WB}R_{WB} \qquad [5.3]$$

$$R_{WB} = \frac{P}{\mu_{WB}Cos\theta_2 + Sin\theta_2} \qquad [5.4]$$

Substituting the angle θ_2 by 2.1° and assuming the coefficient of friction μ_{WB} between the concrete wedges and the concrete barrel is 0.1, equation [5.5] gives R_{WB} as a function of P.

$$R_{WB} = \frac{P}{0.1Cos2.1^{\circ} + Sin2.1^{\circ}} \approx 7P \qquad [5.5]$$

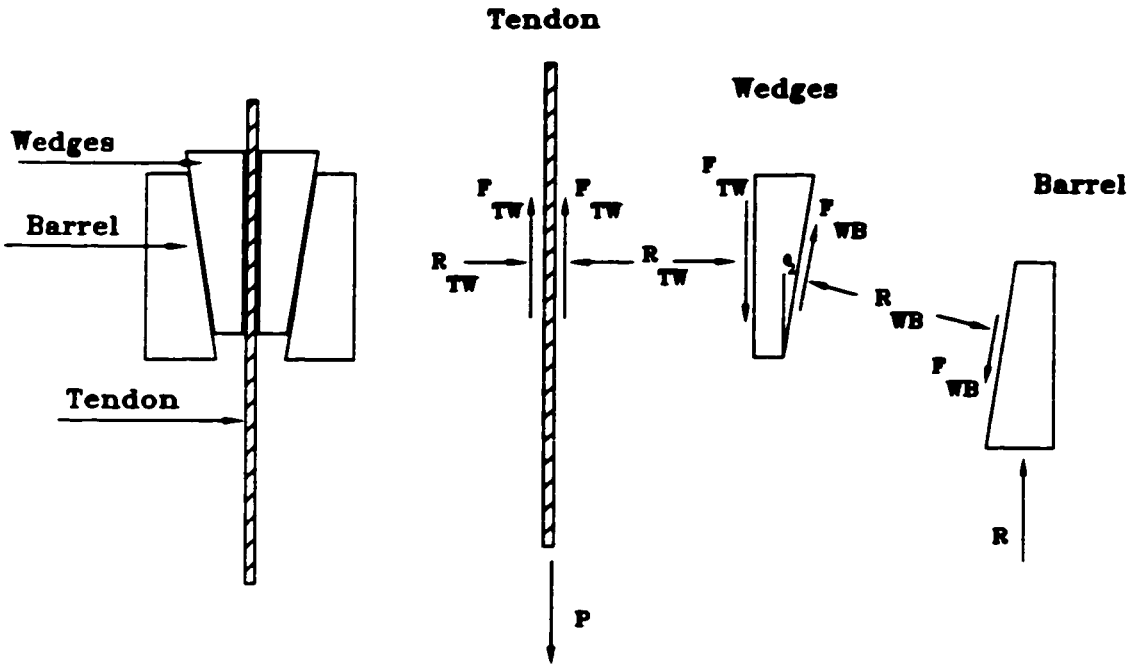

Figure [5.2]: Static model for preliminary anchorage design [Campbell et al. 1997].

5.3.1. Dimensions of the barrel

Assuming linear distribution of the radial stresses exerted on the barrel by the wedges varying from zero at the bottom of the wedges to a maximum at the top of the barrel, the maximum radial stresses σ_{WB} can be estimated in equation [5.6]:

$$\sigma_{WB} = \frac{2 R_{WB}}{\pi d_B l_{BC}} \qquad [5.6]$$

where l_{BC} is the wedge-barrel contact length which can be taken equal to barrel length (l_B)due to the small slope angle used (2°) and d_B is the top inner diameter of the barrel. A first estimate of the tangential stress of the outer barrel σ_T, can be made using thin cylinder theory [Campbell et al. 1997],

$$\sigma_T = \frac{\sigma_{WB} d_B}{2 t_{Bt}} \qquad [5.7]$$

$$\sigma_T = \frac{R_{WB}}{\pi l_B t_{Bt}} \qquad [5.8]$$

$$\text{or } \sigma_T = \frac{2.2 P}{l_B t_{Bt}} \qquad [5.9]$$

Equation [5.9] represents the design equation of the anchorage dimensions. Reducing the barrel length (l_B) or the barrel top thickness (t_{Bt}) will increase the tensile stresses developed in the barrel. Knowing the maximum tendon load, and the barrel tensile strength we can estimate the anchorage dimension. However, the following should be taken into consideration;

1- The barrel length is governed by the need to have enough contact length between the tendon and the wedges to provide enough radial pressure on the tendon without crushing the wedges.

2- Based on the nominal maximum size of the aggregate used in the UHPC mixture (4.0 mm) the minimum wall thickness of the outer barrel (t_{Bt})is 20mm.

3- The bearing stresses developed at the end of the anchorage should be less then the bearing capacity of the anchorage material by a reasonable safety factor.

Assuming the barrel length l_B = 180 mm, the ultimate capacity of the tendon 104 kN,

and UHPC tensile strength of 9 MPa [Oluokun 1991] the required barrel thickness will be 140 mm. This is a very thick unreinforced concrete section. Providing FRP reinforcement will allow this thickness to be reduced. However, a 6 mm diameter FRP reinforcement bar will need a minimum wall thickness of 60 mm which is also impractical.

5.3.2. Wrapping of the barrel

The proposed solution therefore was to wrap the concrete barrel with CFRP Replark™ sheets. These CFRP sheets are needed to provide the necessary circumferential tensile reinforcement to resist the splitting action on the barrel when the tendon is loaded. Table [5.2] gives the engineering properties of the Replark™ CFRP sheets used to wrap the outer barrel. Equation [5.10] is used to estimate the number of CFRP layers required.

Table [5.2]: Engineering Properties of Replark™ CFRP Sheets* [Riad et al. 1998].

Property	
Thickness (mm)	0.110
Width (mm)	250
Strain to failure %	1.5
Modulus of Elasticity (GPa)	228
Tensile Strength (MPa)	3400

*** Mechanical Properties in the longitudinal direction of fibres**

$$t_{sheets} = \frac{2.2\ P}{l_B\ \varphi_{sheets}\ f_{sheets}} \qquad [5.10]$$

With a 104 kN tendon load, a barrel length of 180 mm, a material factor used for CFRP sheets (ϕ_{sheets}) of 0.9 with an ultimate strength of CFRP sheets (f_{sheets}) of 3400 MPa, four layers of Replark™ CFRP sheets are required. The tensile strength of concrete is neglected here as its contribution to overall strength will be very small compared to that of the CFRP sheets. Using these CFRP sheets would allow the barrel wall thickness to be reduced to the minimum

available wall thickness of 20 mm. The anchorage diameter is governed by the bearing strength of the UHPC. Equation [5.11] was used to estimate the outer anchorage diameter.

$$f_{bearing} = \frac{4\gamma P}{\pi (2 d_B t_{Bb} - t_{Bb}^2)} \qquad [5.11]$$

Where d_B is the outer barrel diameter and t_{Bb} is the lower anchor wall thickness, and "γ" is the importance factor defined by the CSA A23.3 [1995]. The lower wall thickness calculated to be 27 mm, allowing for the taper angle while γ was taken as 2.0 to represent the importance of the anchorage in post-tensioning systems.

$$f_{bearing} = 0.85 \phi_c f_c' \qquad [5.12]$$

Equation [5.12] estimates the bearing strength ($f_{bearing}$) using the concrete material factor "ϕ_c" defined by the CSA A23.3 [1995] and characteristic strength of concrete (f'_c). Although ϕ_c for precast concrete is equal to 0.65, ϕ_c was reduced here to 0.35 to represent the uncertainty of the properties of the newly developed UHPC. Considering the 200 MPa characteristic strength of UHPC, the bearing strength will be 60 MPa and an outer barrel diameter of 120 mm would be required. Therefore an outer diameter of 120 mm was initially chosen. This diameter can be changed according to test results.

5.3.3. Dimensions of the wedges

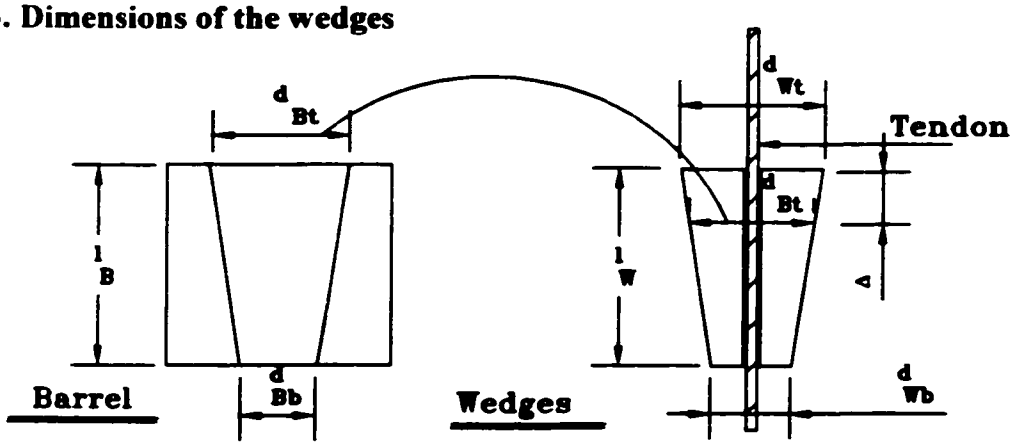

Figure [5.3]: Determination of the wedge dimensions using the barrel dimensions and the seating distance Δ.

d_{Bt} is top inner diameter of the barrel and d_{Bb} is the bottom inner diameter of the barrel connected with a slope angle $\theta_1 = 2°$ through a length of l_B. d_{Wt} is top diameter of the wedges and d_{Wb} is the bottom diameter of the wedges connected with a slope angle $\theta_1 = 2.1°$ through a length of l_w. Considering the Leadline™ tendon diameter of 8 mm and the need to provide enough seating distance (Δ) of the wedges so that they never reach the bottom end of the barrel up to the maximum tendon load, the wedge dimensions can be estimated based on the barrel dimensions as shown in Figure [5.3] through equations [5.13] to [5.15].

$$d_{Bt} = d_{Bb} + 2 l_B \tan 2° \qquad [5.13]$$

$$d_{Wt} = d_{Bt} + 2\Delta \tan 2.1° \qquad [5.14]$$

$$d_{Wb} = d_{Wt} - 2 l_W \tan 2.1° \qquad [5.15]$$

The distance Δ was initially taken as 20 mm but had to be evaluated through anchorage testing. Figure [5.4] shows the proposed dimensions of the non-metallic anchorage system.

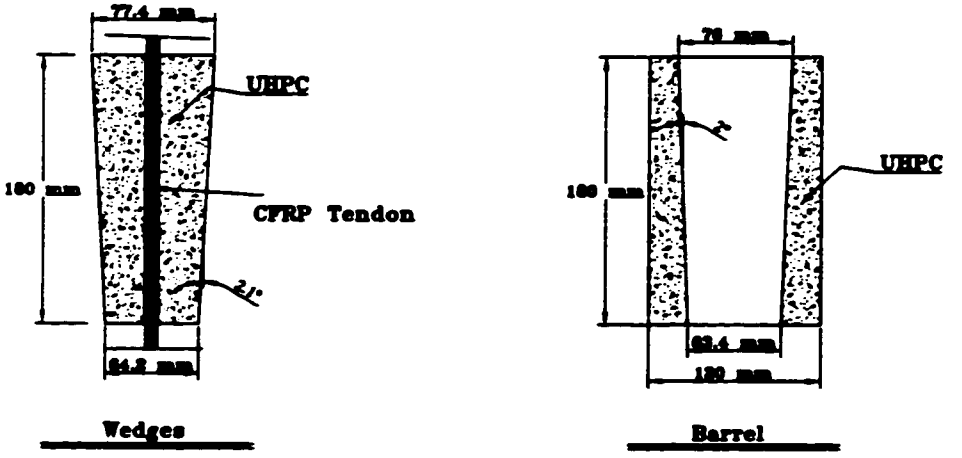

Figure [5.4]: Proposed dimensions of the non-metallic anchorage system.

5.4. Development of the non-metallic anchorage system

5.4.1. Development of casting moulds

The moulds needed to cast the anchorage components constituted a major obstacle. Six consecutive moulds were designed and modified. The difficulties encountered were the need to apply high pressure (80 MPa) to the fresh concrete after being cast in the mould (500 kN for the barrel and 400 kN for the wedges) and the difficulty to demould the concrete elements due to the high bond strength developed between the steel mould and UHPC. The common two-halves cylindrical mould would not allow water to be squeezed out which resulted in very high internal pressures and breaking of the mould. On the other hand, limited removal of water resulted in porous concrete with much lower strength than UHPC.

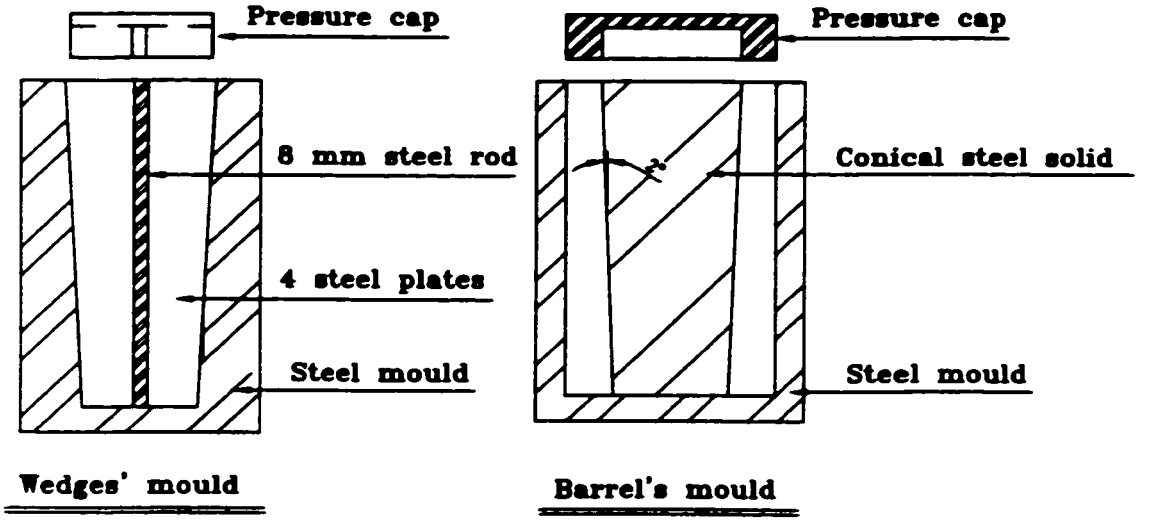

Figure [5.5]: Schematic of the outer barrel and the wedge moulds.

Two moulds were finally designed, one for the barrel and the other for the wedges. The barrel mould consists of an outer -four piece- cylinder and an inner conical part with a slope angle of 2°. The wedge mould consists of an outer -four piece- cylinder with a sloped inner surface. (Trials to cast the wedges in one concrete piece and cut it to four wedges were

unsuccessful due to absence of a very thin accurate concrete saw.) A divider is used in casting the wedges. The divider consists of four perpendicular steel plates (each 1 mm thick) welded to a central steel rod (8 mm diameter). The moulds included small radial grooves at the component interfaces to allow excess fluid to egress. Figure [5.5] shows a schematic of the moulds while Figure [5.6] shows a picture of them. Two head caps were designed for applying pressure to the fresh concrete in these moulds. The head cap for the wedge production was grooved to provide the pressure without touching the cross plates so that the plates did not buckle.

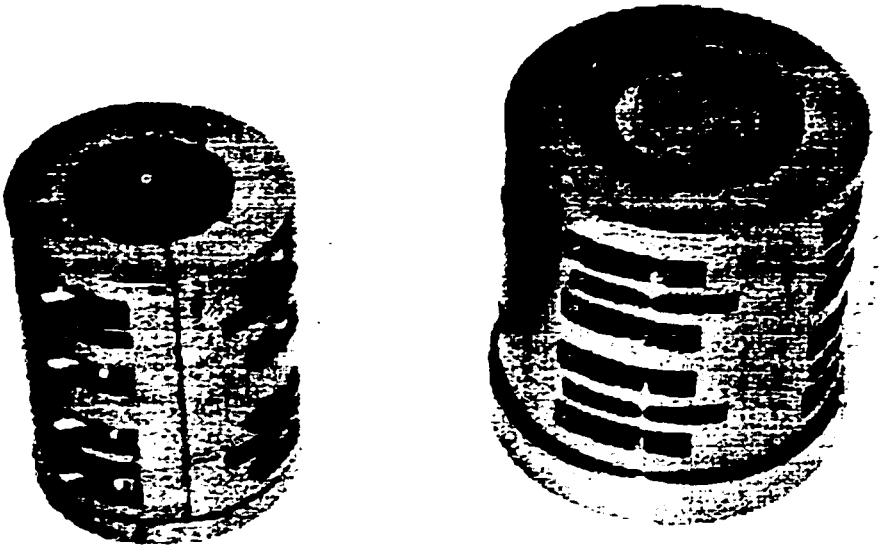

Wedge mould **Barrel mould**

Figure [5.6]: The barrel and the wedge moulds.

The use of oil as a releasing agent for demoulding was not successful because the oil was squeezed out along the water grooves with the water when pressure was applied. A thin wax layer coating the inner conical part of the outer barrel mould and the wedge's divider was able to provide easy demoulding. A very hot wax is needed to create this thin coating. Fast dipping of the steel parts in the hot wax resulted in very thick wax layer. This would provide

a porous surface of concrete. Therefore the steel parts were dipped in the wax for 1 hour and then left to cool slowly for enough time before casting. Alternatively, the steel could have been heated to the wax temperature before dipping. The use of thin wax layers provided concrete pieces with smooth surfaces which was useful in reducing the friction between the barrel and the wedges.

5.4.2. Production of the anchorage components

The aggregate was mixed first, dry, with the cement, silica fume and fibres being added in turn. Half the water was added and after 2 minutes of mixing the rest of the water and the superplasticizer were added. Specimens were then cast. Although the same concrete mixture and mixing procedure as described were always used, changes in the concrete workability used to happen. These changes were attributed to small changes in the time of adding the superplasticizer (parts of a minute). The different workabilities would affect the head cap displacement and the final anchorage dimensions as a result. Therefore, the pressure was applied under load control conditions while keeping track of the head cap displacement so that a constant final displacement was maintained for all casts.

The anchorage components were cured in a 50 °C hot water bath for 5 days after being demoulded, followed by 2 days of dry curing at 200 °C. Changes in the final concrete dimensions were observed. Although these changes were in the range of 2- 4 mm, they affected how the anchorage parts fit together and thus the ability of the anchorage to work effectively as designed. The need to prevent any dimensional changes or to have them consistent on both the outer barrel and the wedges is attributed to the small differential angle of 0.1° needed between the two parts. Any changes would not allow the required seating of the wedges, with the consequence of tendon slippage or wedge cracking. High quality control production conditions were required to prevent undesired dimensional changes. Maintenance of quality requires careful control of the mixing ingredients and mixing procedure, the displacement of the cast concrete in the mould and the time over which pressure is applied, and finally the curing conditions, procedure and period. Optimum values of all parameters have been described previously.

5.4.3. Wrapping of the barrel

Examining the loading capacity of an unwrapped anchorage, the barrel cracked at a seating load of 20 kN. The UHPC was able to provide a tensile strength of 18 MPa prior to cracking [Figure 5.7]. The seating load was increased to 30 kN with no further cracking. The tendon load was then applied and the anchorage failed due to barrel cracking at a tendon load of 6 kN. This test proved that CFRP layers are needed to provide the necessary circumferential tensile reinforcement to resist the splitting action on the barrel as the tendon is loaded.

Consequently, the barrel was wrapped with four layers of CFRP sheets with the fibre direction being circumferential as shown in Figure [5.8]. Each layer was cut to the circumference of the barrel, such that the two ends did not overlap but butted up against each other. This was found to be important since overlapping the ends caused small voids to exist which invariably became the start point of the fibre wrap ripping when the wedges were pushed into the barrel or pulled tighter as load was applied to the tendon. The butt joints of any two successive layers were placed at about 90° to each other around the circumference of the barrel.

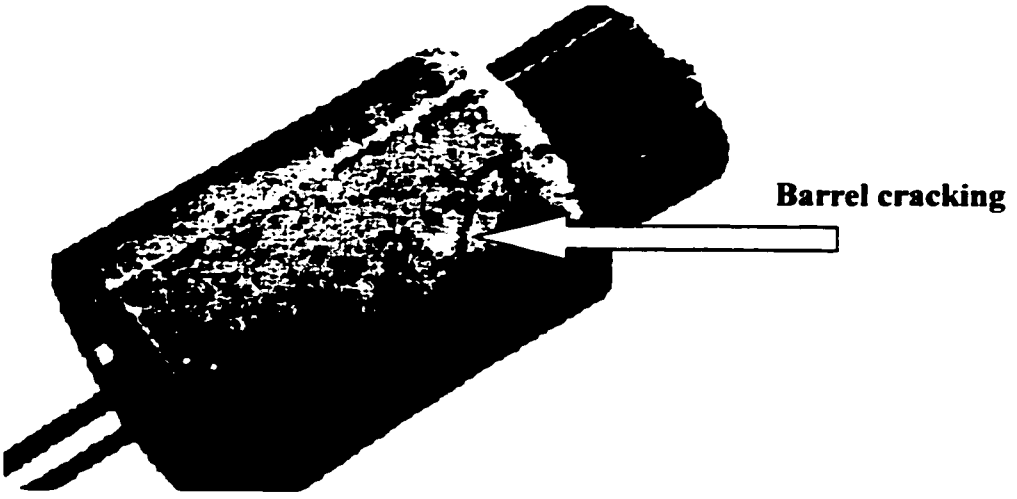

Figure [5.7]: Unwrapped outer barrel cracked during testing.

To ensure full contact between the barrel and the CFRP layers, the friction of the outer surface of the barrel was increased by light sand blasting. The outer surface was then painted with primer and left to dry for 24 hours. Epoxy was then applied to the surface and the first CFRP layer was wrapped. Wax paper was wrapped over the layer and the butt joint and clamped using hose clamps with no transverse spaces between each successive clamp. This forced air out from between the sheet and the barrel, leaving no air voids to constitute crack initiation points. In the following layers the same procedure was applied without sand blasting or applying further primer. Figure [5.8] shows the different stages of wrapping the barrel. The new non-metallic anchorage [Figure 5.9] was designed to be seated before being loaded. The required seating load was determined through testing.

Unwrapped **Primer coated** **Wrapped**

Figure [5.8]: Non-metallic anchorages unwrapped, primer coated and wrapped.

5.5. Testing of the non-metallic anchorage system

A two phase testing programme was planned to test, evaluate, and modify the new non-metallic anchorage system. Thirty-three non-metallic anchorages were examined throughout this testing programme. In the first phase the non-metallic anchorage with dimensions proposed in Figure [5.4] was evaluated in a short-term tension test. This allowed optimization of the anchorage dimensions, verification of the number of layers of the CFRP sheets determined analytically, and examination of the effect of the seating load. Once the different production parameters were determined, the second phase of testing was performed to evaluate the performance of new anchorage performance. In the second phase two tests were performed on the tendon-anchorage assemblies. The first was a short-term tensile test to determine the anchorage efficiency factor (η). The second was fatigue testing to assess the dynamic performance of the new non-metallic anchorage.

5.5.1. Seating of the non-metallic wedges

Before applying any load to the CFRP tendon, the anchorage should be seated. Preparation for seating of the wedges involves three processes. First the internal surface of the barrel is greased to reduce the friction between the barrel and the wedges. This would allow the wedges to slide far enough into the barrel to exert enough pressure on the tendon to grip it. The second process is to roughen the wedge contact surfaces with the tendon. Although the wedge surfaces are not smooth, sometimes a tendon slipped when the surfaces were not roughened. Finally, the third process is to eliminate sharp edge on the wedges. Trials involving wedges with sharp edges showed premature failure of the tendons in the anchorage zone due to the wedges digging into the tendon. The second and the third processes are achieved using a hand file.

The non-metallic anchorage was seated using a hydraulic jack with a 260 kN ENERPAC single-acting-hollow ram and was measured using pressure transducer calibrated in the range of loading 0 ~ 100 kN with accuracy of ± 0.5% of the calibrated range. The load measured was displayed using a digital gauge connected to the pressure transducer. Figure [5.10] shows the seating arrangement.

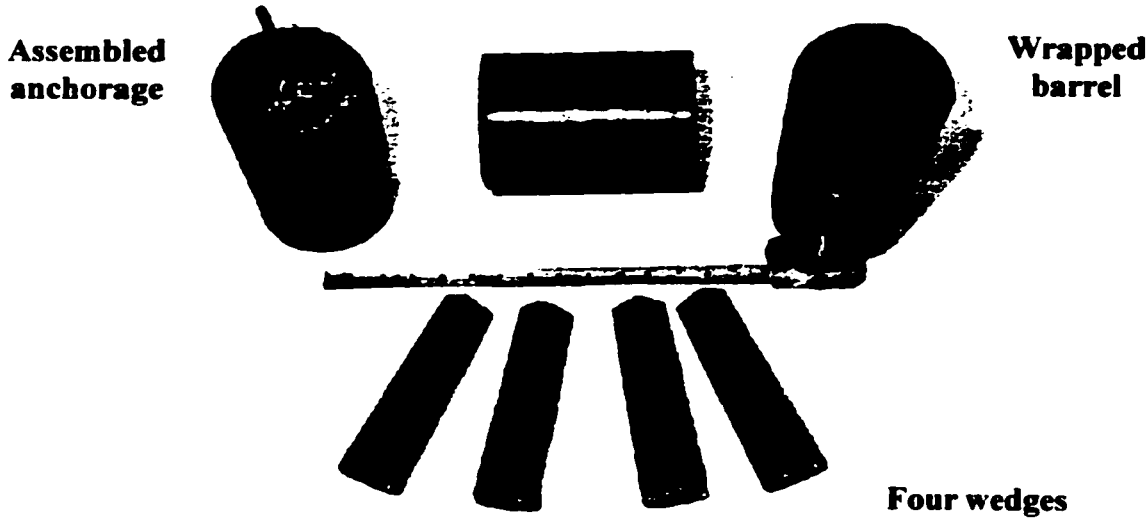

Figure [5.9]: The four wedges, a wrapped barrel and an assembled anchorage.

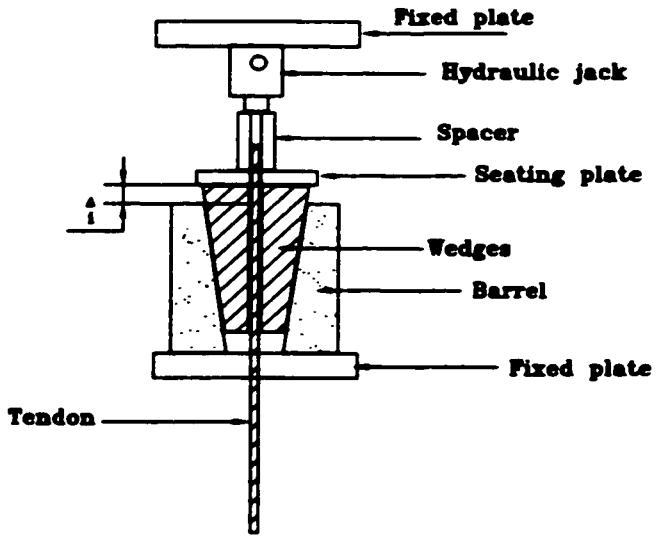

Figure [5.10]: Schematic representation of the seating arrangement.

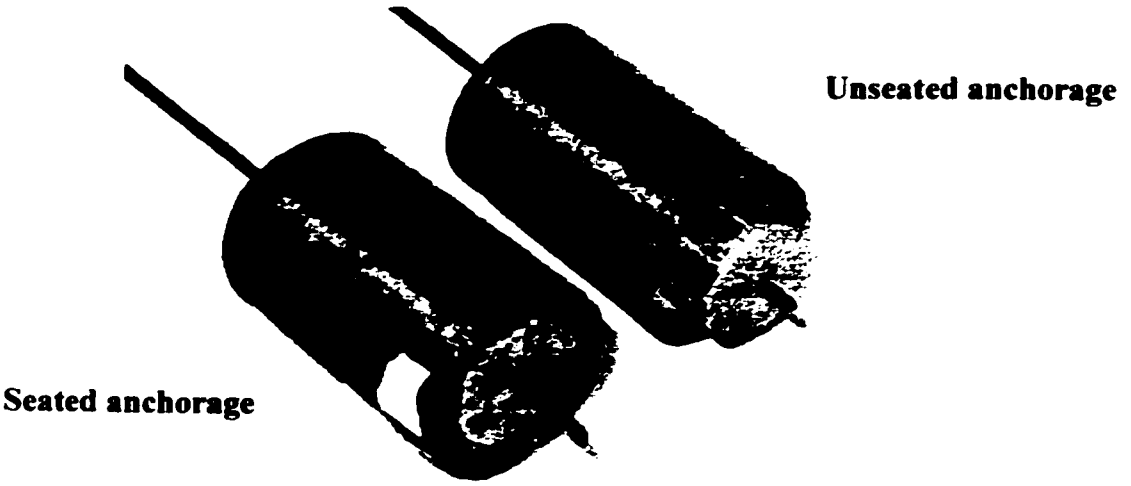

Figure [5.11]: Wedge displacement during anchorage seating.

Two seating displacements can be identified: Δ_1 which is the wedge displacement from the lightly placed initial assembly position to the wedge position after the seating load is applied and Δ_2 which is the wedge displacement between the initial seating and the final position after the tendon has been loaded to its maximum loading capacity or up to failure. Figure [5.11] shows the wedge displacement during anchorage seating (Δ_1). The effect of the seating load on anchorage performance was examined in phase I of the experimental programme.

5.5.2. Phase I

Short-term tensile strength tests were performed with the non-metallic anchorage system anchoring single 8 mm Leadline™ tendon at one end and the steel anchorage developed by Sayed-Ahmed and Shrive [1998] anchoring the other end. In this phase, 15 tests were performed. Table [5.3] gives the different testing parameters examined in phase I.

The 15 tests were divided into three sequential testing groups. In the first group, the initially proposed anchorage dimensions were used with 30 kN seating load and different number of layers of CFRP sheets (Tests 1 to 5). In the second group, the anchorage dimensions were optimized with 4 CFRP layers and the 30 kN seating load (Tests 6 to 10). In the third group, the optimized dimensions of the anchorage were used with 4 CFRP layers: different seating loads of 30, 40, 50, 60 and 65 kN were examined (test 11 to test 15). In the third group the tensile strains of the CFRP sheets were monitored using MM™ (Micro Measurements) strain gauges glued on the outer layer of CFRP sheet.

The tension tests were performed using a Material Testing System (MTS) machine with a load range of 100 kN and a stroke range of ±75 mm with a calibrated accuracy of ± 0.5% throughout the selected range. The load was applied in a load control through a closed-loop system. The rate of loading applied was 0.5 kN/second providing the maximum load within 3 ½ minutes. In each test, the ultimate failure load and the mode and location of failure were recorded.

Table [5.3]: Testing parameters examined in phase I.

Test #	l_B mm	d_{Bt} mm	d_{Bb} mm	l_W mm	d_{Wt} mm	d_{Wb} mm	N^* layers	P_{test} kN
	Proposed Barrel and Proposed Wedges							
1	179.0	76.0	63.5	182.8	77.8	64.4	0	30
2	178.2	75.6	63.2	183.0	78.1	64.4	2	30
3	179.0	76.0	63.0	184.2	78.1	64.6	3	30
4	183.0	76.5	63.7	182.8	77.8	64.4	4	30
5	183.4	76.1	63.3	183.0	77.6	64.2	5	30
	Large Barrel and Proposed Wedges							
6	179.2	80.0	67.4	183.0	78.1	64.4	4	30
7	177.8	80.0	67.6	183.6	77.7	64.3	4	30
	Medium Barrel and Proposed Wedges							
8	178.0	76.5	64.1	184.2	78.1	64.6	4	30
	Medium Barrel and Small Wedges							
9	179.4	76.3	63.8	172.0	75.6	63.0	4	30
	Proposed Barrel and Small Wedges							
10	179.0	76.0	63.5	174.8	76.2	63.4	4	30
	Medium Barrel and Proposed Wedges							
11	180.0	76.5	63.9	183.6	77.7	64.3	4	30
12	178.0	76.5	64.1	184.2	78.1	64.6	4	40
13	179.4	76.7	64.2	182.8	77.8	64.4	4	50
14	180.0	76.6	64.0	182.0	77.4	64.1	4	60
15	180.0	76.5	63.9	183.6	77.7	64.3	4	65

*** N is the number of CFRP Replark™ sheet layers used to reinforce the anchorage.**

5.5.3. Phase II

The anchorage dimensions, the seating load and the number of CFRP sheet layers used in this phase were determined from analysing the results of phase I. Table [5.4] gives the different parameters used in phase II including average anchorage dimensions, the number of layers of CFRP sheets and the seating load. Changes in the dimensions in the range of ± 1.0 % were observed in the tested non-metallic anchorages.

Table [5.4]: Anchorage parameters used throughout phase II.

Parameter	l_g	d_{gs}	d_{gb}	l_w	d_{w1}	d_{w5}	N^*	P_{seat}
	mm	mm	mm	mm	mm	mm	layers	kN
	180.0	76.5	63.9	183.6	77.7	64.3	4	65

5.5.3.1. Short-term tensile strength testing

Short-term tensile strength tests were performed on the non-metallic anchorage system with a single 8 mm Leadline™ CFRP tendon. Two series of short-term tensile testing were performed. The first series involved testing of the new non-metallic anchorage at one end with the steel anchorage developed by Sayed-Ahmed and Shrive [1998] at the other end [Figure 5.12 [a]]. The second series was tested with the non-metallic anchorage at both ends [Figure [5.12 [b]]. In the first series, four non-metallic anchorages were tested while in the second series eight non-metallic anchorages were tested.

5.5.3.1.1. Test set-up and instrumentation

All Leadline™ tendons tested had lengths greater than 1200 mm. Strains of the CFRP sheets wrapping the outer circumference of the non-metallic anchorage were measured using MM™ (Micro Measurements) strain gauges. A similar gauge was attached to CFRP tendon in its mid third. The strain gauges for the CFRP sheets and the tendon were connected to a data acquisition equipment which was linked to a computer system. Figures [5.13] shows a schematic representation of the short-term tensile strength test set-up.

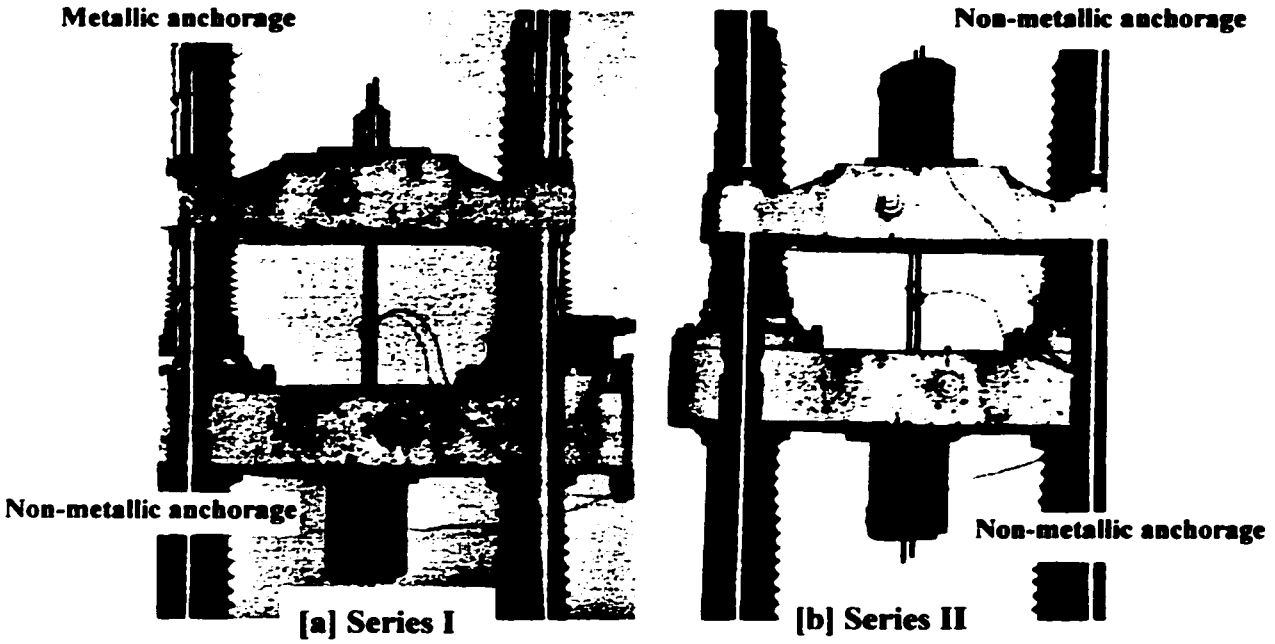

Figure [5.12]: Short-term tensile strength testing [a] series I and [b] series II.

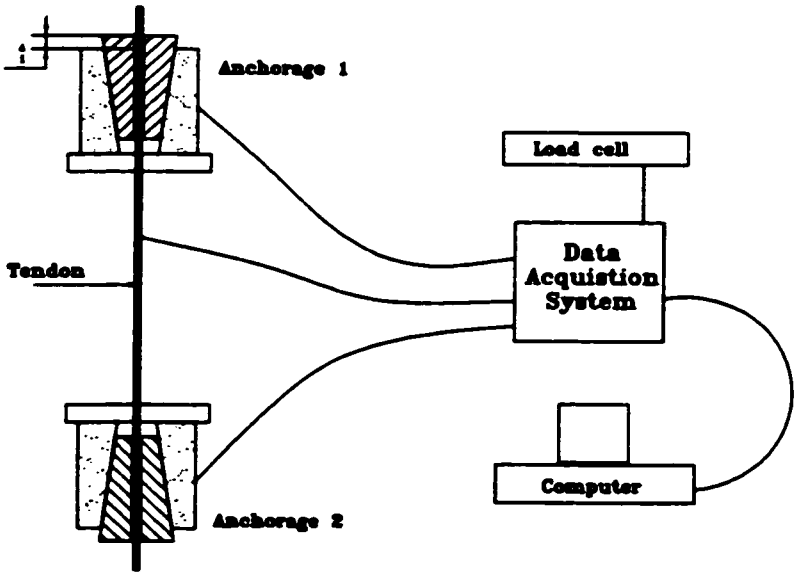

Figure [5.13]: Schematic representation of the short-term tensile strength testing.

A Tinius Olsen universal testing machine was used to apply the tension load. A loading capacity of 300 kN was selected with a calibrated accuracy of ± 0.5% throughout the selected range. Load was applied in load control through a closed-loop system. The rate of loading applied was 0.5 kN/second providing the maximum load within 3 ½ minutes. The output of load and stroke readings was recorded using the data acquisition system. The output data was collected continuously throughout the test at 5 HZ sampling rate. The ultimate tensile load, the location and mode of failure and the wedge displacements ($\Delta_{1 \text{ and } 2}$) were recorded in each test. Readings of the wedge displacement Δ_2 were recorded each 30 kN during loading.

5.5.3.2. Fatigue strength testing

The purpose of the fatigue test was to determine the capacity of the tendon-anchorage assemblies under force fluctuation as an indication of durability and reliability of the system. The evaluation of the fatigue behaviour of the non-metallic anchorage requires the application of cyclic loading on the tendon-anchorage assembly. Two series of testing were performed. In series I, the non-metallic anchorage was at one end with a steel anchorage at the other end [Figure 5.14 [a]]. In series II, non-metallic anchorages were used at both ends [Figure 5.14 [b]]. Two tests were applied in each series giving a total number of six non-metallic anchorages. This complies with the latest CEB-FIP requirements [Rostásy 1998].

5.5.3.2.1. Test set-up and instrumentation

All the fatigue tested Leadline™ tendons were of length greater than 1500 mm. Strains of the CFRP sheets wrapping the outer circumference of the non-metallic anchorage and the tendon were measured using MM™ (Micro Measurements) strain gauges. The strain gauges for the CFRP sheets and the tendon were connected to the data acquisition system which was linked up to a computer system.

The fatigue test was performed using the MTS machine with a load range of ±100 kN and a stroke range of ± 75 mm with a calibrated accuracy of ± 0.5% throughout the selected range. The anchorage was seated first and then the cyclic tension load was applied to the tendon-anchorage assembly. The load was applied in conformance with the PTI standards [PTI 1985]. In this test a total number of 5×10^5 cycles was applied to the tendon- anchorage

assemblies. The application of these cycles was in the following sequence:

1- 500,000 cycles fluctuating between 60-66% of the nominal tendon strength [62 to 68 kN].

2- 50 cycles fluctuating between 50-80% of the nominal tendon strength [52 to 83 kN].

3- A static tension test up to the 95% of the nominal tendon strength [99 kN].

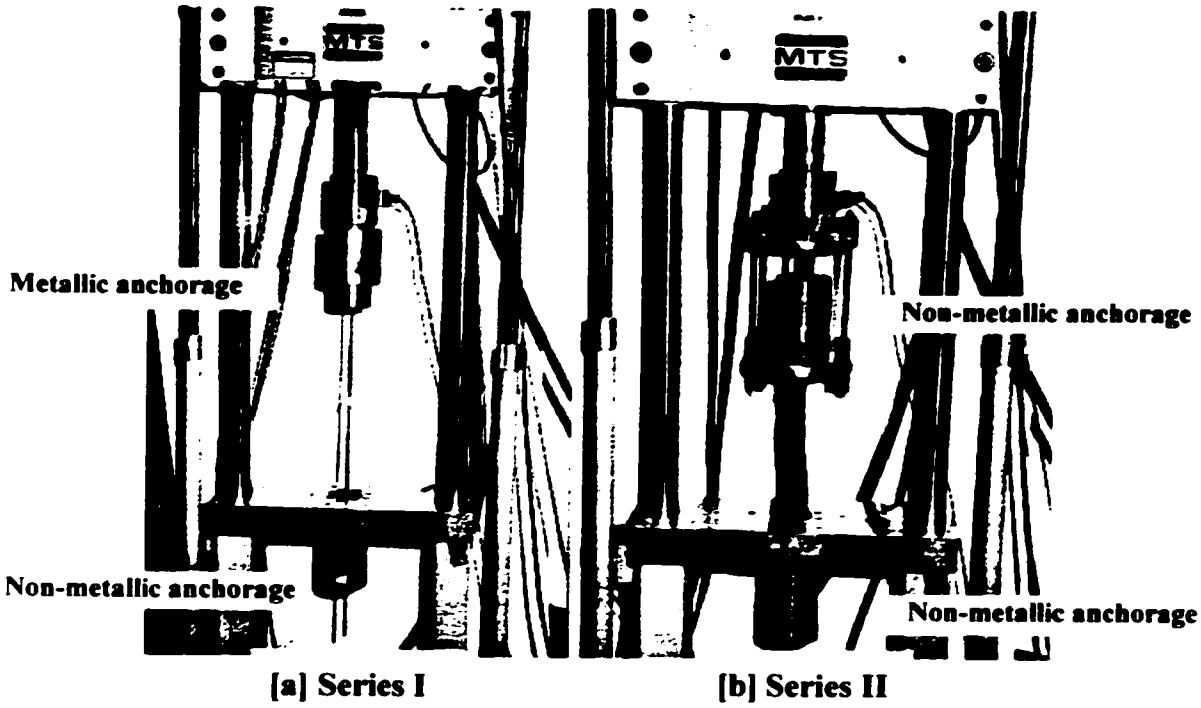

Figure [5.14]: Fatigue strength testing [a] series I and [b] series II.

The output of load and stroke readings was recorded using the data acquisition system. The output data were collected continuously throughout the test at a 0.1 second sampling rate for 10 seconds recorded at 30 minute time intervals. The ultimate tensile load, the location and mode of failure were recorded in each test.

5.6. Test results

5.6.1. Phase I

Table [5.5]: Phase I: short-term tensile strength test results.

Test #	Pult kN	η %	Mode and location of failure
	Proposed Barrel and Proposed Wedges		
1	6	5.7	Barrel cracking [Figure 5.7]
2	30	28.8	Tension failure of the barrel and the CFRP sheets
3	66	63.5	Barrel failure and wedge cracking followed by tendon slip
4	76	73.1	Wedge cracking followed by tendon slip
5	70	67.3	Wedge cracking followed by tendon slip
	Large Barrel and Proposed Wedges		
6	70	67.3	Tendon slip from the non-metallic anchorage
7	66	63.4	Tendon slip from the non-metallic anchorage
	Medium Barrel and Proposed Wedges		
8	72	69.2	Tendon slip from the non-metallic anchorage
	Medium Barrel and Small Wedges		
9	65	62.5	Tendon rupture at the non-metallic anchorage
	Proposed Barrel and Small Wedges		
10	75	72.1	Wedge cracking followed by tendon slip
	Medium Barrel and Proposed Wedges		
11	70	67.3	Tendon slip at the non-metallic anchorage
12	76	73.1	Tendon slip at the non-metallic anchorage
13	89	85.6	Tendon slip at the steel anchorage
14	92	88.5	Tendon rupture at steel anchorage
15	99.2	95.3	Tendon rupture at non-metallic anchorage

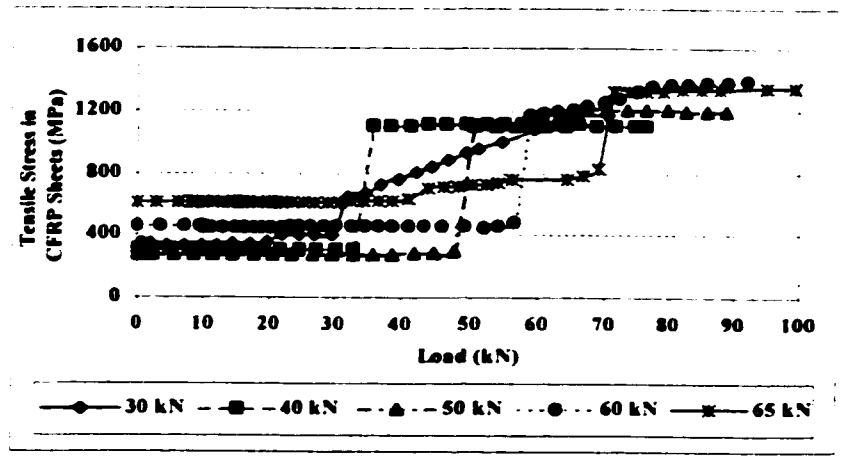

Figure [5.15]: Effect of seating load on the tensile stresses of CFRP sheets. Figure shows the increase in stress in the CFRP sheets when the tendon and the wedges seated themselves as the load exceeded the seating load .

5.6.2. Phase II

5.6.2.1. Short-term tensile strength test results

Table [5.6]: Phase II: short-term tensile strength test results.

Test #	Δ_1	Δ_2	P_{ult}	η	Mode of failure
	mm	mm	kN	%	
	Series I (Non-metallic anchorage - Steel Anchorage)				
1	22.6	6.8	97.9	94.1	Tendon slip from steel anchorage
2	18.7	5.8	99.2	95.3	Tendon rupture in its free length
3	20.9	6.0	99.2	95.3	Tendon rupture at non metallic anchorage
4	19.1	6.4	99.4	95.5	Tendon rupture at steel anchorage
	Series II (Non-metallic anchorage both sides)				
5	17.3/14.2*	5.5/7.2*	98.7	94.9	Tendon rupture at anchorage 1
6	21.7/17.5	5.4/5.3	99.7	95.9	Tendon slip at anchorage2
7	16.2/18.5	6.8/6.2	102.8	98.8	Tendon rupture at free length
8	14.6/16.4	7.0/6.1	101	97.1	Tendon rupture at anchorage 1

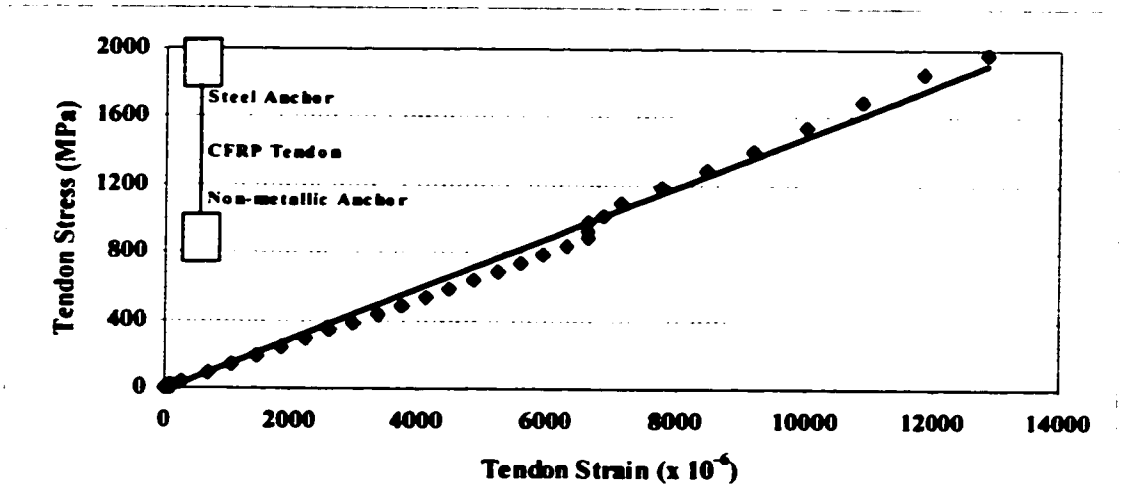

Figure [5.16]: Typical tensile stress-strain of the CFRP Leadline™ [Series I].

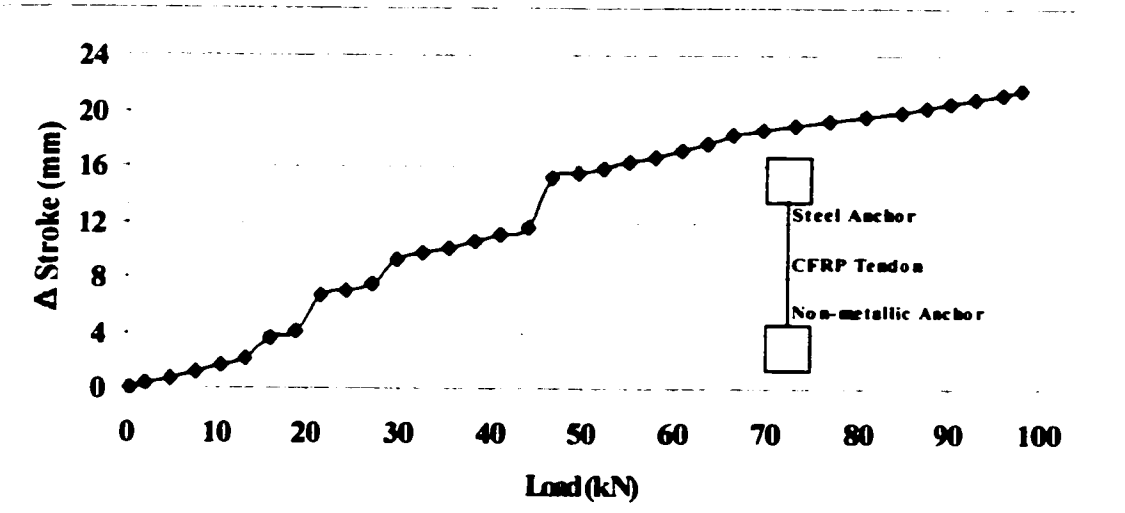

Figure [5.17]: Typical load-stroke in tension showing increase in stroke when the tendon and the wedges seated themselves as the load exceeded 45 kN (70 % of the seating load of 65 kN) [Series I].

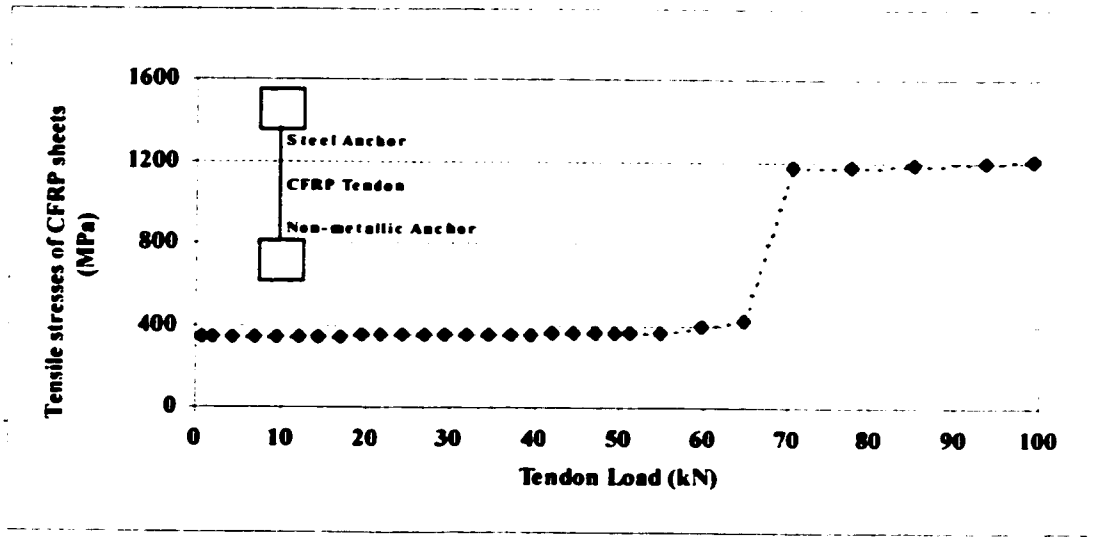

Figure [5.18]: Typical load Vs. tensile stress in CFRP sheets showing increase in the stress of the CFRP sheets when the tendon and wedges seated themselves as the load exceeded the seating load of 65 kN [Series I].

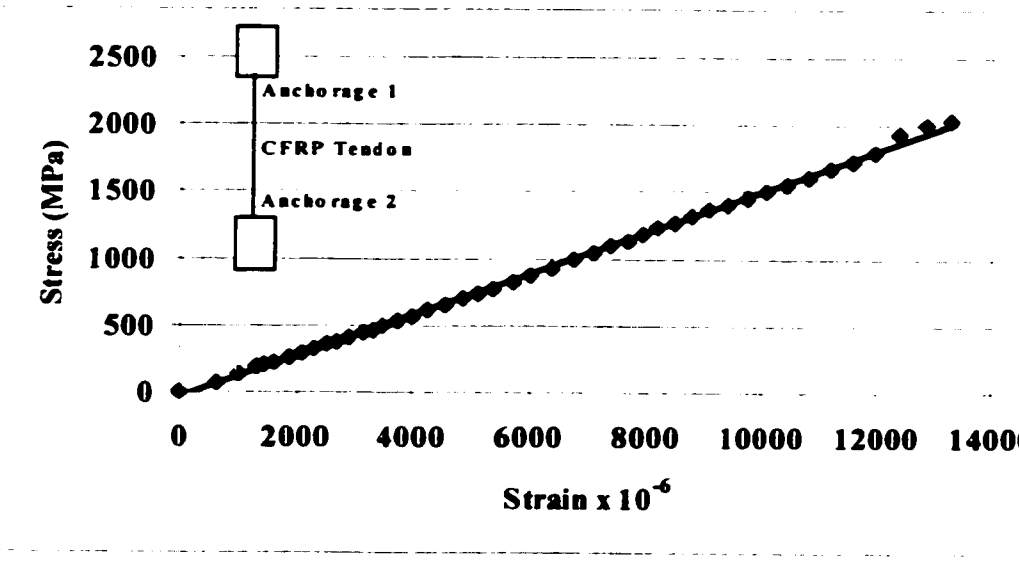

Figure [5.19]: Typical tensile stress-strain of the CFRP Leadline™ [Series II].

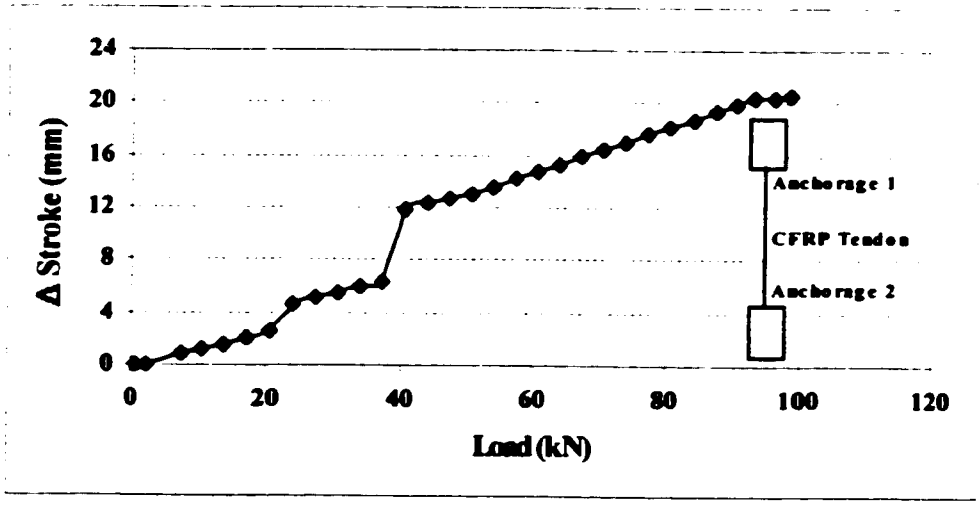

Figure [5.20]: Typical load-stroke in tension showing increase in stroke when the tendon and the wedges seated themselves as the load exceeded 45 kN (60 % of the seating load of 65 kN) [Series II].

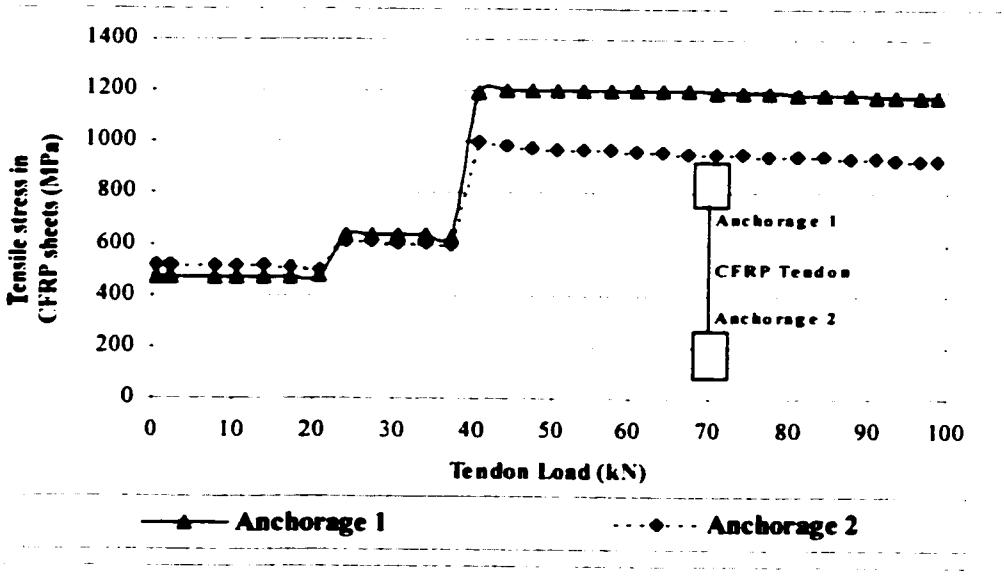

Figure [5.21]: Typical load Vs. tensile stress in CFRP sheets showing increase in the stress of the CFRP sheets when the tendon and wedges seated themselves as the load exceeded the seating load of 45 kN (60 % of the seating load of 65 kN) [Series II].

5.6.2.2.Fatigue test results

Table [5.7]: Phase II: fatigue strength test results.

Test #	Pult kN	η %	Test Result	Mode of failure
	Series I (Non-metallic Anchorage - Steel Anchorage)			
1	99	95.2	Passed	Tendon rupture at free length
2	96.3	92.6	Failed	Tendon rupture at non-metallic anchorage
	Series II (Non-metallic Anchorage both sides)			
3	99.8	96.0	Passed	Tendon rupture at anchorage 1
4	100	96.2	Passed	No failure up to maximum capacity of the machine

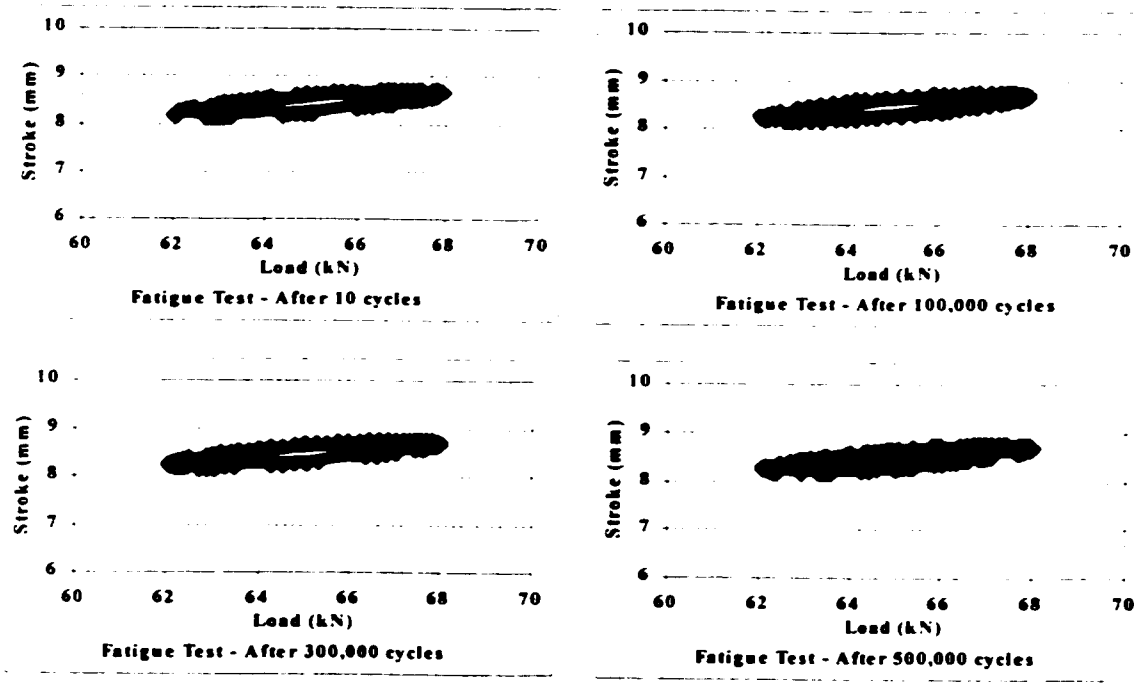

Figure [5.22]: Typical load-stroke in cyclic loading [Step 1- Series I].

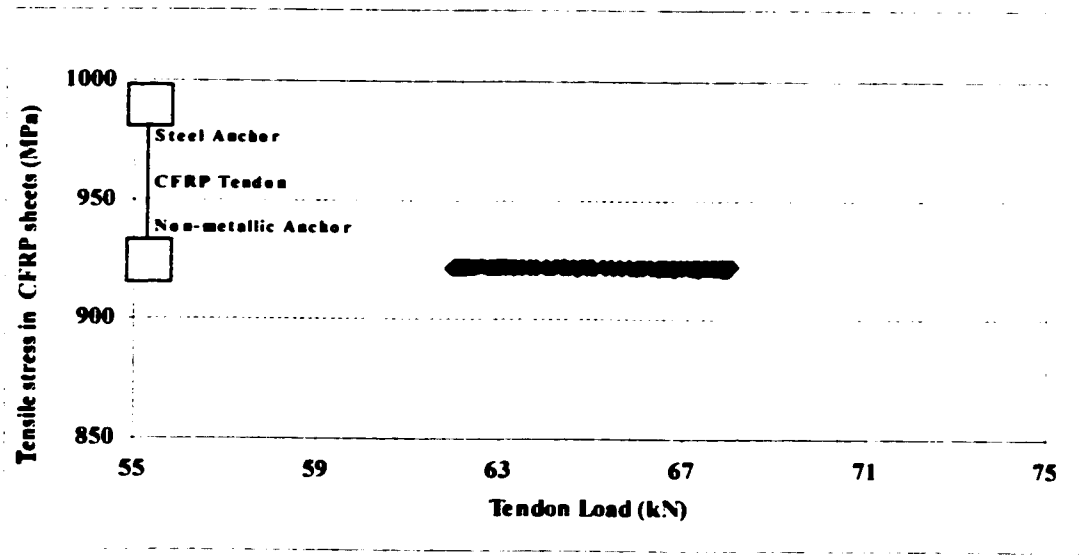

Figure [5.23]: Load Vs. tensile stress in CFRP sheets [Step 1 - Series I].

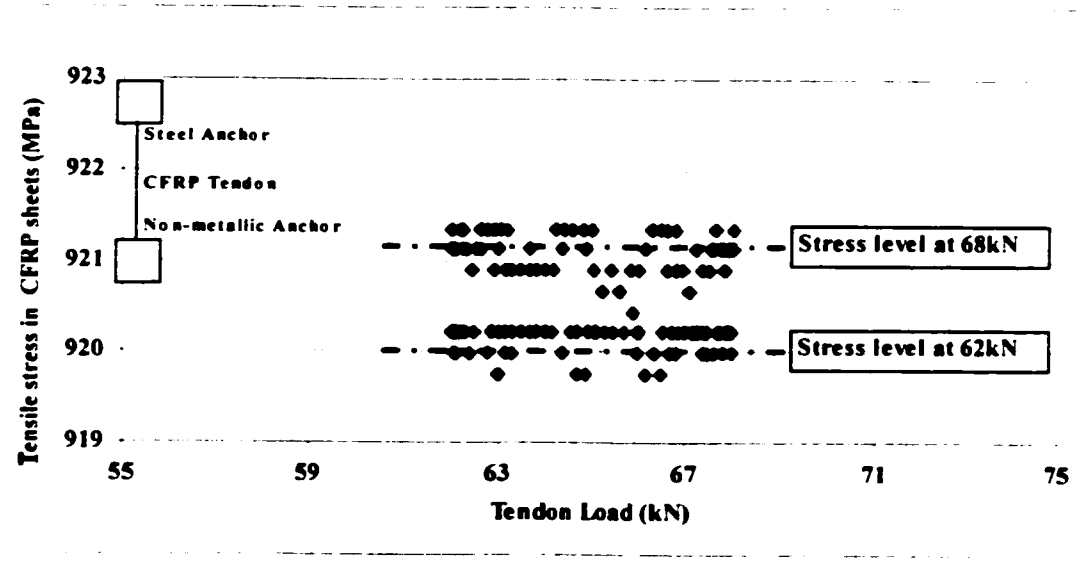

Figure [5.24]: Narrow stress scale showing the fluctuations of the tensile stress of the CFRP sheets during cyclic loading [Step 1- Series I].

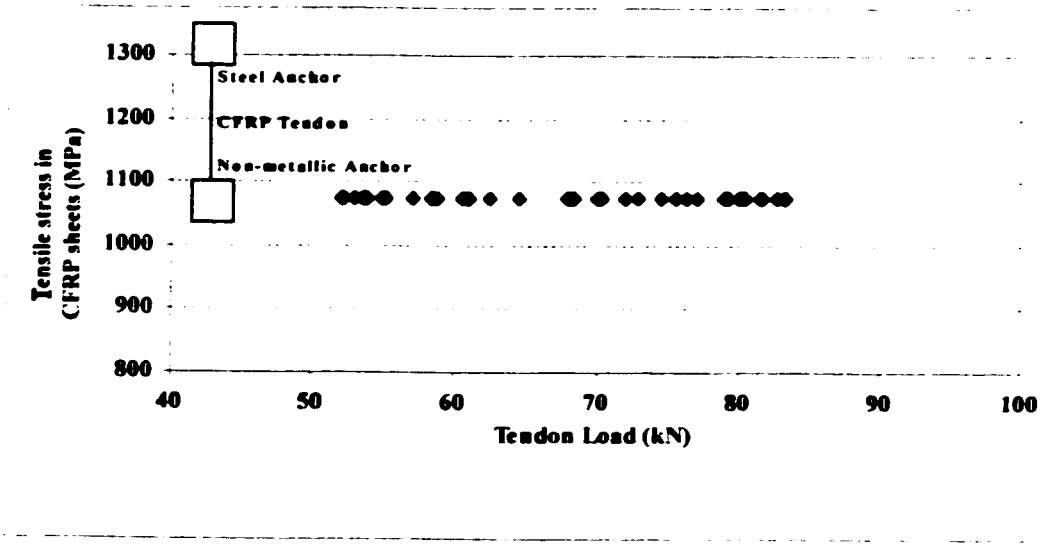

Figure [5.25]: Typical Load Vs. tensile stress in CFRP sheets [Step 2 - Series I].

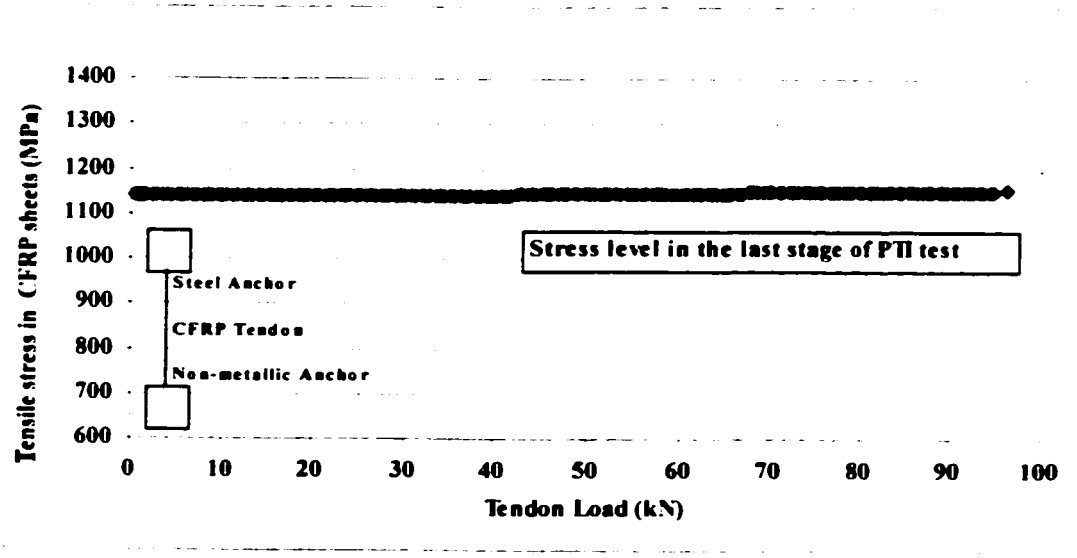

Figure [5.26]: Typical Load Vs. tensile stress in CFRP sheets [Step 3 - Series I].

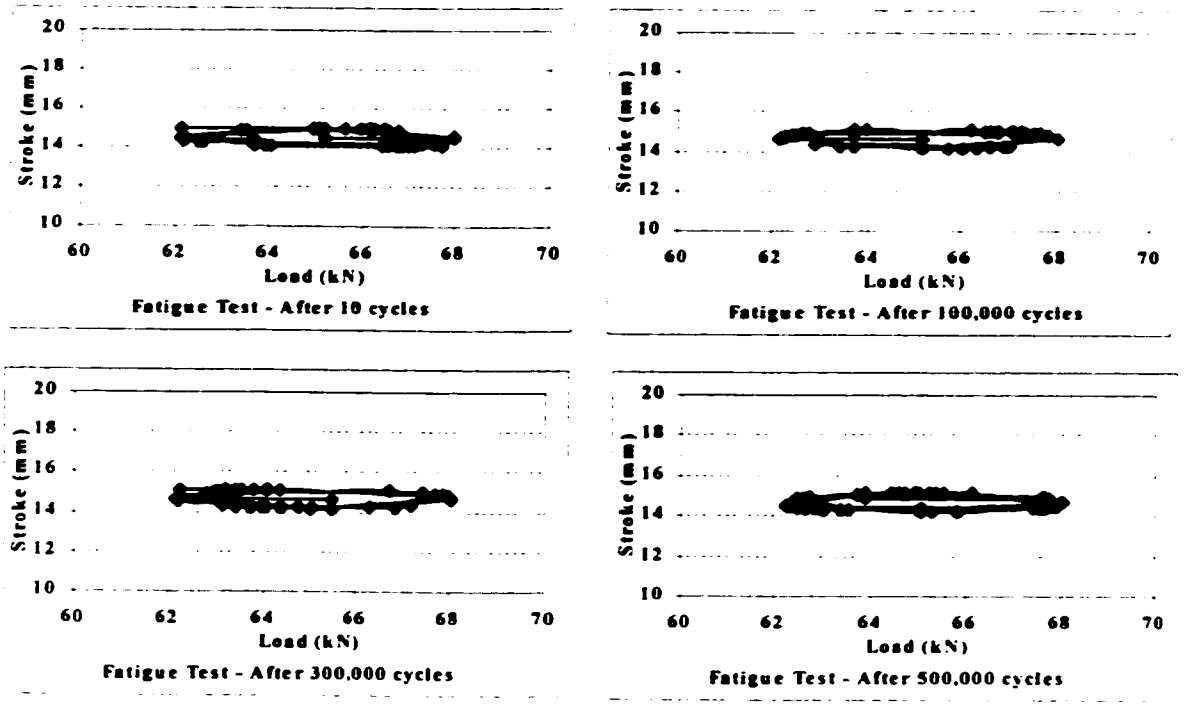

Figure [5.27]: Typical load-stroke in cyclic loading [Step 1 - Series II].

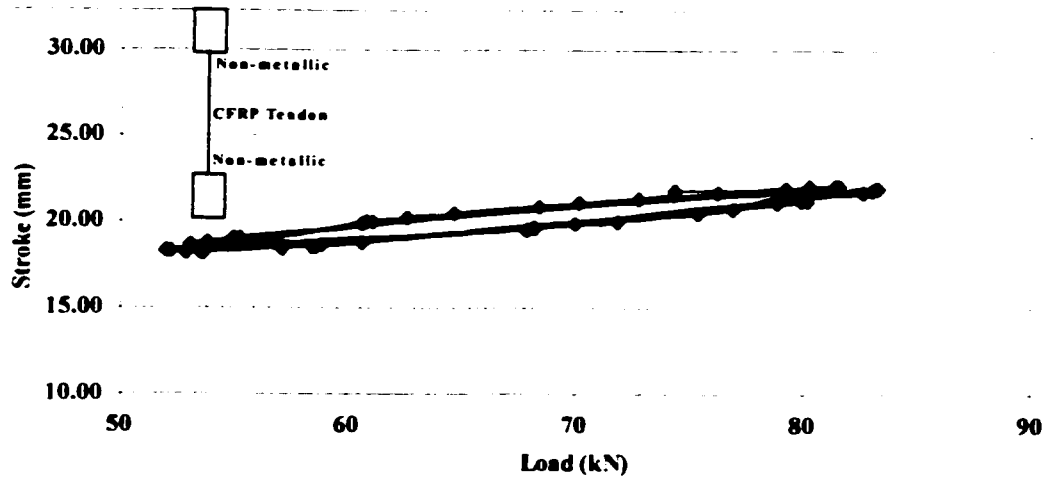

Figure [5.28]: Typical load-stroke in cyclic loading [Step 2 - Series II].

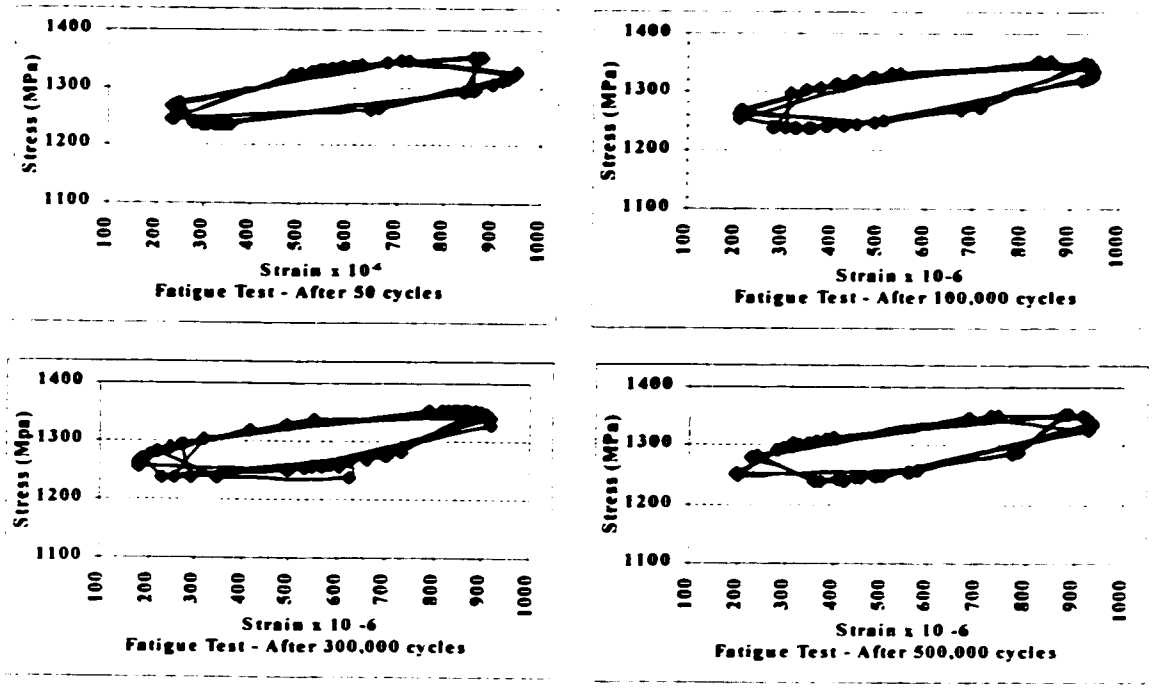

Figure [5.29]: Typical stress-strain of Leadline™ in cyclic loading [Step 1 - Series II].

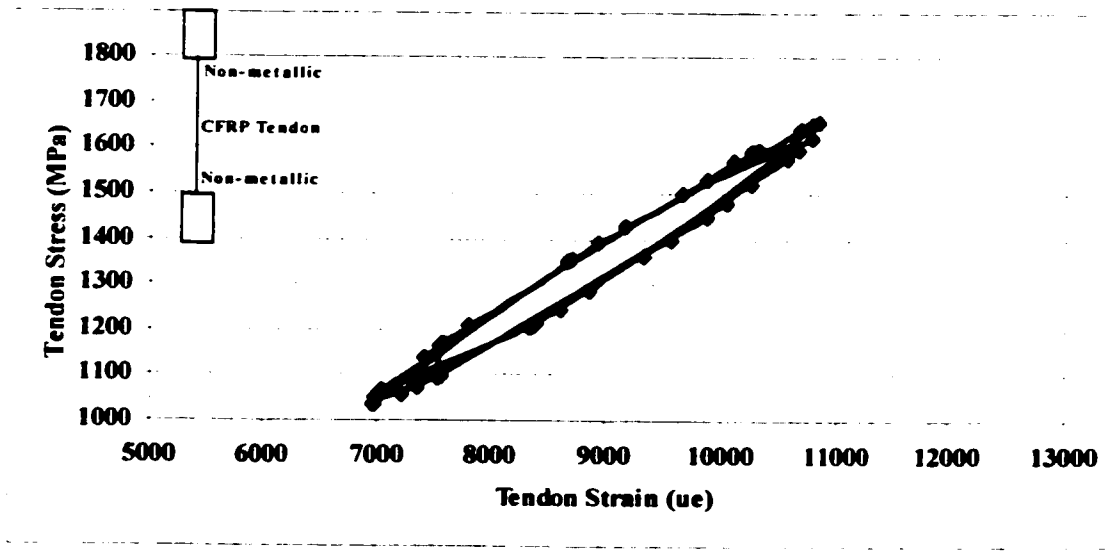

Figure [5.30]: Typical stress-strain of Leadline™ in cyclic loading [Step 2 - Series II].

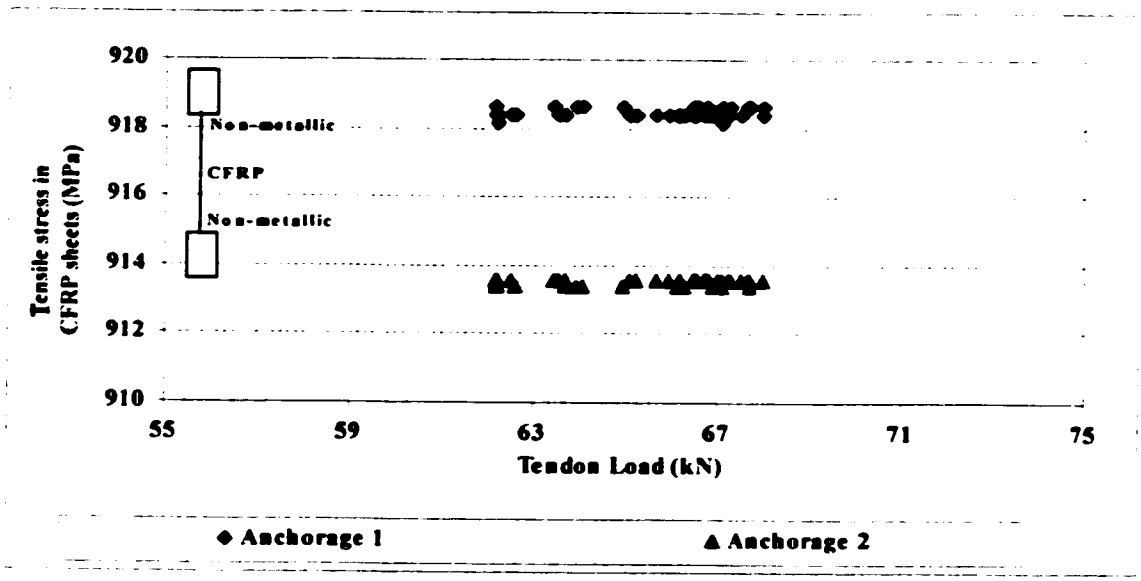

Figure [5.31]: Typical load Vs. tensile stress in CFRP sheets [Step 1- Series II].

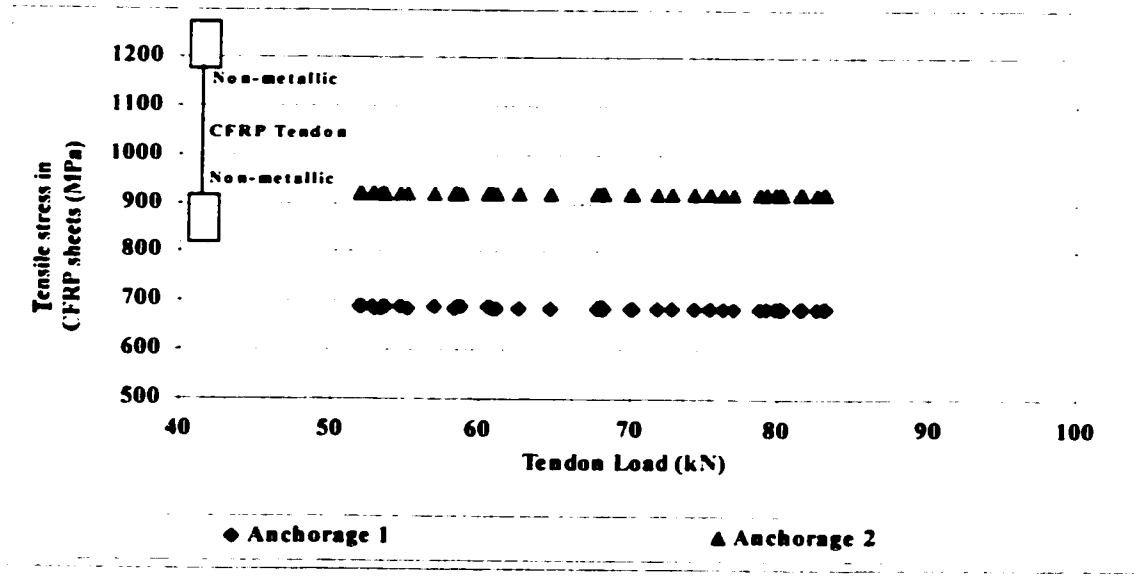

Figure [5.32]: Typical load Vs. tensile stress in CFRP sheets [Step 2 - Series II].

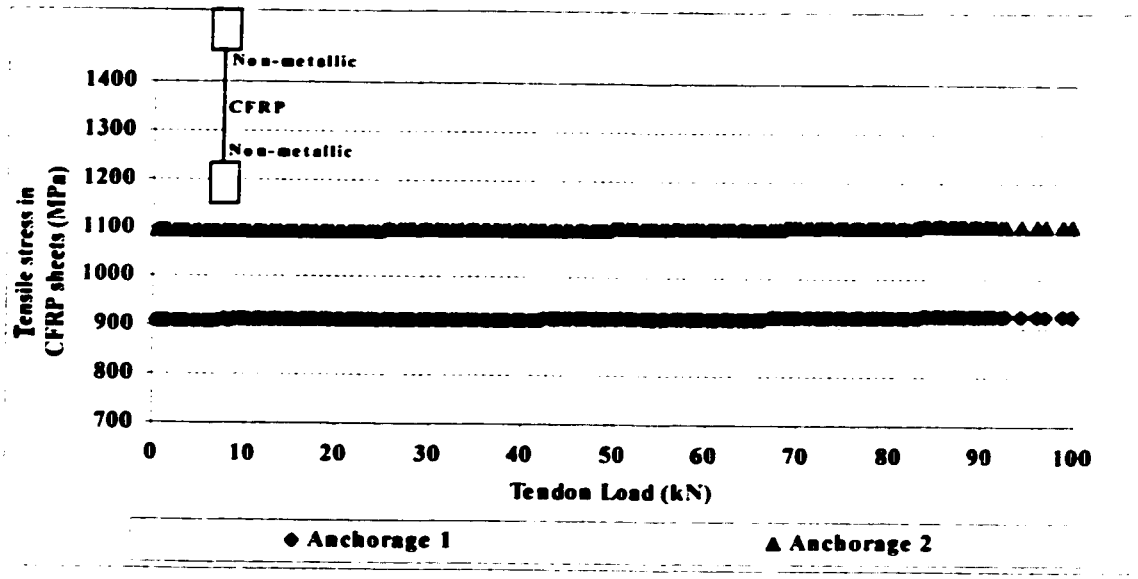

Figure [5.33]: Typical load Vs. tensile stress in CFRP sheets [Step 3 - Series II].

5.7. Analysis and discussions

5.7.1. Phase I

5.7.1.1. Determination of number of CFRP sheet layers

In the first testing group (Tests 1 to 5) the number of CFRP sheet layers required to reinforce the barrel was determined. When no reinforcement was used, the outer barrel was cracked during seating and the cracked barrel showed a load capacity of 6 kN only [Figure 5.7]. An increase of five to ten times of this carrying capacity was achieved when the barrel was wrapped with two and three layers respectively. However in both cases the CFRP sheets ruptured and the barrel failed governing the anchorage load carrying capacity. Figure [5.34] shows a comparison between the experimental and analytical load carrying capacity of the non-metallic anchorage reinforced with 0, 2, 3, 4 and 5 layers of CFRP sheets. The analytical values are based on the static model used in the preliminary design [Figure 5.2].

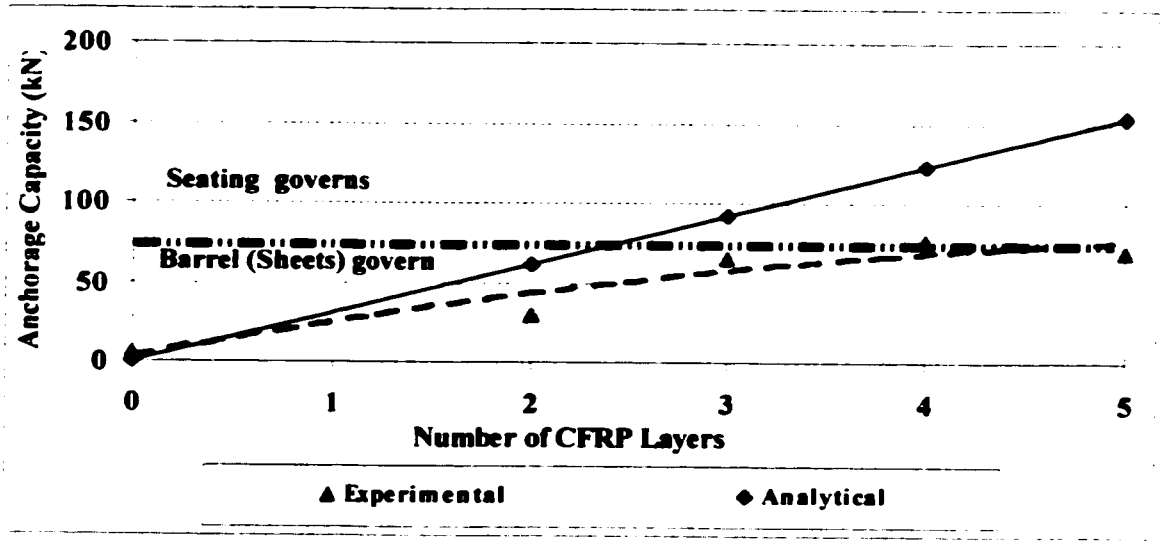

Figure [5.34]: Effect of changing the number of CFRP layers on the carrying capacity of the non-metallic anchorage.

When the anchorage was wrapped with four CFRP layers, the anchorage failed at a tendon load of 76 kN due to cracking of the wedges. Using four CFRP layers or more the barrel will not govern the carrying capacity of the anchorage. The use of five layers of sheets to wrap the barrel did not provide any further increase of the load carrying capacity and the same mode of failure was observed. Therefore, four layers of CFRP Replark™ sheets were required to reinforce the anchorage barrel. This number of CFRP layers was used in the subsequent testing groups of this phase and following phases. Although tiny cracks could be observed in the upper concrete surface of the wrapped barrels when the tendon was loaded, these cracks showed no effect on the anchorage capacity either in tension or in fatigue tests.

5.7.1.2. Optimization of the anchorage geometry.

The second testing group (Tests 6 to 10) was performed to optimize the anchorage geometry so that the wedges are not crushed up to the ultimate tendon capacity. The change in the barrel dimensions was enacted through changing the inner hole diameter by using

different conical parts in the barrel mould. The production of smaller wedges compared to the proposed ones was also performed by changing the wedges' mould head cap, using deeper grooves than that used with the proposed wedge dimensions.

Three barrel types were tested: proposed, large and medium. There were two wedge types: proposed and small [Table 5.3]. Using the proposed barrels and proposed wedges resulted in cracking of the wedges. When large barrels were used with the proposed wedges tendon slip took place. Tendon rupture happened when the medium barrel was used with small wedges while wedge cracking happened again when the proposed barrel was used with smaller wedges. The selection of working anchorage dimensions based on the test results depended on both the maximum attained anchorage capacity and the mode of failure. The optimum combination took place when medium barrel was used with the proposed wedges. No failure of the anchorage was observed but tendon slip occurred. This was attributed to the low seating load of 30 kN used with this testing group. The optimum anchorage dimensions are given in Table [5.4] and shown in Figure [5.35].

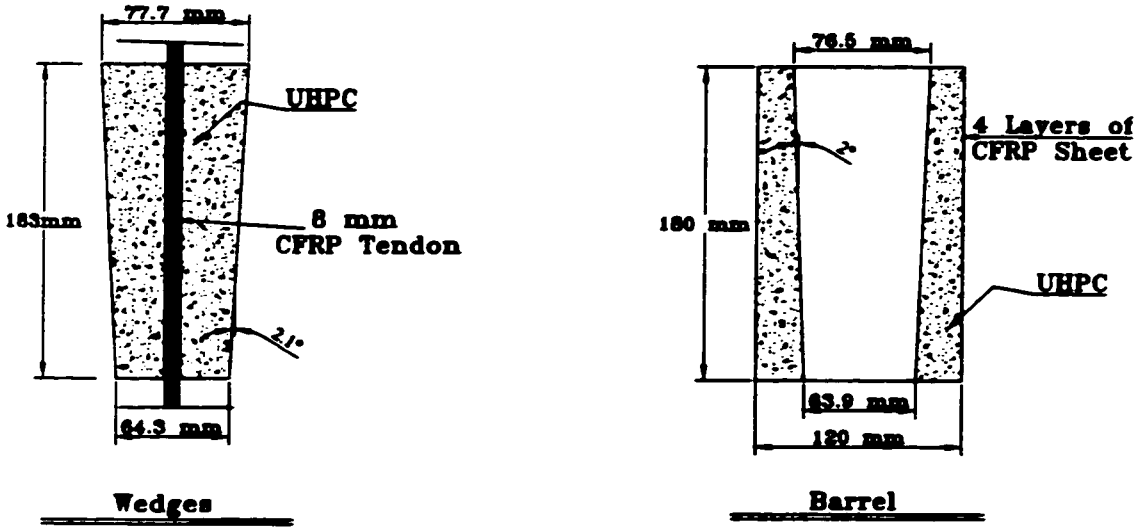

Figure [5.35] Optimized dimensions of the non-metallic anchorage system.

5.7.1.3. Determination of wedge seating load

Optimizing the anchorage dimensions prevent the wedge cracking but showed tendon slip. Increasing the seating load (Test 11 to 15) from 30 kN to 65 kN increased the anchorage carrying capacity to 98 kN and provided the required pressure around the tendon so that tendon rupture rather than tendon slip happened. The increase of the seating load was accompanied by an increase of the wedges' seating displacement (Δ_1)and a reduction of the wedge displacement during loading(Δ_2).

However, increasing the seating load affected the CFRP sheets. When the seating load is applied the sheets are tensioned and when the load is released the sheets continue to be tensioned (prestressed) exerting a confining pressure on the concrete barrel. Applying the tendon load, the sheets and the concrete would not be stressed until the applied load exceeds the seating load. Figure [5.15] shows that changing the seating load resulted in a change of the tendon load needed to provide a rise in the stress (strain) in the CFRP sheets. Having the service load of the Leadline™ in the range of 65 % of the nominal strength of the tendon (67 kN) means applying a seating load of 65 kN will provide no increase in the stress of the sheets throughout service life and full confinement of the barrel. With the optimum number of CFRP sheet layers and the anchorage dimensions, and a high seating load the anchorage was able to show an efficiency factor (η) of 95 %. This is a basic requirement of prestressing anchorage systems [section 2.3.3]. The production parameters determined in this phase were used in subsequent testing phases.

5.7.2. Phase II

The purpose of this phase was to evaluate the mechanical performance of the non-metallic anchorage system.

5.7.2.1. Short-term tensile strength

In phase II eight tests involving twelve non-metallic anchorages were performed examining the short-term tensile strength. These tests were divided in two series as shown in Table [5.6]. With the exception of two anchorages, an efficiency factor in excess of 95% was achieved in phase II. The two failed anchorages showed efficiency factors of 94.1 and 94.9%.

Figure [5.36] shows a histogram of the efficiency factor of the tested non-metallic anchorages. A statistical analysis of the anchorage testing is provided in appendix [C].

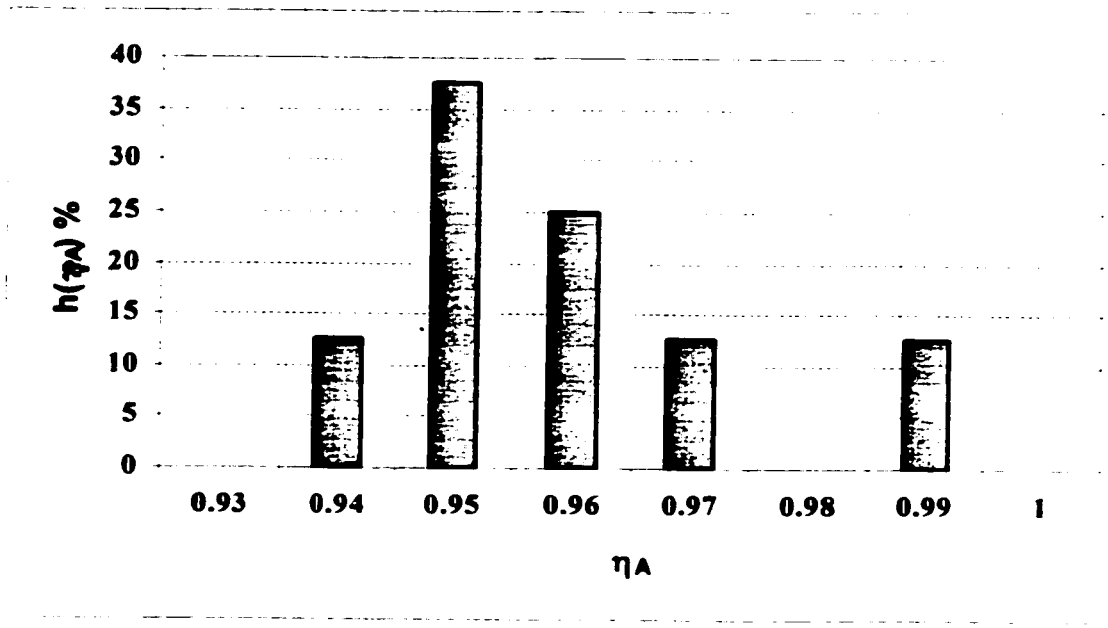

Figure [5.36]: Histogram of short-term tension test of the non-metallic anchorage.

The Leadline™ showed an average elastic moduli of 150 GPa in series I and 153 GPa in series II [Figures 5.16 and 5.19]. These values are higher than the 142 GPa elastic modulus reported in the literature [Table 2.3]. Average ultimate strains of 1.28% and 1.33% were observed in series I and series II respectively which are similar to ultimate strains reported in the literature [Table 2.3]. The non-metallic anchorage showed a load-stroke relation [Figures 5.17 and 5.20] similar to that reported by other anchorages [Sayed-Ahmed and Shrive 1998].

Table [5.6] gives the seating displacement Δ_1 of the wedges after the seating load is applied and Δ_2 the additional displacement after the test was performed up to failure. An average wedge seating displacement Δ_1 of 18 mm was observed [Table 5.6]. Readings of the wedge displacement Δ_2 were recorded at each 30 kN during loading. The final wedge displacement Δ_2 ranged from 5.3 to 7.0 mm with an average of 6.2 mm. This wide range of the

observed seating displacements can be explained by the ± 1% dimensional changes of the anchorage components used in this phase [5.5.3 and Table 5.4]. Tiny changes of the anchorage dimensions would result in a considerable change in seating displacement.

However with a seating load of 65 kN, no wedge displacement was recorded when the tendon/anchorage assembly was loaded up to 70-90% of the seating load. When further load was applied considerable additional displacement was observed especially before failure. Higher seating loads may result in a lower wedge displacements compared to the values observed with a 65 kN seating load. However, higher seating loads may result in premature cracking of the wedges. In post-tensioning applications the tendon stress would not exceed 65% of its nominal strength (67 kN) which will result in a small additional wedge displacement with a seating load of 65 kN.

Observing the development of the tensile stresses[1] in the CFRP sheets provided a view of the anchorage behaviour during tendon loading. Increasing the tendon load did not result in any change of the tensile stresses of the CFRP sheets till the tendon load exceeded at least 70 % of the seating load (45 kN) as shown in Figures [5.18 and 5.21] for series I and series II respectively. All the individual testing graphs are provided in appendix (C). When the tendon load exceeded 80 % of its nominal strength (83 kN) the stresses in the CFRP sheets did not exceed 50% of the nominal strength. This means that although the four layers of CFRP are needed to provide confinement of the concrete barrel, the sheets are not being exploited to their maximum tensile capacity. Comparison of the tensile stresses predicted by the proposed statical model [5.3] to the experimental values showed the analytical values to be much larger than the experimental values. This difference is related to the non-linearity of concrete while the model is built on linear assumptions in addition to the model assumption that the sheets strength will usually govern the anchorage capacity. This assumption did not happen when 4 CFRP layers or more were used. The reduction of stresses of the CFRP sheets can also be explained by the effect of seating load applied to the anchorage before loading [5.7.13]. Figure [5.37]

---

[1] **Tensile stress = Measured tensile strain . E**

shows this comparison between the experimental and analytical values of tensile stresses developed in the CFRP sheets during tendon loading.

No failure of the barrel was observed in any of the non-metallic anchorages examined in phase II. Cracking of the wedges was observed only once [anchorage 2, test 6].This was followed by tendon slip at a load of 99.7 kN. The dominant failure modes are either tendon rupture in its free length [test 2 and 7] or tendon rupture at the anchorage end after exceeding the 95% efficiency load [Test 3, 4, 5, and 8]. It is important to mention that even when tendon rupture happened in the free length, it happened near an anchorage rather than in the middle third of the tendon length. Tiny cracks of the tendon near the anchorage zone were usually observed with all modes of failure. Tendon failure usually began by tiny cracks, fibres splintering followed by sudden catastrophic failure. This sudden failure is attributed to the brittleness of the CFRP tendon.

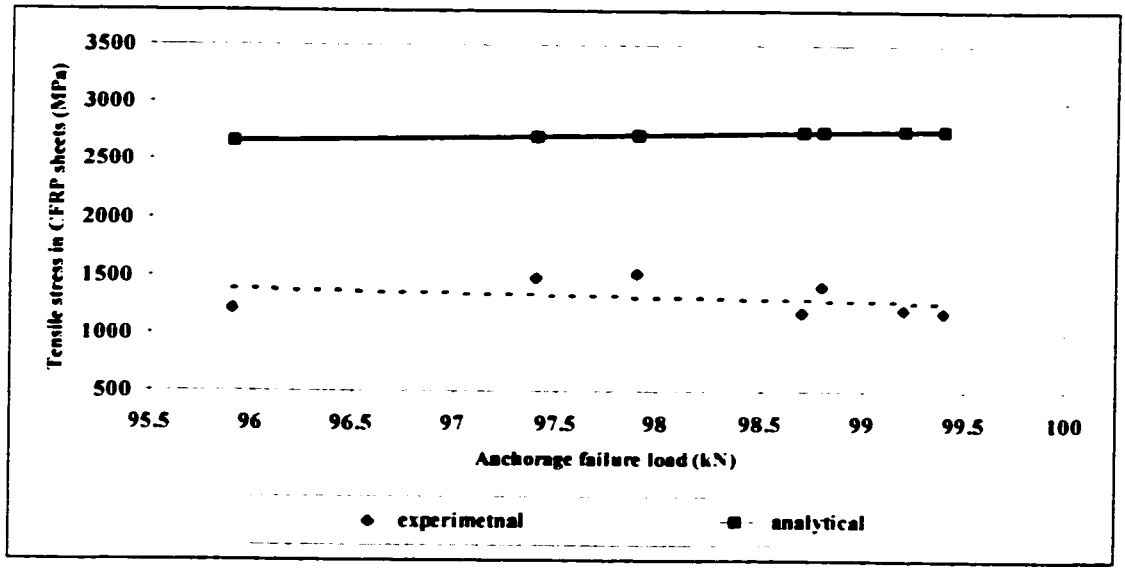

Figure [5.37]: Comparison between the experimental and analytical values of tensile stress developed in the CRFP sheets at anchorage failure load.

5.7.2.2.Fatigue strength

The new non-metallic anchorage passed all the fatigue tests in conformance with the PTI provisions [PTI 1985] with the exception of one test in series I [Table 5.7]. In all the passed tests the cyclic loading did not affect the anchorage efficiency and the tests showed an average efficiency factor (η) of 95%. The maximum capacity of the used fatigue machine was 100 kN which is 96% of the nominal strength and one test did not fail up to the maximum machine capacity. The non-metallic anchorage proved to be able to provide the required fatigue resistance which is a basic requirement for any prestressing anchorage system [2.3.3].

The cyclic loading showed no effect on the stiffness of the tendon-anchorage assembly. This was evaluated by monitoring the load-stroke relation through the first step of the fatigue test after 10 cycles, 100,000 cycles, 300,000 cycles, by the end of the 500,000 cycles and throughout the second step of the fatigue test (50 cycles) [Figures 5.22, 5.27 and 5.28]. There was no effect of cyclic loading on the stiffness of the CFRP tendon itself. This was assessed by monitoring the tendon stress-strain curves at the same loading cycles [Figures 5.29 and 5.30].

The change in the tensile stress[2] in the CFRP sheets wrapping the anchorage barrel was marginal during the first step of the cyclic loading. Monitoring of the tensile stresses began with the application of the cyclic loading with a maximum load 68 kN which exceeds the seating load. Therefore the common increase in stress noticed in the short term tensile strength tests was not observed here [Figures 5.23, and 5.31]. This can be explained by the expected rise of the tensile stress of the CFRP sheets when the load reached its maximum stress at the first cycle and then very narrow fluctuations of the stress were observed on a narrow scale graph as shown in Figure [5.24].

Similarly, when the anchorage was loaded in the second step of the fatigue loading the stress was raised to a certain value when the load reached 83kN for the first time and only minor fluctuations happened in the subsequent cycles [Figures 5.25 and 5.32]. When the tendon was loaded in the third step in direct tension there was no change in the tensile stress of the

[2]**Tensile stress = Measured tensile strain . E**

CFRP sheets up to the maximum load which can be attributed to the pre-tensioning of the sheets at 83 kN in the second step of the test [Figures 5.26 and 5.33]. In all fatigue tests the tensile stresses in the CFRP sheets did not exceed 40% of their nominal strength.

The dominant failure mechanism in all fatigue tests was tendon rupture near the anchorage zone [tests 2 and 3] where in test 1 tendon rupture happened away of the anchorages and in test 4 no failure happened up to the maximum capacity of the machine. Although test 2 did not pass the PTI requirements, the tendon rupture took place at the third step of the test. The anchorage passed the first step of the test of 500, 000 cycles fluctuating between 60-66% of the nominal tendon strength (62 to 68 kN) and passed 50 cycles fluctuating between 50-80% of the nominal tendon strength (52 to 83 kN). Then the anchorage failed at 96.3 kN which is 2.6% less than the required load. Finally, the new non-metallic anchorage system showed a reliable performance under cyclic loading and there was no observed difference in the performance of the tendon/anchorage assembly when the non-metallic anchorage was used on one side or on both sides of the prestressing system.

5.8. Cost analysis

One of the advantages of the non-metallic anchorage system is its cost. The cost[3] of the steel anchorage is roughly $ 45 each; the estimated cost of a ceramic anchorage was $600 each; while the cost of the new anchorage is about $42 each. Table [5.8] shows the cost estimation of the non-metallic anchorage based on market prices in September 1999 which comes finally to $42. The cost of the constituent materials are $12 while $30 indicated for fabrication. This fabrication cost includes a small portion of the cost of the moulds (which can be used many times), the labour cost considering large scale production and the cost for thermal curing. The carbon fibres constitutes 50 % of the constituent cost while the bauxite aggregate constitutes 38 % of the constituent cost [Figure 5.38]. The importance of the carbon fibres to provide high

[3] **$ is Canadian dollars**

fracture toughness has been demonstrated in Chapter 4 and the importance of the bauxite aggregate in developing the high strength has been explained in Chapter 3.

Table [5.8]: Cost analysis of the new non-metallic anchorage system

Constituent	Cost $ /unit*	Amount in Anchorage	Cost $
Cement type 50(kg)	0.17	1.6	0.27
Silica Fume (kg)	0.7	0.2	0.14
Bauxite Aggregate (kg)	1.2	3.7	4.44
Silica Flour (kg)	0.015	1.0	0.16
Silica Sand (kg)	0.06	1.0	0.06
Carbon fibres (kg)	100	0.06	6
Superplasticizer (kg)	1.5	0.04	0.06
CFRP Sheets (m^2)	2.66	0.29	0.77
Fabrication	30	–	30
Total			**≈ 42**

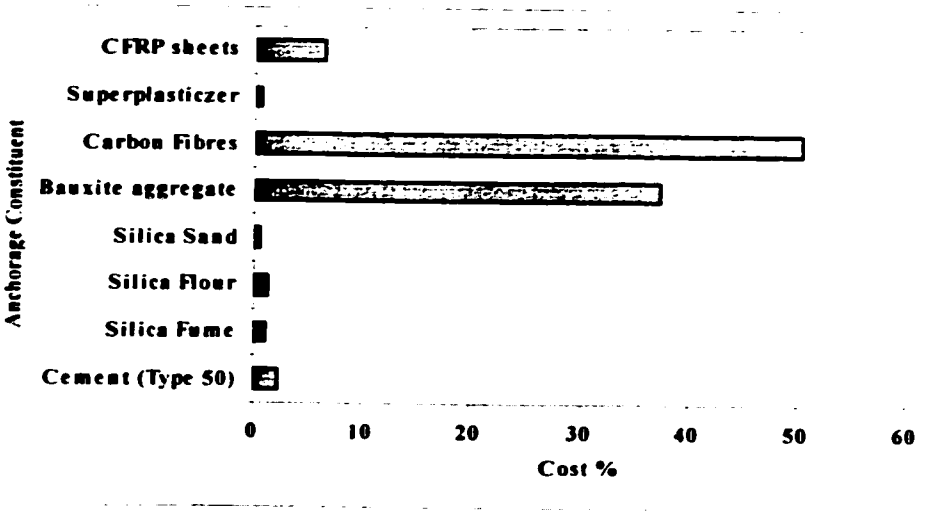

Figure [5.38]: Cost analysis of the constituent materials of the non-metallic anchorage.

5.9. Applications: Post-tensioned masonry diaphragm walls

A promise towards a completely metal-free and thus corrosion-free post-tensioning system does appear. A new wedge-type non-metallic anchorage for post-tensioning applications using CFRP Leadline™ tendons has been developed. The new anchorage showed satisfactory performance and passed the requirements for a post-tensioning anchorage system. Recently, the first post-tensioned masonry diaphragm walls have been constructed and tested in the University of Calgary [Sayed-Ahmed et al. 1999]. In these walls the metallic anchorage [Sayed-Ahmed and Shrive 1998] was used. The non-metallic anchorage will be used in the future for diaphragm walls. The anchorage can be embedded in the capping beam providing outside protection for the CFRP sheets from ultra violet exposures. Figure [5.39] is a schematic drawing showing the utilization of the non-metallic anchorage with a post-tensioned diaphragm wall. Further modifications of the anchorage may be performed before its final industrial utilization. This will be discussed with the final recommendations.

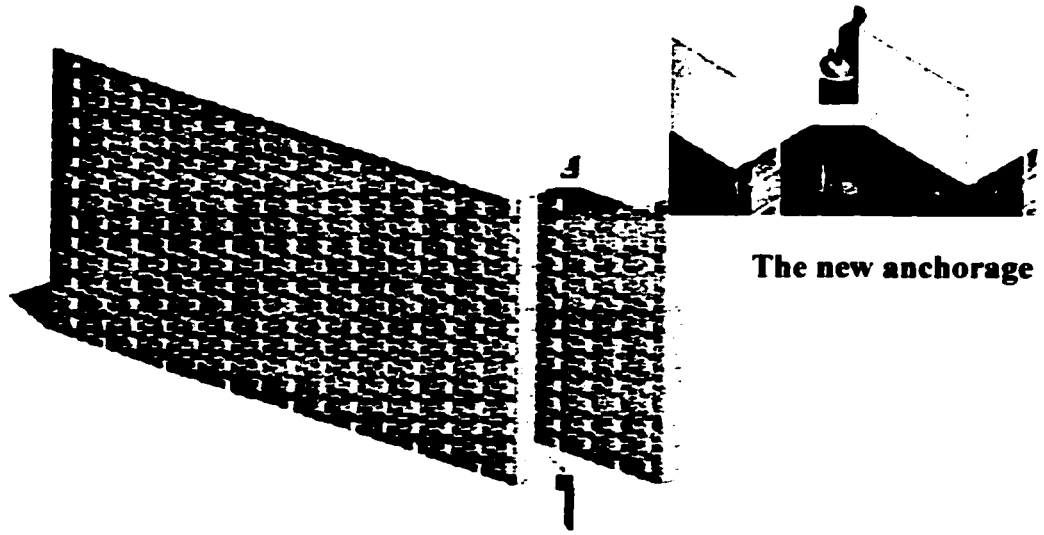

Figure [5.39]: Schematic drawing of the non-metallic anchorage utilized in post-tensioned diaphragm wall.

CHAPTER 6

CONCLUSIONS AND RECOMMENDATIONS

6.1. Summary

The objective of this work was to design, develop and test a new non-metallic anchorage system for post-tensioning applications using CFRP tendons. The use of a non-metallic anchorage should eliminate the corrosion and deterioration concerns of the anchorage zone. The development of a reliable non-metallic anchorage would provide an important contribution to this field of knowledge. The idea of the new anchorage is to hold the tendon through mechanical gripping. The anchor consists of a barrel with a conical housing and four wedges. A 0.1° differential angle between the barrel and wedges is applied.

The new anchorage components are made of concrete. A special concrete with ultra high performance criteria was developed for the anchorage. The UHPC showed compressive strength in excess of 200 MPa. Microstructural investigations including SEM and XRD analysis of the newly developed concrete were performed. The UHPC mixtures showed very dense microstructures with some unique characteristics. The microstructural investigation revealed the role of the carbon fibres in controlling cracking and toughness of the UHPC. An analytical model to predict the optimum fibre length achieving the maximum fracture toughness was applied . This was followed by experimental investigation of the fracture behaviour of UHPC with different fibre lengths. Using 3 mm long carbon fibres a significant increase in the fracture toughness of UHPC was achieved.

Using the developed UHPC with enhanced fracture toughness the new non-metallic anchorage was developed. A linear elastic model was used to determine the dimensions of the new anchorage system. The barrel was wrapped with carbon fibre reinforced polymers (CFRP) sheets to provide the necessary increase in the load carrying capacity of the anchorage system. Thirty-three anchorages were tested with sequential modifications of the anchorage geometry and the different production parameters. The non-metallic anchorage showed excellent

mechanical performance and fulfilled the different requirements of a post-tensioning anchorage system. The anchorage was able to hold the Leadline™ tendon to the maximum required capacity under both static and dynamic loading conditions. The development of the new non-metallic anchorage system will widen the inclusion of CFRP tendons in post-tensioned concrete/masonry structures. The new system will offer the opportunity to avoid corrosion problems and could integrate optical sensors which will create a generation of smart structures.

6.2. Conclusions

6.2.1. A New non-metallic anchorage system

- The issue of corrosion of prestressing steel has become of great concern from both the economic and safety points of view. Replacement of prestressing steel tendons with FRP tendons has been considered as an alternative. The integration of optical sensing techniques will allow monitoring of the behaviour throughout the structure's working life. The inclusion of FRP tendons would need the development of a new anchorage system.

- A new non-metallic anchorage system has been developed. The idea of the new anchorage is to hold the tendon through mechanical gripping. The anchor consists of a barrel with a conical housing and four wedges. A 0.1° differential angle between the slope of the conical housing and the wedges is applied. No sleeve is being used with the new anchorage.

- The new anchorage is made of Ultra High Performance Concrete (UHPC) developed specially for the anchorage. UHPC showed 7 days compressive strength in excess of 200 MPa. Special moulds are developed to cast the anchorage components. The moulds allowed pressuring of fresh concrete up to 80 MPa. The concrete components are cured in 50 °C hot water bath for 5 days and then dry cured in 200 °C for 2 days.

- The geometry of the non-metallic anchorage was optimized through a sequential testing plan. The final anchorage dimensions are shown in Figure [5.35].

- The new non-metallic anchorage showed excellent mechanical performance passing the PTI requirements of post-tensioning anchors [PTI 1985]. The anchorage showed an average efficiency factor (η) of 95.9% under static tension loads and passed the PTI fatigue tests with an average efficiency factor (η) of 95.0%

- Although the elastic statical model was useful in determining the anchorage dimensions, the model did not show good agreement with the experimental data in predicting the anchorage carrying capacity or the tensile stresses developed in the CFRP sheets during tendon loading. This can be attributed to the inaccuracy of using a linear elastic model with concrete which shows inelasticity through cracking.

- A seating load of 65 kN is required to seat the wedges of the anchorage before applying the prestressing load to the tendon. Seating loads lower than 65kN would allow tendon slip.

- Using a differential angle of 0.1° between the inner barrel and the wedges allows the development of uniformly distributed radial pressure on the tendon which prevents premature failure of the tendon in the anchorage zone.

- At least four CFRP sheets are required to be wrapped around the barrel to provide the required confinement. When the sheets are tensioned and released certain confinement pressure will be exerted on the barrel until the tensile stress of the sheets exceeds its initial value. This is practically useful as the 65 kN seating load is in the same range of the maximum anchorage service load 67 kN. This means that the sheets will provide the confinement pressure over the whole service range of the anchorage.

- The common mode of failure was tendon rupture either at the anchorage end or near the anchorage zone. Cracking of the tendon near the anchorage zone was usually observed even when the failure happened away of the anchorage. However, these cracks usually happened at stress levels much higher than the expected stress levels at service loads and the final failure usually happened after the anchorage passed the target strength.

- The non-metallic anchorage is relatively cheap with an estimated cost [1] of $ 42 which is in the same range of the steel anchorage. However, the new anchorage should not need any maintenance as it should not corrode under any environmental conditions in contrast to the metallic anchorages.

6.2.2. Development of UHPC

- Four innovative UHPC mixtures have been developed with 7 days compressive strengths up to 240 MPa.

- Although, the idea of filling the aggregate voids with the cement paste is no longer used in developing HPC, applying an exponential grading curve resulted in minimizing the voids ratio of the aggregate skeleton, reducing the water requirement, thus enhancing the concrete workability for a fixed water content.

- The calcined bauxite aggregate helped produce UHPC with excellent mechanical performance even when no pressure was applied to the fresh concrete. This can be attributed to reaction between Portland cement and the supplementary cementing materials and to the improved bond between the binder and the aggregate.

[1] $ is Canadian dollars

- The inclusion of chopped long carbon fibres in UHPC mixtures allowed the use of thermal curing up to 200 °C and enhanced the concrete ductility compared to unreinforced mixtures.

- Adding the superplasticizer to the concrete mixture about 2-3 minutes after the beginning of the dormant period of the cement enhanced the workability of these UHPC mixtures.

- To produce UHPC it seems crucial to reduce the water/binder ratio as much as possible, to reduce the entrapped air. Applying pressure to the fresh concrete not only reduced the w/c ratio but decreased the porosity of the cement matrix as well. This resulted in much better mechanical performance.

6.2.3. Microstructure of UHPC

- UHPC mixtures showed very dense microstructures compared to the known microstructures of conventional concrete or even High Performance Concrete (HPC).

- UHPC mixtures containing both silica fume and silica flour have generally shown a very dense and uniform microstructure, which was observed in the SEM micrographs. No significant Portlandite (CH) was detected by XRD. The concrete ingredients used, the very low water/cement ratio and the elevated temperature curing regime, created a favourable environment for pozzolanic reactions which consumed most of the weak CH crystals produced during hydration and converted them to strong C-S-H.

- The transition zone observed in the UHPC mixtures examined was of very small thickness with respect to that of HPC and conventional concrete. The microcracks in the vicinity of the aggregate particles were very small with no CH crystals in this vicinity.

- The main hydration products identified had d-values in the range of 2.5 A° and 3.5 A°. Different phases of crystallized C-S-H were observed. Very strong and moderately permeable Xonotlite (C_6S_6H) was a major product in mixtures cured at elevated temperatures.

- No additional transition zones were found adjacent to reinforcing carbon fibres. The bond between the carbon fibres and the cement paste seems to be very good and the microstructure observed in the fibre vicinity was shown to be very dense and homogeneous.

- An unidentified microstructure was observed near the fibre/cement paste interface in some UHPC mixtures. The materials found were gel-like and amorphous in nature. It is suggested that the material may have resulted from a reaction between silica fume and sodium hydroxide (Na OH) released during hydration.

6.2.4. Fracture mechanics of UHPC

- The carbon fibres incorporated in the UHPC mixtures seem to enhance both the strength and the fracture toughness of the matrix with a limited post cracking behaviour. The examination of carbon fibres under SEM has shown these fibres to have a non-smooth surface, which favours a better bond between these fibres and the cement paste.

- A significant increase of the fracture toughness of both High Performance Concrete (HPC) and Ultra High Performance Concrete (UHPC) including fibres can be achieved with the reduction of fibre length towards the critical fibre length.

- UHPC showed fracture toughness four times that of HPC incorporating the same fibres. This can be attributed to the very low porosity of UHPC compared to HPC. The highest fracture toughness of UHPC was attained with fibre lengths of 3 mm.

- Testing of HPC and UHPC incorporating carbon fibres proved the argument that fibre lengths shorter than or equal to the critical fibre length would provide higher fracture toughness than that when fibres longer than the critical length are incorporated. This is because with fibres shorter than the critical fibre length fibe pull-out rather than fibre rupture will be the most dominant mechanism. This would provide a significant increase in the energy consumption and the fracture toughness of the composite as a consequence.

- The shear transfer model used to predict the critical fibre length showed good agreement in the prediction of the critical fibre length with HPC while the model did not show this agreement with UHPC. This can be attributed to the model used to predict the frictional sliding strength which seems to be inaccurate.

- While K_{IC}, G_{IC} and G_F showed sensitivity to fibre inclusion in the matrix, they are statistically insensitive to fibre lengths changes. J_{IC} was the only fracture parameter to be statistically sensitive to changes in fibre length.

6.3. Recommendations

6.3.1. Recommendations for anchorage development

- The common crack observed in the wedges was a transverse crack normal to the longitudinal axis of the wedge which resulted from indirect tensile stresses developed in the longitudinal axis of the wedge. These tensile stresses were developed as a result of the biaxial compressive stresses exerted on the wedges by the barrel. To prevent possible cracking, these wedges could be prestressed using thin FRP wires. Further research is needed to develop this technique.

- To prevent the possible cracking of the barrel when the seating load is applied it is recommended to prestress the CFRP sheets while wrapping on the outer barrel. This would also provide better mechanical performance of the anchorage to the maximum tendon capacity.

- Hercules Aerospace [1995] proposed that a galvanic reaction happens when an aluminum sleeve is in contact with the CFRP tendons. The UHPC used to develop the anchorage included calcined bauxite aggregate which is aluminum based. However, no galvanic reaction between the anchorage and the CFRP tendons is expected as there is no direct contact between the CFRP and metallic aluminum. The long term durability behaviour of the non-metallic anchorage and CFRP tendons needs to be investigated.

- HPC has been reported to have lower creep values than normal strength concrete [Dilger et al. 1996]. The dense microstructure, limited microcracking and low water content of UHPC would also favour low creep of the newly developed non-metallic anchorage system. However, the significance of creep in any prestressing system means that further research on the creep of this new anchorage is required before the anchorage is utilized in prestressed structures.

- For practical considerations a smaller anchorage is recommended to be developed. This would require the reduction of the nominal maximum size of the aggregate which would not allow use of the developed UHPC mixture with 4 mm nominal maximum size. Reactive Powder Concrete (RPC) could be used which has a maximum aggregate size of 160 μm. The problem which will need to be overcome will be the large force developed over the small anchorage length. Prestressing of the barrel and the wedges would provide the required strength of the anchorage.

6.3.2. Recommendations for future research

- Using shrinkage preventing admixtures in the UHPC mixtures. This can provide better dimensional stability and further control of the anchorage dimensions during production. However further research on the effect of these admixtures on UHPC performance is required before its usage.

- Application of the recently developed finite element models for the anchorage systems [Sayed-Ahmed and Shrive 1998 and Campbell et al. 1997] to the new non-metallic anchorage taking into account the quasi-linear behaviour of concrete.

- Testing of the non-metallic anchorage under different fatigue conditions with different stress ranges and stress levels to determine the governing factor during cyclic loading.

- Development of accurate model for the prediction of the frictional sliding strength of the concrete with carbon fibres.

REFERENCES

ACI Committee 440, 1996, "State-of-the-Art Report on Fiber Reinforced Plastic (FRP) Reinforcement for Concrete Structures", 63 p.

Adimi, R., and Benmokrane, B., 1997, "Fatigue Behaviour of GFRP bars Embedded in Concrete", Proceedings of Annual Conference of the Canadian Society of Civil Engineering, Sherbrooke, pp. 121-130.

Aitcin, P.C., Mehta, P.K., 1990, "Effect of Coarse-Aggregate Characteristics on Mechanical Properties of High-Strength Concrete", ACI Materials Journal, Vol. 87, No. 2, pp. 103-107.

Aitcin, P.C., 1992, "How to Make High Performance Concrete?", High Performance Concrete, Publication of Concrete Canada, pp. 27-40.

Andonian, R., Mai, Y. W., Cotterell, B., 1979, "Strength and Fracture Properties of Cellulose Fibre Reinforced Cement Composites", International Journal of Cement Composites, Vol. 1, pp. 151-158.

Anigol, A., M., 1991, "Testing and Evaluation Fibreglass, Graphite and Steel Prestressing Cables for Pretensioned Beams", Ms Thesis, South Dakota School of Mines and Technology, Rapid City, USA, 112 pp.

Aveston, A., Cooper, G. A., and Kelly, A., 1971, "Single and multiple fracture", In the properties of Fibre Composites, Proceedings of Conference National Physical Laboratories, IPC, Science and Technology Press, U.K., pp. 15-24.

Baché, H.H., 1981, "Densified Cement/Ultra Fine Particle Based Materials", Proceedings of the 2nd International Conference on Superplasticizers in Concrete, Ottawa, 35 p.

Balaguru, N. P., and Shah, S. P., 1992, "Fiber-Reinforced Cement Composites", McGraw-Hill Inc., NY., USA, 500 pp.

Ballinger, C.A., 1991, "Development of Composites for Civil Engineering" Proceedings of ASCE - Advanced Composite Material in Civil Engineering, Iyer, S.L., and Sen, R., Ed., N.Y., pp. 288-301.

Banthia, N., 1994, "Carbon Fibre Cements : Structure, Performance, Applications and Research Needs", Fibre Reinforced Cement Development and Innovations, ACI SP- 142, Daniel, J.I. and Shah, S.P., Ed., pp. 91-120.

Barenblatt, G. J., 1962, "The Mathematical Theory of Equilibrium Crack in the Brittle Fracture", Advance in Applied Mechanics, Vol. 7, pp. 55-125.

Bartos, P., 1980, "Analysis of pull-out tests on fibres embedded in brittle matrices", Journal of Material Science, Vol. 15, pp. 3122-3128.

Bazant, Z. P., and OH, B. H., 1983, "Crack Band Theory for Fracture of Concrete", Materials and Structures", RILEM, Vol. 16, pp. 155-177.

Bazant, Z. P., and Kazemi, M. T., 1990, "Determination of Fracture Energy, Process Zone Length, and Brittleness Number from Size Effect, With Application to Rock and Concrete", International Journal of Fracture, Vol. 44, pp. 111-131.

Beaudoin, J. J., 1990, "Handbook of Fibre-Reinforced Concrete, Principles, Properties, Developments and Applications", Noyes Publications, 332 p.

Beaumont, P. W. R., 1974, "A Fracture Mechanics Approach to Failure in Fibrous Composites", Journal of Adhesion, Vol. 6, pp. 107-137.

Begley, J.A., and Landes, J.D., 1972, "The J Intergral as a Fracture Criterion", Fracture Toughness, Proceedings of the 1971 National Symposium on Fracture Mechanics, Prat II, ASTM STP 514, American Society of Testing and Materials, pp. 1-20.

Benmokrane, B., Xu, H., and Nishizaki, I., 1997, "Aramid and carbon fibre-reinforced plastic prestressed ground anchors and their field applications", Canadian Journal of Civil Engineering, Vol. 24, pp. 968-985.

Bentur A., and Mindess, S., 1990, "Fibre Reinforced Cementitious Composites", Elsevier Applied Science, NY. USE., 620 pp.

Bresson, J., 1996, "Mixing and Compacting Techninques for the Production of Very High Performance Precast Concrete Products", 4th International Symposium on Utilization of High Strength / High Performance Concrete, Paris, pp. 269-272.

Broek, D., 1982, "Elementary Fracture Mechanics", Martinus Nijhoff Publishers., 469 pp.

Brown, J. H., 1973, "The Failure of Fibre Glass-Fibre-Reinforced Notched Beams in Flexure", Magazine of Concrete Research, Vol. 25, pp. 31-38.

Budelmann, H., and Rostasy, F.S., 1993, "Creep Rupture Behaviour of FRP Elements for Prestressed Concrete - Phenomenon, Results and Forecast Models", International Symposium of Fibre-Reinforced Plastic Reinforcement for Concrete Structures, Nanni, A., and Dolan, C.W., Ed., ACI SP-138, pp. 87-99.

Burgoyne, C.J., 1998, "Advance Composites- The Challenge to Bridge Designers", Proceedings of 5th International Conference on Short and Medium Span Bridges, Dunaszegi, L. Ed. Calgary, AB, Canada, pp.73-86.

Burgoyne, C.J., 1990, "Properties of Polyaramid ropes and implications for their use as external prestressing tendons", Proceedings of External Prestressing in Bridge, Naaman, A., and Breen, J. Ed., ACI, pp. 107-124.

Campbell, T.I., Keatley, J. P., Barnes, K.M., 1998, "Analysis of an anchorage for CFRP Prestressing Tendons", 2nd Structural Specialty Conference, CSCE, Halifax, Canada, pp. 551-560.

Campbell, T.I., Keatley, J. P., Barnes, K.M., 1997, "Analysis of the Calgary Anchor", Research report, Department of Civil Engineering, Queen's University, Ont., Canada. 33 pp.

Chern, J. C., Young, C. H., and Wu, K. C., 1985, "A Non-Linear Model for Mode I Fracture of Fibre Reinforced Concrete", ACI SP-118, pp. 91-112.

Collepardi, M., 1999, "Damage by Delayed Ettringite Formation: A Holistic Approach and New Hypothesis", ACI International, Volume 21, No. 1, pp.69-74.

Cotterell, B., 1972, "Brittle Fracture in Compression", International Journal of Fracture Mechanics, Vol. 8, No.2, pp. 195-208.

Cox, B. N., and Marshall, D. B., 1994, "Concepts for Bridged Cracks in Fracture and Fatigue", Acta Metallurgy, Vol. 42, No. 2, pp. 341-363.

Cox, H. L., 1952, "The elasticity and strength of paper and other fibrous materials", British Journal of Applied Physics, Vol. 3, pp.72-79.

CSA Standard A23.3-94, 1995, "Design of Concrete Structures", Canadian Standard Association, 220p.

Curtin, W. G., Shaw, G., Beck, J. K., and Bray, W. A., 1982, "Modern Philosophy of Structural Brickwork Design and A Change of Outlook for the Brick Industry" Proceedings of the 6th International Brick Masonry Conference, Rome, Italy, pp. 939-948.

Daniel. M., and Ishai, O., 1994, "Engineering Mechanics of Composite Materials", Oxford University Press, 395 pp.

De Larrard, F., Hu, C., and Sedran, T., 1995, "Best Packing and Specified Rheology: Two Concepts in High - Performance Concrete Mixture Proportioning", Adam Neville Symposium on Concrete Technology, ACI/CANMET, V.M. Malhotra, Ed., Las Vegas, pp. 109-127.

De Larrard, F., 1995, "Ultrafine Particles for the Making of Very High Strength Concretes", Cement and Concrete Research, Vol. 19, pp. 161-172.

Diefendorf, R.J., 1989, "Carbon/Graphite Fibres", Engineering Materials Handbook, Vol. 1: Composites, ASM International Ed., pp. 49-53.

Dilger, W. H., Wang, C., and Niitani, K., 1996, "Experimental Study on Shrinkage and Creep of High Performance Concrete", 4th International Symposium on Utilization of High-Strength /High-Performance Concrete, Paris, pp. 311-319.

Dolan, C.W., 1993, "FRP Development in the United States", Fibre-Reinforced Plastic "FRP" Reinforcement for Concrete Structures: Properties and Applications, Nanni, A., Ed., Elsevier Science Publishers, pp. 129-163.

Domone, P. L. J., and Soutsos, M. N., 1994, "An approach to the proportioning of High Strength Concrete Mixes", Concrete International, Vol. 16, No. 10, pp. 26-31.

Dowling, N. E., 1993, "Mechanical Behaviour of Materials; Engineering Methods for Deformation, Fracture and Fatigue", First edition, Prentice Hall, N.J, 383p.

Doxsee, L E., Janssens, W., Verpoest, I., and DeMeester, P., 1991, "Strength of Aramid Epoxy Composites During Moisture Absorption", Journal of Reinforced Plastics and Composites, Vol. 10, pp. 645-655.

Dugdale, D. S., 1960, "Yielding of Steel Sheets Containing Slits", Journal of Mechanics, Physics and Solids, Vol. 8, pp. 100-104.

Dupont, 1987, Data Manual for Kevlar 49 Aramids, Material Science Corporation, Spring Hill, PA, USA.

Ellis, R. and Gulick, D., 1990, "Calculus with Analytical Geometry", Harcourt Brace Jovanovich Publisher, NY., 4th edition, 1039p.

Ellyin, F., and Kujawski, D., 1992, "Fatigue Testing and Life Predictions of Fibreglass Reinforced Composites", Advanced Composite Materials in Bridges and Structures, Neale and Labossiere, Eds., CSCE, Monteral, pp. 111-118.

Enka, B., 1986, "Arapree-The Twaron resin prestressing element for concrete", Corporate Report, The Netherlands.

Erki, M.A., and Rizkalla, S.H., 1993[a], "FRP Reinforcement for Concrete Structures", Concrete International, Vol. 6, No. 6, pp. 48-53.

Erki, M.A., and Rizkalla, S.H., 1993[b], "Anchorages for FRP Reinforcement", Concrete International, Vol. 6, No. 6, pp. 54-59.

Foote, R., Mai, Y., and Cotterell, B., 1987, "Process Zone Size and Crack Growth Measurement in Fibre Cements", Fibre Reinforced Concrete Properties and Applications, ACI SP-105, Shah, S. P., Batson, G. B., Ed., pp. 55-70.

Fuller, W. B., and Thompson, S. E., 1907, "The laws of proportioning concrete", Trans. ASCE, Vol. 59, pp. 67-143.

GangaRao, H. V. S., and Faza, S. S., 1992, "Bending and Bond Behaviour of Concrete Beams Reinforced with Plastic Rebars"Technical Report, Phase I, West Virginia University, USA, 158 pp.

Gerritse, A., 1992, "Durability Criteria for Non-Metallic Tendons in An Alkaline Environment", Advanced Composite Materials in Bridges and Structures, Nealee, K.W., and Labossiere, P., Ed., CSCE, Montreal, Quebec, pp. 129-137.

Gerritse, A., and Werner, J., 1991, "ARAPREE®, A Non-Metallic Tendon, Performance and Design Requirements", Advanced Composite Materials in Civil Engineering Structures, Proceedings of the Specialty Conference, ASCE, Iyer, S., and Sen, R., Ed., pp. 143-154.

Ghali, A., and Neville, A. M., 1989, "Structural Analysis: A Unified Classical and Matrix Approach", Third edition, E & FN Spon, NY., 870 p.

Gjφrv, O. E., 1996, "Workability Loss of High Strength Concrete", ACI Materials Journal, Vol. 93, No. 5, pp. 427-431.

Gjφrv, O. E., Sφrensen, S. I., and Arnesen, A., 1977, "Notch Sensitivity and Fracture Toughness of Concrete", Cement and Concrete Research, Vol. 7, pp. 333-344.

Glucklich, J., 1963, "Fracture of Plain Concrete", Proceedings of The American Society of Civil Engineers, Vol. 89, No. EM6, pp.127-138.

Goltermann, P., Johansen, V., and Palbφl, L., 1997, "Packing of Aggregates: An Alternative Tool to Determine the Optimal Aggregate Mix", ACI Materials Journal, Vol. 94, Np. 5, pp. 435-443.

Gopalaratnam, V. and Shah, S., 1987, "Failure Mechanisms and Fracture of Fibre Reinforced Concrete", ACI SP-105, Fibre Reinforced Concrete, Properties and Application, S. P. Shah and Baston G. B., Ed., pp. 1-25.

Goode, J., and Lufsey, L., 1962, "A New Graphical Chart for Evaluating Aggregate Gradation", Annual meeting of the Association of Asphalt Paving Technologists, New Orleans, pp. 13-26.

Grabowski, E., and Gillott, J. E., 1989, "Effect of Replacement of Silica Fume with Silica Flour on Engineering Properties of Oilwell Cements At Normal and Elevated Temperatures and Pressures", Cement and Concrete Research, Vol. 19, pp. 333-344.

Grant, L., Tadros, G., and Rizkalla, S., 1995, "Towards Development of Bridges in the Next Century", In Non-metallic (FRP) reinforcement for concrete structures", Taerwe, L., Ed., E&FN Spon, London, UK, pp. 645-662.

Gray, R. J., 1984[a], "Analysis of the effect of embedded fibre length on fibre debonding and pull-out from an elastic matrix, Part 1- Review of theories", Journal of Material Science, Vol. 19, pp. 861-870.

Gray, R. J., 1984[b], "Analysis of the effect of embedded fibre length on fibre debonding and pull-out from an elastic matrix, Part 2- Review of theories", Journal of Material Science, Vol. 19, pp. 1680-1691.

Griffith, A., A., 1921, "The Phenomena of rupture and flow in solids", Philosophy Transaction of Royal Society of London, A221, pp.163-197.

Griffith, A.,A., 1924, "The Theory of Rupture", Proceedings of the 1st International Congress on Applied Physics, Delft, pp. 55-63.

Gutierrez, J.J., and Canovas, M.F., 1996, "High Performance Concrete: Requirements for Constituent Materials and Mix Proportioning", ACI Materials Journal, Vol. 93, No. 3, pp. 223-241.

Halvorsen, G. T., 1980, "J - Integral Study of Steel Fibre Reinfoced Concrete", International Journal of Cement Composites, Vol. 2, pp. 13-22.

Hannant, D. J., Hughes, D. C., and Kelly, A., 1983, "Toughening of Cement and Other Brittle Solids With Fibres", Phil. Trans. Roy. Society of London, A310, pp.175-190.

Harada, T., Matsuda, H., Khin, M., Tokumitsu, S., Enomoto, T., and Idemitsu, T., 1995, "Development of Non-Metallic Anchoring Devices for FRP Tendons", Non-Metallic (FRP) Reinforcement for Concrete Structures, Lactawi, I., Ed., RILEM, pp. 41-48.

Hercules Aerospace Co., 1995,Task 6, "Cable and anchorage technology, state-of-the-art report", Technical Report, 76 pp.

Higdon, A., Olsen, E. H., Stiles, W.B., and Wesse, J. A., 1967, "Mechanics of Materials", Second Edition, John Wiley & Sons Inc. NY. 591 p.

Hillerborg, A., 1985, "The theoretical basis of a method to determine the fracture energy G_F of concrete", Materials and Structures, Vol. 18, no. 106, pp. 291-296.

Hillerborg, A., Modeer, M., and Petersson, P. E., 1976, "Analysis of Crack Formation and Crack Growth in Concrete by Means of Fracture Mechanics and Finite Elements", Cement and Concrete Research, Vol. 6, No. 6, pp. 773-782.

Holte, L.E., Dolan, C.W., and Shmidt, R.J., 1993[a], "Anchorage of Non-Metallic Prestressing Tendons", Department of Civil and Architectural Engineering. University of Wyoming. USA, 102 pp.

Holte, L.E., Dolan, C.W., and Shmidt, R.J., 1993[b], " Epoxy Socketed Anchors for Non-Metallic Prestressing Elements", International Symposium of Fibre-Reinforced Plastic Reinforcement for Concrete Structures, Nanni, A., and Dolan, C.W., Ed., ACI SP-138, pp. 381-400.

Jenq, Y. S., and Shah, S. P., 1985, " A Two Parameter Fracture Model for Concrete", Journal of Engineering Mechanics, ASCE, Vol. 111, No. 4, pp. 1227-1241.

Johnston, C. D., 1982, "Definition and Measurement of Flexural Toughness Parameters for Fibre Reinforced Concrete", ASTM, Cement, Concrete and Aggregates, Vol. 4, No. 2, Winter 1982, pp. 53-60.

Jones, F.R., and Rock, J.W., 1983, "On the Mechanism of Stress Corrosion of E-glass Fibers", Journal of Material Science, Letter 2, pp. 415-418.

Karihalloo, B. L., and Nallathambi, P., 1989, "An Improved Effective Crack Model for the Determination of Fracture Toughness in Concrete", Cement and Concrete Research, Vol. 19, pp. 603-610.

Kakihara, R., Kamiyoshi, M., Kumagai, S., and Noritake, K., 1991, "A New Aramid Rod for the Reinforcement of Prestressed Concrete Structures", Advanced Composite Materials in Civil Engineering Structures, Proceedings of the Specialty Conference, Las Vegas, pp. 134-142.

Kaplan, M. F., 1961, "Crack Propagation and Fracture of Concrete', Journal of The American Concrete Institute, Vol. 58, pp. 591-610.

Kasperkiewicz, J., 1983, "On a Certain Model of Brittle Matrix Composites", Seminar Proceedings, Present state of investigations and applications of Fibre Reinforced Cement Based Materials, RILEM-Polish Academy of Sciences, Cracow Tech. Univ., pp. 58-67.

Katz, A., and Li, V.C., 1995, "Bond Properties of Micro-fibres in Cementitious Matrix", Material Research Society Symposium Proceedings, Vol. 370, pp. 529-537.

Kelly, A., 1973, "Strong Solids", Clarendon Press, Oxford, U.K., 285 p.

Kerstens, J.G.M., Bennenk, W., and Camp, J.W., 1998, "Prestressing with Carbon Composite Rods: A Numerical Method for Developing Reusable Prestressing Systems", ACI Structural Journal, Vol. 95, No. 1, pp. 43-50.

Khin, M., Harada, T., Tokumisu, S., and Idemitsu, T., 1996, "The Anchorage Mechanism for FRP Tendons Using Highly Expansive Materials for Anchoring", Advanced Composite Materials in Bridges and Structures, El-Badry, M.M., Ed., CSCE, Montreal, Quebec., pp. 959-964.

Korczynskyj, Y., Harris, S. J., and Morley, J G., 1981, "The influence of reinforcing fibres on growth of cracks in brittle matrix composites", Journal of Material Science, Vol. 16, pp. 1533-1547.

Kronlöf, A., 1997, "Filler effect of inert mineral powder in concrete", Technical Research Centre of Finland, ESPOO 1997, VTT Publications 322, 155 p. + app. 32 p.

Lawrence, P., 1972, "Some Theoretical Considerations of Fibre Pull-out from an elastic Matrix", Journal of Materials Science, Vol. 7, pp. 1-6.

Laws, V., 1982, "Micromechanical aspects of the fibre-cement bond", Journal of Composites,Vol. 13, No. 2. pp. 145-151.

Lenain, J. C., and Bunsell, A. R., 1979, "The resistance to crack growth of asbestos cement", Journal of Material Science, Vol. 14, pp. 321-332.

Li, S. H., Shah, S. P., Li, Z., and Mura, T., 1995, "Prediction and Verification of Interface Debonding for Fibre Reinforced Cementitious Material", In Interface Fracture and Bond, ACI SP-156, Buyukozturk, O., and Wecharatana, M., Ed., pp. 125-152.

Loov, R.E., 1996, Personal Communications

Luciano, J.J., Nmai, C.K., Delgado, J.R., 1991, "A Novel Approach to Developing High Strength Concrete", Concrete International, Vol. 13, No. 5, pp. 25-29.

Matthews, F.L., and Rawlings, R.D., 1994, "Composite Materials: Engineering and Science", Chapman & Hall, London, UK, 457 pp.

Measure, R.M., Alavie, A.T., Maaskant, R., Ohn, M., Karr, S., and Huang, S., 1995, "A Structurally Integrated Bragg Grating Laser Sensing System for a Carbon Fiber Prestressed Concrete Highway Bridge", Smart Materials and Structures, Vol. 4, pp. 20-30.

Mehta, P.K., 1986, Concrete Structure, Properties and Materials, Prentice-Hall Inc., New Gersy, 390 pp.

Mehta, P.K., and Aitcin, P.C., 1990, "Microstructural Basis of Selection of Materials and Mix Proportions for High-Strength Concrete", Proceedings of 2nd International Symposium on High Strength Concrete, Hester, W.T., Ed., ACI SP-121, pp. 265-286.

Meier, U., 1995, "Extending the Life of Cables by the Use of Carbon Fibres", IABSE Symposium , San Francisco, USA, pp. 1235-1240.

Mindess, S., 1983[a], "The Fracture of Fibre Reinforced and Polymer Impregnated Concretes: A Review", Fracture Mechanics of Concrete, Chapter 6, Wittmann, F. H., Ed., Elsevier Science Publishers, B. V., Amsterdam, pp.481-501.

Mindess, S., 1983[b], "The Cracking and Fracture of Concrete: An Annotated Bibliography 1928-1981", Fracture Mechanics of Concrete, Chapter 6, Wittmann, F. H., Ed., Elsevier Science Publishers, B. V., Amsterdam, pp.539-661.

Mindess, S., and Diamond, S., 1982, "the Cracking and Fracture of Mortar", Matèriaux et Constructions, Vol. 15, no. 86, pp.107-113.

Mindess, S., Lawrence, F.V., and Kesler, C.E., 1977, "The J-Integral As A Fracture Criterion For Fibre Reinforced Concrete", Cement and Concrete Research, Vol. 7, No. 6, pp. 731-742.

Mitsubishi Chemical Corporation, 1996, Personal Communications.

Moavenzadeh, F., and Kuguel, R., 1969, "Fracture of Concrete", Journal of Materials, Vol. 4, pp. 497-519.

Mobasher, B., Li., C. Y., and Arino. a., 1995, "Experimental R-Curves for Assessment of Toughening in Fibre Reinforced Cementitious Compsites", ACI SP-155, Testing of Fibre Reinforced Concrete, Stevens , D. J. et al. , Ed., pp. 93-114.

Mukae, K., Kumagai, S., Nakai, H., and Asai, H., 1993, "Characteristics of Aramid FRP rods", International Symposium of Fibre-Reinforced Plastic Reinforcement for Concrete Structures, Nanni. A., and Dolan, C.W., Ed., ACI SP-138, pp. 35-49.

Naaman, A.E., 1998, "New Fiber Technology", Concrete International, Vol. 20, No. 7, pp. 57-62.

Naaman, A. E., and Shah, S. P., 1976, "Pull-out Mechanism in Steel Fibre-Reinforced Concrete", Proceedings, ASCE, Vol. 102, ST8, pp.1537-1548.

Nanni, A., 1997, "CFRP Strengthening" Concrete International, Vol. 9, No. 6, pp. 19-23.

Nanni, A., Bakis, C. E., O'Niel, P. E., and Dixon, T.O., 1996, "Performance of FRP Tendon-Anchor Systems for Prestressed Concrete Structures" PCI Journal , Vol. 41, No. 1, pp. 34-43.

Nehdi, M., and Mindess, S., 1998, "Modeling the particle Packing, Mechanisms of Hydration and Strength Development in HPC Made with Composite Cements", International Symposium On High Performance And Reactive Powder Concretes, Aitcin, P., and Delagrave, E., Ed., Sherbrooke, Canada, Vol. 4, pp. 125-144..

Neville, A. M., 1996, "Properties of Concrete", 4th Edition, John Wiley & Sons Inc., 797p.

Nikolic-Brzev, S., and Pantazopoulou, S.J., 1995, "Rehabilitation of Masonry Structures Using Non-Metallic Fibre Composite Reinforcement", University of Toronto, Department of Civil Engineering Department, 59 pp.

Nishioka, N., Yamakawa, S., Hirakawa, K., and Akihama, S., 1978. in Testing and Test Methods of Fibre Cement Composites, Swamy, R. N., Ed., RILEM Symposium, Sheffield, Construction Press, Lancaster, pp. 87-98.

Noisternig, J.E., and Jungwirth, D., 1996, "Design and Analysis of Anchoring Systems for A Carbon Fiber Composite Cable" Advanced Composite Materials in Bridges and Structures, M. M. El-Badry, Ed., CSCE, Montreal, Quebec, pp. 935-942.

Ohama, Y., Amano, M., and Endo, M., 1985, "Properties of Carbon Fibre Reinforced Cement with Silica Fume", Concrete International, Vol.7, No. 3, pp.58-62.

Oluokun, F.A., 1991, "Prediction of concrete tensile strength from compressive strength: evaluation of existing relations for normal weight concrete", ACI Materials Journal, Vol. 88, No. 3, pp. 302-309.

Patrick, K.and Meier, U., 1991, "CFRP Cables for Large Structures", Advanced Composite Materials in Civil Engineering Structures, Proceedings, Speciality Conference, Las Vegas, ASCE, NY., pp. 233-244.

Patterson, W. A., and Chan, H. C., 1975, "Fracture toughness of glass reinforced cement", Composites, Vol. 6, pp. 102-104.

Phoenix, S. L., 1979, "Statistical Theory for the Strength of Twisted Fibre Bundles with Applications to Yarn and Cables", Textile Research Journal, Vol. 49, No. 7, pp. 407-417.

Piggott, M. R., 1970, "Theoretical Estimation of Fracture Toughness of Fibrous Composites", Journal of Materials Science, Vol. 5, pp. 669-675.

Porter, M. L., and Barnes, B.A., 1991, "Tensile Testing of Glass Fibre Composite Rod", Advanced Composite Materials in Civil Engineering Structures, Proceedings, Speciality Conference, Las Vegas, ASCE, NY., pp. 123-131.

Post-Tensioning Institute (PTI), 1985, "Post-Tensioning Manual", 4th Edition, Pheonix, Arizona, USA.

Ramouldi, J. P., and Mandel, J. A., 1964, "Tensile Strength of Concrete Affected by Uniformly Distributed and Closely Spaced Short Lengths of Wire Reinforcement" Journal of the American Concrete Institute, Vol. 61, pp. 657-670.

Ramouldi, J. P., and Batson, G. B., 1963, "Mechanism of Crack Arrest in Concrete", Journal of the Engineering Mechanics Division, Proceedings of the American Society of Civil Engineers, EM 3, pp.147-168.

Reda, M.M., Shrive, N.G. and Gillott, J.E., 1999, "Micorstructural Investigations of Ultra High Performance Concretes", Vol. 29, No. 3, pp. 323-329.

Reda, M.M., and Shrive, N.G., 1998, "A New Ultra High Performance Concrete Using Micro Carbon Fibers", Proceedings of the 2th CSCE Conference, Halifax, pp. 329-338.

Reda, M.M., Sayed-Ahmed, E.Y., and Shrive, N.G., 1997[a], "Advanced Composite Materials for Post-Tensioning Applications: Merits, Shortcomings and Possibilities", Proceedings of the International Conference on Engineering Materials, Ottawa, Canada, Vol1, No. 21

Reda, M.M., Sayed-Ahmed, E.Y., and Shrive, N.G., 1997[b], "Towards a New Non-Metallic Anchorage System for Post-Tensioned Applications With Carbon Fibre Reinforced Plastic Tendons", Proceedings of the 42nd International SAMPE Symposium, Anaheim, USA, pp. 288-297

Riad, A., Sayed-Ahmed, E. Y., Tadros, G., Loov, R. E., and Shrive, N. G., 1998, "Design Recommendations for HC-Type Bridge Girders Retrofitted with CFRP strips", Proceedings of 5th International Conference on Short and Medium Span Bridges, Dunaszegi, L., Ed., Calgary, Canada, 13 pp.

Rice, J.R., Paris, P.C., and Merkle, J.G., 1973, "Some Further Results of J-Integral Analysis and Estimates", Progress in Flaw Growth and Fracture Toughness Testing, ASTM STP 536, American Society of Testing and Materials, pp. 231-245.

Rice, J, R., 1968, "A Path Independent Integral and the Approximate Analysis of strain Concentration by Notches and Cracks", Journal of Applied Mechanics, Transactions of ASME, Vol. 35, pp. 379-386.

Richard, P., 1996, "Reactive Powder Concrete, A New Ultra-High Strength Cementitious Material" 4th International Symposium on Utilization of High Strength / High Performance Concrete, Paris, pp. 1343-1349.

Richard, P., and Cheyrezy, M., 1995, "Composition of Reactive Powder Concretes", Cement and Concrete Research, Vo. 25, No. 7, pp. 1501-1511.

RILEM Committee 50-FMC on Fracture Mechanics of Concrete, 1985, "Determination of the Fracture Energy of Mortar and Concrete by Means of Three-Point bend Tests on Notched Beams", Materials and Structures, Vol. 18, No. 106, pp 285-290.

Rizkalla, S., 1998, "Advanced Composite Materials for Bridges" Proceedings of 5th International Conference on Short and Medium Span Bridges, Dunaszegi, L. Ed. Calgary, AB, Canada, pp.48-58.

Rossi, P., and Renwez, S., 1996, "High Performance Multi Modal Fibre Reinforced Cement Composites (HPMMFRCC)" Proceedings of the 4th International Symposium on Utilization of High Strength/High Performance Concrete, Paris, pp. 687-694.

Rostàsy, F. S., 1998, "Draft Guidelines For The Acceptance Testing of FRP Posttensioning Tendons", Journal of Composites For Construction, ASCE, Vol. 2, No. 1, pp. 2 - 6.

Rostàsy, F.S., 1993, "FRP Tensile Elements for Prestressed Concrete- State of the Are, Potentials and Limits", International Symposium of Fibre-Reinforced Plastic Reinforcement for Concrete Structures, Nanni, A., and Dolan, C.W., Ed., ACI SP-138, pp. 347-365.

Rostàsy, F.S., and Budelmann, H., 1993, "Principles of Design of FRP Tendons and Anchorages for Post-Tensioned Concrete", International Symposium of Fibre-Reinforced Plastic Reinforcement for Concrete Structures, Nanni, A., and Dolan, C.W., Ed., ACI SP-138, pp. 633-649.

Rostàsy, F.S., and Budelmann, H., 1991, "FRP-Tendons for the Post-Tensioning of Concrete Structures", Advanced Composite Materials in Civil Engineering Structures, Proceedings of the Specialty Conference, Las Vegas, pp. 155-166.

Rubinsky, I.A., and Rubinsky, A., 1954, "An Investigation into the Use of Fibre-Glass for Prestressed Concrete", Magazine of Concrete Research, Vol. 6

Saadatmanesh, H., and Tannous, F. E., 1999, "Relaxation, Creep and Fatigue Behaviour of Carbon Fibre Reinforced Plastic Tendons", ACI Materials Journal, Vol. 96, No. 2, pp.143-153.

Santoh, N., 1993,"CFCC "Carbon Fibre Composite Cable)", Fibre Reinforced Plastic (FRP) Reinforced For Concrete Structures, Nanni, A., Ed., Elsevier Science Publishers, NY., pp. 223-248.

Sarkar, S.L., 1994, "The Importance of Microstructure in Evaluating Concrete", Advances in Concrete Technology, 2nd edition, Malhotra, V.M., Ed., CANMET, pp. 125-160.

Sayed-Ahmed, E. Y., Lissel, S. L., Tadros, G., and Shrive, N. G., 1999, "Carbon fibre reinforced polymer (CFRP) post-tensioned masonry diaphragm walls: prestressing, behaviour, and design recommendations" Canadian Journal of Civil Engineering, Vol. 26, pp. 1-26.

Sayed-Ahmed, E.Y., and Shrive, N.G., 1998, "A new steel anchorage system for post-tensioning applications using carbon fibre reinforced plastic tendons", Canadian Journal of Civil Engineering, Vol. 25, pp. 113-127.

Schmiedmayer, R., and Schachinger, I., 1998, "Influence of Superplasticizer Dosage and Mixing Procedure on the Density and Strength of Reactive Powder Concrete", International Symposium On High Performance And Reactive Powder Concretes, Aitcin, P., and Delagrave, E., Ed., Sherbrooke, Canada, Vol. 3, pp. 145-152.

Sedran, T., and De Larrard, F., 1996, "Rene-LCPC Software to Optimize The Mix Design of High Performance Concrete", 4th International Symposium on Utilization of High Strength / High Performance Concrete, Paris, pp. 167-178.

Shaw, G., 1996, "Innovative Development of Prestressed Masonry", In Worldwide advances in structural concrete and masonry, Proceedings of the Committee on Concrete and Masonry Structures Symposium, Schultz, A.E., and McCabe, S.L., Ed., ASCE, NY., pp. 13-24.

Shah, S. P. 1996, "High Performance Concrete: Controlled Performance Concrete", Magazine

of Concrete Research, Vol. 49, No. 178, pp.1-3.

Shah, S.P., Swartz, S.E., and Ouyang, C., 1995, "Fracture Mechanics of Concrete: Applications of Fracture Mechanics to Concrete, Rock and Other Quasi-Brittle Materials", John Wiley & Sons Inc., 552 p.

Shah, S. P., and McGarry, F. J., 1971, "Griffith Fracture Criterion and Concrete", Journal of the Engineering Mechanics Devision, ASCe, Vol. 97, pp. 1663-1676.

Shrive, N.G., Sayed-Ahmed, E.Y., Damson, E., Tilleman, D., and Tadros, G., 1996, "Prestressing anchorage system for fibre reinforced plastic prestressing tendons", U.S. Patent Application # 08/754186.

Shrive, N. G., and El-Rahaman, M., 1985, "Understanding the Cause of Cracking in Concrete: A Diagnostic Aid", Concrete International, Vol. 7, No. 5, pp. 39-44.

Shrive, N.G., 1983, "Compression Testing and Cracking of Plain Concrete", Magazine of Concrete Research, Vol. 35, No.122, pp. 27-38.

Shwarz, M. M., 1992, "Composite Materials Handbook", First edition, McGraw Hill Inc. NY.

Sippel, T.M., 1992, "Design, Testing and Modeling of an Anchorage System for Resin Bonded Fibreglass Rods Used as Prestressing Tendons", Advanced Composite Materials in Bridges and Structures, Neale, K.W., and Labossiere, P., Ed., CSCE, Montreal, Canada, pp. 363-372.

Soroushian, P., Aouadi, F., and Hsu, J., 1995, "Theroetical Optimization of Fiber Reinforced Cement Comopsites", ACI Materials Journal, Vol. 92, No. 4, pp. 373-381.

Stang, H., and Shah, S. P., 1986, " Failure of Fibre Reinforced Concrete by Pull-out Fracture", Journal of Material Science, Vol. 21, No. 3, pp. 953-957.

Sumida, A., Okamoto, T., and Tanigaki, M., 1995, "Experiences of MCC on Aramid RP", SP-150, Annual Conference of Expo 95, Cincinnati, OH.

Swamy, N.R., 1979, "Fracture Mechanics Applied to Concrete", Developments in Concrete Technology -1, Lydon, F.D., Ed., Applied Science Publisher Ltd., London, Chapter 6, pp. 221-281.

Tada, H., Paris, P. C., and Irwin, G. R., 1985, "The Stress Analysis of Cracks Handbook", Second edition, Paris Production Inc., St. Louis, USA.

Taerwe, L.R., 1993, "FRP Development and Applications in Europe", Reinforcement for Concrete Structures: Properties and Applications, Nanni, A., Ed., Elsevier Science Publishers, pp. 99-114.

Tanigaki, M., and Mikami, H., 1990, "Braided High Strength Fiber Rods for Reinforcing Concrete', Proceedings of the 11th FIP Congress, Hamburg, Germany, 2p.

Tannous, F.E., and Saadatmanesh, H., 1998, "Environmental Effects on the Mechanical Properties of E-Glass FRP Rebars", ACI Materials Journal, Vol. 95, No. 2, pp. 87-100.

Taylor, M. R., Lydon, F. D., and Barr, B.T.G., 1996, "Toughness characterization of fibre-reinforced concrete", Indian Concrete Journal, Vol. 70, No. 10, pp. 525-531.

Todd, J. D., 1974, "Structural Theory and Analysis", First edition, William Clowes & Sons Ltd. London, 353p.

Tokyo Rope, 1990, Product data sheet.

Umoto, T., and Hodhod, H., 1993, "Properties of Fiber Reinforced Plastic Rods for Prestressing Tendons", International Symposium of Fibre-Reinforced Plastic Reinforcement for Concrete Structures, Nanni, A., and Dolan, C.W., Ed., ACI SP-138, pp. 101-115.

Velazco, G., and Visalvanich, K., and Shah, P. S., 1980, "Fracture Behaviour and Analysis of Fiber Reinforced Concrete Beams", Cement and Concrete Research, Vol. 10, pp. 41-51.

Vernet, C., Lukasik, J., and Prat, E., 1998, "Nanostructure, porosity, permeability, and diffusivity of Ultra High Performance Concretes (UHPC)"International Symposium On High Performance And Reactive Powder Concretes, Aitcin, P., and Delagrave, E., Ed., Sherbrooke, Canada, Vol. 3, pp.17-35.

Visalvanich, K., and Naaman A. E., 1983, "Fracture Model for Fibre Reinforced Concrete", ACI Journal, Vol. 83, No. 2, pp. 128-138.

Walton, J.M., and Yeung, Y.T.C., 1986, "The Fatigue Performance of Structural Strands of Pultruded Composite Rods", Journal of the Institute of Mechanical Engineering, London, C/286/86, pp. 315-320.

Ward, R. J., Yamanobe, K., Li, v. C., and Backer, S., 1989, "Fracture Resistance of Acrylic Fibre Reinforced Mortars in Shear and Flexure", ACI SP- 118, Fracture Mechanics: Application to Concrete , Li, V. C., and Bazant, Z. P., Ed., ACI, Detriot, Michigan, pp. 17-67.

Wang, E.Z., and Shrive, N.G., 1995, "Brittle Fracture in Compression: Mechanisms, Models and Criteria", Engineering Fracture Mechanics, Vol. 52, No. 6, pp. 1107-1126.

Wecharatana, M., and Shah, S. P., 1983, "A Model for Predicting Fracture Resistance of Fibre Reinforced Concrete", Cement and Concrete Research, Vol. 13, pp. 819-829.

Weiss, V., 1973, "Crack development in concrete with closely-spaced reinforcement and in similar materials", Cement and Concrete Research, Vol. 3, pp. 189-205.

Wolff, R., and Miesser, H. J., 1989, "New Materials for Prestressing and Monitoring Heavy Structures", Concrete International, Vol. 11, No. 9, pp. 86-89.

Yamaguchi, T., Kato, Y., Nishimura, T., Uomoto, T., 1997, "Creep rupture of FRP rods made of Aramid, Carbon, and Glass Fibres", Proceedings of 3rd International Symposium on Non-Metallic (FRP) Reinforcement for Concrete Structures, Sapporo, Japan, Vol. 2, pp. 179-186.

Yamashita, T., and Inukai, H., 1990, "Prestressed Concrete Bridge Using FRP Tendons-Shinmiya Bridge", Prestressed Concrete Engineering Association, Tokyo, Japan, pp. 53-56.

Young, J.F., 1997, "Densified Cement Pastes and Mortars", Advanced Cement Based Materials, Vol. 9, No. 2, pp.4-5.

Zhang, B., Benmokrane, B., 1997, "Development of Anchorage System for Fibre Reinforced Plastic (FRP) Tendons", Proceedings of Annual Conference of the Canadian Society of Civil Engineering, Sherbrooke, pp. 131-140.

Zhang, J., Stang, H., 1998, "Applications of Stress Crack Width Relationship in Predicting The Flexural Behaviour of Fibre-Reinforced Concrete", Cement and Concrete Research, Vol. 3, No. 3, pp. 439-452.

Zoltek, 1996, "Panex 33CF -Product Data Sheer".

APPENDIX

Appendix A

A.1. Individual test results of UHPC

A.1.1. Individual results of 7 days compressive strength of UHPC

Group #	Spec. 1	Spec. 2	Spec. 3	Av. (MPa)	St. dev. (MPa)
1	120	122	118	**120**	**1.6**
2	128	130	132	**130**	**1.6**
3	120	122	118	**120**	**1.6**
4	164	157	159	**160**	**2.9**
5	129	130	131	**130**	**0.8**
6	144	141	136	**140**	**3.3**
7	188	191	192	**190**	**1.7**
8	178	184	179	**180**	**2.6**
9	195	185	190	**190**	**4.1**
10	214	221	225	**220**	**4.5**
11	130	131	130	**130**	**0.5**
12	139	138	138	**138**	**0.5**
13	169	168	174	**170**	**2.6**
14	181	182	182	**182**	**0.5**
15	167	168	158	**164**	**4.5**
16	210	210	209	**210**	**0.5**
17	129	134	128	**130**	**2.6**
18	150	148	151	**150**	**1.2**
19	158	159	163	**160**	**2.2**
20	207	199	195	**200**	**5.0**
21	165	159	157	**160**	**3.4**
22	187	188	195	**190**	**3.6**
23	184	184	173	**180**	**5.2**
24	246	241	234	**240**	**4.9**
25	118	119	114	**117**	**2.2**
26	138	122	130	**130**	**6.5**
27	169	170	172	**170**	**1.2**

Av. : Average
St. dev. : Standard Deviation

A.1.2. Individual results of 28 days compressive strength of UHPC

Group #	Spec. 1	Spec. 2	Spec. 3	Av. (MPa)	St. dev. (MPa)
1	130	133	132	132	1.2
2	144	144	140	143	1.9
3	142	140	138	140	1.6
4	164	168	164	165	1.9
5	140	141	140	140	0.5
6	144	147	135	142	5.1
7	192	198	195	195	2.4
8	201	197	188	195	5.4
9	190	203	192	195	5.7
10	229	228	234	230	2.6
11	142	142	144	143	0.9
12	164	164	162	163	0.9
13	175	178	172	175	2.4
14	190	190	192	191	0.9
15	180	187	187	185	3.3
16	216	218	218	217	0.9
17	142	138	140	140	1.6
18	168	164	164	165	1.9
19	172	171	168	170	1.7
20	204	211	214	210	4.2
21	180	170	175	175	4.1
22	195	191	198	195	2.9
23	196	190	198	195	3.4
24	242	244	233	240	4.8
25	140	144	144	143	1.9
26	144	150	140	145	4.1
27	176	173	176	175	1.4

Av. : Average
St. dev. : Standard Deviation

A.2. Statistical analysis of UHPC test results

Assuming a level of significance α = 5%, all probabilities < 5% means that there is a significant difference between the compared groups

Examining the effect of fibres and drying on 7 days strength

Effect of fibres

Compared Groups	t- Probability	Result
3 to 5	0.48%	Significantly different
17 to 18	0.31%	Significantly different
21 to 23	1.45%	Significantly different

Effect of drying

Compared Groups	t- Probability	Result
5 to 7	0.00%	Significantly different
8 to 10	0.13%	Significantly different
18 to 20	0.13%	Significantly different
23 to 24	0.31%	Significantly different

Examining the effect of fibres and drying on 28 days strength

Effect of fibres

Compared Groups	t- Probability	Result
3 to 5	80.42%	Non-different
17 to 18	0.02%	Significantly different
21 to 23	0.69%	Significantly different

Effect of drying

Compared Groups	t- Probability	Result
5 to 7	0.07%	Significantly different
8 to 10	0.44%	Significantly different
18 to 20	0.13%	Significantly different
23 to 24	0.07%	Significantly different

Appendix B

B.1. Derivation of fibre pull-out work of fracture equation

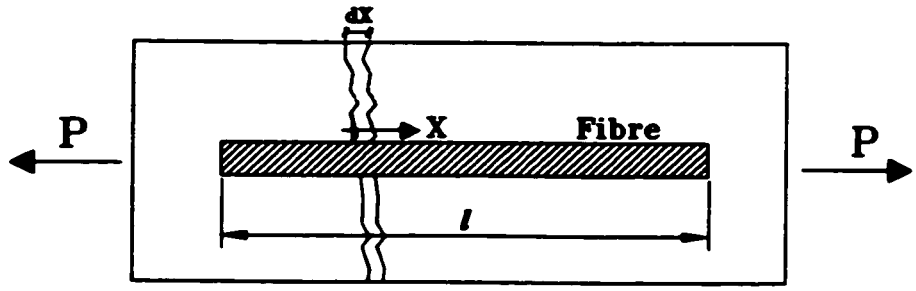

Figure [B.1]: A fibre being pull-out from a cracked matrix.

Figure [B.1] shows a fibre being pulled out from a cracked matrix. The total fibre pull-out work of fracture W_T can be estimated using equations [B.1] to [B. 4].

$$dW_T = F\,dx \qquad \text{[B.1]}$$

$$dW_T = \pi\ d\ \tau_{av}\ x\,dx \qquad \text{[B.2]}$$

$$W_T = \int_0^l \pi\, d\, \tau_{av}\, x\, dx \qquad \text{[B.3]}$$

$$W_T = \tfrac{1}{2}\pi\, d\, \tau_{av}\, l^2 \qquad \text{[B.4]}$$

To estimate the average pull-out work per unit fibre length W_P two different cases should be considered:

Case 1 : $l < l_c$

In this case fibre pull-out is more dominant than fibre rupture and pull-out can happen for embedded fibre lengths between 0 and $l/2$. The average pull out work can be estimated as given in equation [B.5].

$$W_P = \frac{\int_0^{l/2} W_T \, dx}{\int_0^{l/2} dx} \qquad [B.5]$$

Case 2 : $l > l_c$

In this case fibre rupture is more dominant than fibre pull-out and pull-out can happen for embedded fibre lengths between 0 and $l_c/2$. The average pull out work can be estimated as given in equation [B.6].

$$W_P = \frac{\int_0^{l_c/2} W_T \, dx}{\int_0^{l/2} dx} \qquad [B.6]$$

Consequently the average fibre pull-out work W_P can be estimated using equation [B.7].

$$W_P = \begin{cases} \frac{1}{24} \pi \, d \, \tau_{av} \, l^2 & for \; l < l_c \\ \frac{1}{24} \pi \, d \, \tau_{av} \, l^2 \left(\frac{l_c}{l} \right) & for \; l > l_c \end{cases} \qquad [B.7]$$

B.2. Fracture toughness testing data

B.2.1. Fracture toughness testing data of HPC series

For all beams the following properties is constant

Beam width (mm)	100
Beam depth (mm)	75
Beam length (mm)	350
Loaded span (mm)	300
Initial crack length (mm)	25
Poisson's ratio	0.17

Mix HPC0 .

	HPC0-1	HPC0-2	HPC0-3
W (kg)	6.542	6.561	6.482
P_c (kN)	5.120	4.800	1.530
Δ_c (mm)	0.061	0.080	0.079
P_i (kN)	3.450	3.590	3.448
Δ_i (mm)	0.040	0.053	0.049
Δ_{max} (mm)	0.767	0.509	0.554
$CMOD_{max}$(mm)	0.798	0.528	0.627
A_1 (kN.mm)	0.280	0.170	0.174
A_2 (kN.mm)	0.064	0.054	0.045
A_3 (kN.mm)	0.733	0.661	0.664

Mix HPC3

	HPC3-1	HPC3-2	HPC3-3
W (kg)	6.281	6.383	6.162
P_c (kN)	4.945	5.230	5.716
Δ_c (mm)	0.085	0.101	0.082
P_i (kN)	4.025	4.310	4.652
Δ_i (mm)	0.045	0.063	0.043
Δ_{max} (mm)	1.273	1.340	1.001
$CMOD_{max}$(mm)	1.154	1.367	1.032
A_1 (kN.mm)	0.275	0.327	0.308
A_2 (kN.mm)	0.063	0.073	0.095
A_3 (kN.mm)	1.506	1.624	1.713

Mix HPC6

	HPC6-1	HPC6-2	HPC6-3
W (kg)	6.031	6.098	6.258
P_c (kN)	5.400	5.730	5.420
Δ_c (mm)	0.077	0.080	0.092
P_i (kN)	4.280	4.350	4.410
Δ_i (mm)	0.045	0.052	0.065
Δ_{max} (mm)	0.946	1.216	1.281
$CMOD_{max}$(mm)	0.978	1.243	1.139
A1 (kN.mm)	0.254	0.268	0.291
A2 (kN.mm)	0.066	0.071	0.066
A3 (kN.mm)	1.156	1.285	1.409

Mix HPC10

	HPC10-1	HPC10-2	HPC10-3
W (kg)	6.538	6.501	6.472
P_c (kN)	4.750	4.869	4.776
Δ_c (mm)	0.082	0.092	0.094
P_i (kN)	3.480	3.569	3.520
Δ_i (mm)	0.046	0.050	0.055
Δ_{max} (mm)	1.200	1.152	1.289
$CMOD_{max}$(mm)	1.245	1.076	1.229
A1 (kN.mm)	0.228	0.267	0.249
A2 (kN.mm)	0.074	0.074	0.074
A3 (kN.mm)	1.627	1.197	1.826

B.2.2. Fracture toughness testing data for UHPC series

For all beams the following properties are constant

Beam width (mm)	25
Beam depth (mm)	25
Beam length (mm)	100
Loaded span (mm)	75
Initial crack length (mm)	7.5
Poission's ratio	0.17

Mix UHPC0 (Control)

	UHPC0-1	UHPC0-2	UHPC0-3
W (gm)	175.00	183.00	176.00
P_c (N)	1297.00	1717.00	1502.00
Δ_c (mm)	0.07	0.06	0.05
P_i (N)	1094.00	1200.00	1000.00
Δ_i (mm)	0.04	0.04	0.02
Δ_{max} (mm)	1.02	0.36	0.43
A_1 (N.mm)	55.39	62.64	54.94
A_2 (N.mm)	17.18	20.36	18.47
A_3 (N.mm)	176.33	227.53	193.08

Mix UHPC3

	UHPC3-1	UHPC3-2	UHPC3-3
W (gm)	183.00	186.00	179.00
P_c (N)	2498.00	2726.00	2249.00
Δ_c (mm)	0.11	0.11	0.10
P_i (N)	1500.00	2000.00	1500.00
Δ_i (mm)	0.05	0.06	0.06
Δ_{max} (mm)	1.56	1.81	1.84
A_1 (N.mm)	146.00	152.47	133.00
A_2 (N.mm)	36.60	44.45	34.16
A_3 (N.mm)	516.13	608.20	467.00

Mix UHPC6

	UHPC6-1	UHPC6-2	UHPC6-3
W (gm)	176.00	179.00	182.00
P_c (N)	1893.00	1941.00	2007.00
Δ_c (mm)	0.06	0.08	0.07
P_i (N)	1200.00	1000.00	1400.00
Δ_i (mm)	0.02	0.03	0.04
Δ_{max} (mm)	1.00	0.98	1.12
A_1 (N.mm)	91.98	95.94	93.55
A_2 (N.mm)	33.39	27.71	39.55
A_3 (N.mm)	325.52	346.26	340.44

B.3. Sample of spread sheets

B.3.1. Sample of spread sheets used with HPC notched specimens

HPC0 Notched

100*75*350 mm specimen
Two point loads at one third
Notched with 3 mm wide, 25 mm depth, one mid span notch.

P_c	**0.021**	kN
Δ_c	**0.061**	mm
P_e	**3.450**	kN
Δ_e	**0.040**	mm
Δ_{max}	**5.120**	mm
$CMOD_{max}$	**0.767**	mm

To calculate the area under the curve the trapezoidal rule is used: $A = \Sigma A_i = \Delta xi * Y_{av}$

(A_1) Area under the curve till P_c **0.218** kN.mm

(A_3) total area under the whole curve **0.733** kN.mm

Raw data			*Final data*					
P (kN)	Δ (mm)	CMOD (mm)	CMOD (m	Δ (mm)	P (kN)	Δx	Y_{av}	A_i
0.090	-0.027	0.000	0.000	0.000	0.000			
0.090	-0.027	0.000	0.000	0.000	0.000	0.000	0.000	0.000
0.090	-0.027	0.000	0.000	0.000	0.000	0.000	0.000	0.000
0.090	-0.027	0.000	0.000	0.000	0.000	0.000	0.000	0.000
0.100	-0.028	0.000	0.000	-0.001	0.010	-0.001	0.005	0.000
0.110	-0.028	0.001	0.001	-0.001	0.020	0.000	0.015	0.000
0.120	-0.028	0.001	0.001	-0.001	0.030	0.000	0.025	0.000
0.110	-0.028	0.000	0.000	-0.001	0.020	0.000	0.025	0.000
0.100	-0.028	0.001	0.001	-0.001	0.010	0.000	0.015	0.000
0.110	-0.028	0.001	0.001	-0.001	0.020	0.000	0.015	0.000
0.120	-0.028	0.001	0.001	-0.001	0.030	0.000	0.025	0.000
0.110	-0.028	0.001	0.001	-0.001	0.020	0.000	0.025	0.000
0.120	-0.027	0.001	0.001	0.000	0.030	0.001	0.025	0.000
0.150	-0.027	0.001	0.001	0.000	0.060	0.000	0.045	0.000
0.160	-0.026	0.001	0.001	0.001	0.070	0.001	0.065	0.000
0.150	-0.026	0.001	0.001	0.001	0.060	0.000	0.065	0.000
0.140	-0.026	0.001	0.001	0.001	0.050	0.000	0.055	0.000
0.130	-0.026	0.001	0.001	0.001	0.040	0.000	0.045	0.000
0.140	-0.026	0.001	0.001	0.001	0.050	0.000	0.045	0.000
0.120	-0.026	0.001	0.001	0.001	0.030	0.000	0.040	0.000
0.140	-0.026	0.001	0.001	0.001	0.050	0.000	0.040	0.000

B.3.2. Sample of spread sheets used with UHPC notched specimens

UPHC0 Notched

25*25*100 mm specimen
Two point loads at one third with 75 mm span
Notched with 0.5 mm wide, 7.5 mm depth, one mid span notch.

P_c	**1297**	N
Δ_c	**0.072**	mm
P_e	**1094**	N
Δ_e	**0.043**	mm
Δ_{max}	**1.020**	mm

To calculate the area under the curve the trapezoidal rule is used: $A = \Sigma A_i = \Delta xi * Y_{av}$

(A_1) Area under the curve till P_c **55.39** N.mm

(A_3) total area under the whole curve **176.33** N.mm

Raw data		***Final data***				
P (N)	Δ (mm)	Δ (mm)	P (N)	Δx	Y_{av}	A_i
0	0	0.000	0.000			
0	0.003	0.003	0.000	0.003	0.000	0.000
0	0.004	0.004	0.000	0.001	0.000	0.000
0	0.001	0.001	0.000	-0.003	0.000	0.000
0.4	0	0.000	0.400	-0.001	0.200	0.000
1.9	0	0.000	1.900	0.000	1.150	0.000
4.7	0.001	0.001	4.700	0.001	3.300	0.003
7	0.002	0.002	7.000	0.001	5.850	0.006
9.3	0.004	0.004	9.300	0.002	8.150	0.016
10.9	0.005	0.005	10.900	0.001	10.100	0.010
13.2	0.004	0.004	13.200	-0.001	12.050	-0.012
14	0.003	0.003	14.000	-0.001	13.600	-0.014
15.6	0.004	0.004	15.600	0.001	14.800	0.015
17.1	0.004	0.004	17.100	0.000	16.350	0.000
19.5	0.002	0.002	19.500	-0.002	18.300	-0.037
21.4	0.002	0.002	21.400	0.000	20.450	0.000
23	0	0.000	23.000	-0.002	22.200	-0.044
24.1	0	0.000	24.100	0.000	23.550	0.000
26.1	0.001	0.001	26.100	0.001	25.100	0.025
28	0.001	0.001	28.000	0.000	27.050	0.000
30	0.001	0.001	30.000	0.000	29.000	0.000
30.8	0.001	0.001	30.800	0.000	30.400	0.000
32.3	0.001	0.001	32.300	0.000	31.550	0.000

B.4. Derivation of the deformation equation for notched specimens

The following is the mathematical derivation of the equation used to estimate the deflection at the centre span of a notched beam loaded in third point bending as shown in Figure [B.2].

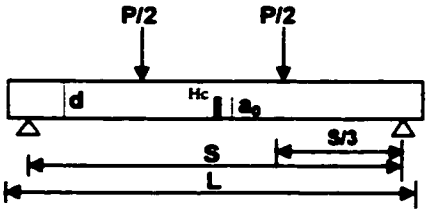

Figure [B.2]: Notched beam loaded in third point bending.

B.4.1. Basic Parameters

Two concentrated loads acting at one third of the span each of *P/2* are considered, *w* is the self weight of the beam per unit length, *S* is the loaded span, b is the beam width, *d* is the depth and *a* is the crack depth at the centre span. *E* is the modulus of elasticity in bending, *G* is the modulus of rigidity. The total deflection at the mid span is the summation of the three basic deflections; δ_f the elastic deflection, $_v$ the shear deflection and *c* the deflection due to cracking.

$$\delta = \delta_1 + v + c \qquad [B.8]$$

B.4.2. Estimation of the elastic deflection.

The elastic deflection at centre span due to two concentrated loads *P/2* and uniform load w can be estimated using the theory of virtual work or by applying superposition to the formulae provided by Ghali and Neville [1989].

$$\delta_1 = \delta_{11} + \delta_{12} \qquad [B.9]$$

Where δ_{l1} is the elastic deflection at centre span due to concentrated loads and δ_{l2} is the elastic deflection due to uniform loads

$$\delta_{l1} = \frac{23PS^3}{1296EI} \qquad [B.10]$$

$$\delta_{l2} = \frac{5wS^4}{384EI} \qquad [B.11]$$

Considering a rectangular cross section

$$I = \frac{bd^3}{12} \qquad [B.12]$$

The elastic deflection at centre span can be evaluated using equation [B.13]:

$$\delta_l = \frac{23PS^3}{108bd^3E} + \frac{5wS^4}{32bd^3E} \qquad [B.14]$$

B.4.3. Shear Defelction

The shear deflection can be evaluated by integrating equation [B.15] [Todd 1974].

$$\frac{dv}{dx} = \frac{QK}{bdG} \qquad [B.15]$$

Where Q is the shear force acting at the point of concern and K is a constant to convert the average shear stress to the maximum shear stress for a particular section. This value would be 3/2 for rectangular sections [Todd 1974]. G can be evaluated as in equation [B.16] where ν is Poisson's ratio of concrete ranging from 0.15 to 0.2 [Neville 1996].

$$G = \frac{E}{2(1+\upsilon)} \qquad [B.16]$$

The shear force Q can be given as

$$Q(x) = \begin{cases} \dfrac{P}{2} + \dfrac{w(S-x)}{2} & \text{for } 0 < x < \dfrac{S}{3} \\ \dfrac{w(S-x)}{2} & \text{for } \dfrac{l}{3} < x < \dfrac{S}{2} \end{cases} \qquad \text{[B.17]}$$

$$v = \int_0^{S/2} \frac{Qk}{bdG} dx \qquad \text{[B.18]}$$

$$v = \frac{3(1+\upsilon)}{bdE}\left[\int_0^{\frac{S}{3}} Q\,dx + \int_{\frac{S}{3}}^{\frac{S}{2}} Q\,dx\right] \qquad \text{[B.19]}$$

$$v = \frac{(1+\upsilon)}{bdE}\left[\frac{PS}{2} + \frac{23wS^2}{48}\right] \qquad \text{[B.20]}$$

B.4.4. Cracking deflection

Considering a dummy load dA acting at the centre span. The deflection due to cracking can be estimated by differentiating the strain energy (U) with respect to dA when A is equal to zero. This is a direct application of Castigliano's theorem for deflection by energy method [Higdon et al. 1967].

$$G_I = \frac{K^2{}_I}{E} \qquad \text{[B.21]}$$

Where G_I is the strain energy release rate and E is the plane strain modulus of elasticity and K_I is the stress intensity factor.

$$\frac{dU}{da} = G_I\, b = \frac{K_I^{\,2}\, b}{E} \qquad \text{[B.22]}$$

$$K_I = g_1(\alpha)\sigma\sqrt{\pi a} \qquad \text{[B.23]}$$

Where $\alpha = \frac{a}{d}$, a is the crack depth and d is the beam depth. $g_I(\alpha)$ is the geometry function to calculate the stress intensity factor for pure bending reported by Tada [1985].

$$g_1(\alpha) = 1.122 - 1.40\,\alpha + 7.33\,\alpha^2 - 13.08\,\alpha^3 + 14.0\,\alpha^4 \qquad \text{[B.24]}$$

$$g(\alpha) = g_1(\alpha)\sqrt{\pi} \qquad \text{[B.25]}$$

$$\frac{dU}{da} = \frac{\sigma^2\, a\, b\, g^2(\alpha)}{E} \qquad \text{[B.26]}$$

$$da = d\,(d\alpha) \qquad \text{[B.27]}$$

$$dU = \left(\frac{\sigma^2\, d^2\, b}{E}\right) \alpha\; g^2(\alpha)\; d\alpha \qquad \text{[B.28]}$$

$$U = \left[\frac{\sigma^2\, d^2\, b}{E}\right] \int_0^{\alpha_i} \alpha\; g^2(\alpha)\, d\alpha \qquad \text{[B.29]}$$

Defining $F(\alpha_i) = \int_0^{\alpha_i} \alpha\, g^2(\alpha)\, d\alpha$ [B.30]

$$U = \frac{\sigma^2 d^2 b F(\alpha_i)}{E} \quad [B.31]$$

$$\sigma = \frac{6M}{bd^2} \quad [B.32]$$

$$M = \frac{PS}{6} + \frac{AS}{4} + \frac{wS^2}{8} \quad [B.33]$$

$$\frac{dM^2}{dA} = 2M\frac{dM}{dA} \quad [B.34]$$

$$U = \frac{36 M^2 F(\alpha_i)}{b d^2 E} \quad [B.35]$$

$$c = \left[\frac{dU}{dA}\right]_{A=0}. \quad [B.36]$$

$$c = \frac{F(\alpha_i)}{E b d^2}\left[3PS^2 + \frac{9wS^3}{4}\right] \quad [B.37]$$

B.4.5. Evaluation of the total deflection δ

$$\delta = \delta_1 + v + c \quad [B.38]$$

$$\delta = \left[\frac{S^3}{bd^3E}\left[\frac{23P}{108} + \frac{5wS}{32}\right]\right] + \left[\frac{(1+\upsilon)S}{bdE}\left[\frac{PS}{2} + \frac{23wS^2}{48}\right]\right] + \left[\frac{F(\alpha_i)}{bd^2E}\left[3PS^2 + \frac{9wS^3}{4}\right]\right] \quad [B.39]$$

defining $\chi = \frac{S}{d}$ and $\eta = \frac{w}{P}$

$$\delta = \frac{PS^3}{Ebd^3}\left[\left[\frac{23}{108} + \frac{5wS}{32P}\right] + \left[\frac{(1+\upsilon)d^2}{S^2}\left(\frac{1}{2} + \frac{23wS}{48P}\right)\right] + \left[F(\alpha_i)\left(3 + \frac{9wS}{4P}\right)\right]\right] \quad [B.40]$$

$$\delta = \frac{P\chi^3}{Eb}\left[\left[\frac{23}{108} + \frac{5}{32}\eta S\right] + \left[\frac{(1+\upsilon)}{\chi^2}\left(\frac{1}{2} + \frac{23}{48}\eta S\right)\right] + \left[F(\alpha_i)\left(3 + \frac{9}{4}\eta S\right)\right]\right] \quad [B.41]$$

Equation [B.41] is the final formula used to evaluate the mid span deflection of a notched beam loaded in third point bending.

B.5. MathCad™ program for evaluation of the fracture toughness parameters for FRC

The following program is used to determine the different fracture toughness parameters for concrete. The estimation of the effective crack length is based on the elastic crack model developed by Karilahoo and Nallathambi [1989]. The following equations assume a simple beam notched at mid span and loaded in third point bending as shown in figure.

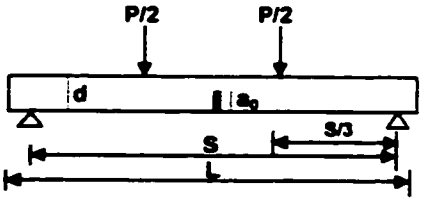

Beam parameters

$b := 100$ (beam width in mm) $d := 75$ (beam depth in mm)

$L := 350$ (beam length in mm) $S := 300$ (beam loaded span in mm)

$a_0 := 25$ (initial notch depth in mm) $H_0 := d - a_0$ (Initial un-cracked ligament in mm)

$W := 6.542$ (Beam wt. in kgs)

Concrete properties

$v := 0.17$ Poisson's ratio of concrete

Testing data

$P := 3.45$ (Load in kN) $\delta := 0.04$ (Deflection in mm)

P and δ are any load and its corresponding deflection within the elastic range of loading

$P_c := 5.12$ (Load in kN) $\delta_c := 0.061$ (Deflection in mm)

P_c is the maximum load in N and δ_c is the deflection corresponding to maximum load in mm

First data analysis

$A_1 := 0.218$ kN .mm

Area under the P-d curve of notched specimen up to P_c and d_c.

$A_2 := 0.0639$ kN . mm

Area under the P-d curve of similar unnotched specimen up to P_c and d_c of the notched specimen.

$A_3 := 0.733$ kN . mm

Area under the total P-d curve of notched specimen.

$\delta_{max} := 0.767$ mm

Maximum deflection to calculate G_F

Processing Parameters

$w := \frac{W \cdot 10}{L}$ N per mm $\quad \eta := \frac{w}{P \cdot 10^3} \quad \phi := \frac{a_0}{d} \quad \chi := \frac{S}{d}$

$i := 0 .. 10000$ Iteration counter $\quad a_{i+1} := a_i + 0.0001\ d \quad \beta_i := \frac{a_i}{d}$

Considering the stress intensty factor function $g_1(\alpha)$

$g_1(\alpha) := 1.122 - 1.40\ \alpha + 7.33\ \alpha^2 - 13.08\ \alpha^3 + 14.0\ \alpha^4$ **(Tada et al. 1985)**

$g(\alpha) := \sqrt{\pi} \cdot g_1(\alpha)$ float, 4 $\rightarrow 1.989 - 2.482 \cdot \alpha + 13.0 \cdot \alpha^2 - 23.19 \cdot \alpha^3 + 24.82 \cdot \alpha^4$

$F(\alpha) := \int \alpha \cdot g(\alpha)^2 d\alpha$

$F(\alpha) := -3.29 \cdot \alpha^3 + 63.5 \cdot \alpha^6 + 14.4 \cdot \alpha^4 + 148. \cdot \alpha^8 - 103. \cdot \alpha^7 - 31.2 \cdot \alpha^5 + 1.98 \cdot \alpha^2 - 128. \cdot \alpha^9 + 61.6 \cdot \alpha^{10}$

Evaluation of E based on Elastic analysis

$$E := \frac{P \cdot 10^3 \cdot \chi^3}{\delta \cdot b} \cdot \left[\frac{23}{108} + \frac{5}{32} \cdot \eta \cdot S + \left[\frac{1+\nu}{\chi^2} \cdot \frac{1}{2} + \frac{23}{48} \cdot \eta \cdot S \right] + \left[\frac{F(\phi)}{\chi} \cdot 3 + \frac{9}{4} \cdot \eta \cdot S \right] \right]$$

$E = 2.25 \cdot 10^4$

Evaluation of the E for cracked specimen $E_{cracked}$

$$E_{cracked_i} := \frac{P_c \cdot 10^3 \cdot \chi^3}{\delta_c \cdot b} \cdot \left[\frac{23}{108} + \frac{5}{32} \cdot \eta \cdot S + \left[\frac{1+\nu}{\chi^2} \cdot \frac{1}{2} + \frac{23}{48} \cdot \eta \cdot S \right] + \left[\frac{F\ \beta_i}{\chi} \cdot 3 + \frac{9}{4} \cdot \eta \cdot S \right] \right]$$

Determination of the effective crack length

$$i_{critical}(\Delta,\rho) := \left| \begin{array}{l} i \leftarrow 1 \\ \text{while } \Delta_i \le \rho \\ \quad i \leftarrow i + 1 \\ i \end{array} \right. \qquad \Delta_i := \frac{E_{cracked_i} - E}{E}$$

$$i_{critical}(\Delta, 0.0005) = 105$$

The counter at which the value of difference between the two moduli comes to 0.05%.

Critical crack depth (a_c)

$$c := i_{critical}(\Delta, 0.0005)$$

$E = 2.25 \cdot 10^4$ MPa $\qquad E_{cracked_c} = 2.25 \cdot 10^4$ MPa

$a_c = 25.788$ mm $\qquad \beta_c = 0.34$

Evaluation of Fracture toughness

1 - LEFM parameters (Broek 1982)

$$E_{plst} := \frac{E \cdot 10^{-3}}{1 - \nu^2} \qquad E_{plst} = 23.19 \text{ GPa}$$

(*Plane strain modulus of elasticity*)

$$\sigma_c := \frac{P_c \cdot 10^3 \cdot S + 0.75 \cdot w \cdot S^2}{b \cdot d^2} \qquad \sigma_c = 2.75 \text{ MPa}$$

$$K_{IC} := \sigma_c \cdot g\, \beta_c \cdot \sqrt{a_c \cdot 10^{-3}} \qquad K_{IC} = 0.9 \text{ MPa . m}^{1/2}$$

$$G_{IC} := \frac{K_{IC}^2 \cdot 10^3}{E_{plst}} \qquad G_{IC} = 36.35 \text{ N / m}$$

2- EPFM parameters

2.1. Estimation of the $CTOD_c$ ***Tada et al. (1985) and Shah et al. (1995)***

$$g_2(\alpha) := 0.8 - 1.7\,\alpha + 2.4\,\alpha^2 + \frac{0.66}{1 - \alpha^2}$$

$$CMOD_c := \frac{4 \cdot \sigma_c \cdot a_c \cdot g_2\ \beta_c}{E_{plst} \cdot 10^3} \qquad CMOD_c = 0.0153 \quad mm$$

$$\theta := \frac{a_0}{a_c} \qquad \theta = 0.97$$

$$g_3(\alpha, x) := \left[(1 - x^2) + (1.081 - 1.149 \cdot \alpha)\ x - \alpha^2 \right]^{0.5}$$

$$CTOD_c := 1000 \cdot CMOD_c \cdot g_3\ \beta_c, \theta \qquad CTOD_c = 12.2614 \quad \mu m$$

2.2. Evaluation of J_{IC}. ***Begley and Landes (1972) and Mindess et al. (1977)***

$$H_c := d - a_c \qquad H_c = 49.21 \quad mm$$

H_c The uncracked legment the cracked specimen

$$A := A_1 - A_2 \qquad A = 0.15 \quad kN.mm$$

$$J_{IC} := \frac{2 \cdot A \cdot 10^6}{b \cdot H_c} \qquad J_{IC} = 62.63 \quad N / m$$

2.3. Evaluation of G_F ***Hillerborg (1985)***

$$G_F := \frac{A_3 + W \cdot \delta_{max} \cdot 10^{-2} \cdot 10^6}{b \cdot H_0} \qquad G_F = 156.64 \quad N / m$$

B.6. Compressive strength and modulus of rupture of HPC series

Compressive strength (MPa)

MIX	Spec. 1	Spec. 2	Spec. 3	Av. (MPa)	St. dev. (MPa)
HPC0	48.7	51.8	54.6	**51.7**	**2.4**
HPC3	50.8	52	51	**51.3**	**0.5**
HPC6	54.6	55	49.6	**53.1**	**2.5**
HPC10	55.5	52.5	58.3	**55.4**	**2.4**

Modulus of rupture (MPa)

MIX	Spec. 1	Spec. 2	Spec. 3	Av. (MPa)	St. dev. (MPa)
HPC0	5.3	7.5	5.6	**6.1**	**1.0**
HPC3	7.5	7.9	8.6	**8.0**	**0.5**
HPC6	9.2	8.3	7	**8.2**	**0.9**
HPC10	8.6	7.9	6.6	**7.7**	**0.8**

B. 7. Individual fracture toughness results

B.7.1. Individual fracture toughness results of HPC series

	HPC0-1	HPC0-2	HPC0-3	average	st dev.
a_c (mm)	25.788	28.308	30.393	**28.2**	**2.31**
E (GPa)	23.190	18.200	18.900	**20.1**	**2.70**
σ_c (MPa)	2.750	2.580	2.440	**2.6**	**0.16**
K_{IC} (MPa. $m^{1/2}$)	0.900	0.900	1.000	**0.9**	**0.06**
G_{IC} (N / m)	36.350	48.430	48.100	**44.3**	**6.88**
$CTOD_C$ (μm)	12.200	17.060	17.300	**15.5**	**2.88**
J_{IC} (N / m)	62.600	49.860	58.020	**56.8**	**6.45**
G_F (N / m)	156.600	138.880	140.600	**145.4**	**9.77**
	HPC3-1	**HPC3-2**	**HPC3-3**	**average**	**st dev.**
a_c (mm)	35.425	32.125	33.850	**33.8**	**1.65**
E (GPa)	24.000	18.350	26.680	**23.0**	**4.25**
σ_c (MPa)	2.660	2.810	3.070	**2.8**	**0.21**
K_{IC} (MPa. $m^{1/2}$)	1.300	1.200	1.400	**1.3**	**0.10**
G_{IC} (N / m)	65.580	74.750	69.740	**70.0**	**4.59**
$CTOD_C$ (μm)	18.936	22.440	18.280	**19.9**	**2.24**
J_{IC} (N / m)	107.190	118.440	103.590	**109.7**	**7.75**
G_F (N / m)	317.190	341.850	354.950	**338.0**	**19.17**
	HPC6-1	**HPC6-2**	**HPC6-3**	**average**	**st dev.**
a_c (mm)	32.718	29.178	28.698	**30.2**	**2.20**
E (GPa)	25.510	22.460	18.180	**22.1**	**3.68**
σ_c (MPa)	2.900	3.080	2.920	**3.0**	**0.10**
K_{IC} (MPa. $m^{1/2}$)	1.200	1.200	1.100	**1.2**	**0.06**
G_{IC} (N / m)	59.860	59.360	63.900	**61.0**	**2.49**
$CTOD_C$ (μm)	17.137	17.299	19.768	**18.1**	**1.47**
J_{IC} (N / m)	85.190	84.720	93.770	**87.9**	**5.09**
G_F (N / m)	243.570	272.810	298.380	**271.6**	**27.43**
	HPC10-1	**HPC10-2**	**HPC10-3**	**average**	**st dev.**
a_c (mm)	32.658	32.598	32.598	**32.6**	**0.03**
E (GPa)	41.820	19.170	21.960	**27.7**	**12.35**
σ_c (MPa)	3.420	2.620	2.570	**2.9**	**0.48**
K_{IC} (MPa. $m^{1/2}$)	1.500	1.100	1.100	**1.2**	**0.23**
G_{IC} (N / m)	50.360	64.230	53.990	**56.2**	**7.19**
$CTOD_C$ (μm)	12.270	20.454	17.521	**16.7**	**4.15**
J_{IC} (N / m)	76.380	92.350	86.170	**85.0**	**8.05**
G_F (N / m)	339.870	253.450	381.930	**325.1**	**65.50**

B.7.2. Individual fracture toughness results of UHPC series

	UHPC0-1	UHPC0-2	UHPC0-3	average	st dev.
a_c (mm)	10.320	9.230	11.080	10.2	0.93
E (GPa)	12.450	16.310	22.200	17.0	4.91
σ_c (MPa)	6.230	8.250	7.210	7.2	1.01
K_{IC} (MPa. $m^{1/2}$)	1.400	1.700	1.800	1.6	0.21
G_{IC} (N / m)	165.800	175.990	147.130	163.0	14.64
$CTOD_C$ (μm)	24.230	20.880	17.400	20.8	3.42
J_{IC} (N / m)	208.300	214.450	209.690	210.8	3.23
G_F (N / m)	407.100	521.560	443.060	457.2	58.53
	UHPC3-1	UHPC3-2	UHPC3-3	average	st dev.
a_c (mm)	9.007	9.225	8.470	8.9	0.39
E (GPa)	13.590	15.520	12.650	13.9	1.46
σ_c (MPa)	12.000	13.090	10.800	12.0	1.15
K_{IC} (MPa. $m^{1/2}$)	2.400	2.700	2.100	2.4	0.30
G_{IC} (N / m)	427.110	465.500	333.380	408.7	67.96
$CTOD_C$ (μm)	35.230	34.810	31.190	33.7	2.22
J_{IC} (N / m)	547.260	547.800	478.450	524.5	39.88
G_F (N / m)	1190.000	1400.000	1070.000	1220.0	167.03
	UHPC6-1	UHPC6-2	UHPC6-3	average	st dev.
a_c (mm)	12.410	10.612	10.035	11.0	1.24
E (GPa)	27.950	18.120	18.020	21.4	5.70
σ_c (MPa)	9.090	9.190	9.640	9.3	0.29
K_{IC} (MPa. $m^{1/2}$)	2.700	2.200	2.200	2.4	0.29
G_{IC} (N / m)	253.790	264.080	257.690	258.5	5.19
$CTOD_C$ (μm)	20.770	25.550	24.860	23.7	2.58
J_{IC} (N / m)	372.220	379.380	288.670	346.8	50.43
G_F (N / m)	748.070	795.470	782.820	775.5	24.54

B.8. Statistical analysis of fracture toughness testing

B.8.1 Statistical analysis of HPC fracture toughness

Assuming a level of significance α = 5%, all probabilities < 5% means that there is a significant difference.

Examining the effcet of fibre length on K_{IC}

Compared Groups	t- Probability	Result
G0 to G3	1.00%	Significantly different
G0 to G6	0.78%	Significantly different
G0 to G10	14.65%	Non different
G3 to G6	13.36%	Non different
G3 to G10	68.05%	Non different
G6 to G10	67.08%	Non different

Examining the effcet of fibre length on G_{IC}

G0 to G3	0.84%	Significantly different
G0 to G6	3.94%	Significantly different
G0 to G10	10.73%	Non different
G3 to G6	5.67%	Non different
G3 to G10	5.84%	Non different
G6 to G10	36.57%	Non different

Examining the effcet of fibre length on $CTOD_C$

G0 to G3	11.09%	Non different
G0 to G6	26.61%	Non different
G0 to G10	69.75%	Non different
G3 to G6	31.44%	Non different
G3 to G10	33.05%	Non different
G6 to G10	64.59%	Non different

Examining the effcet of fibre length on J_{IC}

G0 to G3	0.09%	Significantly different
G0 to G6	0.34%	Significantly different
G0 to G10	1.02%	Significantly different
G3 to G6	2.02%	Significantly different
G3 to G10	1.85%	Significantly different
G6 to G10	62.78%	Non different

Examining the effcet of fibre length on G_f

G0 to G3	0.06%	Significantly different
G0 to G6	0.89%	Significantly different
G0 to G10	3.90%	Significantly different
G3 to G6	3.14%	Significantly different
G3 to G10	77.02%	Non different
G6 to G10	29.27%	Non different

B.8.2. Statistical analysis of UHPC fracture toughness

Assuming a level of significance $\alpha = 5\%$, all probabilities < 5% means that there is a significant difference.

Examining the effec\t of fibre length on K_{IC}

Compared Groups	t- Probability	Result
G0 to G3	2.68%	Significantly different
G0 to G6	0.19%	Significantly different
G3 to G6	49.79%	Non different

Examining the effect of fibre length on G_{IC}

G0 to G3	2.04%	Significantly different
G0 to G6	0.50%	Significantly different
G3 to G6	6.48%	Non different

Examining the effect of fibre length on $CTOD_C$

G0 to G3	0.10%	Non different
G0 to G6	3.27%	Non different
G3 to G6	0.62%	Non different

Examining the effect of fibre length on J_{IC}

G0 to G3	0.43%	Significantly different
G0 to G6	4.08%	Significantly different
G3 to G6	0.71%	Significantly different

Examining the effect of fibre length on G_f

G0 to G3	1.16%	Significantly different
G0 to G6	0.41%	Significantly different
G3 to G6	4.25%	Significantly different

Appendix C

C.1. Statistical analysis of anchorage testing

Statistical analysis of anchorage efficiency

The following statistical analysis is used to represent the efficiencies of the non-metallic anchorage (η_A) tested in stage II through the experimental programme.

Test Results

Test #	P_{ult}	η_A
1	97.9	0.94
2	99.2	0.95
3	99.2	0.95
4	99.4	0.96
5	98.7	0.95
6	99.7	0.96
7	102.8	0.99
8	101	0.97
	Average	**0.96**
	St. dev.	**0.01**

Statistical Analysis

η_A	Frequency	h (η_A)%
0.93	**0**	**0**
0.94	**1**	**13**
0.95	**3**	**38**
0.96	**2**	**25**
0.97	**1**	**13**
0.98	**0**	**0**
0.99	**1**	**13**
1	**0**	**0**
Sum	**8**	

C.2. Individual test results of phase II - short-term tensile strength test

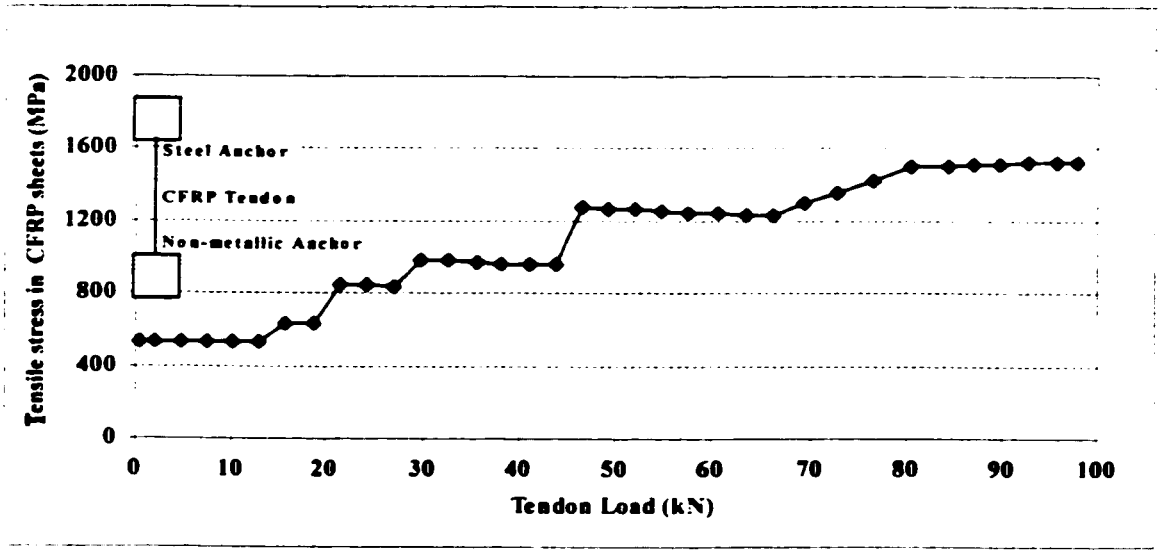

Figure [C.1]: Tensile stress of CFRP sheets Vs. tendon load (Test 1 - Series I).

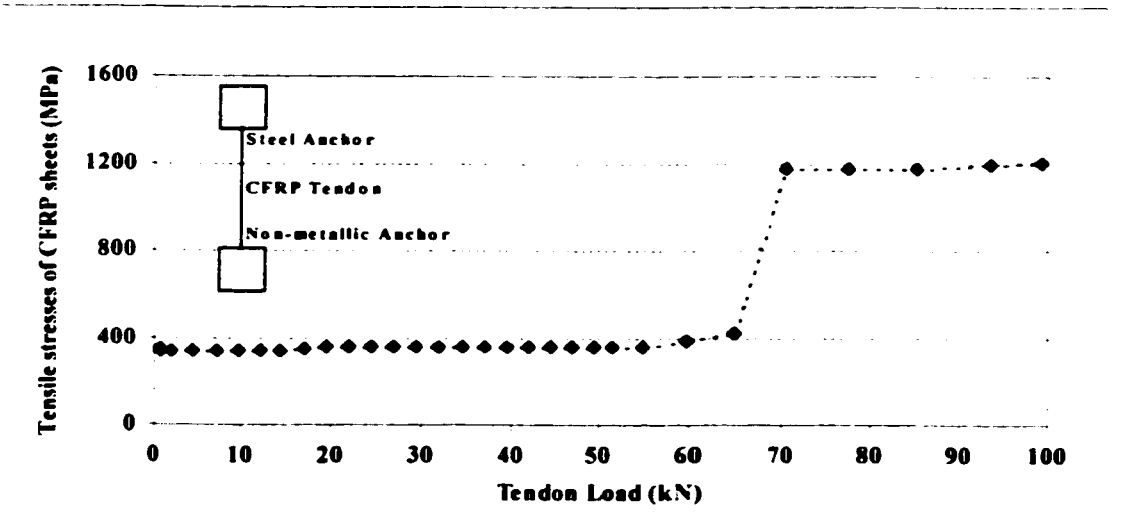

Figure [C.2]: Tensile stress of CFRP sheets Vs. tendon load (Test 2 - Series I).

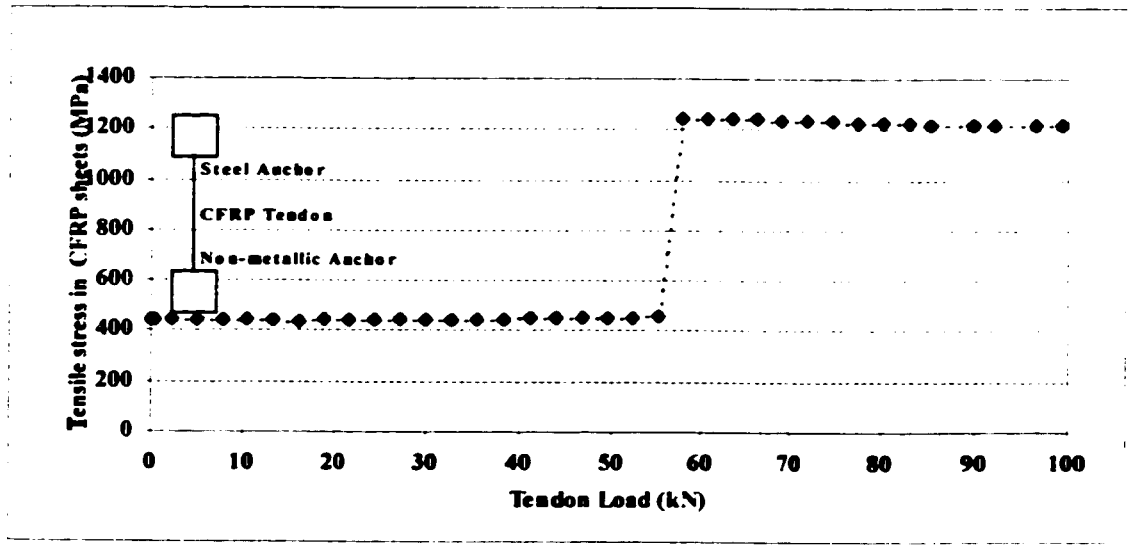

Figure [C.3]: Tensile stress of CFRP sheets Vs. tendon load (Test 3 - Series I).

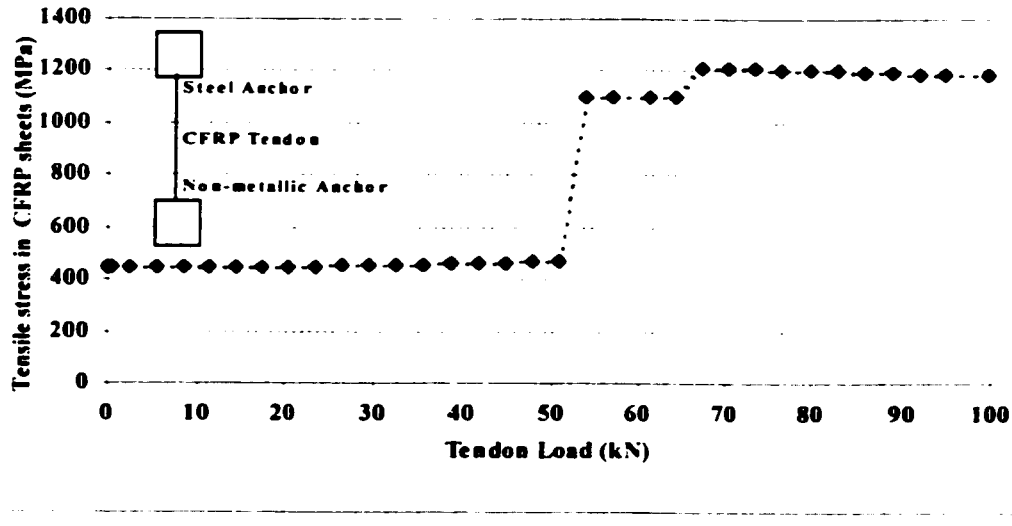

Figure [C.4]: Tensile stress of CFRP sheets Vs. tendon load (Test 4 - Series I).

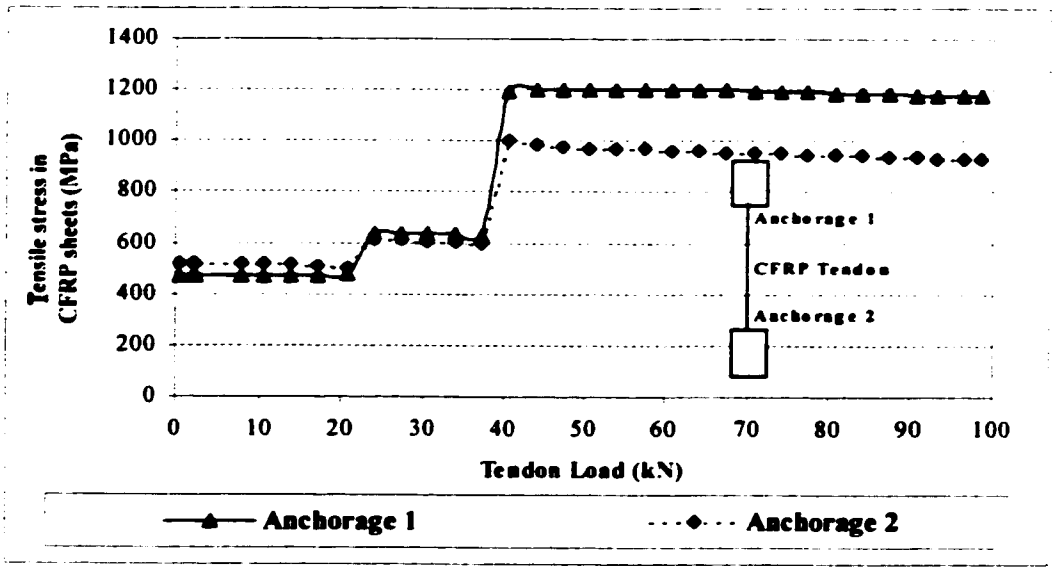

Figure [C.5]: Tensile stress of CFRP sheets Vs. tendon load (Test 1 - Series II).

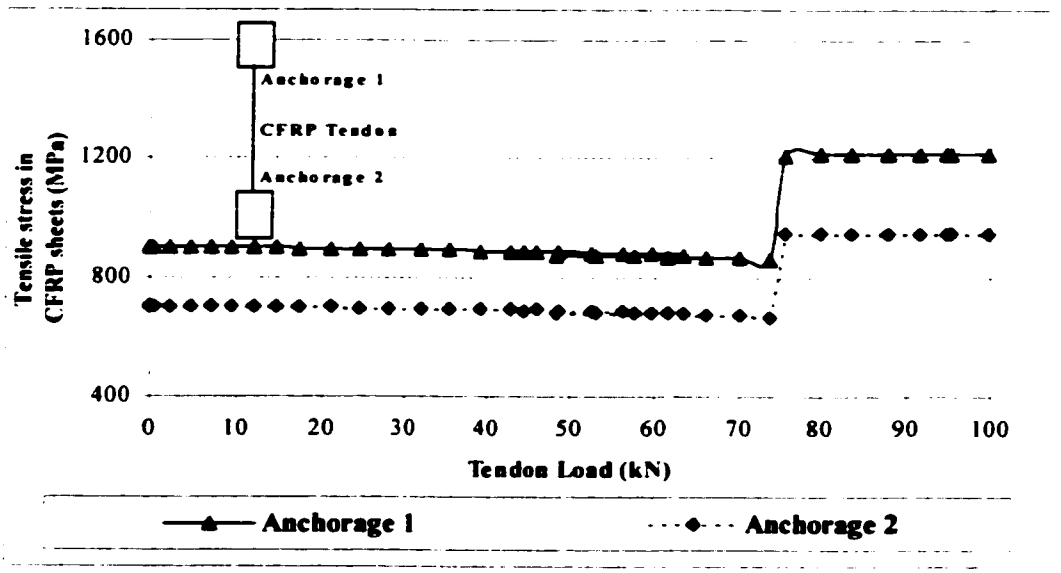

Figure [C.6]: Tensile stress of CFRP sheets Vs. tendon load (Test 2 - Series II).

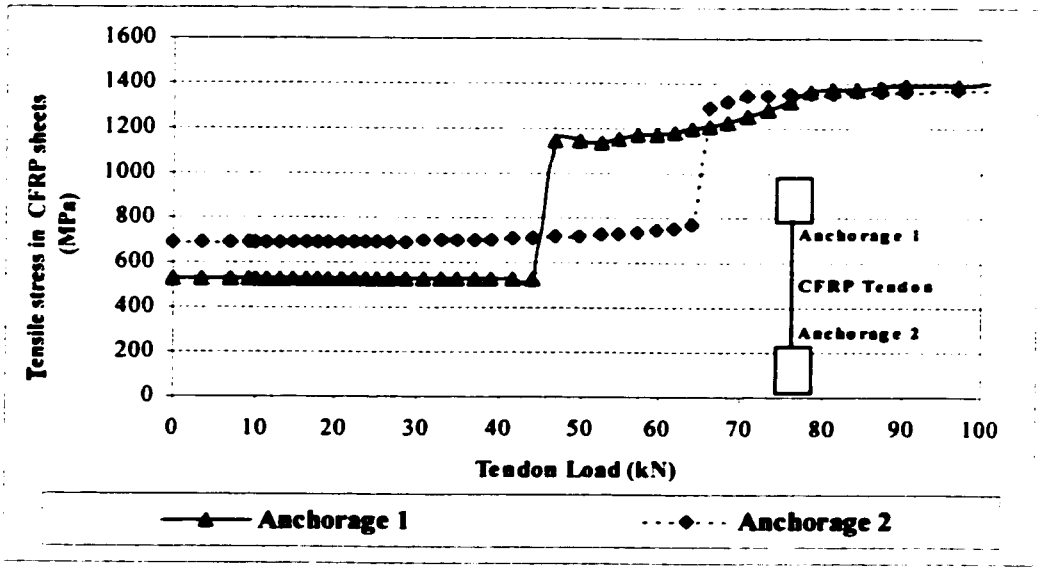

Figure [C.7]: Tensile stress of CFRP sheets Vs. tendon load (Test 3 - Series II).

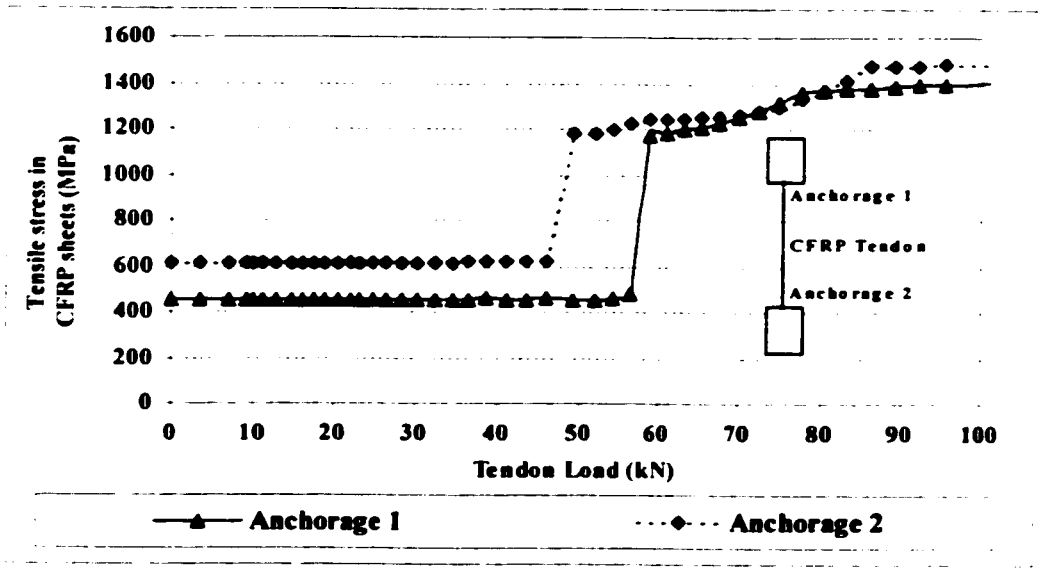

Figure [C.8]: Tensile stress of CFRP sheets Vs. tendon load (Test 4 - Series II).